Best

Available

Copy

AD

AD 675458

USAAVLABS TECHNICAL REPORT 68-41

ANALYSIS OF NOISE GENERATED BY UH-1 HELICOPTER TRANSMISSION

By

I. Laskin

F. K. Orcutt

E. E. Shipley

June 1968

U. S. ARMY AVIATION MATERIEL LABORATORIES
FORT EUSTIS, VIRGINIA

CONTRACT DA 44-177-AMC-416(T)

MECHANICAL TECHNOLOGY INCORPORATED

LATHAM, NEW YORK

This document has been approved for public release and sale; its distribution is unlimited.

Reproduced by the
CLEARINGHOUSE
for Federal Scientific & Technical
Information Springfield Va. 22151

318

Disclaimers

The findings in this report are not to be construed as an official Department of the Army position unless so designated by other autorized documents.

When Government drawings, specifications, or other data are used for any purpose other than in connection with a definitely related Government procurement operation, the United States Government thereby incurs no responsibility nor any obligation whatsoever; and the fact that the Government may have formulated, furnished, or in any way supplied the said drawings, specifications, or other data is not to be regarded by impication or otherwise as in any manner licensing the holder or any other person or corporation, or conveying any rights or permission, to manufacture, use or sell any patented invention that may in any way be related thereto.

Trade names cited in this report do not constitute an official endorsement or approval of the use of such commercial hardware or software.

Disposition Instructions

Destroy this report when no longer needed. Do not return it to originator.

DEPARTMENT OF THE ARMY
U. S. ARMY AVIATION MATERIEL LABORATORIES
FORT EUSTIS, VIRGINIA 23604

This report was prepared by Mechanical Technology Incorporated under the terms of Contract DA 44-177-AMC-416(T).

The objective of the program was to develop effective technology for the computation of helicopter gearbox operating noise. The program included the application of the derived technology to an analysis and evaluation of the UH-1 helicopter main transmission.

This command concurs in the contractor's conclusions. A further validation of the technology is being conducted, using the CH-47 helicopter power train as the model.

Task 1G121401D14414
Contract DA 44-177-AMC-416(T)
USAAVLABS Technical Report 68-41
June 1968

ANALYSIS OF NOISE GENERATED BY UH-1 HELICOPTER TRANSMISSION

By
I. Laskin
F. K. Orcutt
E.E. Shipley

Prepared by

Mechanical Technology Incorporated
Latham, New York

This document has been approved for public release and sale; its distribution is unlimited.

for

U. S. ARMY AVIATION MATERIEL LABORATORIES
FORT EUSTIS, VIRGINIA

FOREWORD

This report was prepared by I. Laskin, F. K. Orcutt, and E. E. Shipley of Mechanical Technology Incorporated, under Contract DA-44-177-AMC-416(T). The contract was carried out under the technical cognizance of Mr. E. R. Givens, U.S. Army Aviation Materiel Laboratories, Fort Eustis, Virginia.

A major contribution to the program was made by D. W. Dudley, who was at MTI when the contract was initiated. He provided the general direction which the program followed and also served as consultant in many areas of gear technology.

Consultation in the design and interpretation of the noise and vibration measurements was provided by Mr. Edward F. Noonan of Noonan, Knopfle, and Feldman.

This program was carried out with the cooperation and assistance of many individuals and organizations. Special credit is due Mr. John Nobles of USAAVLABS; Mr. Charles W. Bowen, Jr. of Bell Helicopter Company; Dr. Jorgen Lund and Mr. David Hu of MTI, who contributed the torsional response analysis; and Mr. Paul M. Dean of MTI, who assisted in the interpretation of the gear measurements.

ABSTRACT

This study is part of an effort to create a technology for reducing internal helicopter noise at its source. The objectives were as follows:

1. Development of an effective method of computing helicopter gearbox noise.

2. Use of measurements in the helicopter and on its gearbox components to provide a basis for and to validate the computational method.

3. Application of the method for the evaluation of noise-reducing design changes.

Only one helicopter model, the UH-1D, was investigated in detail, but the approach was made general enough to apply to all similar helicopters.

To develop a firm, empirical basis for the analytical methods, three groups of measurements were made: in-flight noise and vibration measurements on four helicopters, laboratory vibration measurements on the gearbox casing, and precision inspection measurements on two sets of gears. These measurements identified the major factors in the generation and transmission of gearbox noise and at the same time demonstrated that some commonly accepted factors were of minor significance. The most objectionable noise was shown to originate in the meshing action of the gear teeth. When the gears are heavily loaded, high-level noise components are produced whose frequencies correspond to the first three harmonics of each tooth meshing rate. The broad-band noise characteristics of the gearbox are determined by the total pattern of the magnitudes and frequencies of these components. The excitation of the noise comes primarily from the variable tooth deflection of the gears meshing under load, with some contribution from manufactured profile errors. The other gear errors - tooth spacing and runout - do not play a major role. The bearings themselves are not a significant source of noise production, but they do transmit the gear-induced vibration to the gearbox casing, which serves as an important "broadcaster" of this gear noise.

A computerized calculation procedure was developed for predicting noise levels from design and operating data. This procedure was checked by applying it to the UH-1D helicopter operating under cruise conditions, for which it gave calculated noise levels in good agreement with the in-flight measured noise levels.

This analytical procedure makes it possible to identify, for the first time, the individual noise components which will dominate the noise spectrum, and to find out how much each of these components must be reduced in order to drop the noise to an acceptable level. With this procedure, it is now also possible to evaluate quantitatively the improvement to be obtained from any of a broad range of design changes often proposed for noise reduction.

The calculations on the UH-1D gearbox revealed that a variety of design modifications will be required to reduce all of the high-level noise components. They also showed that some of the modifications must be carefully optimized to avoid increasing one component while reducing another.

A partial investigation of the gear noise reductions possible with design changes points to a potential decrease of 10 db or more along the entire frequency spectrum. The 10-db improvement can be obtained from relatively minor changes, such as tooth profile modifications and system stiffness modifications which shift the relations between excitation and resonant frequencies. Only where greater reduction is required will it be necessary to introduce major changes, such as more accurate gear manufacture, helical gears in place of spur gears in the planetary stages, or gearbox casing redesign.

TABLE OF CONTENTS

	Page
ABSTRACT	iii
FOREWORD	v
LIST OF ILLUSTRATIONS	ix
LIST OF TABLES	xiv
INTRODUCTION	1
DESCRIPTION OF PROGRAM	5
DISCUSSION OF RESULTS	8
Introduction	8
Noise Measurements	10
Gearbox Vibration Measurements	28
Cabin Surface Vibration Measurements	32
Gearbox Casing Resonance Measurements	35
General Description of Analysis	44
Gear Excitation Analysis	47
Dynamic Force Analysis	62
Noise Level Analysis	65
MODIFICATIONS FOR NOISE REDUCTION	74
Introduction	74
Gear Tooth Modifications	74
Drive System Modification	77
Gearbox Casing Modifications	81
CONCLUSIONS	85
LITERATURE CITED	87
APPENDIXES	
I. Noise and Vibration Measurements	88
Description of Instrumentation and Calibration Procedures	88
Sound Pressure Level Measurements	93
Vibration Measurements	93
Measurements on Cabin Surfaces	107

TABLE OF CONTENTS (CONT.)

		Page
II.	Measurement of Gearbox Housing Structural Response	115
III.	Gear Measurements	121
	General Methods of Gear Inspection	121
	Gear Errors and Analytical Measurement Techniques	122
	Composite Measuring Techniques	124
	Inspection of UH-1D Transmission Gearing	128
IV.	Gear Excitation Analysis	143
	Introduction	143
	Limitations and Assumptions	143
	Description of Analysis	145
	Derivation of Analytical Relationships	148
	Description of Computer Program	186
	Data Reduction	215
V.	Gear Tooth Force Analysis	218
	Introduction	218
	Limitations and Assumptions	218
	Description of Analysis	220
	Derivation of Analytical Relationships	223
	Description of Main Computer Program	240
	Description of Auxiliary Computer Program	274
VI.	Predicted Noise Level Analysis	288
	Introduction	288
	Description of Analysis and Calculated Results	288
DISTRIBUTION		300

LIST OF ILLUSTRATIONS

Figure		Page
1	Comparison of Measured Noise on the UH-1D With Present and Proposed Specifications	2
2	Comparison of Noise Levels at Normal Cruise Power on UH-1D and UH-1A	2
3	Overall Program for a New Method of Reducing Noise From Helicopter Gearboxes	3
4	Factors in Helicopter Gearbox Noise	9
5	Noise Measurements in Third-Octave Bands, Helicopter No. 66-1038, Cruise Operation	11
6	Noise Measurements in Third-Octave Bands, Helicopter No. 66-1039, Cruise Operation	12
7	Noise Measurements in Third-Octave Bands, Helicopter No. 66-1043, Cruise Operation	13
8	Microphone Locations for Sound Pressure Level Measurements on Three Helicopters	14
9	Comparative Noise Levels Among Three Helicopters, Measured at Gearbox Compartment	16
10	Noise Levels for Two Microphone Locations, Helicopter No. 66-1038, Cruise Operation	18
11	Schematic Diagram of Main Rotor Drive Gearing Stations in the UH-1D Helicopter Transmission	23
12	Portion of Narrow-Band Sound Pressure Level Frequency Spectrum, Measured at Hatch to Gearbox Compartment, Cruise Operation, Helicopter No. 66-1038, With Calculated Gear Teeth Meshing Frequencies	25
13	Noise Attenuation From Gearbox Compartment to Location Behind Pilot	27
14	Surface Vibration Velocity Measurements at Three Locations on Gearbox Housing, Helicopter No. 66-1038, Cruise Operation	29
15	Surface Vibration Velocity Measurements at Locations Above and Below Lift Link, Helicopter No. 66-1038, Cruise Operation	30

Figure		Page
16	Accelerometer Locations for Some of the In-Flight Vibration Measurements	31
17	Comparison of Noise and Vibration Measurements	33
18	Vibration Attenuation Across Gearbox Lift Link and Mounts	34
19	Vibration Measurements on Cabin Surfaces, Helicopter No. 66-1039, Cruise Operation	36
20	Location of Excitation and Some of the Accelerometers Used in Gearbox Casing Resonance Measurements	38
21	Gearbox Casing Vibration Response - Measured at Point of Excitation	39
22	Gearbox Casing Vibration Response - Driving Force Applied at Input Shaft Bearing Support	40
23	Gearbox Casing Vibration Response - Driving Force Applied at Ring Gear	41
24	Gearbox Casing Vibration Response - Driving Force Applied at Mast Upper Bearing Support	42
25	Flow Chart Description of Predicted Noise Calculation	45
26	Gear Tooth Unit Deflection Curves	48
27	Gear Mesh Pulsations for Upper Sun Driving Planet With Involute Profiles on Both	50
28	Sun Gear Tooth Profiles	51
29	Ring Gear Tooth Profiles	52
30	Gear Mesh Pulsations for Upper Sun Driving Planet for Non-Involute Profiles	54
31	Gear Tooth Profile Measurements on the Sun Gear	55
32	Gear Tooth Profile Measurements on the Ring Gear	55
33	Gear Tooth Profile Measurements on the Planet Gear	56
34	Gear Mesh Pulsations for Upper Sun Driving Planet Under Various Load Conditions	59

Figure		Page
35	Dynamic Forces at the Bevel Gear Teeth for Unit Excitation at the Same Point	63
36	Dynamic Forces at Upper Planetary Gear Teeth for Excitation at Sun-Planet Gear Mesh	66
37	Dynamic Forces at Upper Planetary Gear Teeth for Excitation at Planet-Ring Gear Mesh	67
38	Dynamic Forces at Lower Planetary Gear Teeth for Excitation at Sun-Planet Gear Mesh	68
39	Dynamic Forces at Lower Planetary Gear Teeth for Excitation at Planet-Ring Gear Mesh	69
40	Comparison of Calculated and Measured Noise Levels Adjacent to the Gearbox, Cruise Condition	72
41	Planet Gear Design and Sun-Ring Excitation Phasing	80
42	Instrumentation Arrangements for Recording and Analyzing Sound and Vibration Data	89
43	Installation of Recording and Readout Equipment in Helicopter	91
44	Typical Filter Frequency Selectivity Characteristics	92
45	Microphone Locations for Sound Pressure Level Measurements	94
46	Accelerometer Locations for Vibration Measurements in the First and Second Flight Series	105
47	Location of Excitation and Accelerometers for Gearbox Housing Structural Response Measurements	116
48	Gearbox Housing With Electromagnetic Shaker and Accelerometers for Structural Response Measurements	120
49	Schematic Diagram of a Gear Rolling Fixture	125
50	Chart of Gear Tooth Errors of a Typical Gear When Run With a Master Gear on a Gear Rolling Fixture	125
51	Gear Cardiograph	127
52	Portion of a Sample Cardiogram	127

Figure		Page
53	Measurement of Runout on the Input Stage Spiral Bevel Pinion Performed by the Hofler Gear Measuring Machine ...	129
54	Measurement of Runout on the Input Stage Spiral Bevel Gear Performed by the Hofler Gear Measuring Machine	130
55	Measurement of Runout on the Lower Stage Planetary Sun Gear Performed by the Hofler Gear Measuring Machine	131
56	Measurement of Runout on the Planet Gear Performed by the Hofler Gear Measuring Machine	132
57	Measurement of Tooth Spacing on the Input Stage Spiral Bevel Gear Performed by the Hofler Gear Measuring Machine	133
58	Measurement of Profile on the Lower Stage Planetary Sun Gear Performed by the Hofler Gear Measuring Machine	134
59	Measurement of Profile on the Upper Stage Planetary Sun Gear Performed by the Hofler Gear Measuring Machine	135
60	Measurement of Profile on the Planet Gear Performed by the Hofler Gear Measuring Machine	136
61	Measurement of the Lower Stage Planetary Sun Gear on the Gear Cardiograph	137
62	Runout Measurement of the Lower Planetary Stage Sun Gear as Measured on the Hofler Gear Measuring Machine	138
63	Tooth Spacing Measurement of the Lower Planetary Stage Sun Gear as Measured on the Hofler Gear Measuring Machine	139
64	Profile Measurement of the Lower Planetary Stage Sun Gear as Measured on the Hofler Gear Measuring Machine	140
65	Portion of the Composite Gear Measurement of the Lower Stage Sun Gear as Measured on the Gear Cardiograph	141
66	External Gear Tooth Driving External Gear Tooth	153
67	External Gear Tooth Driving Internal Gear Tooth	156
68	Outline of External Gear Tooth	160
69	Outline of Internal Gear Tooth	164

Figure		Page
70	Beam Deflections in the Gear Tooth	168
71	Two Successive Pairs of Teeth in Mesh and the Division of Transferred Tooth Load	181
72	Diagram Representing Two Successive Pairs of Gear Teeth in Mesh	182
73	General Case of Distributed Mass Between Stations	226
74	General Portion of the Torsional Syster	226
75	Schematic Diagram of Planetary Gearing ·tion	232
76	Schematic Diagram of Torsional Vibration ystem for the UH-1D Drive System	241
77	Third-Octave Filter Characteristic	296
78	Curve for Calculating DB Level of Combination of DB Levels of Two Signals	297

LIST OF TABLES

Table		Page
I	Calculated Excitation Frequencies - Gear Teeth Meshing Frequencies and Their Harmonics	19
II	Calculated Excitation Frequencies - Main and Tail Rotor Rotational Frequencies and Their Harmonics	20
III	Calculated Excitation Frequencies - Miscellaneous Shaft Rotational Frequencies	21
IV	Calculated Excitation Frequencies - Ball and Roller Passing Frequencies	22
V	Comparison of Gear Excitation — Effect of Manufacturing Profile Error	57
VI	Comparison of Gear Excitation — Effect of Operating Load	60
VII	Computed Gear Excitation Components — Cruise Flight Condition	61
VIII	Computed Gear Tooth Dynamic Forces — Cruise Flight Condition	70
IX	Comparison of Gear Excitation — Effect of New Modified Profile	76
X	Comparison of Gear Excitation — Effect of Operating Load With New Modified Profile	78
XI	Comparison of Planetary Dynamic Forces — Effect of Sun-Ring Excitation Phasing	82
XII	Comparison of Planetary Dynamic Forces — Effect of Planet Support Compliance	83
XIII	Overall Sound Pressure Levels	95
XIV	Tabulated One-Third-Octave Frequency Analysis of Sound Measurements, Flight Idle Operation, Helicopter No. 66-1038	96
XV	Tabulated One-Third-Octave Frequency Analysis of Sound Measurements, Flight Idle Operation, Helicopter No. 66-1039	97

Table		Page
XVI	Tabulated One-Third-Octave Frequency Analysis of Sound Measurements, Flight Idle Operation, Helicopter No. 66-1043	98
XVII	Tabulated One-Third-Octave Frequency Analysis of Sound Measurements, Cruise Operation, Helicopter No. 66-1038	99
XVIII	Tabulated One-Third-Octave Frequency Analysis of Sound Measurements, Cruise Operation, Helicopter No. 66-1039	100
XIX	Tabulated One-Third-Octave Frequency Analysis of Sound Measurements, Cruise Operation, Helicopter No. 66-1043	101
XX	Narrow-Band Frequency Analysis of SPL Measurements for Cruise Operation, Helicopter No. 66-1038	102
XXI	Narrow-Band Frequency Analysis of SPL Measurements for Cruise Operation, Helicopter No. 66-1039	103
XXII	Narrow-Band Frequency Analysis of SPL Measurements for Cruise Operation, Helicopter No. 66-1043	104
XXIII	Vibration Levels Measured on Gearbox and Supporting Structure During Initial Series of Measurements	106
XXIV	Vibration Levels Measured on Gearbox During Final Series of Tests	108
XXV	Tabulated One-Third-Octave Frequency Analysis of Vibration Data, Helicopter No. 66-1038, Cruise Operation	109
XXVI	Tabulated One-Third-Octave Frequency Analysis of Vibration Data, Helicopter No. 66-1039, Cruise Operation	110
XXVII	Tabulated One-Third-Octave Frequency Analysis of Vibration Data, Helicopter No. 66-1043, Cruise Operation	111
XXVIII	Tabulated One-Third-Octave Frequency Analysis of Vibration Data, Helicopter No. 66-1038, Flight-Idle Operation	112

Table		Page
XXIX	Tabulated One-Third-Octave Frequency Analysis of Vibration Data, Helicopter No. 66-1039, Flight-Idle Operation	113
XXX	Tabulated One-Third-Octave Frequency Analysis of Vibration Data, Helicopter No. 66-1043, Flight-Idle Operation	114
XXXI	Measured Casing Response	117
XXXII	Measurements Made on UH-1D Transmission Gears	142
XXXIII	Dynamic Equations for Planetary Gear Stage With Equal, Synchronized Excitation Among Planets	237
XXXIV	Dynamic Equations for Single Planet of Planetary Gear Stage With Equal Excitations Among Planets of Non-Zero, Uniformly Spaced Phase Relationship	239
XXXV	Computation of Sound Pressure Levels of Gear Noise Components - Cruise Flight Condition	295
XXXVI	Combination of Gear Noise Components Simulating Third-Octave Analysis - Cruise Flight Condition	299

INTRODUCTION

Helicopter cabin noise, particularly that due to the drive gearbox, is already well recognized as one of the important problems in the present and future use of helicopters. The nature and extent of the problem are seen when present noise levels are compared to existing and proposed noise specifications. Figure 1 gives such a comparison for the UH-1D, in which cabin noise levels exceed MIL-A-8806 by as much as (Reference 1) 14 db. The excessively high levels, incidentally, occur only in the higher frequency octave bands, where the noise is associated primarily with the gearbox, in contrast with the lower frequency range, where the noise is associated with the rotors (References 1 and 2).

Another aspect of the helicopter noise problem is the continuing increase in noise levels as new helicopters are introduced with more and more power transmitted through the gearbox. This trend is demonstrated in Figure 2, which compares measured cabin noise levels of the UH-1A in 1961 with those of the UH-1D in 1967. A significant difference in the two aircraft is in the cruise horsepower, which has increased from 465 HP in the former to 680 HP in the latter. It is not unreasonable to project further power increases in the future and to expect a corresponding rise in the already excessive noise levels. Thus, the need for better methods of noise reduction in helicopters is becoming all the more urgent.

One approach to noise reduction has been the addition of sound-absorbing materials. Although potential benefits have been demonstrated, these are necessarily accompanied by significant weight penalties. As was concluded (Reference 1), "Greater efficiency in noise control can be achieved by reduction at the source," and "Such achievement will require research into several basic mechanisms of aircraft noise." Since the most objectionable cabin noise comes from the gearbox, this is the component of the aircraft that should receive attention first.

The benefits of any new method of reducing noise from helicopter gearboxes will materialize only when they are written into a technical specification and applied to new helicopter designs. This will require an overall program containing a sequence of stages of engineering study and testing. Such a program is shown in the flow chart in Figure 3. It concentrates first on the development of analytical tools which can be used to predict noise levels from design data. The study covered by this report has been devoted to accomplishing a practical and usable major portion of this first stage.

The objectives of this effort were as follows:

1. Development of an effective method of computing the noise produced in a helicopter gearbox, including:

    a. Identification of the major sources of this noise.

    b. Consideration of the influence of vibrational resonances in the overall drive system and in the gearbox casing.

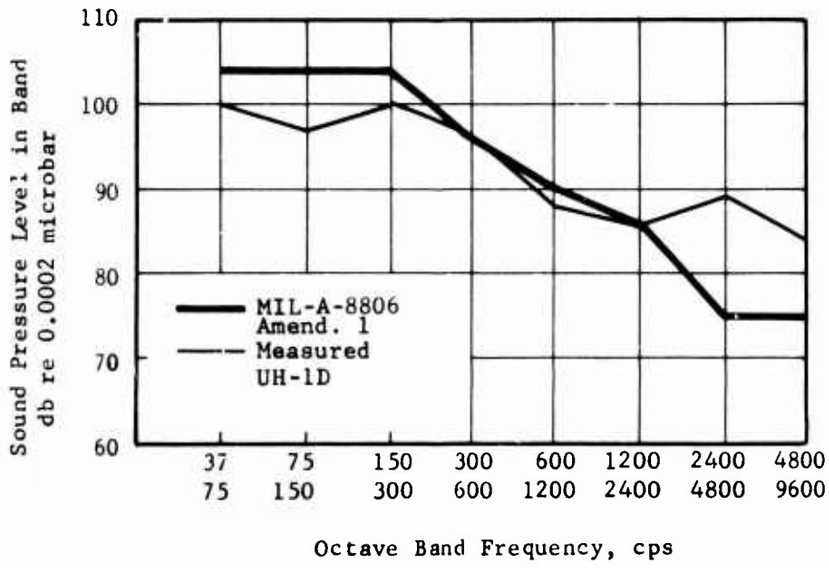

Figure 1. Comparison of Measured Noise on the UH-1D With Present and Proposed Specifications.

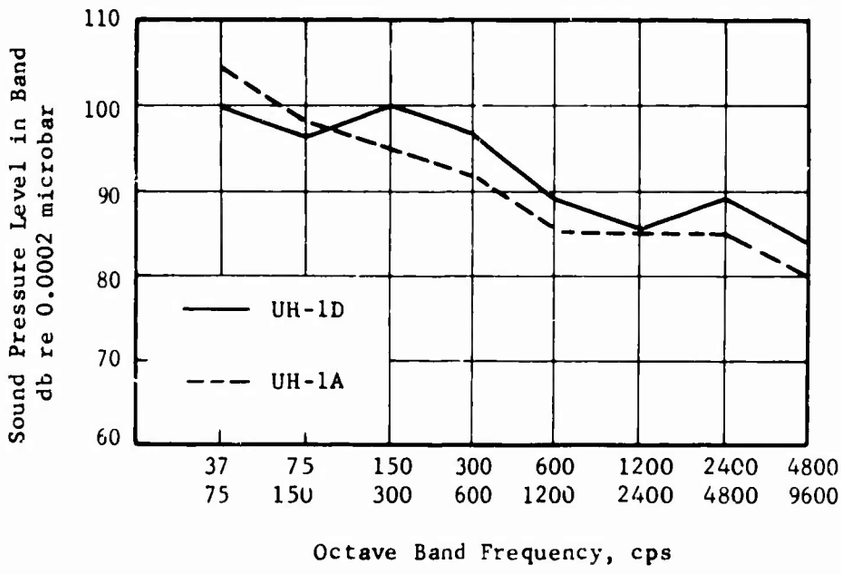

Figure 2. Comparison of Noise Levels at Normal Cruise Power on UH-1D and UH-1A.

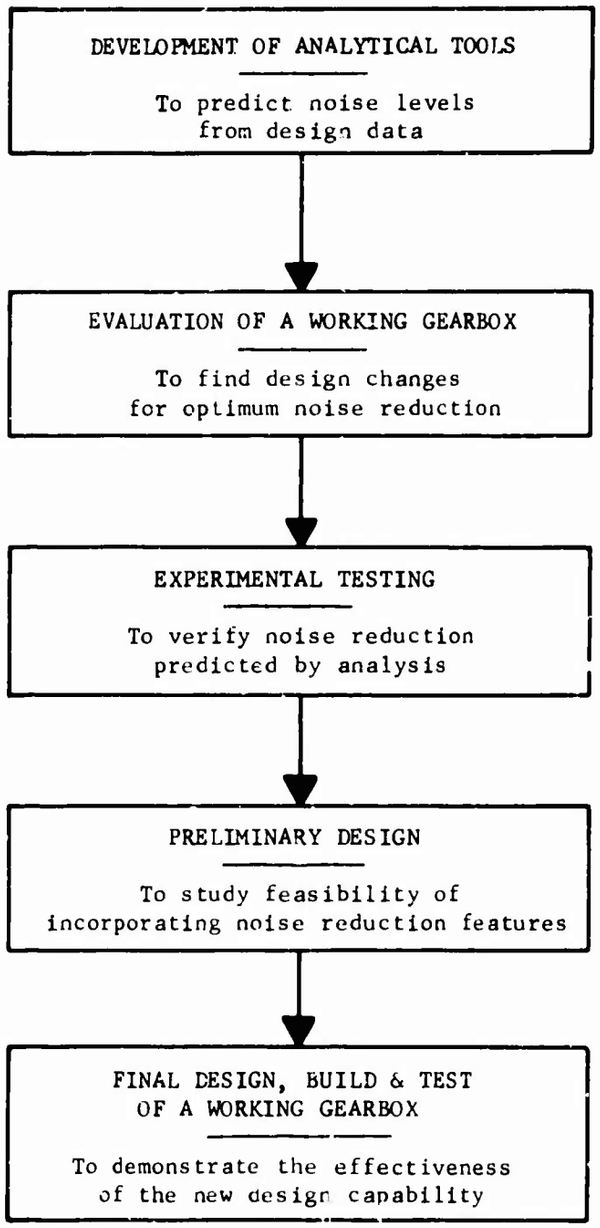

Figure 3. Overall Program for a New Method of Reducing Noise From Helicopter Gearboxes.

c. Evaluation of the mode of transmission of noise from the gearbox to the pilot's location in the cabin.

d. Preparation of a computerized noise calculation which starts with design data, operating conditions, and manufacturing imperfections.

e. Validation of the calculation method by comparison of calculated and measured results for the UH-1D helicopter.

2. Recommendation of design modifications which will reduce the amount of noise generated.

DESCRIPTION OF PROGRAM

This study of helicopter gearbox noise reduction was conducted in three tasks. The individual efforts of each task are summarized below, with more detailed descriptions and explanations reserved for the Discussion of Results and the appropriate Appendixes.

TASK I — GEAR MEASUREMENT

For this task, the Government provided two of each of the main drive gears: input stage spiral bevel pinion and gear, lower planetary stage sun gear, upper planetary sun gear, planet gear common to both planetary stages, and combined ring gear for the two planetary stages. Because working-quality gears could not be released from Government inventories, these gears were selected from rejected production parts but, insofar as possible, of representative, acceptable quality in those features which related to the measurements planned.

The types of measurements made were those judged to be most commonly used to control gear quality and most likely to relate to noise generation. They included measurement of tooth spacing errors and runout on all gears, tooth profile on all spur gears, and composite gear errors on all external spur gears. The most precise inspection equipment available was used.

TASK II — ANALYSIS

In this task, it was necessary to treat three distinct subjects. These were the excitation developed by gears and bearings, the dynamic forces that resulted, and the noise generated from the vibrating gearbox casing.

The treatment of the subject of excitation started with a review of recognized causes of gear and bearing noise. After possible gear and bearing excitation frequencies were calculated and related to frequency spectra of measured noise, the significant forms of excitation were selected and the formal analysis was undertaken. Since this analysis proved to rest heavily on gear tooth deflection, it was necessary first to research thoroughly and then to adapt suitable relationships for beam deflections of gear teeth and also for Hertian contact deflections. The gear excitation analysis was completed and then programmed for computer solution. This program was run for all the cases of the gears in the UH-1D gearbox, with a variety of loads and profiles. Besides studying standard profiles, computations were made for measured profiles with manufacturing inaccuracies and for some specially modified profiles.

The second portion of the analysis, determination of the dynamic forces resulting from the excitation, received a more direct analytical treatment. This started with the torsional vibration analysis of a multi-branched transmission system with provision for damping at its bearings. The next step was the addition of the dynamic analysis of a simple gear set with displacement excitation at the gear mesh. Finally, the analysis was extended to include the case of a planetary gearing system with displacement excitation at each gear mesh. This last addition had to be made in two

distinct parts, corresponding to two different conditions of planet excitation phasing. This total analysis was programmed for computer solution, including provision for calculating torsional inertias and stiffnesses directly from component dimensions. The program was run for the main drive system, from turbine to main rotor, in the UH-1D helicopter. This required reduction of the design data from the transmission design drawings into the format required by the program. The specific applications of the program were in calculating the gear tooth forces resulting from the excitation under cruise operating conditions. It was also used to calculate the extent to which force levels are influenced by selected conditions of changing frequency, compliance, and excitation phasing.

The final subject of the analysis, the conversion of gear excitation and dynamic forces into noise levels, started with a study of an earlier quasi-analytical method for calculating marine gearing noise. This was revised and adapted to approximate more closely the conditions of the helicopter gearbox. The new analysis was reduced to a manual calculating procedure to give a calculated noise level for each excitation frequency. Added to this procedure was a calculation which simulates the function of the frequency spectrum analyzer used to analyze measured noise and vibration data. It thereby permits the combination of the noise levels at individual frequencies into equivalent third-octave wide-band noise levels. This feature permits convenient comparison of calculated and measured results. This completed portion of the analysis was then used to calculate the noise levels for the cruise operating conditions considered in the earlier computations.

TASK III — NOISE AND VIBRATION MEASUREMENT AND ANALYSIS

A preliminary set of measurements was first made on one UH-1D helicopter at Fort Eustis. Noise levels were measured under three flight conditions and at four locations within the aircraft. During the same test flight, vibration measurements were also made at 10 locations on the gearbox housing and on the aircraft structure close to mounting points. The measurements were reduced to overall levels and to wide-band and narrow-band analyses. These preliminary measurements were reviewed to select the most significant test conditions and locations for the final set of in-flight measurements. These preliminary measurements served an additional purpose. The frequencies of the peak values in the analyzed noise measurements were compared to the exciting frequencies calculated for the gearbox components, thereby serving to identify the major sources of noise in the gearbox.

The final set of measurements was made in flight on three UH-1D helicopters at Fort Rucker. Two operating conditions were used, with three locations for the cabin noise measurements and five locations for the gearbox housing vibration measurements. These were later reduced to overall levels and to wide- and narrow-band analyses. On one helicopter, additional vibration measurements were made at 16 bulkhead locations. The results of this final series of measurements were studied to obtain information on the uniformity of noise and vibration among aircraft, the relationship between noise and gearbox housing vibrations, and the mode of

noise transmitted from gearbox to pilot's location in the cabin. The noise measurements at cruise were used to make the comparison with the noise levels calculated in Task II for the same operating condition.

In addition to the measurements made in the helicopter, gearbox casing resonances were investigated using an unpowered, assembled gearbox, complete except for the mast and rotor. Casing resonances were investigated by externally driving the casing with a vibrational force and measuring casing motion through accelerometer pickups. The driving force was applied in turn at three locations, and measurement was made at six locations.

DISCUSSION OF RESULTS

INTRODUCTION

In this program, a great many of the factors which come into play in the creation of helicopter gearbox noise and its transmittal to the cabin area and the pilot have been studied, or at least touched upon. The factors and their relationships are pictured in flow chart form in Figure 4. The first factor is the excitation inside the gearbox which sets up torsional vibration in the drive system. Depending on the response of the system, dynamic forces are developed at the gear teeth, superimposed on the steady forces transmitting power from engine to rotor. These dynamic forces act through the shafts and bearings to set up lateral vibrations in the gearbox housing, with the magnitude of vibration being influenced by any natural resonances in the housing. One result of this vibration is the transfer of vibratory motion from the large areas of the housing to the air, thus generating noise. At the same time, some of the vibration of the housing is transferred through its mounting into the aircraft structure. At this point, the direct role of the gearbox in influencing cabin noise has ceased, indicating the logical cutoff point for the area of concern of this program. Indeed, the intensive study of the program was confined to those noise factors directly related to the gearbox. However, when in-flight measurements were being made, and because of the convenience of doing so, the investigation was to a limited extent carried over to some of the factors associated with the aircraft proper. Figure 4 continues on to show these factors relating to the transmittal of noise to the pilot after it leaves the gearbox. The upper path in the chart shows, in highly simplified fashion, how the noise in the air surrounding the gearbox housing passes through the gearbox compartment bulkhead and continues through the air until it reaches the pilot. Since this mode of transmittal originated and continued with the vibration in the form of noise, or air pressure pulsations, the noise using this path is referred to as airborne noise. The lower path in the chart shows, again in highly simplified fashion, that the gearbox vibration transmitted to the structure is carried by the structure to the cabin bulkheads, where it is for the first time transformed into noise reaching the pilot. Since the structure played a pronounced role in this mode of noise transmittal, the noise at the end of the path is referred to as structure-borne noise.

The factors described above have been investigated in some portion of the three tasks making up the program. Task III, devoted to noise and vibration measurements, served to identify the sources of excitation and the mode of noise transmittal. It also described the nature of the resonances in the gearbox housing. Task II, containing the analytical treatments, provided the quantification of the major form of excitation and of the gear tooth forces that result from this excitation. It further revealed the contribution of torsional resonances in the drive system. Task I, dealing with the gear measurements, helped to identify the manufacturing imperfections that contributed directly to the major forms of excitation and to what extent.

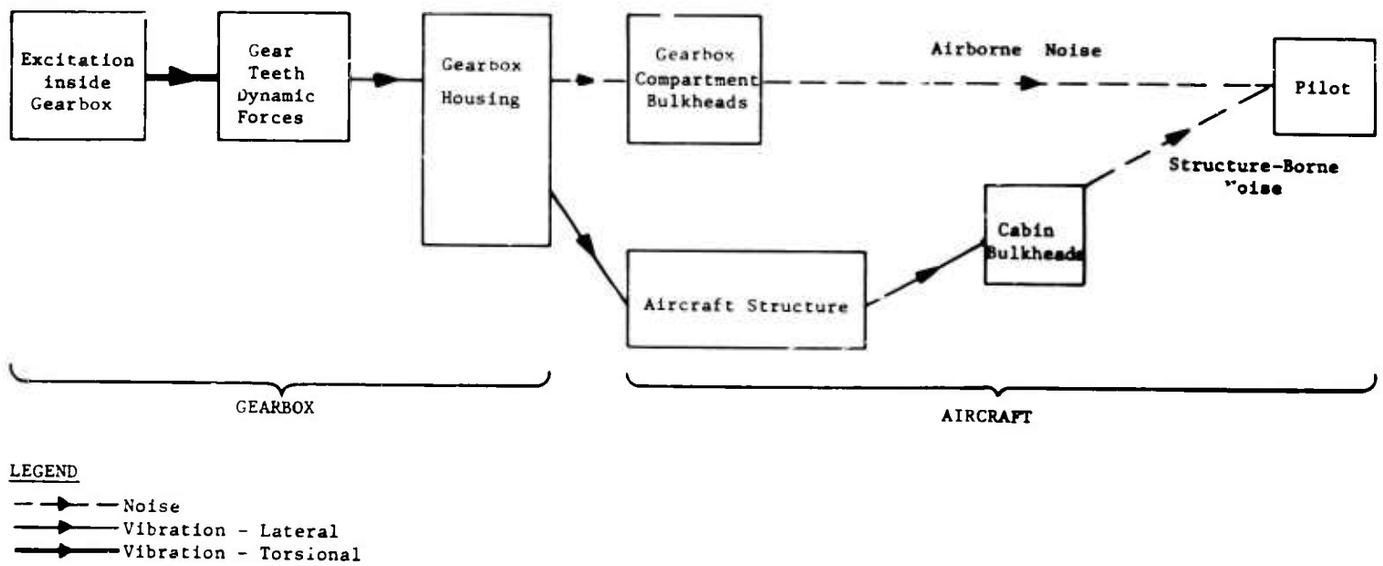

Figure 4. Factors in Helicopter Gearbox Noise.

This section of the report, following the sequence just given, will describe how each of these factors has been investigated in the program, will give some representative results, and will discuss their interpretation leading to the conclusions. The comprehensive data collected, the instrumentation and methods used, and the derivation and justification of the analyses have been reserved for the various appendixes.

NOISE MEASUREMENTS

The noise measurements made on three helicopters during cruise operation are presented in Figures 5, 6, and 7. The cabin locations referred to in these figures are identified in Figure 8.

Before an analysis of these results is undertaken, it may be useful to review briefly some of the pertinent basic information about complex sound and its measurement. More detailed information may be found in Reference 3.

Typical noise, such as that measured in the helicopter, may be considered a blend of two kinds of sounds. In one, the sound is distributed essentially continuously in frequency (meaning that all frequencies are present) and is fairly constant in sound pressure level over a wide frequency range. This kind of sound is often referred to as "white noise". The other kind consists of discrete frequencies (meaning a limited number of isolated frequencies), which are greater in sound pressure level than the "white noise" of adjacent frequencies. Instrumentation used to measure sound cannot measure the sound pressure level of each individual frequency; instead, by using the adjustable band-pass filters, it measures the combined effect of all the frequencies within each selected band. Because the filters cannot be made with perfectly sharp cutoff limits, an actual measurement combines also part of the effect of frequencies in adjoining bands. The bandwidth is referred to as a "narrow band" if its width is small, perhaps one-thirtieth of an octave. The term "wide band" is used for bandwidths of one-third, one-half, and full octave. If the instrument measures the entire sound frequency range as one band, the measurement is an "overall" sound pressure level. The indication of the sound pressure level instrument is not based on a linear measure; instead, the unit used is the decibel (db), which is based on a logarithmic scale. The sound pressure is indicated as proportional to the logarithim of its ratio to a very small standard pressure. The significance of the decibel is such that a sound having 10 times the pressure level of another will be indicated as measuring 20 db higher.

The selection of the bandwidth depends on the purpose for which the measurements are to be used. A narrow-band plot is useful to pinpoint the exact values of the discrete frequencies, especially when these are crowded close together. The full octave bandwidth, on the contrary, obscures the individual frequency values and instead shows the manner in which the general noise level varies over the full frequency range. Figures 1 and 2 are of this type. The third-octave bandwidth, used in Figures 5, 6, and 7, and most other figures in this report, performs the combined function of calling attention to the location of the discrete

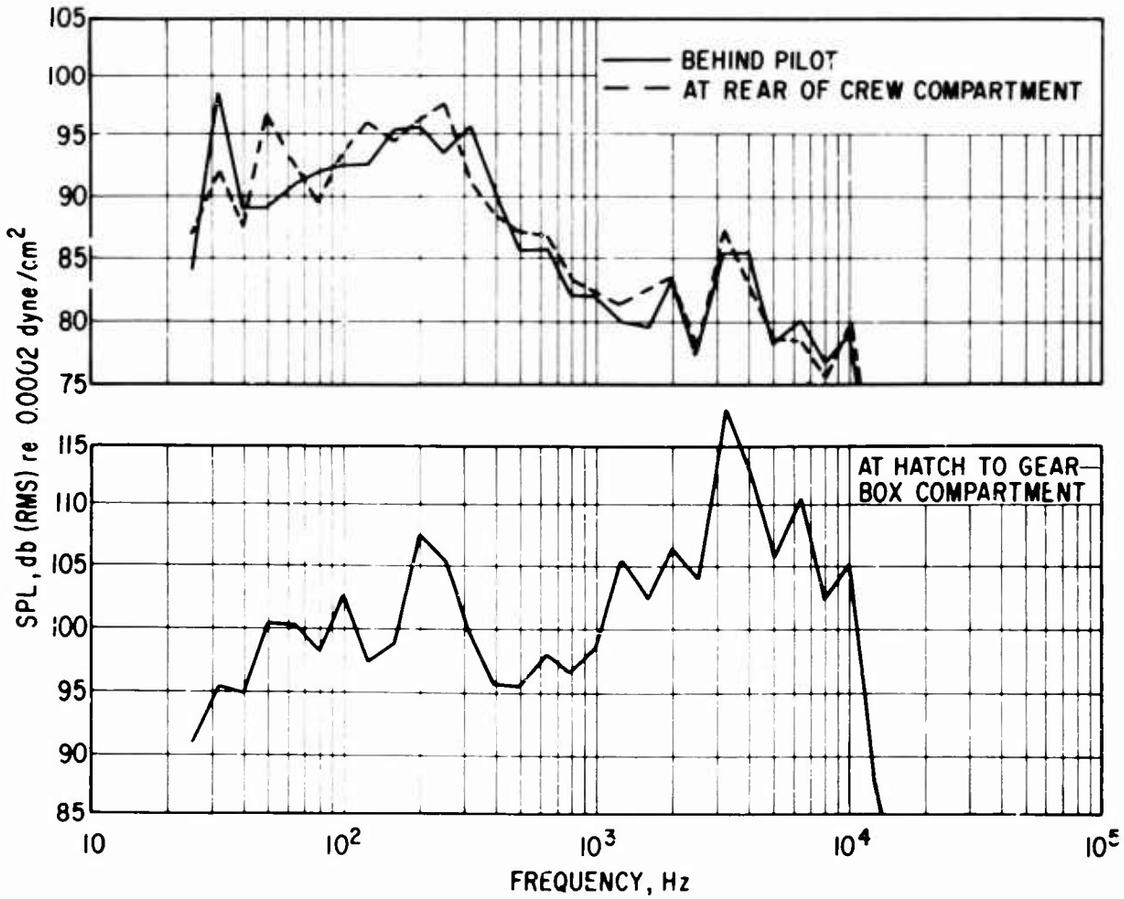

Figure 5. Noise Measurements in Third-Octave Bands, Helicopter No. 66-1038, Cruise Operation.

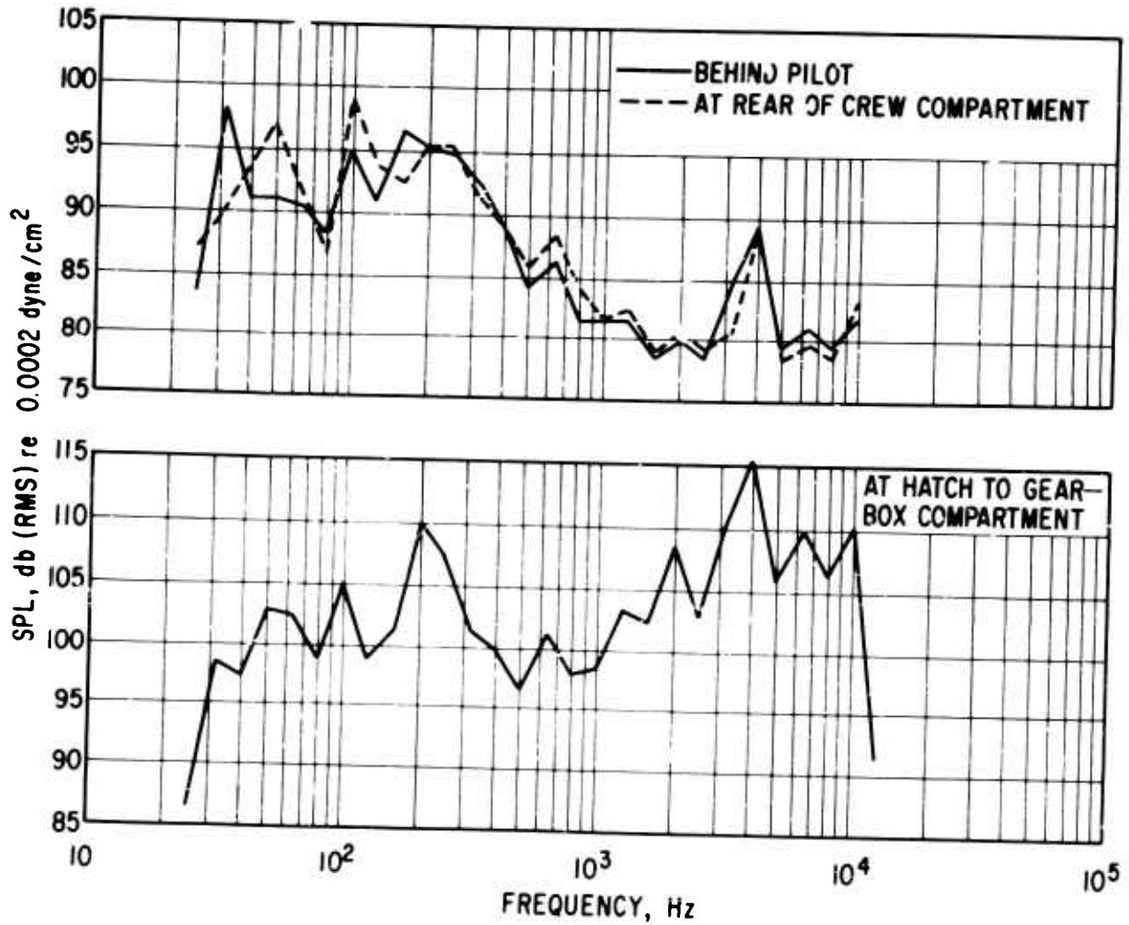

Figure 6. Noise Measurements in Third-Octave Bands, Helicopter No. 66-1039, Cruise Operation.

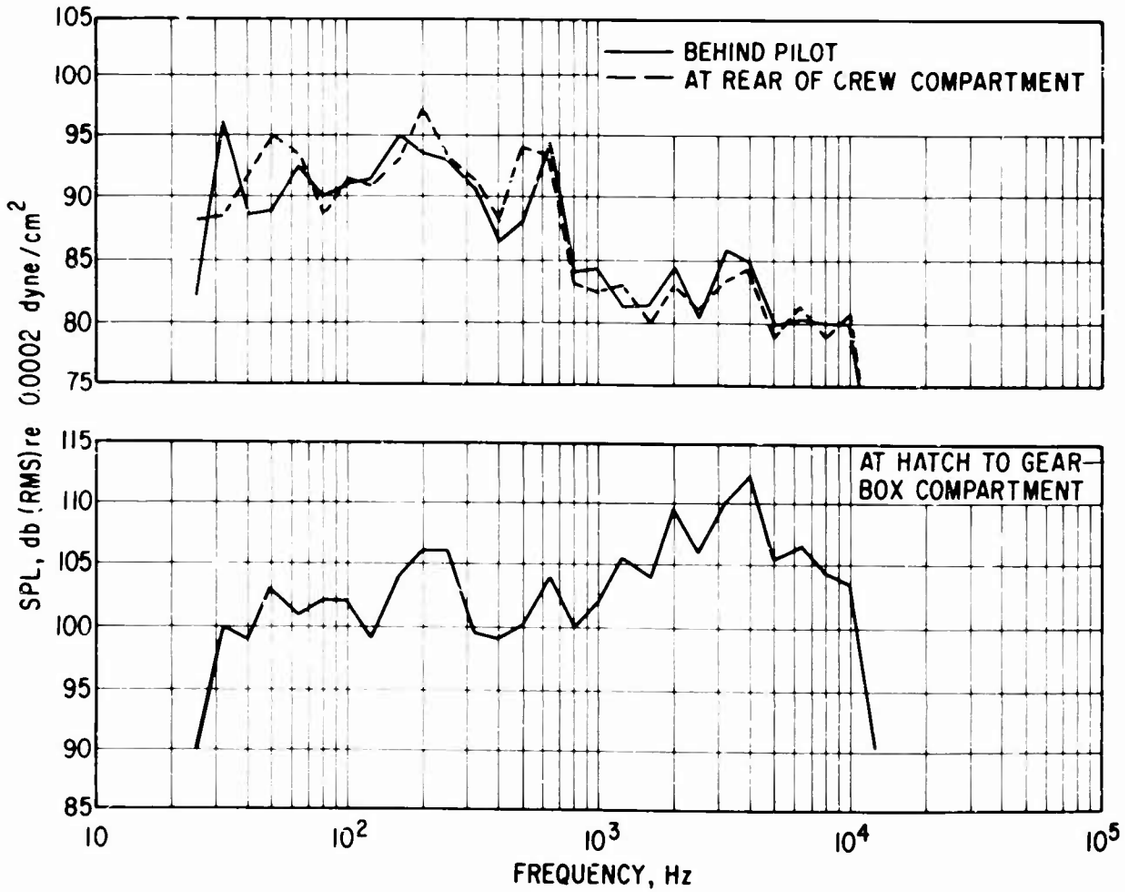

Figure 7. Noise Measurements in Third-Octave Bands, Helicopter No. 66-1043, Cruise Operation.

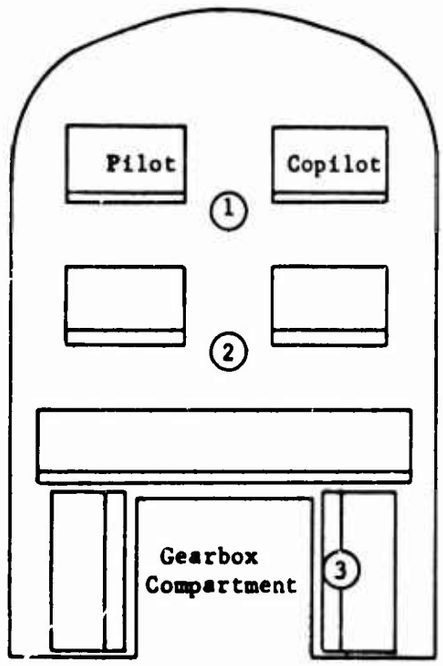

(1) Behind pilot
(2) At rear of crew compartment
(3) At hatch to gearbox compartment

Figure 8. Microphone Locations for Sound Pressure Level Measurements on Three Helicopters.

frequency components of the noise and, in a special way to be explained later, of conveying the general level as it varies across the entire frequency range.

In these plots, a series of straight lines connect points whose frequency values are at the "mid-points" of the bands. The purpose of the line segments is merely to convey the association of the points. Unlike conventional plotted curves, intermediate points on the line segments have no significance.

Interpretation of these third-octave band curves is based on the locations and heights of the peak values. These peak values generally signify that one or more discrete frequency noise components are present within the particular band of frequencies. While the height of the peak represents the combined effect of all frequency noise components in the band, because of the nonlinear manner in which the combination takes place, the one or two dominant discrete frequency components generally determine the value of the peak. For example, adding a second discrete frequency component to one of the same magnitude will raise the peak by only 3 db. If the second component is 5 db smaller than the first, when the two combine, the increase over the first component alone will be only 1 db. Hence, to get a general picture of how the curve would look if it were plotted with a wider bandwidth in place of third-octave, it is necessary only to imagine a line almost "skimming" the peaks. Furthermore, any overall noise level would be almost completely determined by any one portion of the noise spectrum which is higher than the rest. For example, in Figure 2 the overall level for each of the curves would be determined by the higher levels shown in the low-frequency end of the frequency spectrum with practically no influence from the lower levels at the high-frequency end.

With this explanation in mind, it will be recognized that the "valleys" appearing between peaks in the third-octave band plots are of little significance. The value read out by the instrumentation consists of a combination of the continuous-frequency "white noise" and low-level discrete frequency components within the particular band and, in addition, a portion of the high-level discrete frequency components in the adjacent band, especially those whose frequencies are just beyond the particular band limits. As mentioned earlier, these "outside" contributions result from the inadequately sharp cutoff capabilities of the band-pass filters. Very often, if the high peaks in the adjacent bands are reduced, the values of the valleys would also drop accordingly.

Returning to Figures 5, 6, and 7, some conclusions may now be drawn. First, there is a high degree of similarity in both levels and curve shape for the three aircraft. This may be recognized more easily in Figure 9, in which the measurements at the gearbox compartment are shown in superimposed curves. The frequency bands with the peak or near-peak values are remarkably consistent for the three curves. In addition, the sound pressure levels show remarkable consistency, with differences between curves at any one band rarely exceeding 5 db. This absence of large, random variation among aircraft reinforces the concept that a reliable, analytical method for computing noise levels can be developed.

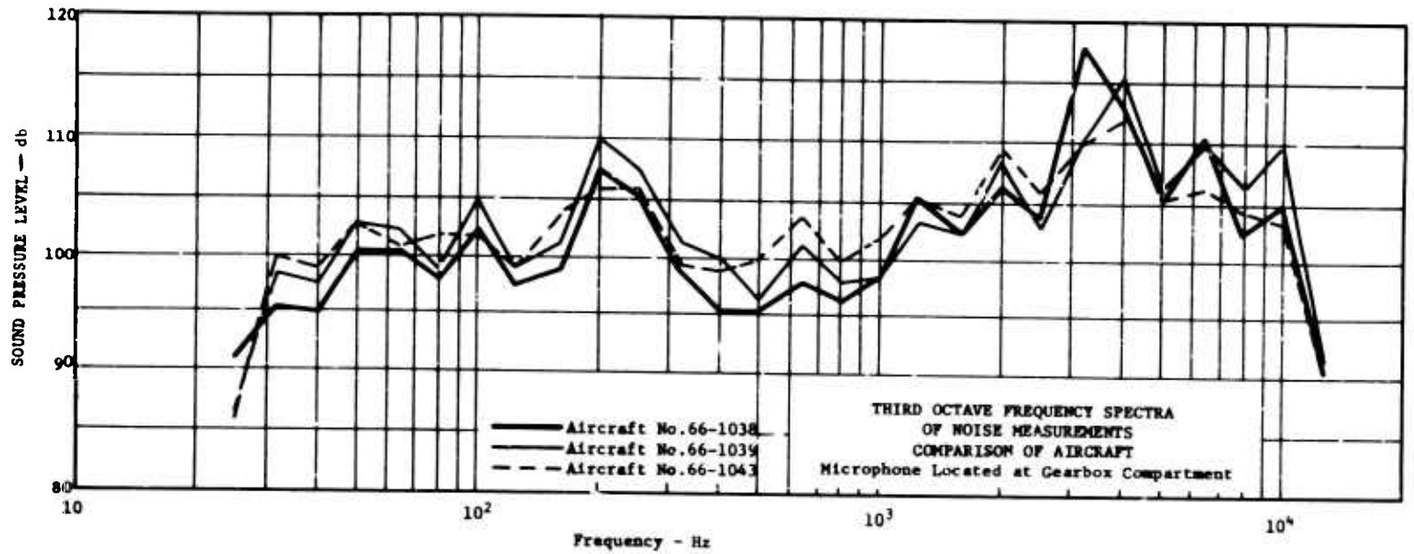

Figure 9. Comparative Noise Levels Among Three Helicopters, Measured at Gearbox Compartment.

The influence of microphone location may be considered by again referring to Figures 5, 6, and 7. One noteworthy item is the similarity over a broad range of frequencies between the measurements at the rear of the crew compartment to those behind the pilot, for each of the three helicopters. The range of closest similarity is that above 600 Hz. As mentioned in the Introduction and as will be demonstrated later, this range is the one particularly related to the gearbox. Another item of interest in these figures is the major difference between the measurements taken at the gearbox compartment and those in the cabin proper. This difference takes the form of contrasting general shapes of the curves, with one showing generally lower sound levels as frequency increases and with the other showing the opposite relationship. The difference also shows up in the absolute sound level reached, especially at the high-frequency end. Less obvious, but also significant, is the one similarity among all the curves, that they peak almost always in the same frequency band. These differences and similarities can be examined more effectively if two of the widely differing curves are plotted superimposed on one set of coordinates. This has been done for the "behind pilot" and "at gearbox compartment" readings taken on one of the helicopters, No. 66-1038, with the results shown in Figure 10. This comparison reveals that the relationship between the two curves is different in the frequency range below about 500 Hz from what it is in the range about 500 Hz. In the lower range, the two curves are closer but the locations of individual peaks are not very similar. In the upper range, on the other hand, the curves are widely separated but the peaks show identical locations on the frequency scale. This differing relationship between the curves in the two frequency ranges suggests significant differences in the sources and modes of transmittal of their individual noise components.

Before proceeding further with the analysis of these noise measurements, it is possible to narrow the problem down to only one of the two frequency ranges. Figure 1 shows the measurements for the "behind pilot" location replotted on a full-octave band frequency scale in comparison to the maximum noise level limits of MIL-A-8806. The measured noise levels exceed the specification limits but only in the higher portion of the overall frequency range. Further discussion will therefore emphasize the higher frequency noise components, and only occasional reference will be made to the lower frequency range.

The sources of the discrete frequency noise components which create the noise peaks may be traced through comparison to the calculated frequencies of all possible excitations connected with the drive system. These calculated frequencies, based on in-flight transmission input speed of 6600 rpm, are given in Tables I through IV. In each table, each individual frequency is associated with the third-octave band in which it falls. If the frequency is close to the value dividing two adjacent bands, it is located between the two, indicating that its effect on measurements will be about equal in the two bands. Table I is of particular interest because the frequencies that it contains lie in the upper portion of the overall frequency range. The first three columns of listed frequencies are for the main rotor drive gearing stations in the transmission. A schematic diagram of these stations is given in Figure 11. Matching the values

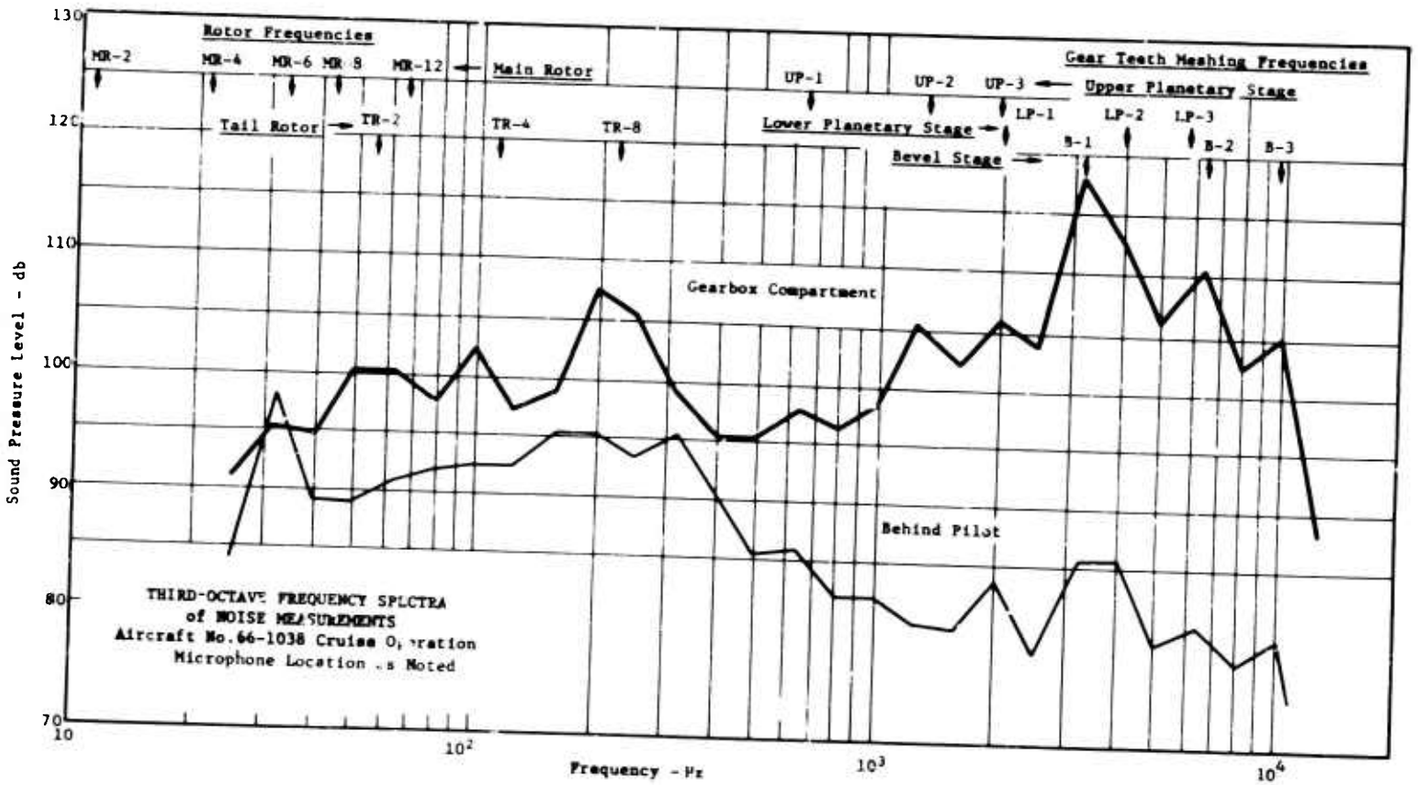

Figure 10. Noise Levels for Two Microphone Locations, Helicopter No. 66-1038, Cruise Operation.

TABLE I. CALCULATED EXCITATION FREQUENCIES - GEAR TEETH MESHING FREQUENCIES AND THEIR HARMONICS*

Third-Octave Band Midpoints Hz	Transmission Main Rotor Drive			Transmission Tail Rotor Drive		Turbine Reduction	Turbine Coupling
	Upper Stage Planetary Hz	Lower Stage Planetary Hz	Bevel Set Hz	Takeoff Spur Hz	Drive Bevel Hz	Secondary Stage Hz	Transmission Input Hz
500							
640	644						
800							
1000							
1250	1288(2)						
1600							
2000	1932(3)	1982			1860		
2500	2576(4)						
3200			3190	2830			
4000		3964(2)			3720(2)		
5000							
6400		5946(3)	6380(2)	5660(2)	5590(3)	5940	6600
8000		7928(4)		8490(3)	7440(4)		
10000			9570(3)				
12500			12760(4)	11320(4)		12880(2)	13200(2)

*Figures in parentheses show order of harmonic.

TABLE II. CALCULATED EXCITATION FREQUENCIES - MAIN AND TAIL ROTOR ROTATIONAL FREQUENCIES AND THEIR HARMONICS*

Third Octave Band Midpoints, Hz	Main Rotor Hz	Tail Rotor Hz
10	11 (2)	
12.5		
16		
20	21 (4)	
25		28
32	33 (6)	
40	43 (8)	
50	54 (10)	55 (2)
63	65 (12)	
80		
100		110 (4)
125		
160		165 (6)
200		220 (8)
250		275 (10)
320		330 (12)

*Figures in parentheses show order of harmonics. Each rotor has two blades; hence, even-numbered harmonics are blade-passing frequencies.

TABLE III. CALCULATED EXCITATION FREQUENCIES - MISCELLANEOUS SHAFT ROTATIONAL FREQUENCIES

Third-Octave Band Midpoints Hz	Transmission Shafts Main Rotor Drive			Transmission Shafts Tail Rotor Drive		Power Turbine
	Inter-planetary Hz	Quill Hz	Input Hz	Takeoff Hz	Drive Hz	Shaft Hz
16	17					
20						
25						
32						
40						
50		52				
63				69		
80					72	
100						
125			110			
160						
200						
250						
320						
400						353

TABLE IV. CALCULATED EXCITATION FREQUENCIES - BALL AND ROLLER PASSING FREQUENCIES*

Third-Octave Band Midpoints Hz	Mast		Quill		Input		Planets	
	Upper Brg. (Ball) Hz	Lower Brg. (Roller) Hz	Upper Brg. (Ball) Hz	Lower Brg. (Roller) Hz	Outer Brg. (Ball) Hz	Inner Brg. (Roller) Hz	Upper Planetary (Roller) Hz	Lower Planetary (Roller) Hz
50	48							
63	60	69					64	
80		83						
100							94	
125								
160								
200			197					198
250			238	245 290				
320								294
640					661	688		
300								
1000					1022	960		

*The two frequencies given for each bearing correspond to excitation frequencies which would be generated by loaded balls or rollers passing over a defect in the outer and inner bearing races.

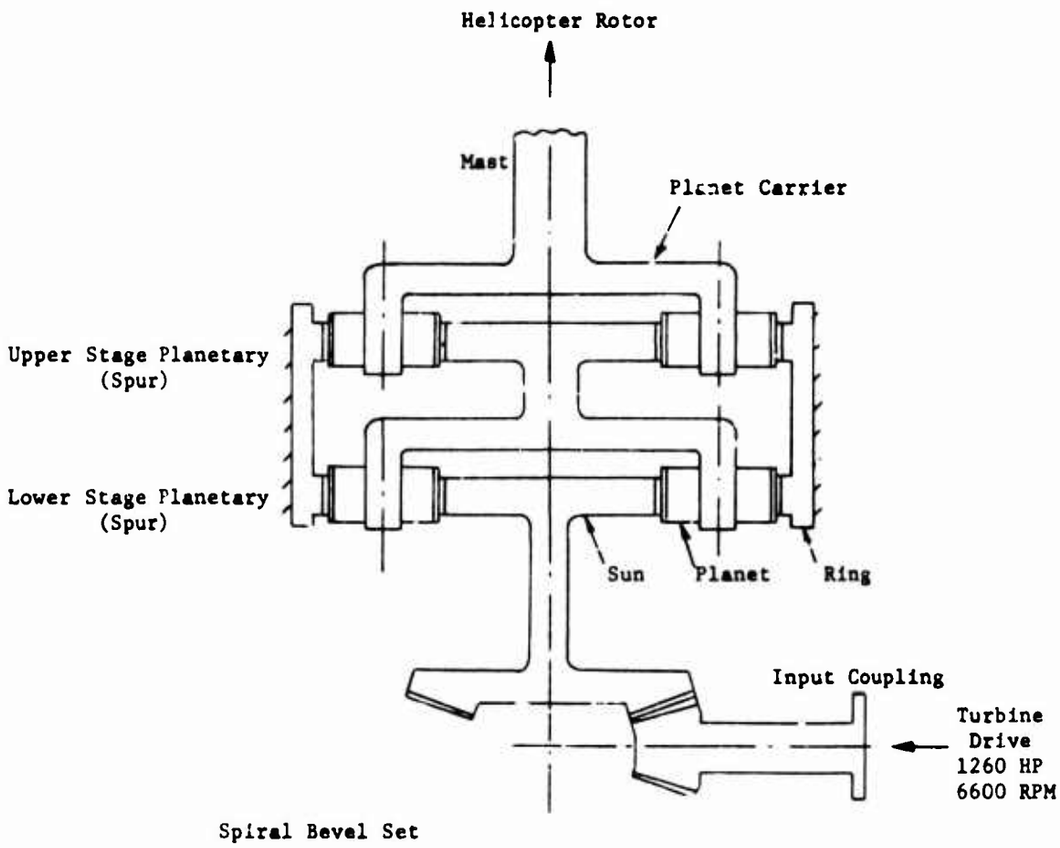

Figure 11. Schematic Diagram of Main Rotor Drive Gearing Stations in the UH-1D Helicopter Transmission.

in the table to the peak noise level frequencies in Figure 10 reveals a clear relationship between the frequencies for all three gearing stations, from the fundamental frequency up to the third harmonic. The fourth harmonic for all three stations, however, corresponds with a "valley" in the noise plot. The exciting frequencies are indicated in the upper right of Figure 10. This correspondence is shown even more emphatically when the calculated frequencies are compared to the peak values in the narrow-band analysis, as shown in Figure 12. The narrow-band analysis, to some extent, helps to distinguish the effects of two exciting frequencies which are close enough to each other to be within the same third-octave band. The upper planetary third harmonic exciting frequency falls so close to the fundamental of the lower planetary that even the narrow-band analysis cannot separate their effects. On the other hand, the second harmonic of the bevel set exciting frequencies is sufficiently removed from the third harmonic of the lower planetary that, in Figure 12, it is seen as not contributing significantly to the noise level peak in the 6400 Hz third-octave band.

The other frequencies listed in Table I may also be compared to the peak noise level frequencies in Figures 10 and 12. The transmission gears that are part of the tail rotor drive do not appear to make any significant contribution to the noise peaks, most likely because of the relatively small power they transmit. The fundamental frequency from the second stage of the turbine reduction gears is almost identical to the third harmonic from the lower stage planetary of the main transmission; hence, it is impossible to evaluate its contribution. The last column in Table I shows the tooth meshing frequencies in the coupling connecting the turbine to the transmission. Although these teeth are not gear teeth in the strict sense, their meshing action is somewhat similar. In any case, comparison of the calculated frequencies shows no significant role in the gearbox noise.

The frequencies shown in Table II are derived from the rotation of the main and tail rotors. Since each of these rotors has two blades, the even-numbered harmonics given in the table correspond to blade passing frequencies. Some of these frequencies have been indicated in Figure 10, where they appear to identify the rotors as major sources of the noise in the lower frequency range. A similar identification was made in a Bell Helicopter Company noise study on the UH-1A (Reference 2).

Miscellaneous shaft rotational frequencies are given in Table III. Excitations of these frequencies could arise from eccentricities of shafts, gears, or bearing races. Any gear manufacturing error which introduces a variation from tooth to tooth in an irregular pattern is likely to excite a fundamental frequency equal to the rotational frequency, and also its higher harmonics. Since the frequencies listed in Table II are confined to the lower frequency range, and in any case do not correspond in a clear-cut fashion to individual peaks in Figure 10, these possible sources of excitation may be discounted as major contributions to the gearbox noise problem.

The part played by the ball and roller bearings as sources of excitation

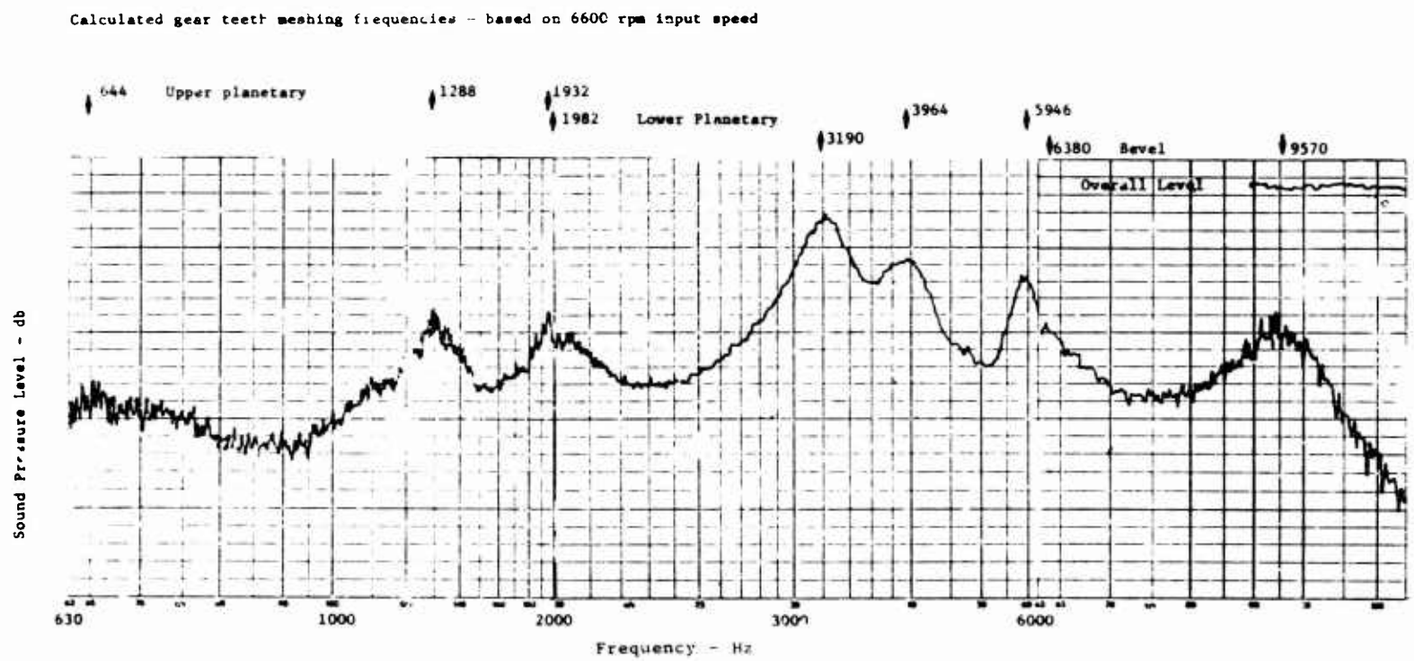

Figure 12. Portion of Narrow-Band Sound Pressure Level Frequency Spectrum, Measured at Hatch to Gearbox Compartment, Cruise Operation, Helicopter No. 66-1038, With Calculated Gear Teeth Meshing Frequencies.

may also be derived from the noise measurements. It is necessary, first, to recognize the special character of rolling-element bearing noise. "While bearing sound is not composed purely of superimposed continuous tones, it can, in most cases, be analyzed as such. It consists principally of repeated sets of impacts and rapidly induced vibrations followed by decaying transients, all intermingled." (Reference 4) The basically continuous-frequency character of this noise will therefore not show up as discrete-frequency peaks in the noise measurement plots. Instead, the ball and roller bearings may be regarded as major contributives to "white noise" throughout the entire frequency range. This "white noise" plays a secondary role in producing objectionable noise. This is true especially in the upper frequency range, where the excessive noise levels are to be found. In this frequency range, the higher peaks stand out at much higher sound levels than the valleys, and it is the valleys which reflect the "white noise" in combination with other influences.

The one exception to the continuous-frequency character of the rolling-element bearing would arise in the presence of race defects over which loaded balls or rollers were passing. The excitation frequencies associated with such conditions have been calculated and listed in Table IV. Except for the input shaft bearings, these frequencies lie in the lower frequency range, and even these show no clear-cut relationship to the peak-value frequencies. In the case of the two sets of higher frequencies, the frequencies for the outer races fall close to the peak attributed to the upper planetary gear teeth meshing excitation. Since this peak itself is so low, it is unlikely that the two bearings make any significant contribution. The frequencies for the two inner races of these bearings likewise fail to correspond to any major noise components.

The relationship between the noise measurements at the two microphone positions, as plotted in Figure 10, reveals something about the mode of transmittal of the noise from the gearbox to the pilot's location in the cabin. The spacing between the two curves at each frequency is a measure of the attenuation, or reduction, of sound level experienced by the noise component of that particular frequency. If the noise is structure-borne from gearbox to helicopter cabin, the attenuation is likely to vary with frequency because resonances in the structure tend to influence the transmittal of vibration. On the other hand, airborne noise is more likely to be independent of frequency. To facilitate examination of the attenuation characteristics contained in Figure 10, the differences between its two curves have been replotted in Figure 13. The point-by-point plot is accompanied by straight lines showing averaged values over broader ranges of frequency. This figure emphasizes the basic difference between the noise components at the lower ends, and the higher ends, of the overall frequency range, showing also an intermediate transition range. Most significant is the nearly constant attenuation, deviating 5 db or less, from a mean of 27.5 db, in the frequency range over 1000 Hz. This significance is based on the premise that structure-borne noise is more likely than airborne noise to reflect resonances, which would appear as major variations in attenuation with changing frequency. The absence of such variations in the frequency range covering the major gearbox noise components, suggests that a large part of the gearbox noise reaching the pilot is airborne.

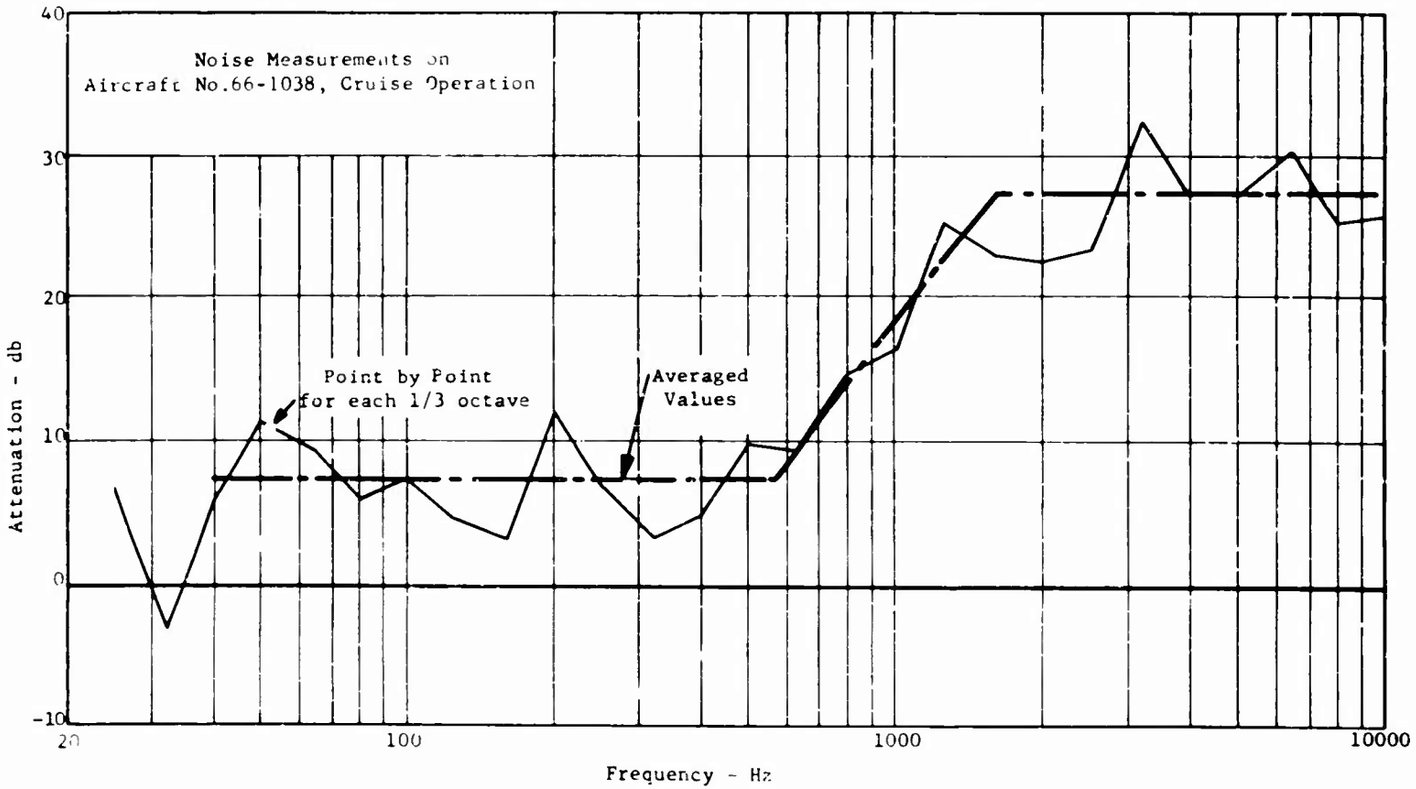

Figure 13. Noise Attenuation From Gearbox Compartment to Location Behind Pilot.

GEARBOX VIBRATION MEASUREMENT

Some typical in-flight measurements of gearbox vibration are shown in Figures 14 and 15, with the locations identified in Figure 16. These plots are on the same third-octave band frequency scale as was used with the noise measurements, and are subject to the same interpretation as to the significance of peaks and valleys. The vertical scale gives the vibration in terms of velocities, to which the initial acceleration measurements were converted. Since the pressure levels of sound are directly proportional to the velocities of the vibrating surfaces that produce them, vibration measurements in the form of velocities will most easily permit comparison with sound measurements. The velocity scale used is also similar to that of the sound pressure level, in that measurements are given in the same logarithmic or db scale. In the case of the velocity measurements, however, the db levels are calculated in relation to an arbitrary reference: the velocity which is equivalent to 1 g acceleration at 1000 Hz is taken as 85 db. Therefore, there is no direct relationship between individual db levels in noise and vibration velocity plots; however, differences in db levels in one plot are directly equivalent to differences in the second.

Identification of the gear teeth meshing frequencies shown in the noise plots has also been added to the vibration plots. Again, there is a close relationship between these frequencies and the frequencies of the vibration peaks. It is interesting to note that, although the fundamental bevel set meshing frequency does not appear as a peak in the ring gear housing vibration curve, it does appear in both base vibration curves. One peak not associated with any gear teeth meshing frequency is to be found in the upper frequency range of most of these vibration measurements. This peak is at 1000 Hz and is present in all the curves except that of the ring gear housing. It also appears in the "behind pilot" noise measurements but not in the "gearbox compartment" noise measurements. See Figures 5, 6, and 7. A possible explanation for this peak is that its source is external to the gearbox and that it is being transmitted into the gearbox base from the aircraft structure by the lift link.

No thorough analysis has been made of the vibration curves in the lower frequency range. However, it is interesting to note that two of the most prominent peaks in each of the vibration curves coincide with the frequencies of 43 and 67 Hz, at which the planets in the upper and lower stages, respectively, pass any point in the ring gear. These, then, are the frequencies at which the somewhat flexible ring gear is forced to pulsate under the moving planet gear steady loads. It is also worth noting that, although these peaks are dominant in the vibration curves, they hardly appear, if at all, in the noise measurements. Quite possibly, the low frequency of these ring gear vibrations contributes to their almost complete attenuation.

In the range of gear teeth meshing frequencies, it is possible to go somewhat further in relating the vibration measurements to the noise measurements than by simply pointing out the matching relationship of peaks to excitation frequencies. Not only the frequencies but also the levels

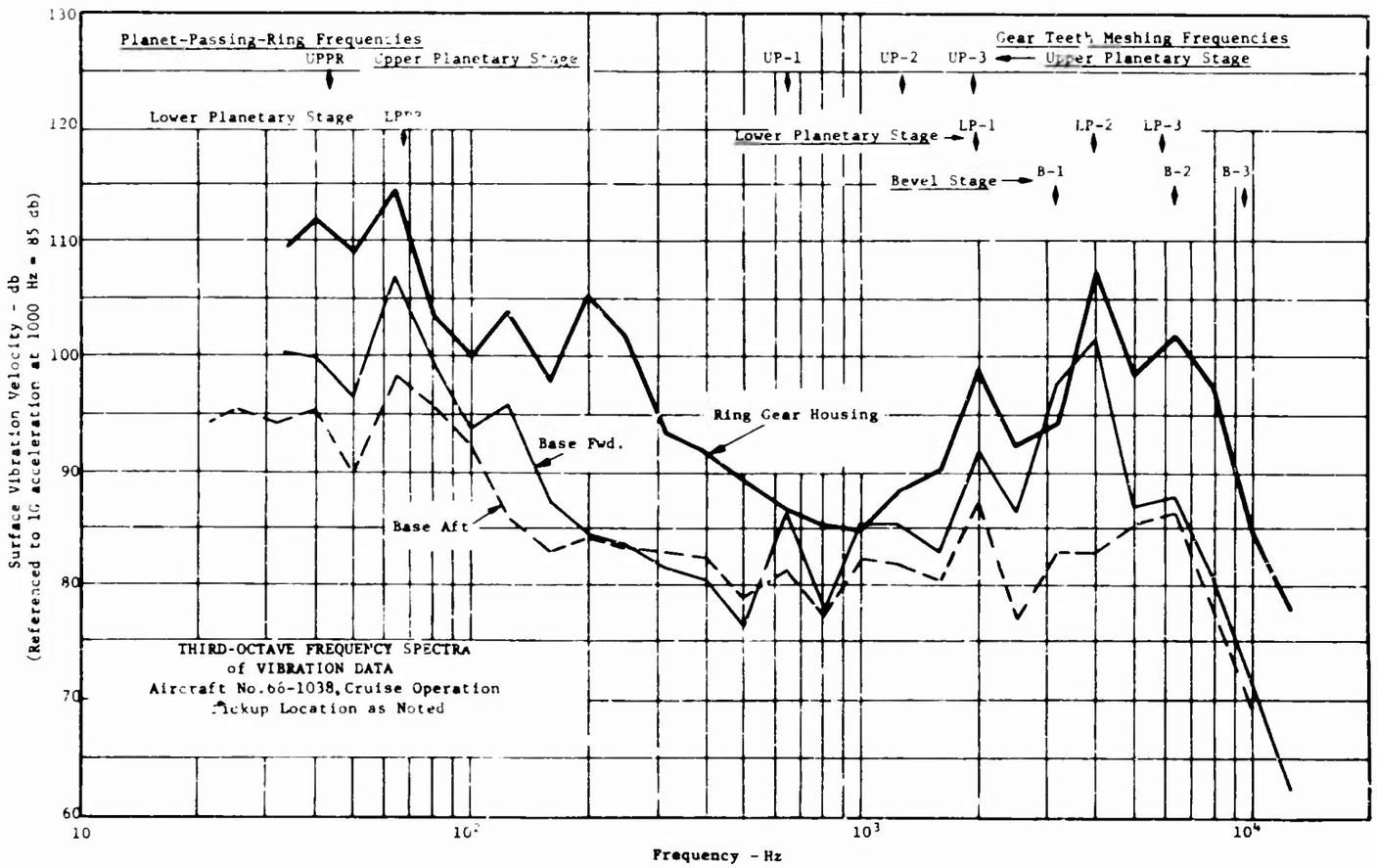

Figure 14. Surface Vibration Velocity Measurements at Three Locations on Gearbox Housing, Helicopter No. 66-1038, Cruise Operation.

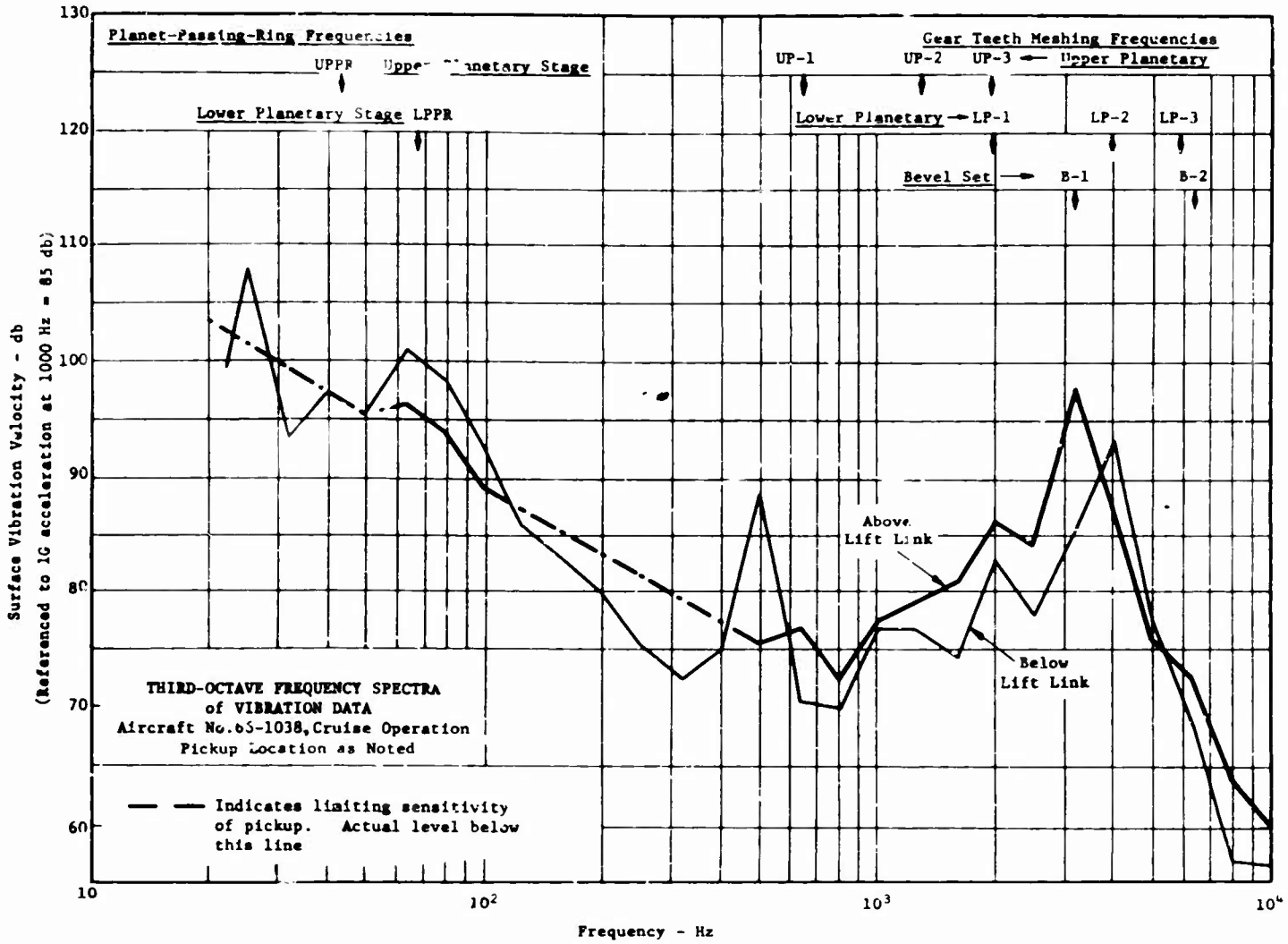

Figure 15. Surface Vibration Velocity Measurements at Locations Above and Below Lift Link, Helicopter No. 66-1038, Cruise Operation.

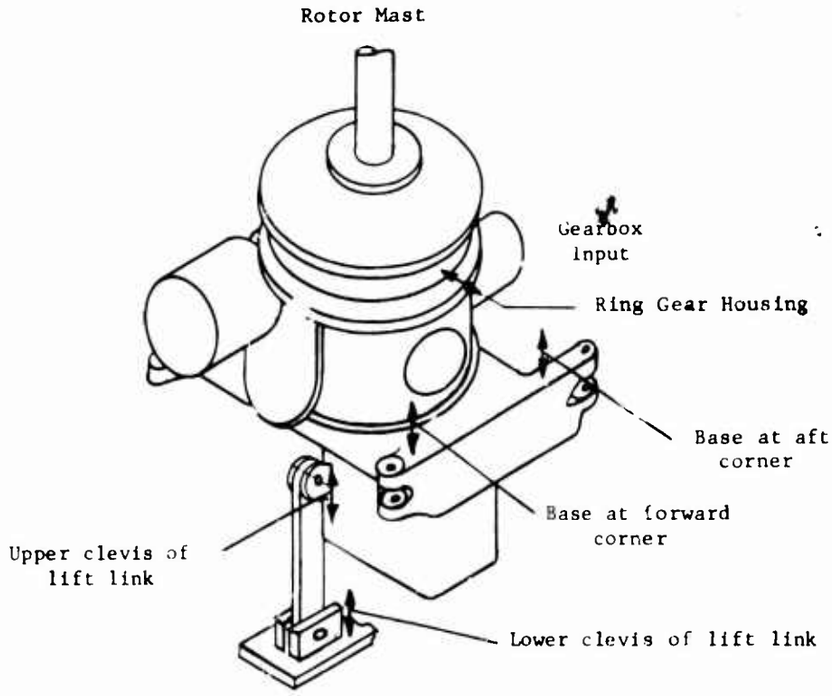

(a) Entire gearbox with lift link.

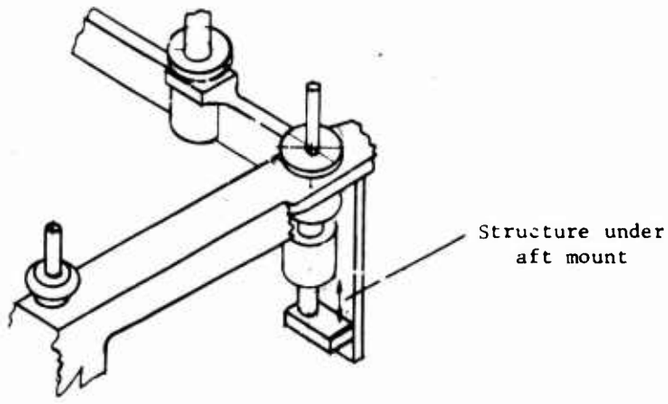

(b) Enlarged detail of aircraft structure showing corner mount and damper.

Figure 16. Accelerometer Locations for Some of the In-Flight Vibration Measurements.

associated with each of the peaks have a general similarity when the two kinds of measurements are compared, especially when the vibration measurements of the base are used. This is demonstrated in Figure 17, in which the noise measurements were taken from the upper curve in Figure 10 and the vibration measurements were taken as a composite of the velocities of the forward and aft portions of the housing base. Note that the offset of one curve from the other has no significance, in that it results from the arbitrary selection of the reference values in the db scales. The peaks in the vibration plot fail to follow those in the noise plot only at two frequencies. The vibration curve shows a superfluous peak at 1000 Hz and fails to have a peak at 10,000 Hz. A possible explanation for the former peak was offered earlier, but no explanation for the latter is apparent.

Now that the relationship between gearbox vibration and noise has been established, it is possible again to consider in what manner and to what extent this vibration might be transmitted into the aircraft structure. The measurements shown in Figure 15 show very similar vibration at both ends of the lift link, indicating that only overall attenuation has been effected by the lift link or its fasteners. A similar set of vibration measurements was made on both sides of one of the [illegible]x mounts on one of the other helicopters tested. The positions of the two accelerometers were the "base at aft corner" in Figure 16(a) and the "structure under after mount" in Figure 16(b). The attenuation across the mount, that is, the difference between the two measurements, has been plotted in Figure 18 along with th attenuation across the lift link, for the above 500 Hz portion of the frequency range. The plot shows that, while the lift link transmits vibration from gearbox to the aircraft structure with only little loss, the corner mounts are highly effective in isolating the gearbox, at least in the gear noise frequency range.

The relationships shown in Figures 17 and 18 lead to an observation on the mode of transmittal of noise from the gearbox to the cabin. Since the spectrum of noise levels at the gearbox compartment corresponds so closely to the spectrum of gearbox base vibrations, the casing vibrations may well be the direct source of the radiating noise. Since so little of the base vibrations are transmitted directly through the corner mounts into the aircraft structure and since even the lift link offers some overall attenuation, the structural path of noise transmittal may be of reduced signifiance. In this way, the observed relationships lend support to the suggestion made earlier that a large part of the gearbox noise reaching the pilot is airborne.

CABIN SURFACE VIBRATION MEASUREMENTS

These measurements were included as a possible source of additional information on the mode of noise transmittal into the cabin area. Practical considerations limited the measurements to overall levels of acceleration. These measurements and their locations in the cabin are shown in Figure 19.

Before any analysis of these measurements is attempted, the limitations of overall levels as a source of information must be considered. As explained earlier in connection with noise level measurements, the overall value for

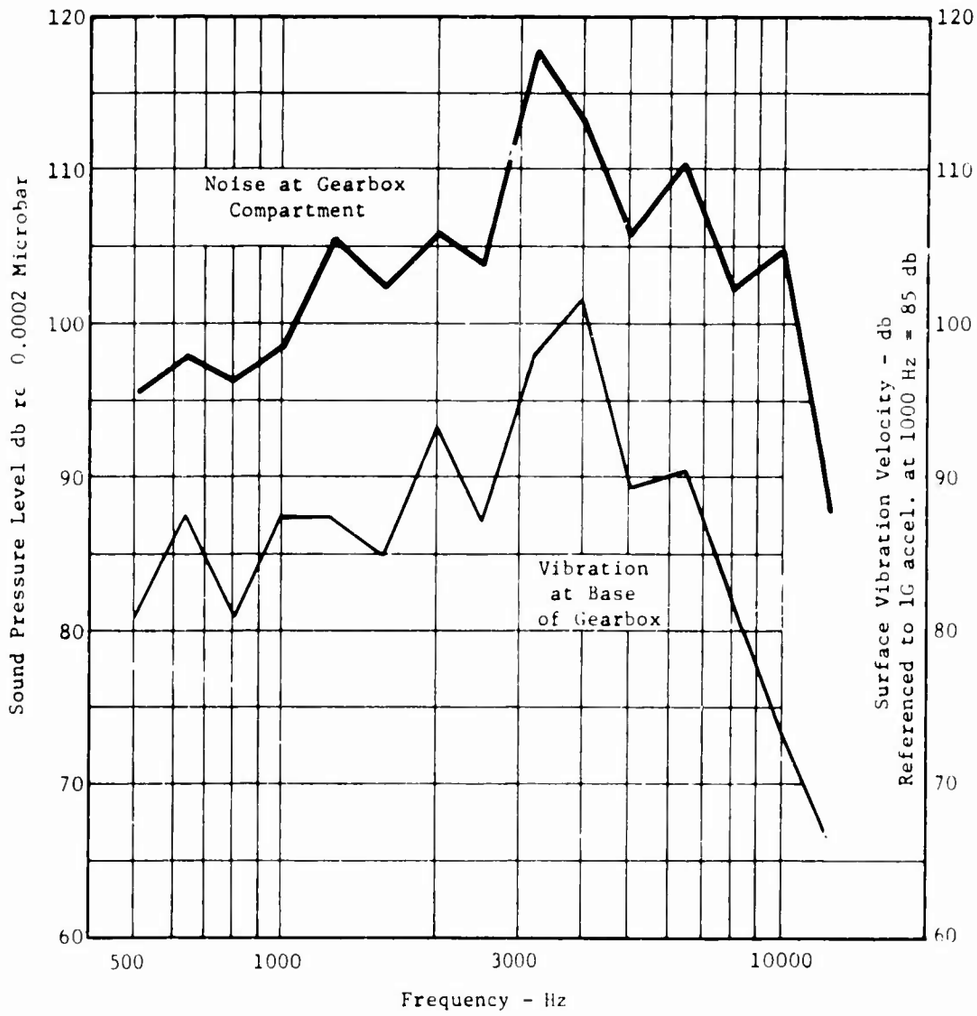

Figure 17. Comparison of Noise and Vibration Measurements.

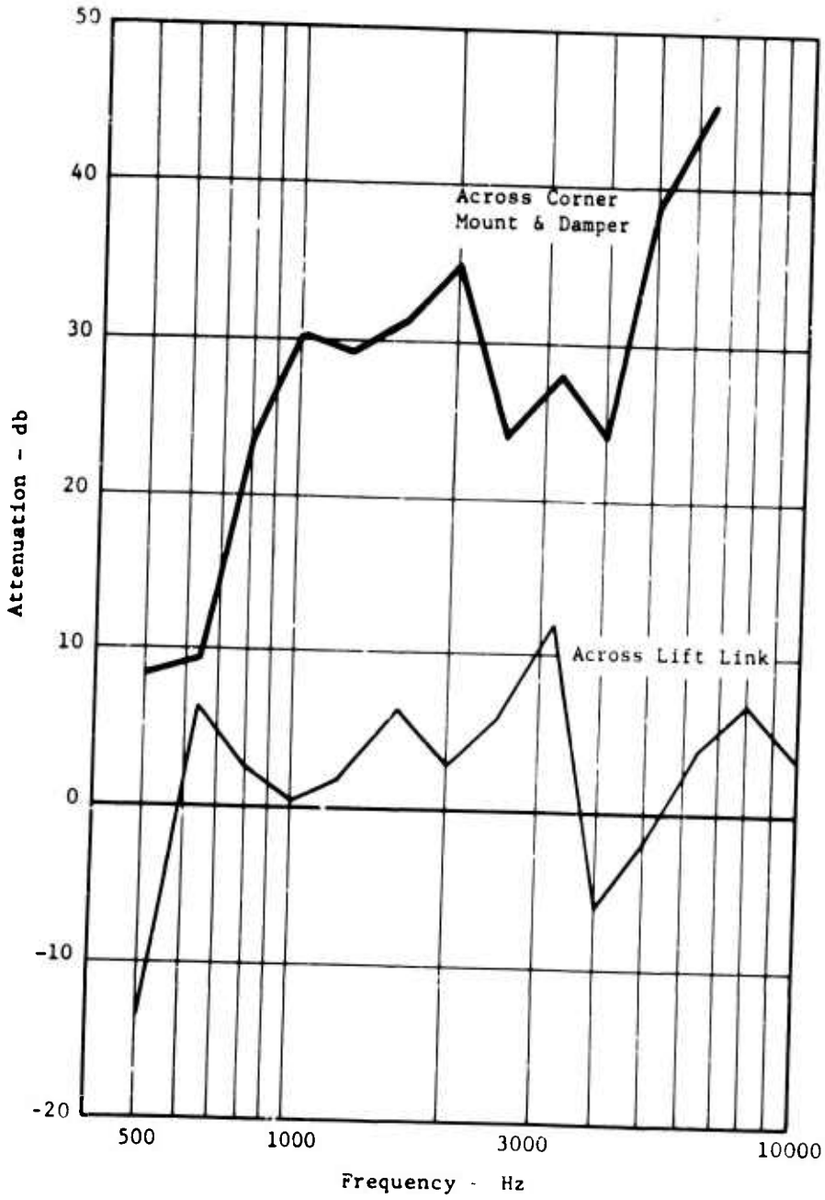

Figure 18. Vibration Attenuation Across Gearbox Lift Link and Mounts.

the entire frequency range reflects almost exclusively the highest levels attained anywhere in the frequency spectrum. For example, in the noise measurements shown in Figure 10, the overall level for the noise at the gearbox compartment would be slightly greater than the highest peak in the upper, or gear noise, frequency range. This is demonstrated very clearly in the narrow-band analysis of Figure 12, in which the overall noise level is shown in the upper right. In a similar way, the overall level for the noise at the pilot's station would again be only somewhat higher than the highest peak, which occurs in the lower, or rotor noise, frequency range. As the cabin surface vibration measurements were made in the cabin, it is reasonable to expect that the overall levels indicated will more likely reflect peaks in the lower frequency range. Hence, these overall level measurements will tell more about the transmittal of rotor noise than that of gear noise.

The tabulated data in Figure 19 show that vibration levels are fairly uniform on most of the cabin surfaces. Only two general locations stand out with measurements of higher vibration. The greater vibration on the side of the rear door, position 11, suggests that this is a point of entry of external rotor noise. The other high levels are at various locations on the gearbox compartment bulkhead, positions 12 through 16. The vibration at the last of these positions was recorded and reduced to a narrow-band analysis. The major peaks in this analysis are plotted on a velocity db scale in Figure 19. While most of the gear meshing frequencies appear, the highest peaks, as anticipated, from the crew compartment noise measurements of Figures 5, 6, and 7, are in the low-frequency end of the scale. Thus, the high overall vibration levels measured at the bulkhead represent rotor pulsations, which find a relatively direct path through the bulkhead into the cabin area.

Since these cabin wall vibration measurements were not in a form which throws further light on the mode of transmittal of gearbox noise, any final conclusions must rest on the indirect evidence discussed earlier. This evidence pointed to the airborne mode, radiation of noise directly from the gearbox, as having major significance.

GEARBOX CASING RESONANCE MEASUREMENTS

These measurements were undertaken to determine if any isolated resonances exist in the gearbox casing which will impose a specific character on the noise produced. With this as the sole reason, no attempt was made to conduct a detailed study of vibration modes or to identify all closely spaced individual resonant frequencies.

The general procedure followed was that of applying a constant-amplitude vibrational force of a preset frequency to a selected point on the casing, while accelerometers fixed to the casing at various points recorded the magnitude of the resulting local vibrations. The procedure was repeated for other set frequencies at closely spaced intervals over the entire frequency range of interest, all the while keeping the vibrational force at the same level. Then the force was shifted to other locations. The accelerometers remained in position, except for one which moved so that it would

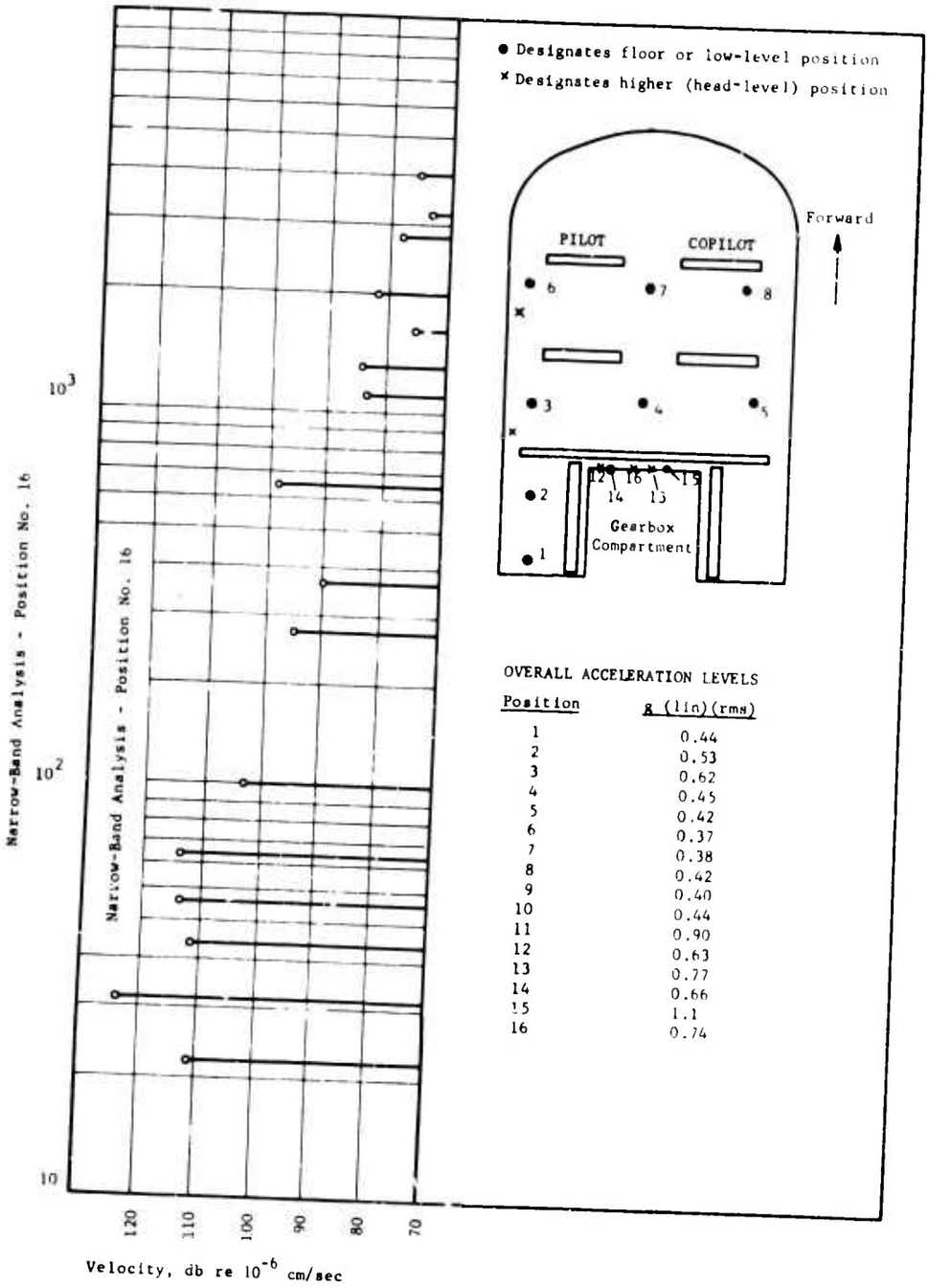

Figure 19. Vibration Measurements on Cabin Surfaces, Helicopter No. 66-1039, Cruise Operation.

always be at the point of force application. A total of three force locations were investigated. These are identified in Figure 20, as are those of the accelerometer locations which have been chosen for consideration in the discussion which follows.

Representative measurements from these accelerometer locations have been plotted in Figures 21 through 24. Before the plotted results are discussed, the format of these curves will be explained. Although they appear very similar to the third-octave plots of noise and vibration measurements presented earlier, there are basic differences. Each measurement was made with excitation at a single, discrete frequency. Hence, the response recorded is for that frequency only and, unlike the third-octave measurements, does not show the combined effect with response at other frequencies, adjacent or otherwise. The line segments connecting the recorded points merely show that the connected points came from the same accelerometer. Peaks and valleys have no special significance; the peak measurement is merely greater than its neighbors and the valley measurement is just smaller than its neighbors. The individual frequencies used for measurement were selected on the basis of practical considerations; they were sufficiently closely spaced to pick up a large number of resonances, but not so closely spaced that the testing would be unnecessarily drawn out. All the measurements taken are tabulated in Appendix II, but the plots in Figures 21 through 24, for reasons of brevity and clarity, show only a representative portion of these measurements. The frequencies selected for these plots were those closest to the conventional third-octave midpoints. Use of these values gave an unbiased selection and gave approximately uniform spacing between the measurements as plotted on a logarithmic frequency scale. Although individual resonances appeared at frequencies that fell between these selected values, their levels followed the same general trends shown. The vertical scale in the plots gives the motion of the casing surfaces as acceleration, so that the constant driving force used would give constant response except where a resonance effect is present. The db scale is used to compress the large range of response. The db reference values for the various accelerometers are sufficiently alike that relative positions of the curves may be interpreted as shown.

Figure 21 compares the response just alongside the excitation for the three different driving points. Although the driving points are widely separated on the gearbox, and the casing construction at each point is quite different, the three sets of results show strong similarities. In general, they all start from a minimum at 200 cycles, rise more or less uniformly until about 2000 to 4000 cycles, and then drop off slightly until the highest frequency measured, 10,000 cycles, is reached. The nearly-matching response curves would seem to indicate that despite apparent case construction differences, there is an overriding similarity throughout the casing as far as dynamic response is concerned. At the same time, it must be recognized that the similarities may result from an unknown common influence originating in the test technique. If this is the case, the results recorded may also be describing the dynamic characteristics of the test system, and not purely those of the casing alone. Because it was not possible to identify any such influence on the part of the test methods, it has not been taken into account in interpreting the results. However,

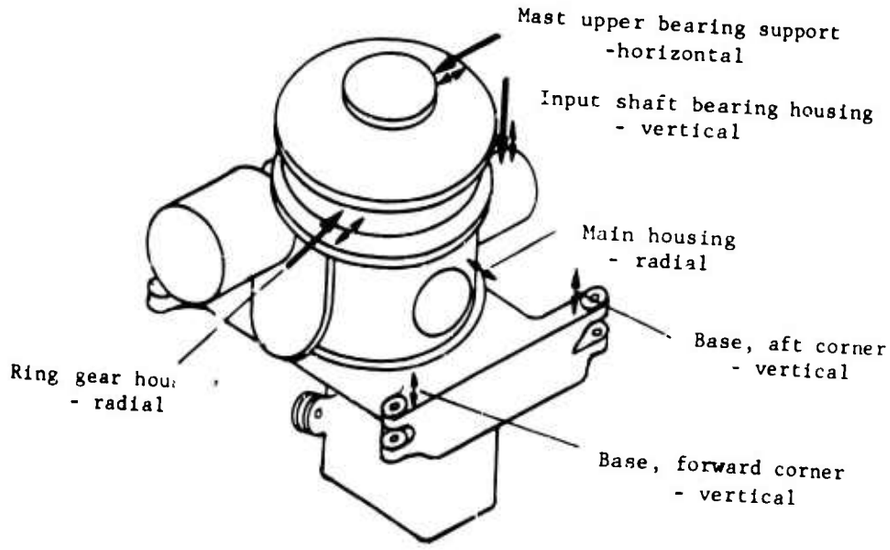

Legend:

Location and orientation of excitation force

Location and orientation of accelerometer

Notes:

Accelerometers shown alongside excitation force changed location with change of excitation.

Accelerometers shown alone remained in position for all excitations

Figure 20. Location of Excitation and Some of the Accelerometers Used in Gearbox Casing Resonance Measurements.

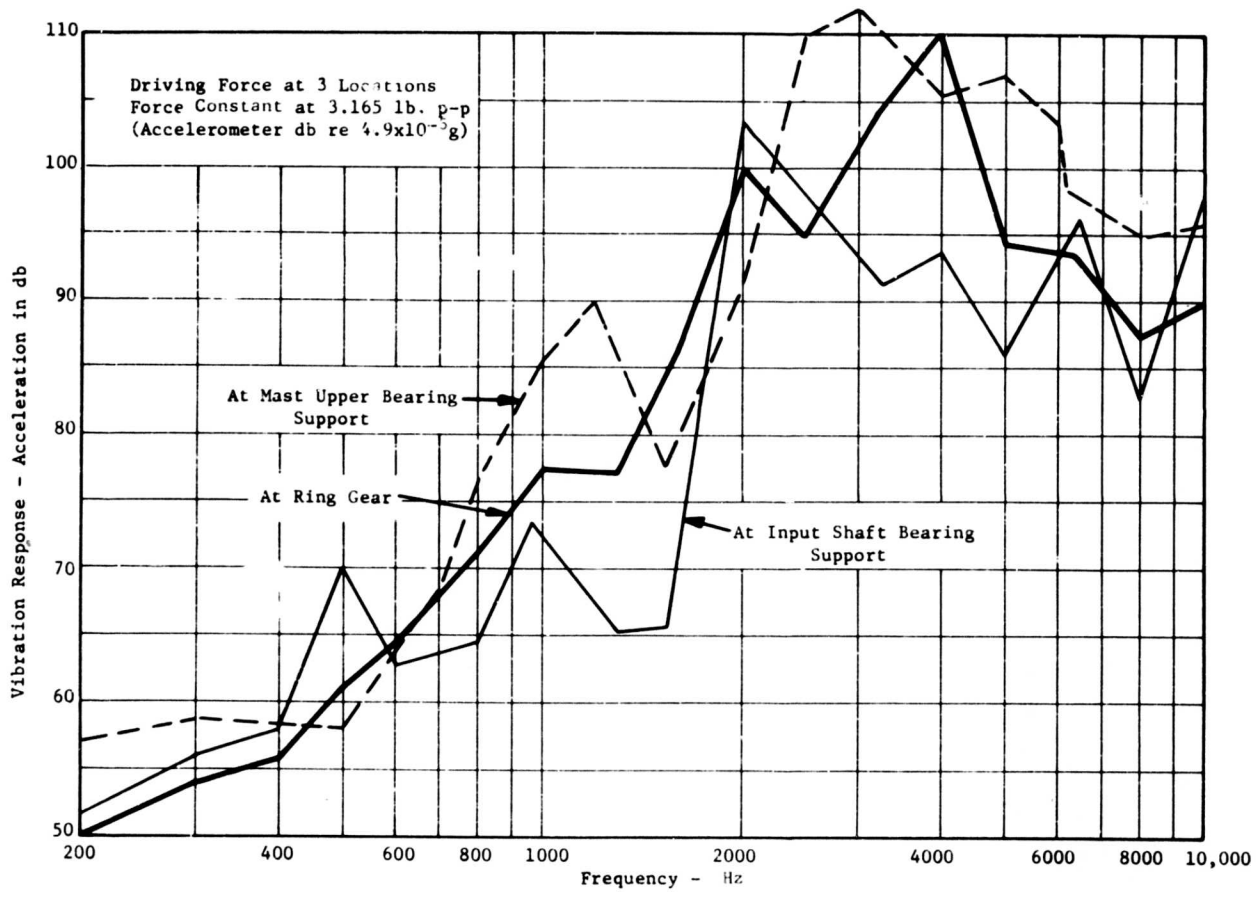

Figure 21. Gearbox Casing Vibration Response - Measured at Point of Excitation.

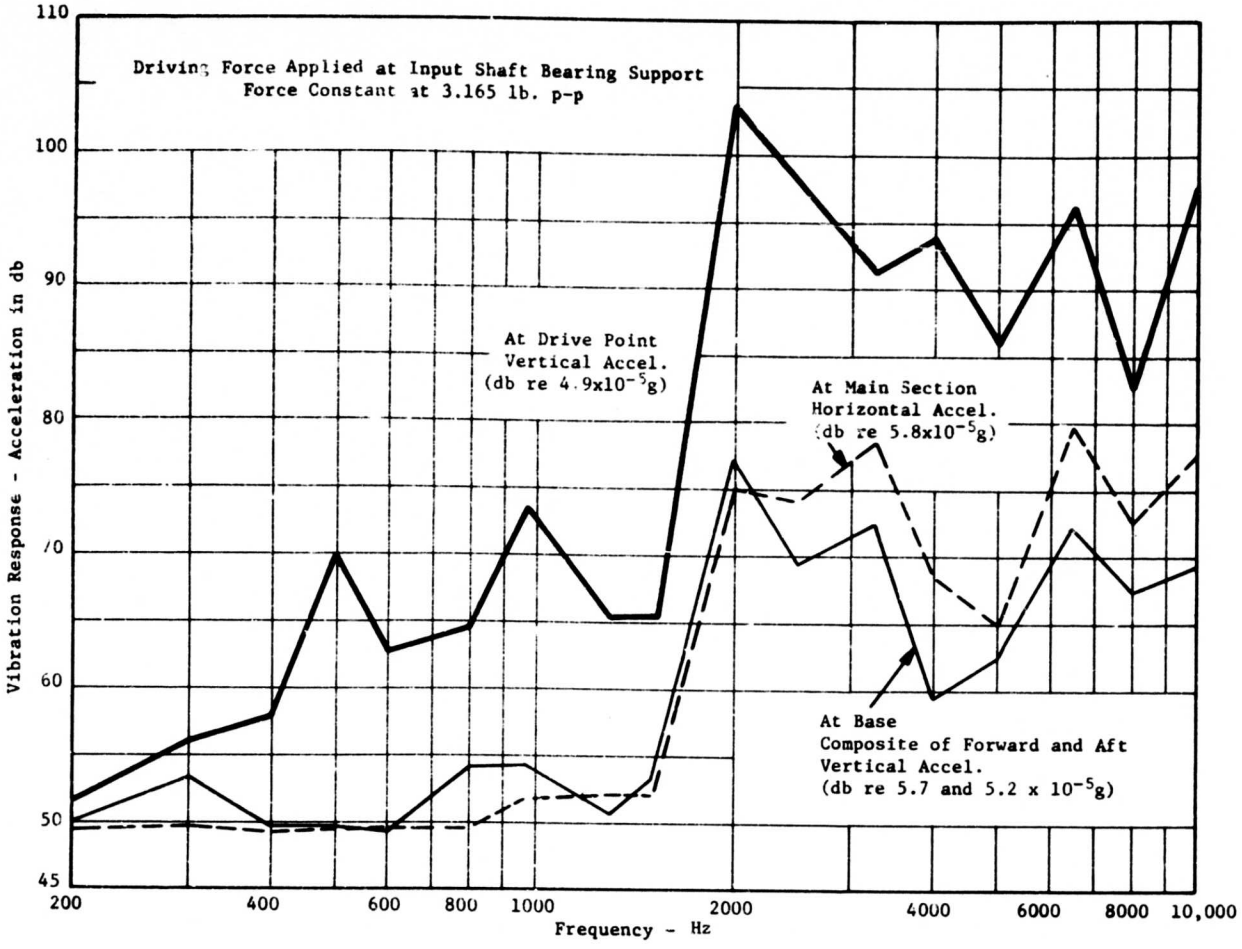

Figure 22. Gearbox Casing Vibration Response - Driving Force Applied at Input Shaft Bearing Support.

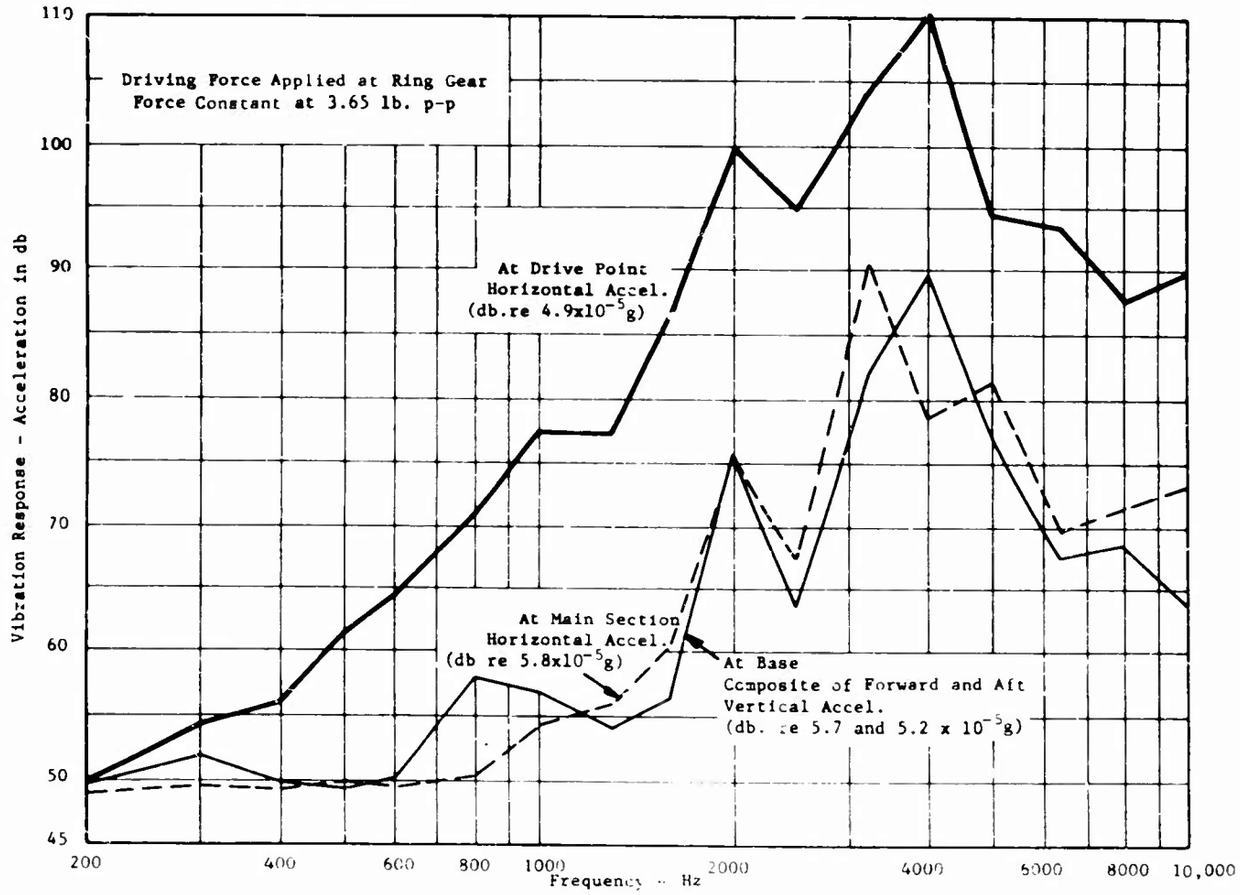

Figure 23 Gearbox Casing Vibration Response - Driving Force Applied at Ring Gear.

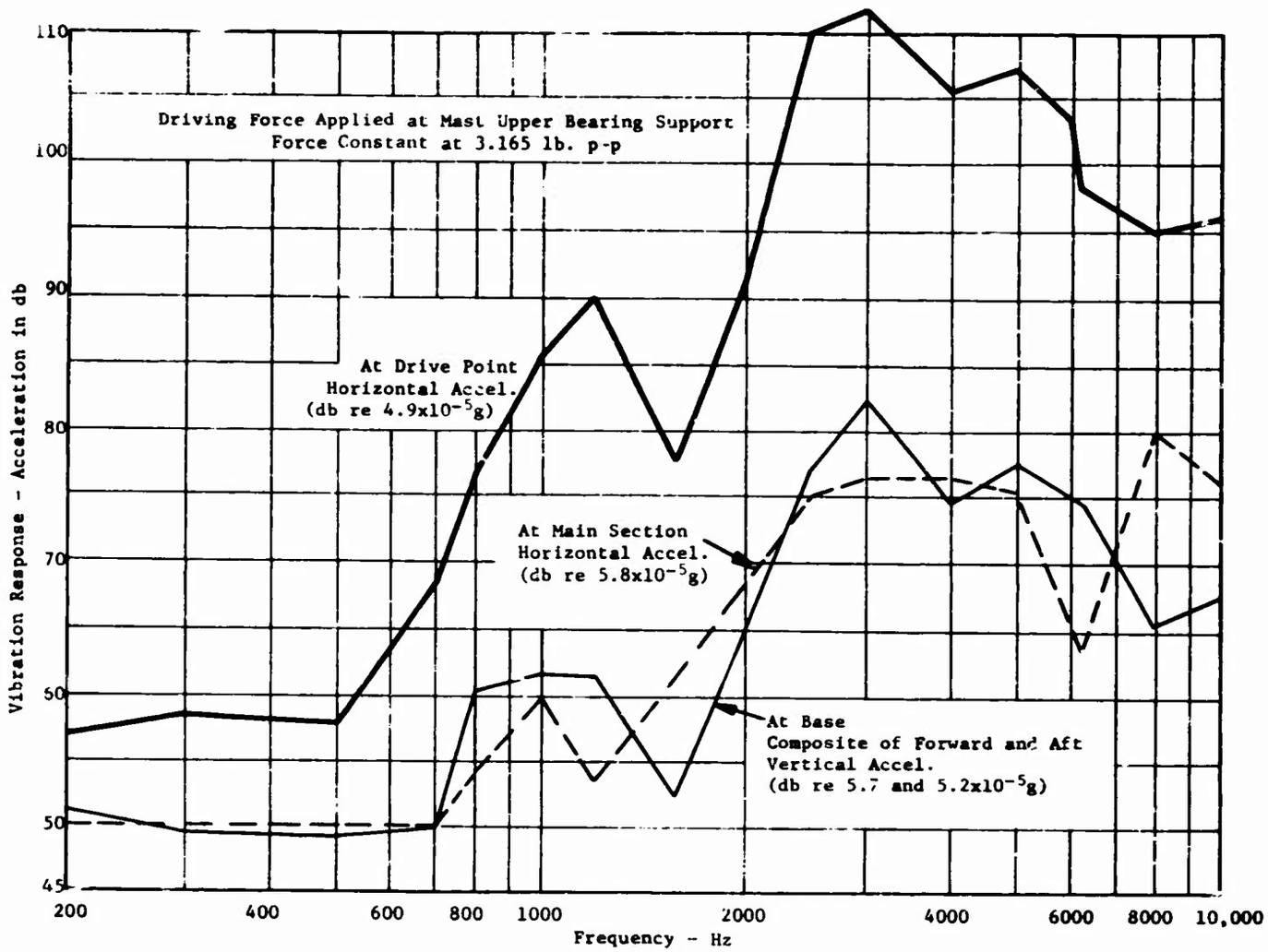

Figure 24. Gearbox Casing Vibration Response - Driving Force Applied at Mast Upper Bearing Support.

most, if not all, of the conclusions drawn from the measurements would not be changed if such an influence on the general shape of the response curves were to be confirmed.

Referring again to Figure 21, the differences between the curves are quite significant. There are no isolated frequencies at which all the curves show a common maximum response. For example, at 3000 cycles, the ring gear response is at its highest level but the response at the mast bearing is more than 5 db below its highest and the response at the input bearing is about 10 db below its highest. If all three locations were excited simultaneously, as might be expected in the operating gearbox, it is quite likely that the composite response at each of the frequencies would be less variable than the individual responses are shown to be. The overall effect of casing resonance at the drive points therefore appears to be fairly uniform, at least in the frequency range above about 2000 cycles. This range, incidentally, includes those frequencies previously demonstrated to have the major gear noise components.

Figures 22, 23 and 24 each compare the casing response at the drive point to the response at other locations. One of these locations is on the main casing section, below the ring gear. The other two locations are on the base, and their measurements have been averaged to give some rough idea of a composite response. The measurements at these non-driving-point locations all show certain common characteristics. First of all, at frequencies up to about 1600 cycles, the response stays fairly constant at close to 50 db. This simply indicates that at these frequencies and at these locations, the applied force is simply shaking the casing as a rigid body in its soft mounts. At higher frequencies, the response plot starts to follow the response at the driving points, but at levels of 20 to 30 db lower. The shapes of the response curves for base and main section locations, especially the former, are very similar to the higher response curves.

These other curves tend to reinforce the conclusion stated after study of Figure 21, that a composite response with excitation at all locations has no isolated resonance, and that the many individual resonances tend to combine to give a more or less uniform response at frequencies above 2000 cycles. The relationship between the response at the non-driving locations to that at the drive points leads to some additional conclusions. Although the excitation force is applied in a fairly restricted area, its effect is felt throughout the casing. The response at the other locations may be 20 or 30 db lower than that at the drive point, but this reduction may be more than offset by the larger surfaces involved. Another conclusion derives from the similarity in the response of the base, in its variation from frequency to frequency, to that of the portion of the structure where the driving force is applied. This similarity suggests that it is the resonance in the drive point structure, rather than in the connecting structure or the base itself, which determines the general character of the overall response of the gearbox casing.

GENERAL DESCRIPTION OF ANALYSIS

The analytical method developed in this program for predicting gear noise levels is described in basic form in Figure 25. The data used in the calculation are derived primarily from the design of the gearbox and other components in the main drive system. If a new gearbox design is to be analyzed, information normally found in a design layout will suffice. Data from the operating conditions is also required, specifically the horsepower transmitted and the speed. The final information needed is related to the as-manufactured condition of the gears. Ideally, this information will be taken from measurements on representative gears. In the case of a new design, where the gears have not yet been manufactured, it is possible to use information derived from past measurements of similar gears. When the gears have been precision ground, as is typical of helicopter transmission gearing, the significance of the manufacturing deviations may be rather small and estimates of gear errors based on design specifications will suffice. The computation procedure involves three steps, which are briefly described below. Representative results will be presented in later portions of the Discussion section. Detailed descriptions of the analyses and computer programs are presented in Appendixes IV, V and VI.

The first step, using a computer program, is an evaluati[illegible] the magnitude of the excitation or disturbance introduced into the gearbox vibrational system. This excitation comes predominantly from the meshing, or clashing, of the gear teeth, as was demonstrated in the noise and vibration measurements discussed earlier. Hence, the first computer program considers in very thorough fashion many aspects of the gear meshing phenomenon. The present program is written specifically for spur gears, which make up most of the gearing in the conventional helicopter gearbox. A more general program would also consider helical gears, but it was found to be most impractical to take on this more complex problem without first gaining some experience with the simpler spur gear case. The first reduction gears in the helicopter gearboxes are generally spiral bevel gears. Although these gears cannot be analyzed exactly, the existing program does assist in obtaining usable estimates of the excitation they produce.

The output of this first program is in the form of a series of excitation amplitudes, corresponding to frequencies equal to the gear teeth meshing rate and its harmonics. The program also provides a computed value of the mean combined stiffness of the meshing gear teeth.

The second step is a vibration response calculation performed by a main computer program supplemented by an auxiliary program. The main program treats the entire main power drive system, from engine to rotor, as a torsionally vibrating system excited by displacement pulsations in each gear mesh. This program is written around the conventional gearing arrangement of helicopter gearboxes: a simple stage of reduction gears used together with two planetary reduction stages. There are several unique features in this program. Excitation is introduced as a displacement instead of in the more conventional manner of exciting forces or torques. The planetary systems are subjected to a thorough dynamic analysis, which considers

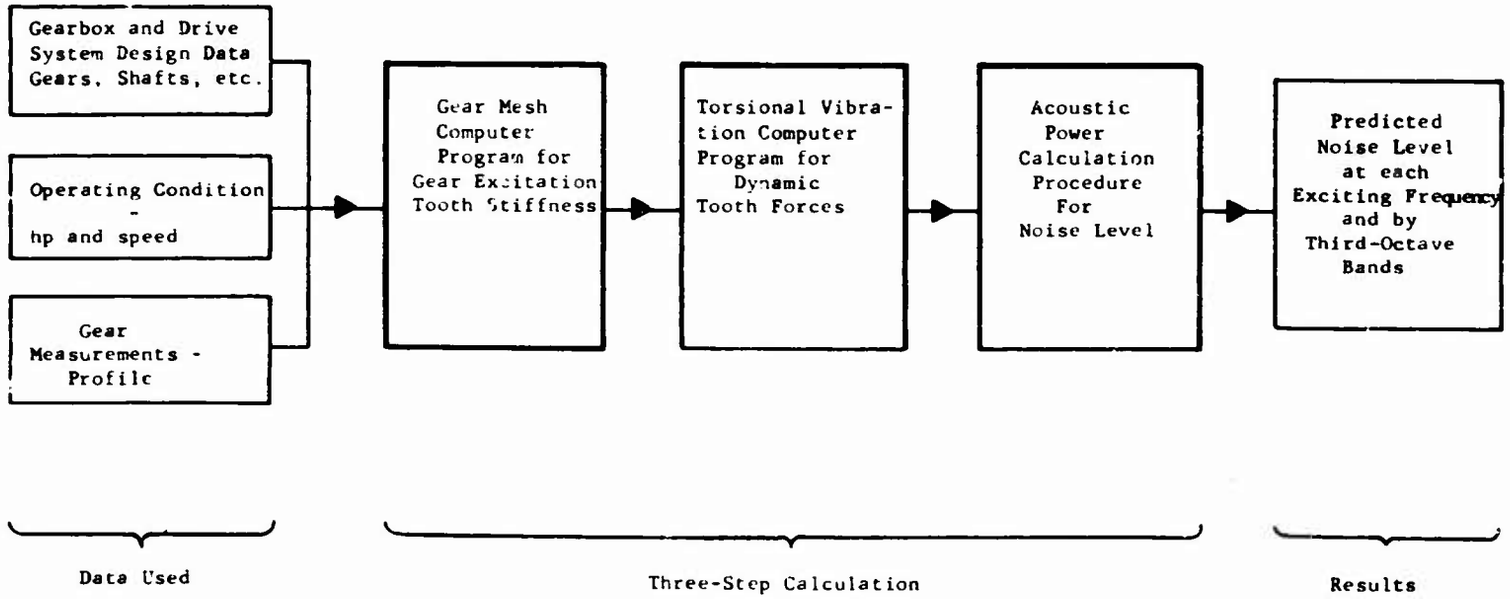

Figure 25. Flow Chart Description of Predicted Noise Calculation.

elasticity at all gear teeth meshing points, in the planet carrier, and even in the mounting restraint of the ring gear. Likewise, the individual inertias of all of the components are included. The program has provision for damping at bearing locations, but not of the gear teeth meshing points. Although this additional feature is highly desirable, it would have added considerable complexity, and it was best deferred to a future refinement of the program.

The results of this response calculation are in the form of dynamic torques which act on the driving gears. Under certain conditions of planet phasing, it is necessary to use the supplementary computer program on each of the planetary stages in order to get the forces associated with the individual planets.

The final step of the calculation process takes the excitation values from the first computation and the dynamic forces from the second computation and translates them into predicted noise levels. The actual process through which excitation leads to noise is extremely complex and very dependent on many specific design features of the particular gearbox and its environment in the helicopter. Development of a rigorous analysis which follows in step-by-step fashion the actual noise production process was judged to be unrealistic, considering the present state of knowledge in the field. Instead, the calculation employs a very direct method which has more of an empirical than an analytical basis. This method was adopted from one which demonstrated its effectiveness when used for noise level predictions on other types of gear transmission systems (see Reference 5). The original analysis postulates that for each excitation frequency there is a scalar quantity akin to power which is introduced at the excitation points and which finds its way through the shafts and bearings into the casing. This "power" shows up in the casing in the form of casing surface vibrations, and a known small portion of it is thereby converted into acoustical power. The "power" at the source is taken as the product of the absolute excitation displacement times the absolute dynamic force of the same frequency developed at the same point. Zero attenuation while passing through the bearings is assumed. This assumption is reasonable because the bearings are both laterally stiff and free of lateral damping. A response of the casing independent of frequency is presupposed. Measurements of the gearbox casing response described earlier do indeed indicate that there is no isolated, dominant casing resonant frequency and that, instead, the overall level of response in almost all of the gear noise frequency range was relatively uniform. The assumption that noise is directly produced by the vibration of the gearbox housing and that it is not dependent on the aircraft structure is also supported by measurements made in the program. These noise and vibration measurements, it may be recalled, strongly pointed to the airborne mode of noise transmittal.

After finding the noise power levels, the calculation procedure converts them to sound pressure levels as measured by the noise level instruments. To facilitate comparison of calculated to measured noise levels in third-octave band spectra, the procedure also includes a means of simulating the effect of noise analyzer filters in combining noise levels of close frequencies. Thus the final result of predicted noise levels is very similar

in presentation to the results of actual measurement.

GEAR EXCITATION ANALYSIS

The gear excitation of vibration comes from the imperfect action of the meshing gear teeth. Perfect gear action takes place when the ratio of instantaneous velocity of the two gears remains absolutely constant and no varying loads are introduced by the meshing action. This perfect action is not achieved in actual gearing because of a combination of the following conditions (References 5, 6, and 7):

1. Nonuniform deflection of gear teeth under a steady load

2. Imperfect geometry of the gear due to manufacturing and sometimes also design

3. Variable frictional forces acting at the teeth contact points

4. Variable hydraulic forces due to oil pocketing in the spaces between meshing teeth

The analysis developed considers the first two items for those characteristics which show up uniformly from tooth to tooth. Any characteristics of deflection or geometry which are not uniform in this manner will not generate disturbances of the tooth meshing frequency or its harmonics and therefore do not contribute to the noise components under study. Items 3 and 4 were judged to contribute less to gear excitation in helicopter gearboxes than Items 1 and 2 and were set aside for future refinement of the present analysis.

As part of its procedure for calculating the excitation components, the analysis and its computer program finds the point-by-point variation in gear teeth deflection. This is illustrated in Figure 26(a), which gives the unit normal deflections calculated for a single tooth on the upper sun driving a single tooth on the planet under a tangential load of 2500 pounds. As shown in the figure, total gear tooth deflection is the sum of the flexural displacement of the driving and driven teeth plus the combined contact or Hertzian deformation. The form of the individual tooth displacement curves may be explained in the following manner. Since the driving tooth comes into mesh with the load applied near its root, it experiences very little flexural displacement at its load point. As the driving tooth continues in mesh, the load point moves out toward the tip of the tooth, and this displacement increases rapidly. The driven gear tooth comes into mesh with the load applied at its tip, and therefore its displacement characteristic is in reverse. When the two curves are combined, a more nearly uniform displacement results. The addition of the contact deformation, which is uniform throughout the gear teeth engagement, gives the total deflection curve.

Figure 26 shows how this total deflection curve for one pair of teeth applies only during that part of the meshing action in which only one pair transmits load. When load transmission is shared with adjoining teeth, the

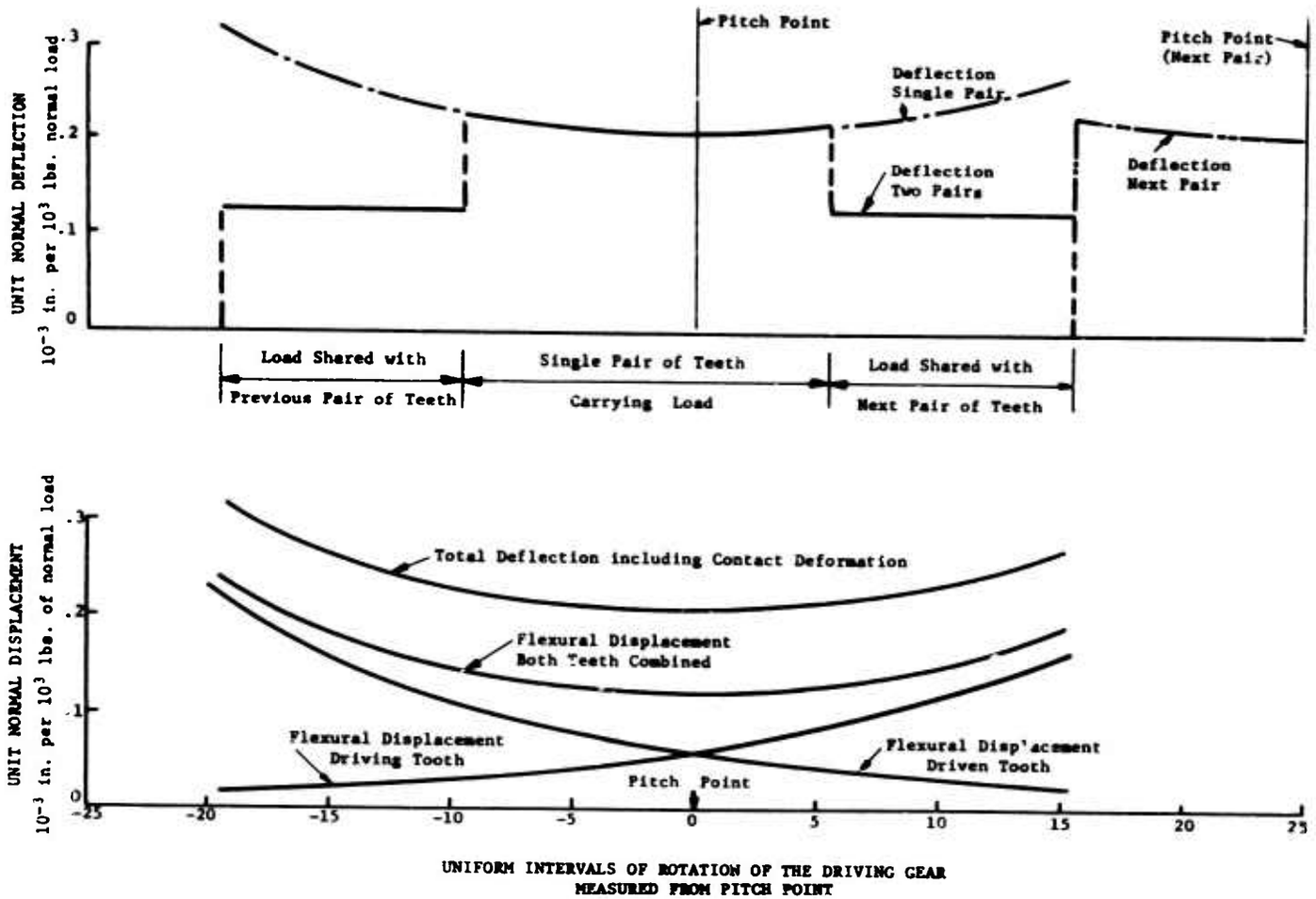

Figure 26. Gear Tooth Unit Deflection Curves - (a) Lower - Single Pair of Teeth; (b) Upper - Combined Action of Adjoining Pairs.

single pair in question has only a fraction of the total load and deflects correspondingly less. The individual pair of teeth therefore experiences a pattern of no deflection at no load, partial deflection when load is shared, full deflection when the load is carried alone, partial deflection as load is again shared, and, finally, no deflection as the pair of teeth goes completely out of mesh.

The gear as a whole does not experience the intervals of no deflection, for when the single pair is out of mesh, other teeth are carrying the load and deflecting in a similar manner. The pattern for the entire gear may also be seen in Figure 26(b). The right-hand part of the deflection curve has been augmented by the deflection of the next pair. Going from the pitch point of one pair to that of the next gives a repeating pattern for the entire gear of full deflection, partial deflection, and back to full deflection.

This same pattern is shown in the upper part of Figure 27. It is a duplicate of the right-hand portion of Figure 26(b) except that the ordinate is given as measured on the pitch circle. The lower part of the figure describes the manner in which load is transferred from the first to the second pair of mating teeth. Each pair carries the full load except when both pairs are in contact and sharing the load. When the second pair of teeth comes into contact, the load on the first pair suddenly drops off to about 60 percent, decreases to about 40 percent during the load-sharing interval, and then drops to zero as the pair of teeth separates. This cycle of variable deflection described in the upper part of Figure 27 prevents the driven gear from keeping a perfectly uniform speed relationship with respect to the driving gear. As the steps in the deflection curve are experienced, the driven gear will attempt to instantaneously speed up and slow down. To do so, it must overcome the stiffness and inertia of the gears and other components in the drive system. The result is the excitation of vibration into this system. The fundamental frequency of this vibration will be the frequency corresponding to the deflection curve cycle, that is, the tooth meshing frequency. Because the deflection curve shows sharp changes, in practice not so sharp as shown in the plotted curves but nevertheless abrupt, the excitation will also include components of higher harmonics. These harmonics are evaluated in the computer program by means of a Fourier analysis, so that the total excitation is expressed in a series of sine and cosine curves related in phase with the pitch point as a reference.

The deflection curves discussed above were based on perfect involute teeth with no profile deviations, either in design or in manufacturing. The introduction of any such changes in the tooth profile will require a new curve to describe the variability of rotation of the driven gear relative to the driving.

Some of the gears in the UH-1D gearbox have been designed with teeth profiles which are not true involutes. The specified profiles for sun and ring gears have been modified so that the trace of a profile measurement will be inclined rather than a parallel straight line. Figures 28 and 29 give profile data for the sun and ring gears respectively. The dotted line in the

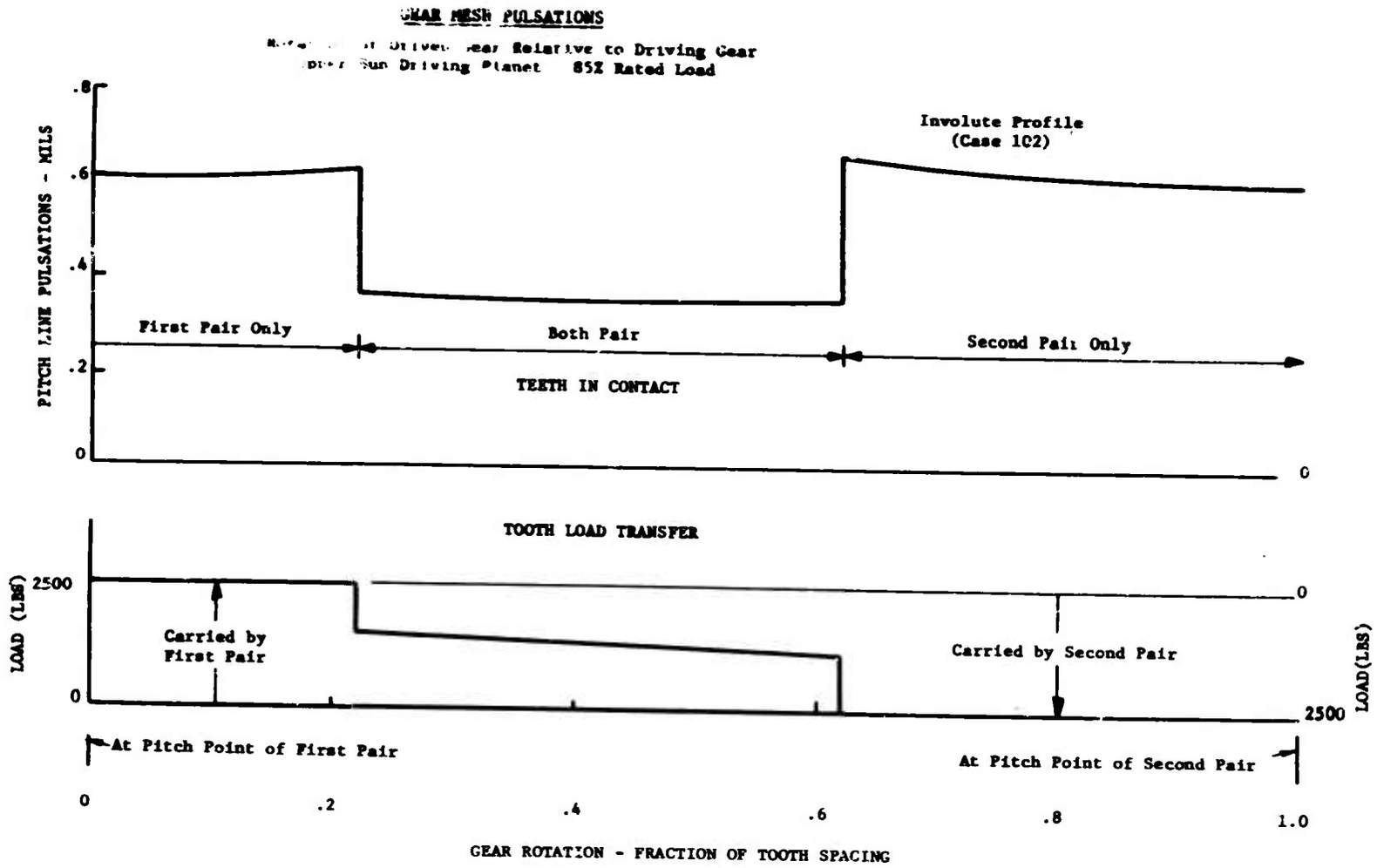

Figure 27. Gear Mesh Pulsations for Upper Sun Driving Planet With Involute Profiles on Both.

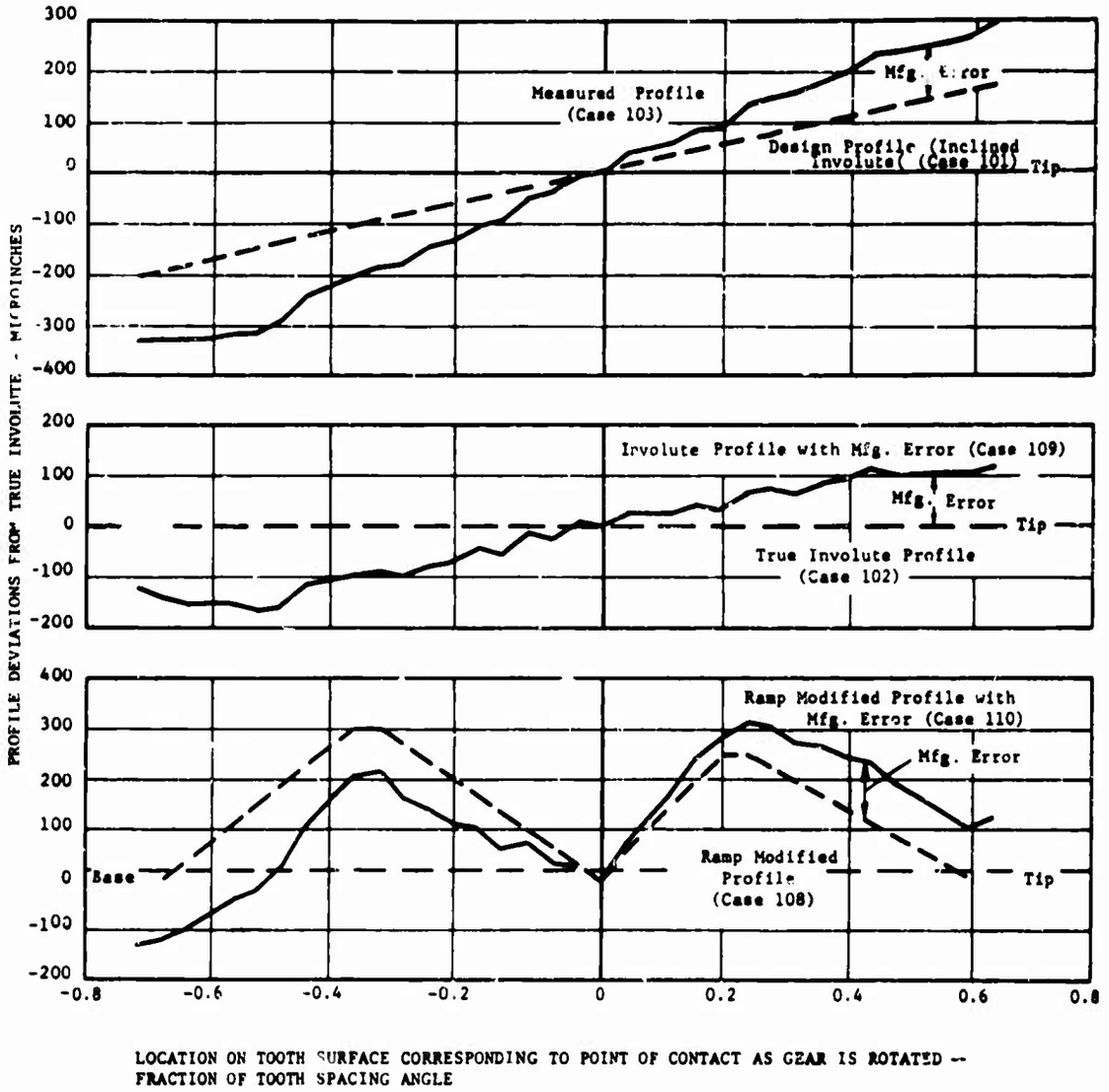

Figure 28. Sun Gear Tooth Profiles.

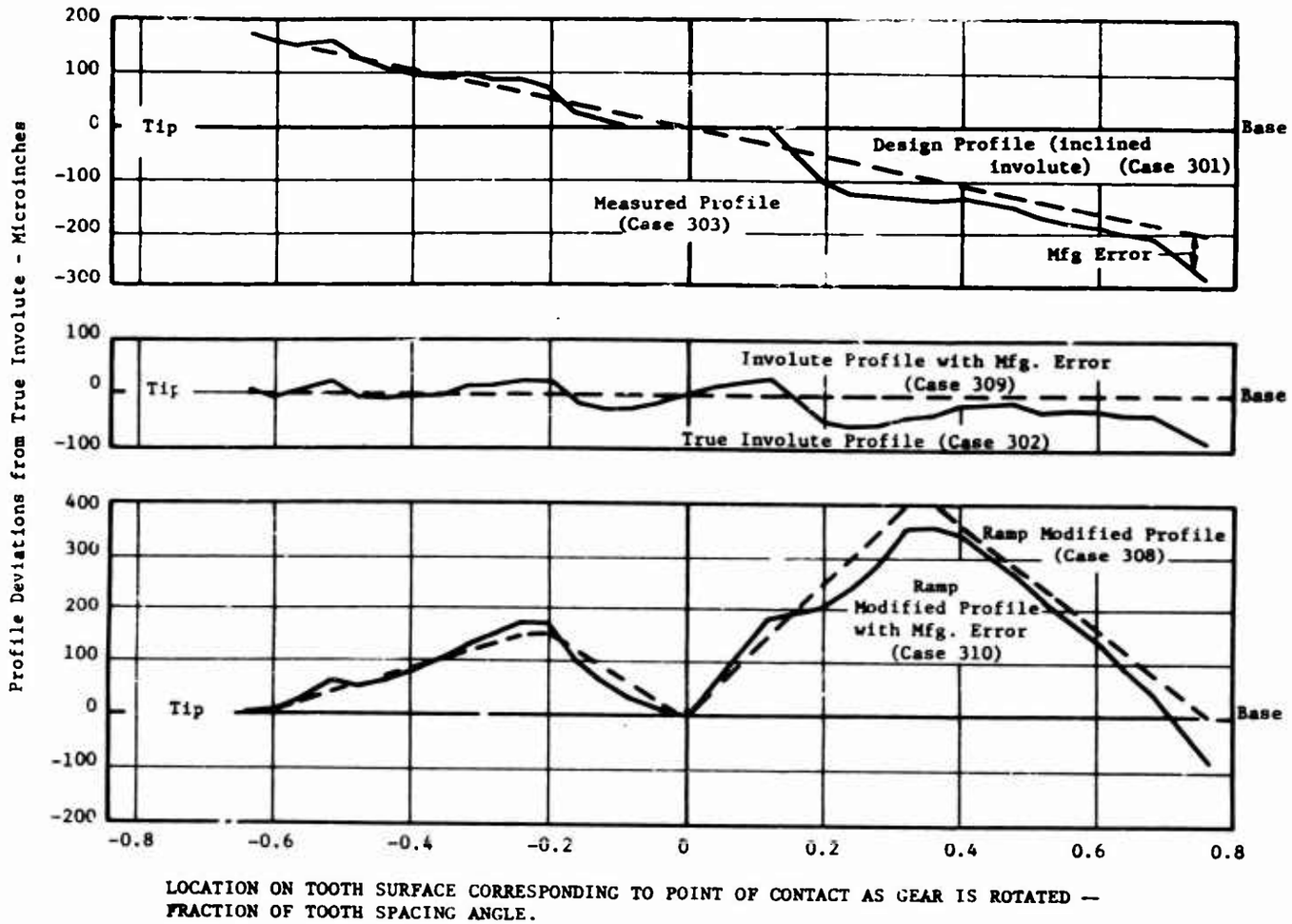

Figure 29. Ring Gear Tooth Profiles.

upper plot of each figure shows the design profile as an inclined line, while the dotted line in the center plot of each figure shows the true involute profile as a parallel line.

The effect of this design modification is illustrated in Figure 30. By comparing the pulsation curve for the design profile with that of the true involute profile in Figure 27, it is seen that the profile modification has reduced the abrupt step as the second pair comes into contact, but has increased the step as the first pair goes out of contact. The load transfer curve in Figure 30 shows how the design profile results in the first pair's carrying most of the load until it goes out of mesh.

Other types of profile modifications may be made part of the gear design. One such modification, designed to reduce gear excitation, will be discussed in a later section of the report.

Deviations from a true involute profile as actually found in gears also include the effects of manufacturing errors. Measured profiles show point-to-point irregularities as well as more extended deviations from the ideal design profile. As long as these deviations remain within the tolerance band normally specified with the design profile, the gear will be accepted for use. However, these deviations, very often repeated from tooth to tooth, influence the gear mesh pulsation effect and hence the gear excitation.

Actual profile measurements are shown in Figures 31, 32, and 33. For one profile in each of the first two sets of curves, point-by-point deviations from a parallel line, or true involute profile, have been measured using the pitch point as the zero deviation. (The third set of curves, taken from a planet gear, are already so close to a true involute that the deviations have been neglected in the calculations used in the illustrations in this report.) These point-by-point deviations have been plotted alongside the design profile curves in Figures 28 and 29. These measured profiles show both types of profile deviations: the extended deviations in the case of the sun gear in Figure 28 and the point-by-point deviations around the design profile in the case of the ring gear in Figure 29. In both figures, the manufacturing error, taken as the point-by-point difference between the measured and design profiles, has also been plotted as it would appear if superimposed on a true profile.

The gear excitation computer program includes the effects of the manufacturing errors of both meshing gears along with any profile design modifications in calculating pulsation and load transfer curves. As an illustration, Figure 30 shows these curves for the measured profile of the sun gear. When this pulsation curve is compared to that for the design profile, the small contribution of manufacturing errors as compared to gear deflection is recognized. This minor effect of manufacturing errors is seen again when the magnitudes of the computed excitation components for the two profiles are compared. Table V gives these magnitudes for the fundamental and first two harmonics resulting from the design and measured profiles for the case of the upper sun driving the planet and the case of the upper planet driving the ring. With the former case, the effect of manufacturing

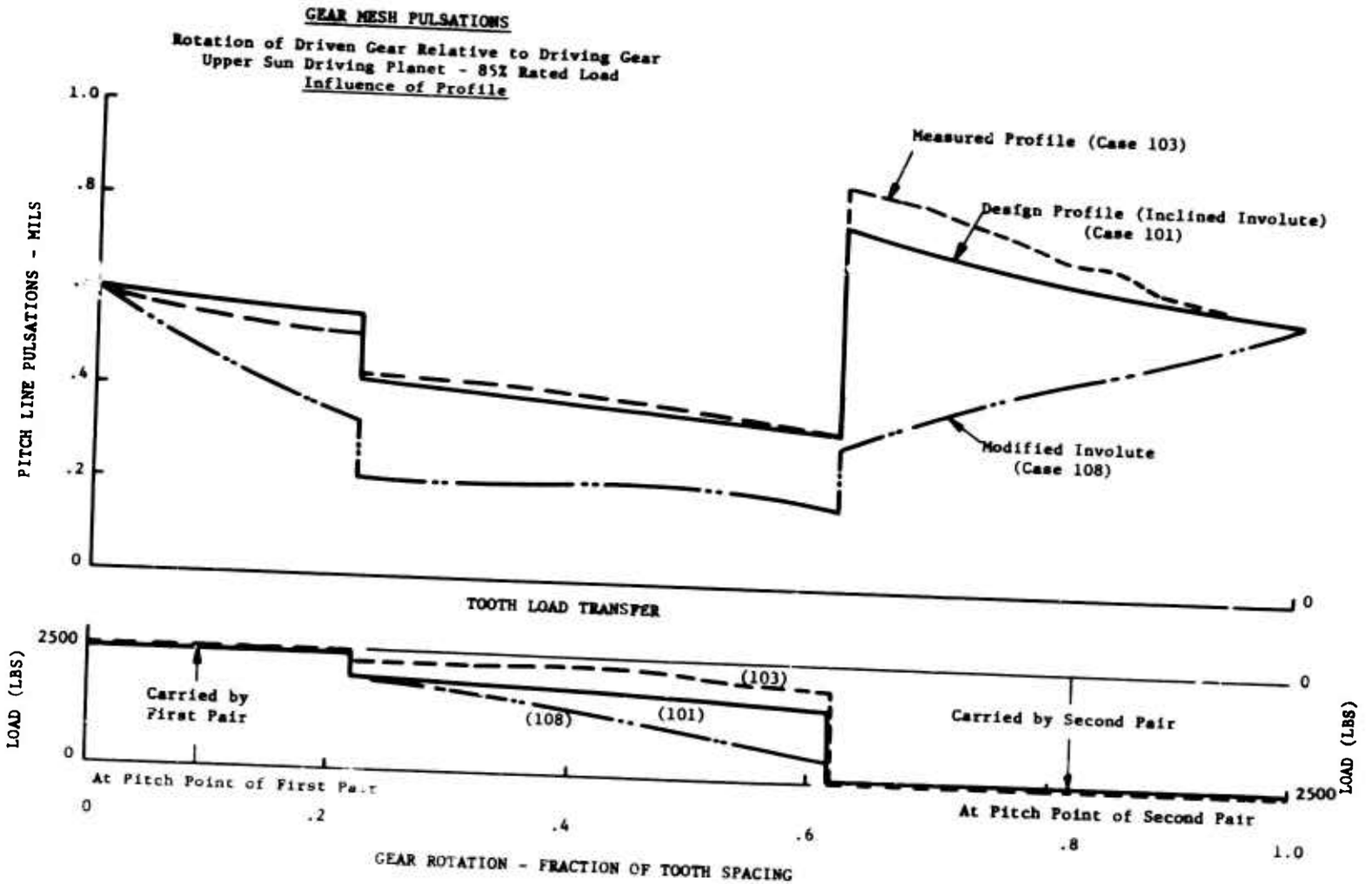

Figure 30. Gear Mesh Pulsations for Upper Sun Driving Planet for Non-Involute Profiles.

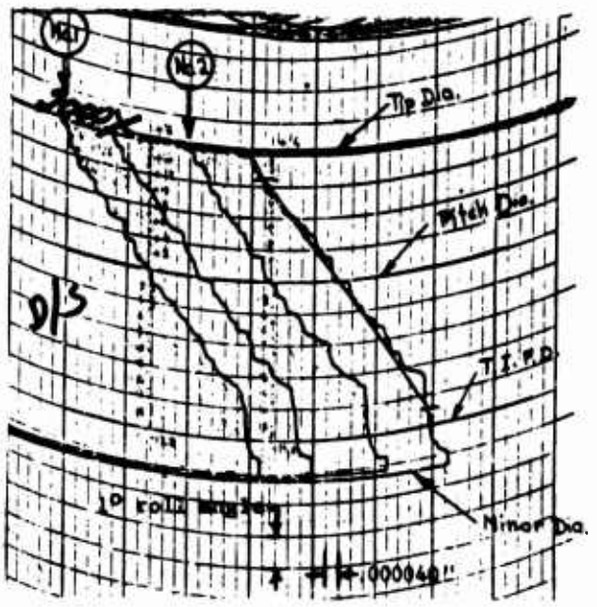

Figure 31. Gear Tooth Profile Measurements on the Sun Gear.

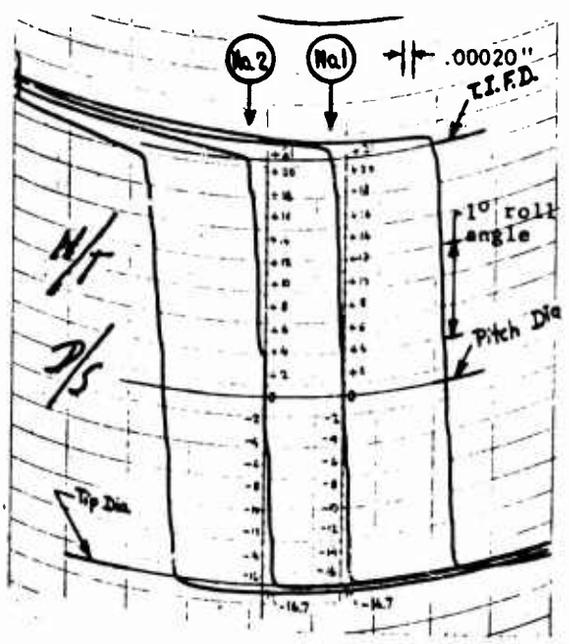

Figure 32. Gear Tooth Profile Measurements on the Ring Gear.

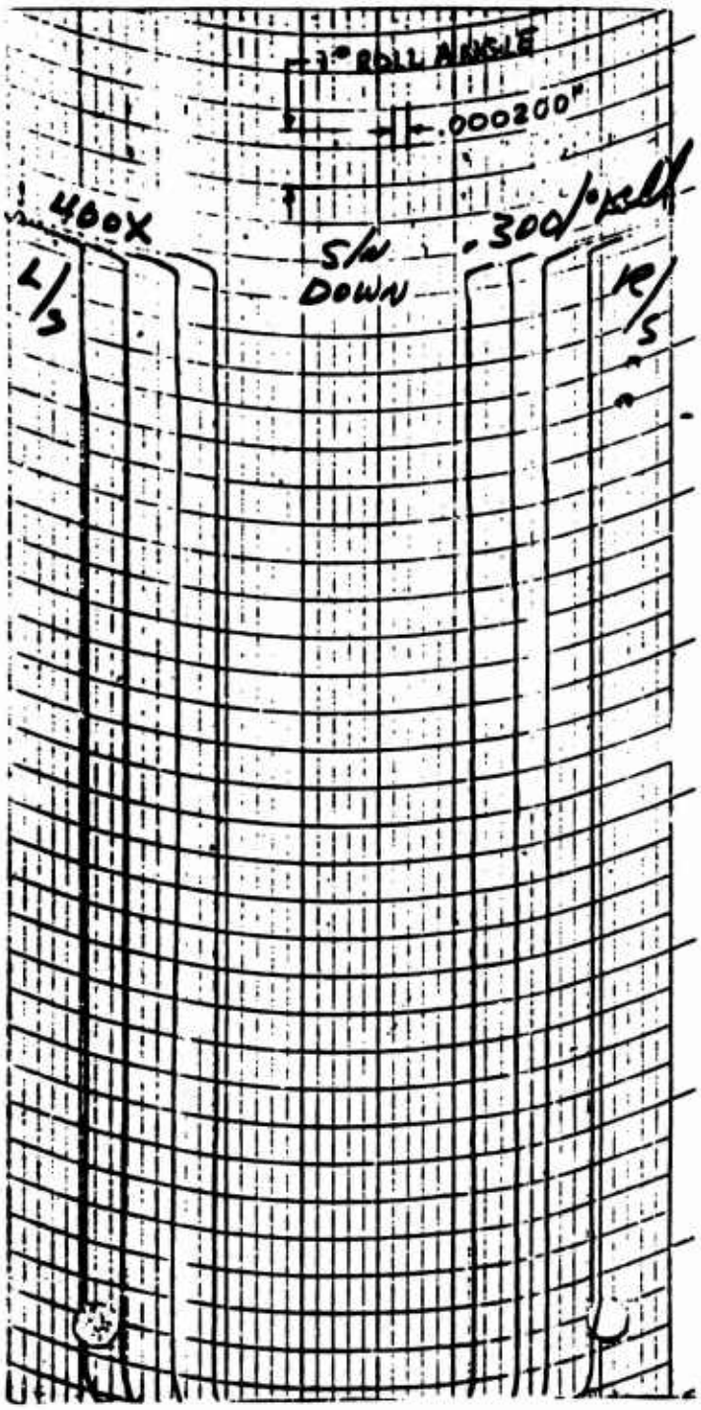

Figure 33. Gear Tooth Profile Measurements on the Planet Gear.

TABLE V. COMPARISON OF GEAR EXCITATION - EFFECT OF MANUFACTURING PROFILE ERROR

	Fund.	2nd Harm.	3rd Harm.
Upper sun driving planet at 85% rated load			
Excitation with Design Profile - mils (Case 101)- no manufacturing error	.160	.070	.043
Excitation with Measured Profile - mils (Case 103)- with manufacturing error	.174	.088	.057
Effect of Manufacturing Error on Noise Level	0.7 db	2.0 db	2.4 db
Upper planet driving ring at 85% rated load			
Excitation with Design Profile - mils (Case 301)- no manufacturing error	.161	.053	.041
Excitation with Measured Profile - mils (Case 303)- with manufacturing error	.156	.054	.048
Effect of Manufacturing Error on Noise Level	-0.3 db	0.2 db	1.4 db

Note: The excitation amplitudes given in this table are the resultants of the sine and cosine components for each harmonic. These resultants do not reflect the phase shift for each harmonic which may accompany the changed profile.

The noise level changes are based on the assumption that each excitation component acts alone to excite dynamic forces and noise. In the planetary stages, excitation from sun and ring gear meshes interact and effective noise changes may not correspond to those shown in the table.

error on noise level is very small at the fundamental and reaches a maximum of a 2.4-db noise increase at the third harmonic. In the case of the ring gear and planet, where the manufacturing error showed only point-to-point variation about the design profile, the effect on noise level is even smaller, showing a maximum of 1.4 db at the third harmonic.

The gear excitation computer program may also be used to study the influence of any other gear design or operating parameter. As an illustration, the effect of gear loading on the upper sun and planet gearing has been examined. Figure 34 shows the pulsation curves for four load conditions ranging from 45 percent to 105 percent of rated gearbox load. The gear tooth profiles used are the design profiles, that is, inclined involute on the sun and true involute on the planet. This figure shows how the pulsations are increased as the load increases. Table VI gives the individual components of the gear excitation for both the sun-planet and planet-ring cases with design profiles. Increasing load brings up the excitation amplitude for all harmonics. Relative noise levels based on these amplitudes also increase with load, but not necessarily by a uniform amount. In the case of the planet-ring combination, load change from 45 percent to 105 percent of rated load will increase the noise level by 6.6 db in the fundamental component and by 6.9 db in the third harmonic component, but only by 4.2 db in the second harmonic component.

When the practical gear is considered, the manufacturing error present will take an added significance as the gear tooth deflection decreases with decreased load. At low loads, this manufacturing error will be the major source of gear excitation and noise, and further load reduction will have little benefit in reducing noise. Table VI shows this for the sun-planet mesh. Dropping the load from 85 percent to 1 percent of rated load drops the noise level less than 10 db.

Excitation components were computed for the conditions matching those under which in-flight noise measurements were made. These are tabulated in Table VII. The profiles used in the computation were taken from one of the measured profiles available for each type of gear. The loads used were those corresponding to the 85 percent of rated load observed during the cruise flight condition. Gear design data were taken from manufacturing drawings.

Since the computer program treats only spur gears, calculations for the spiral bevel gears involved a series of approximations. First of all, the bevel configuration was converted to an approximately equivalent parallel axis gear configuration using Tregold's approximation. Second, the spiral feature, already converted into an equivalent helical feature, was further reduced to an equivalent spur gear set. The spur tooth proportions, taken from the normal plane of the helical set, were used by the computer program to get tooth deflections. The fundamental of the mesh pulsations was estimated from these deflections after taking into account that load is shared by two or three pairs. No attempt was made to estimate the higher harmonic components for several reasons. The approximations made in converting the spiral bevel gears into equivalent spur gears lose their relevancy if the program is to be used to find higher harmonics in the

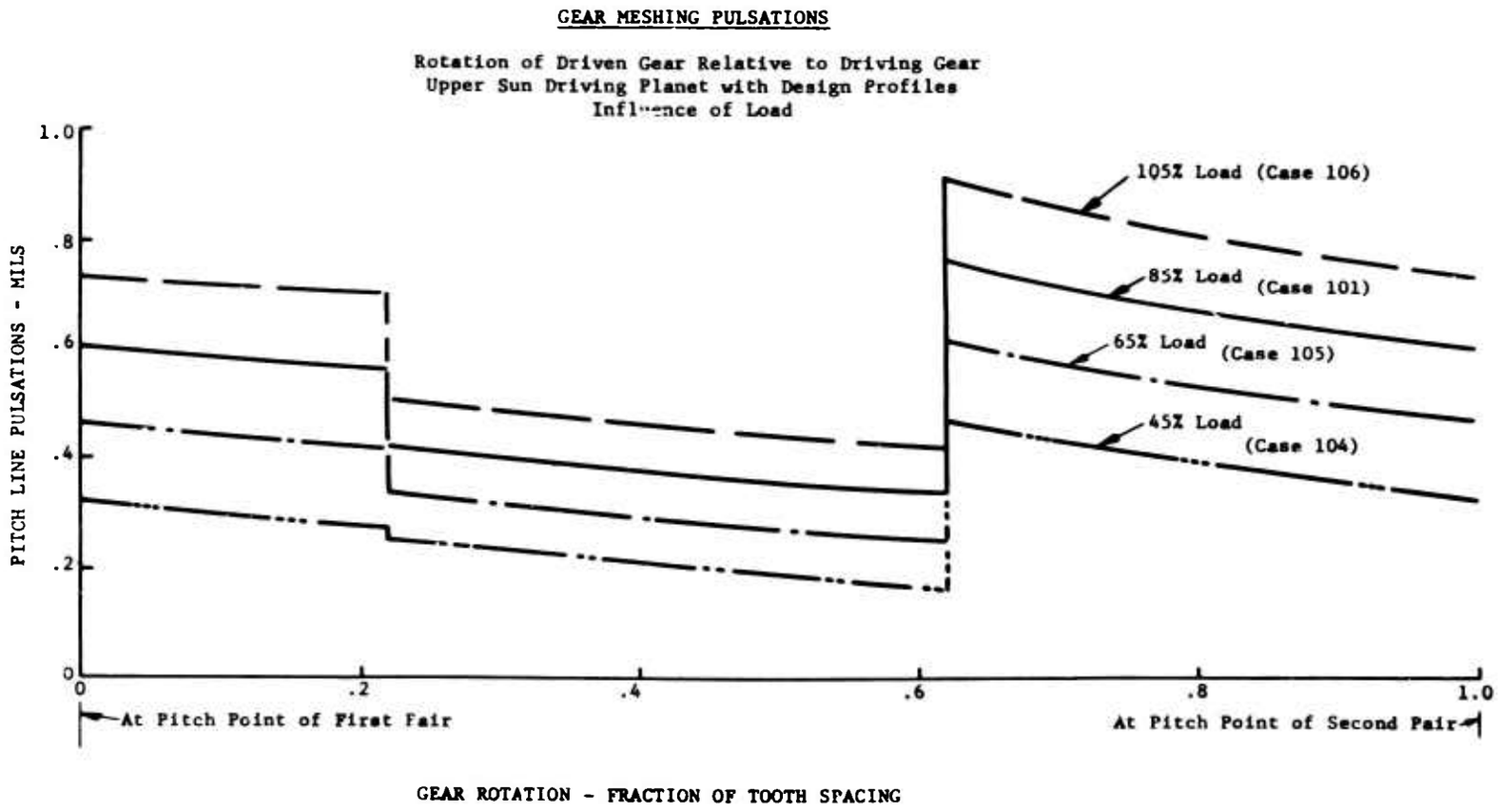

Figure 34. Gear Mesh Pulsations for Upper Sun Driving Planet Under Various Load Conditions.

TABLE VI. COMPARISON OF GEAR EXCITATION - EFFECT OF OPERATING LOAD

	Fund.		2nd Harm.		3rd Harm.	
	Ampl'-tude	Relative Noise Level	Ampli-tude	Relative Noise Level	Ampli-tude	Relative Noise Level
Upper Sun Driving Planet -with design profiles						
45% rated load (case 104)	.095 mil	-4.5 db	.048 mil	-3.3 db	.031 mil	-2.8 db
65% rated load (case 105)	.126	-2.1	.058	-1.6	.036	-1.6
85% rated load (case 101)	.160	0	.070	0	.043	0
105% rated load (case 106)	.192	1.6	.082	1.4	.049	1.1
Upper Planet Driving Ring -with design profiles						
45% rated load (case 304)	.090 mil	-5.0 db	.038 mil	-2.9 db	.023 mil	-5.0 db
65% rated load (case 305)	.125	-2.2	.045	-1.4	.301	-2.4
85% rated load (case 301)	.161	0	.053	0	.041	0
105% rated load (case 306)	.195	1.6	.061	1.2	.051	1.9
Upper Sun Driving Planet -with measured profile						
85% rated load (case 103)	.174 mil	0 db	.083 mil	0 db	.057 mil	0 db
1% rated load (case 114)	.081	-6.6	.044	-6.0	.023	-7.9

Note: The excitation amplitudes given in this table are the resultants of the sine and cosine components for each harmonic. These resultants do not reflect the phase shift for each harmonic which may accompany the changed load.

The noise level changes are based on the assumption that each excitation component acts alone to excite dynamic forces and noise. In the planetary stages, excitation from sun and ring gear meshes interact and effective noise changes may not correspond to those shown in the table.

TABLE VII. COMPUTED GEAR EXCITATION COMPONENTS - CRUISE FLIGHT CONDITION
Amplitudes - Zero to Peak - Microinches

				Fundamental			Second Harmonic			Third Harmonic		
Stage	Mesh	Profile	Tang. Load	Cos	Sine	Result.	Cos	Sine	Result.	Cos	Sine	Result.
Upper Planetary	Sun Planet	Measured	2500 lb	-55	165	174	65	-59	88	-57	-3	57
	Planet Ring	Measured	2500 lb	-153	28	156	47	26	54	40	-26	48
Lower Planetary	Sun Planet	Measured	1610 lb	-39	126	132	54	-45	70	-46	-3	46
	Planet Ring	Measured	1610 lb	-135	40	141	40	34	52	35	-33	48
Bevel	-	Involute	4300 lb	-	-	120						

mesh pulsation curves. Tooth profile information could not be obtained because profile measurements on spiral bevel teeth cannot be made with commercial inspection equipment. The true action between bevel gears is very much influenced by assembly dimensions, and this variable cannot be treated in the present gear excitation analysis. Furthermore, the multi-pair load sharing and the spiral gear action tend to eliminate the abrupt load transfer and associated abrupt change in tooth deflections which are present in spur gears. The smoother action gives a mesh pulsation curve closer to a sine wave than to a square wave. Hence, the higher harmonics, especially the second harmonic, will be less prominent. This reduced significance of the second harmonic of the bevel set was recognized in the narrow-band noise analysis, Figure 12.

DYNAMIC FORCE ANALYSIS

The typical study of the helicopter drive as a torsionally vibrating system has as its objective the determination of critical speeds and vibration modes, especially at the low frequencies associated with rotor rotation or similar excitation sources (see Reference 9). In such studies, practical considerations result in the neglecting of inertias and compliances of internal gearbox components, a simplification which does not introduce any major error in the results required. However, when the drive system is to be studied for torsional vibration in the range of frequencies associated with gear noise, the analysis must be more sophisticated. The inertias and compliances of internal components must be included, especially the inertias of the gear bodies and the compliances of the gear teeth. Furthermore, the exact dynamics of the planetary stages must also be considered. The new torsional vibration computer program contains these elements and, when applied to the helicopter drive system, begins to reveal the great complexity of the system, especially in the gearbox portions. Some of this complexity is observed in Figure 35. This is a frequency plot of the undamped dynamic forces developed at the bevel gear mesh by a unit displacement excitation introduced at the same point. This plot shows many critical speeds in the frequency range of from 500 to 5000 Hz. At frequencies above this range, the critical speeds are even more closely spaced, and the computer program as presently applied is unable to give a clear description of response characteristics. This limitation does not particularly handicap the noise level calculation. The frequency range below 5000 Hz contains all the gear excitation frequencies except the higher harmonics of the bevel gear set. As explained earlier, the excitation magnitude of these higher harmonics cannot be properly evaluated by the present gear excitation program because of the spiral character of the bevel gears. If the gear excitation program is extended to helical gears, however, the torsional vibration program will have to be revised to handle the higher frequencies.

Figure 35 shows the dynamic force going to infinite values at the critical speeds and also dropping to zero at those frequencies at which vibration absorption is taking place. The bevel gear excitation frequency in the test helicopter gearbox is at about 3000 Hz and falls at neither of these two conditions. It is therefore possible to accept the calculated dynamic force as a reasonable measure of the force actually existing in the gearbox

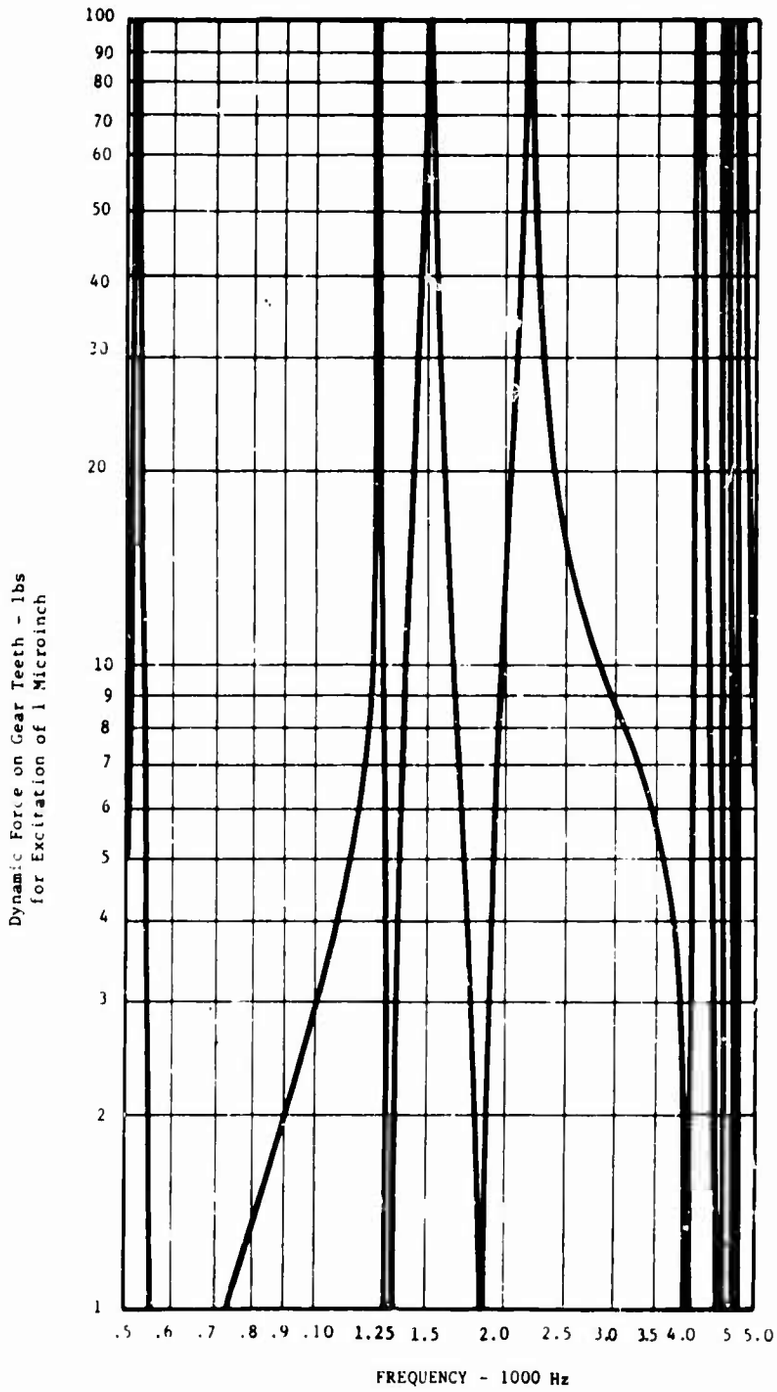

Figure 35. Dynamic Forces at Bevel Gear Teeth for Unit Excitation at the Same Point.

under the specified conditions. Dynamic forces from excitations whose frequencies are closer to the infinite or zero response points cannot be as reliably evaluated. Actual conditions in the drive system, specifically damping, prevent the infinite or zero response. Because the computer program permitted the introduction of damping at the bearings, this kind of influence was investigated. It was found that damping at these locations had an insignificant effect, even at the frequencies close to the critical speeds. Further consideration of the dynamics of the gearbox system indicated that the response at this gear excitation frequency range is dominated by the conditions in effect at or near the gear mesh points. These conditions include the gear teeth compliance and the gear body inertia and, very likely, also the gear teeth damping. Since the computer program, as explained earlier, was not written to include this factor, it could not be investigated. If gearboxes are operated with gear excitation frequencies near the critical speeds of the system, proper evaluation of the dynamic forces will require extension of the torsional vibration computer program to handle gear mesh damping.

The complexity of the torsional system is even more pronounced when the planetary stations are considered. While a simple gear set has only one meshing point associated with a particular excitation frequency, the planetary gearing has many. This plurality of excitations is due first to the number of planets and second to the meshing of each planet on both the sun and the ring gears. The multiple excitations introduce special problems. Although uniform magnitude of excitation has been assumed for all the meshing points around the sun, the phase relationship among these excitations is not necessarily identical. The actual phase relationship is determined by the relationship between the number of teeth on the sun gear, the number of planets, and the order of the harmonic. Only if the product of the number of teeth and the order of the harmonic is an exact multiple of the number of planets will the particular excitation be synchronized among the planets. When this is the case, the main torsional vibration computer program sums up the individual excitations and computes the combined dynamic forces. Under these conditions, the dynamic response within the planetary system can be influenced by such variables as the elastic compliance of the ring gear support or the elastic compliance of the planet carrier with respect to the output shafting or to changes in the adjacent portions of the overall drive system.

This system of synchronous excitation, however, is not the typical situation in planetary designs. Most often the number of sun gear teeth is intentionally selected so as not to have a common factor with the number of planets. In such a case, there will be no synchronous excitation among the planets until an order of the harmonic equal to the number of planets is reached. For example, in the lower planetary stage of the test helicopter gearbox, the number of teeth on the sun is 57 and the number of planets is 4. For the fundamental and second and third harmonics, the product of the number of teeth on the sun and the order of the harmonic is not an exact multiple of the number of planets. As a result, the excitation among the planets is not synchronous. Instead, the phase relationship is such that any impulse applied to the sun at one planet will be exactly countered by an identical impulse at the diametrically opposite

planet, at least as long as excitations of uniform magnitude are assumed. These phased excitations, fully balanced, cannot excite vibration of those system elements which are acted on by all planets simultaneously, elements such as the ring gear, the sun gear, the planet carrier, and elements of the drive system external to the planetary stage. The vibration which is excited under those conditions is of the individual planets vibrating against the compliant restraints of the meshing gear teeth and the planet bearing. At each planet, excitation will be introduced at both the sun-planet mesh and the planet-ring mesh. Excitation at either point will develop tooth forces at both points. The resultant dynamic tooth forces will be determined by the combination of the two excitations.

This condition of nonsynchronous excitation of the planets is analyzed by the auxiliary vibration computer program. Response curves calculated by this program are shown in Figures 36, 37, 38, and 39. For each of these curves, a unit excitation was applied at only one of the excitation points on the planet. Only when a particular relationship between the excitations at the sun and at the ring is assumed can the combined effect be shown.

All of these figures show a common patter[illegible]ly constant response at the lowest frequencies which falls off to [illegible]sponse at some intermediate frequency and which goes on at high[illegible]encies to give two critical speed conditions. The response curves for the two mesh points as caused by the same excitation are similar, but not identical. The first zero response frequencies for the two curves differ somewhat, but the infinite response frequencies are the same. Within one planetary stage, these infinite response frequencies are the same, regardless of the point at which the excitation is applied.

The vibration computer programs have been applied to the test helicopter drive system using dimensional data taken from design drawings. The previously calculated gear excitations, listed in Table VII, have been introduced. The calculated dynamic tooth forces are tabulated in Table VIII. The static tooth forces for the particular flight condition have been included. They show, in every case, that the dynamic forces are well below the level to cause tooth separation.

One value in this table stands out as especially noteworthy. This is the high force for the second harmonic of the lower planetary planet-ring mesh. The explanation for the high value lies in the closeness of the excitation frequency of 3964 Hz to the critical speed, or resonant frequency, of about 4200 Hz, shown in Figures 38 and 39.

NOISE LEVEL ANALYSIS

This final step in the noise calculation procedure is least supported by established and well accepted analytical methods. Justification for the validity of the calculation is more empirical in nature than analytical. Some of this empirical basis has been derived from the limited amount of testing performed. The selection of gear excitation frequencies has been

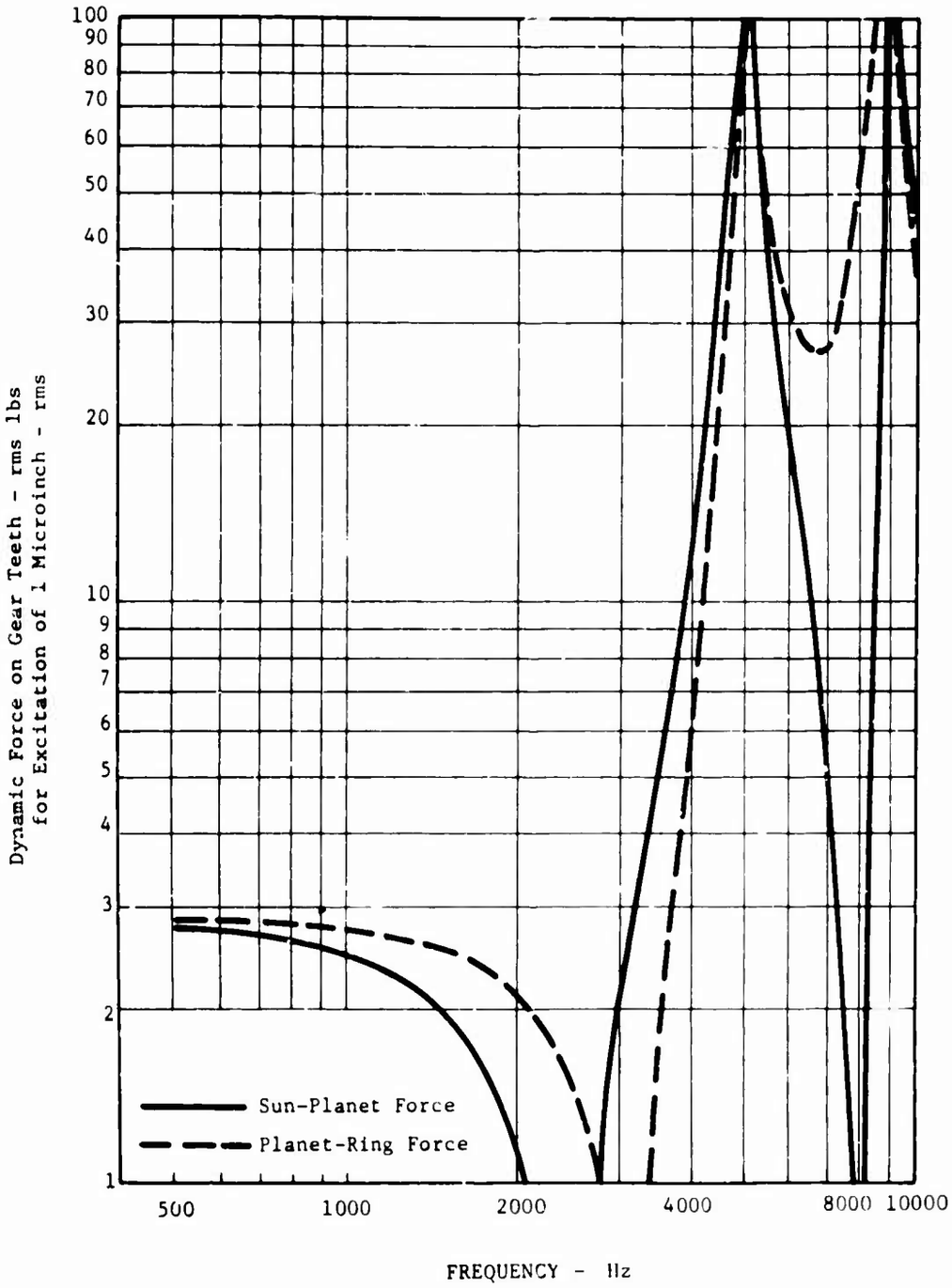

e 26. Dynamic Forces at Upper Planetary Gear Teeth for Excitation at Sun-Planet Gear Mesh.

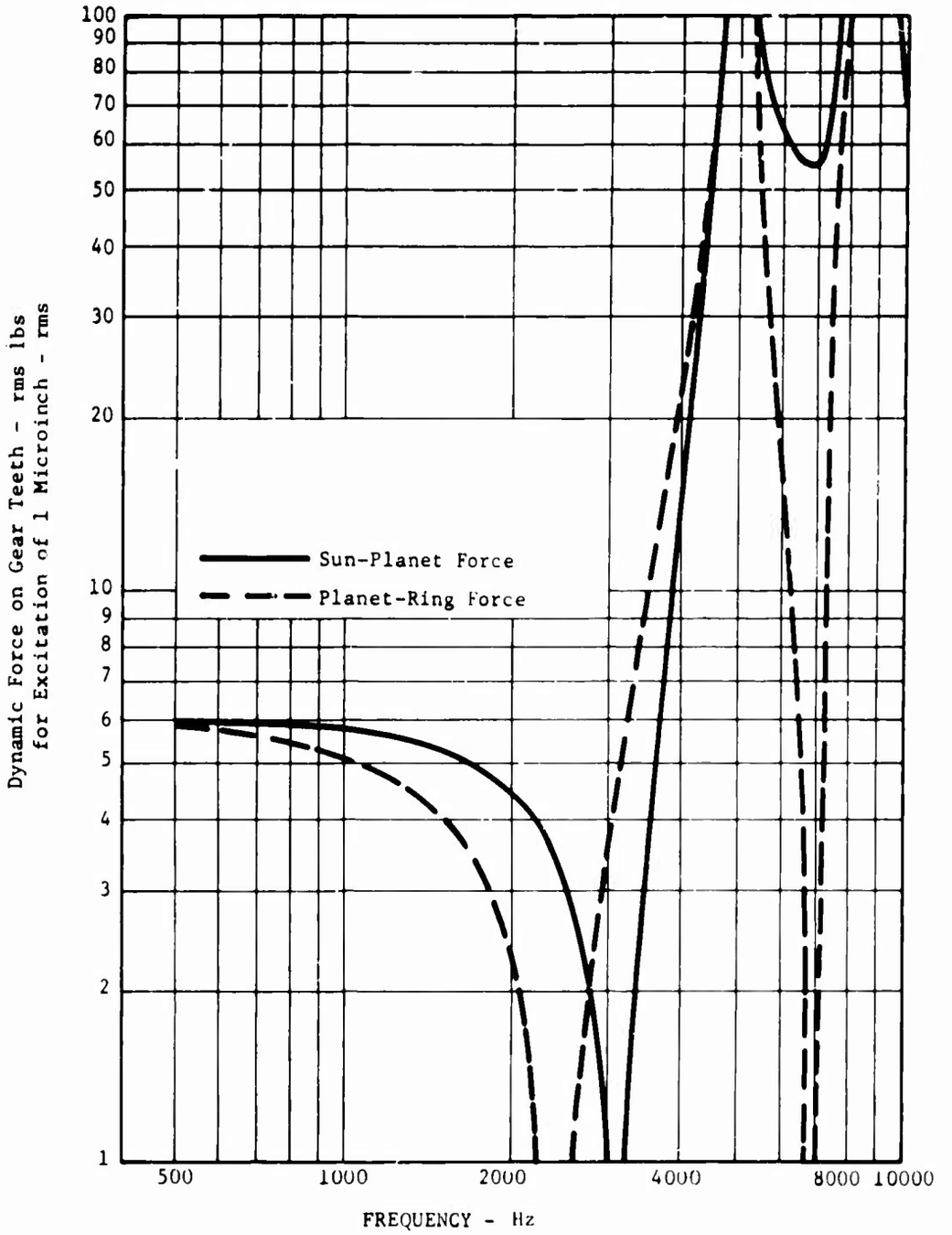

Figure 37. Dynamic Forces at Upper Planetary Gear Teeth for Excitation at Planet-Ring Gear Mesh.

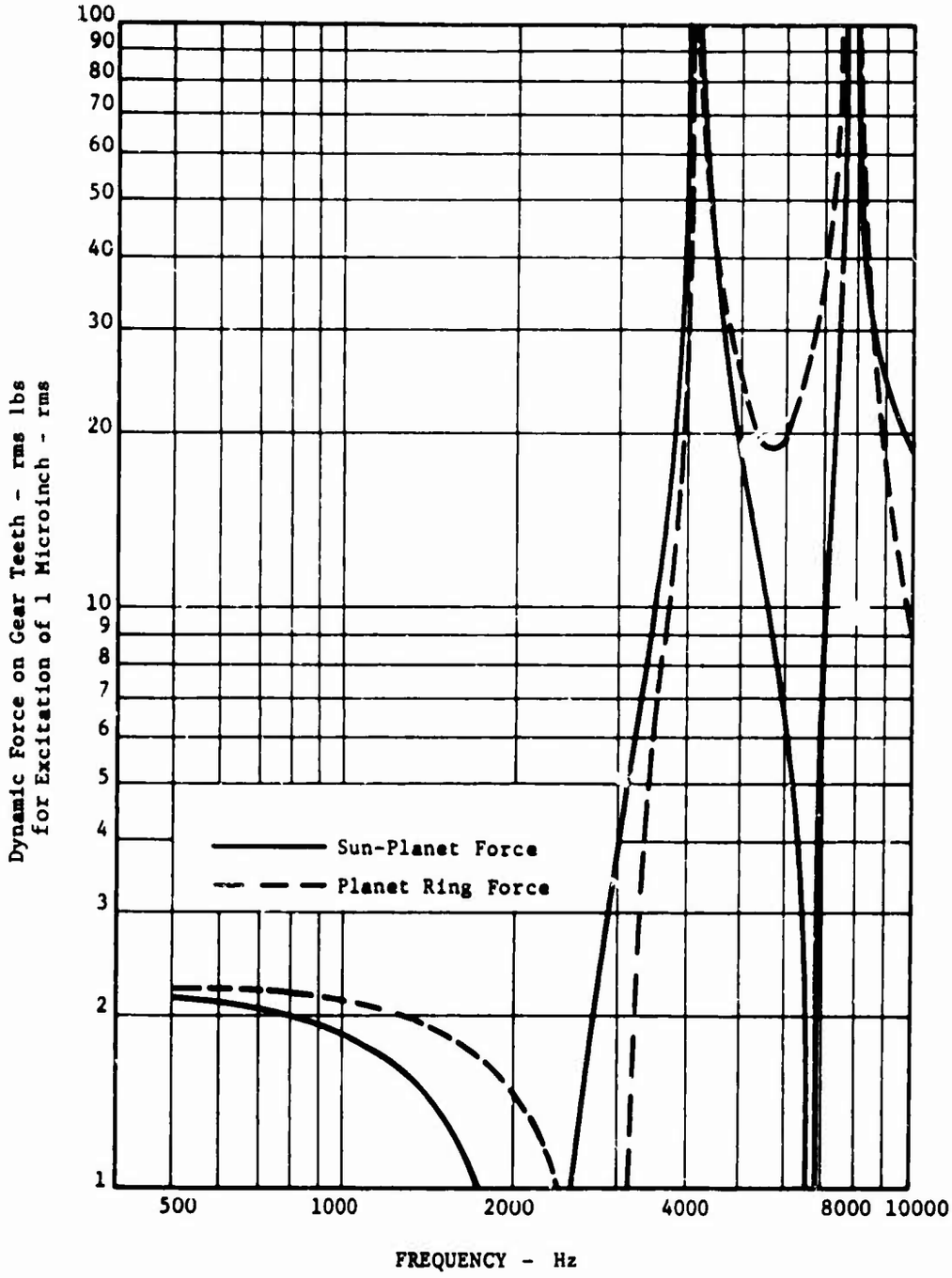

Figure 38. Dynamic Forces at Lower Planetary Gear Teeth for Excitation at Sun-Planet Gear Mesh.

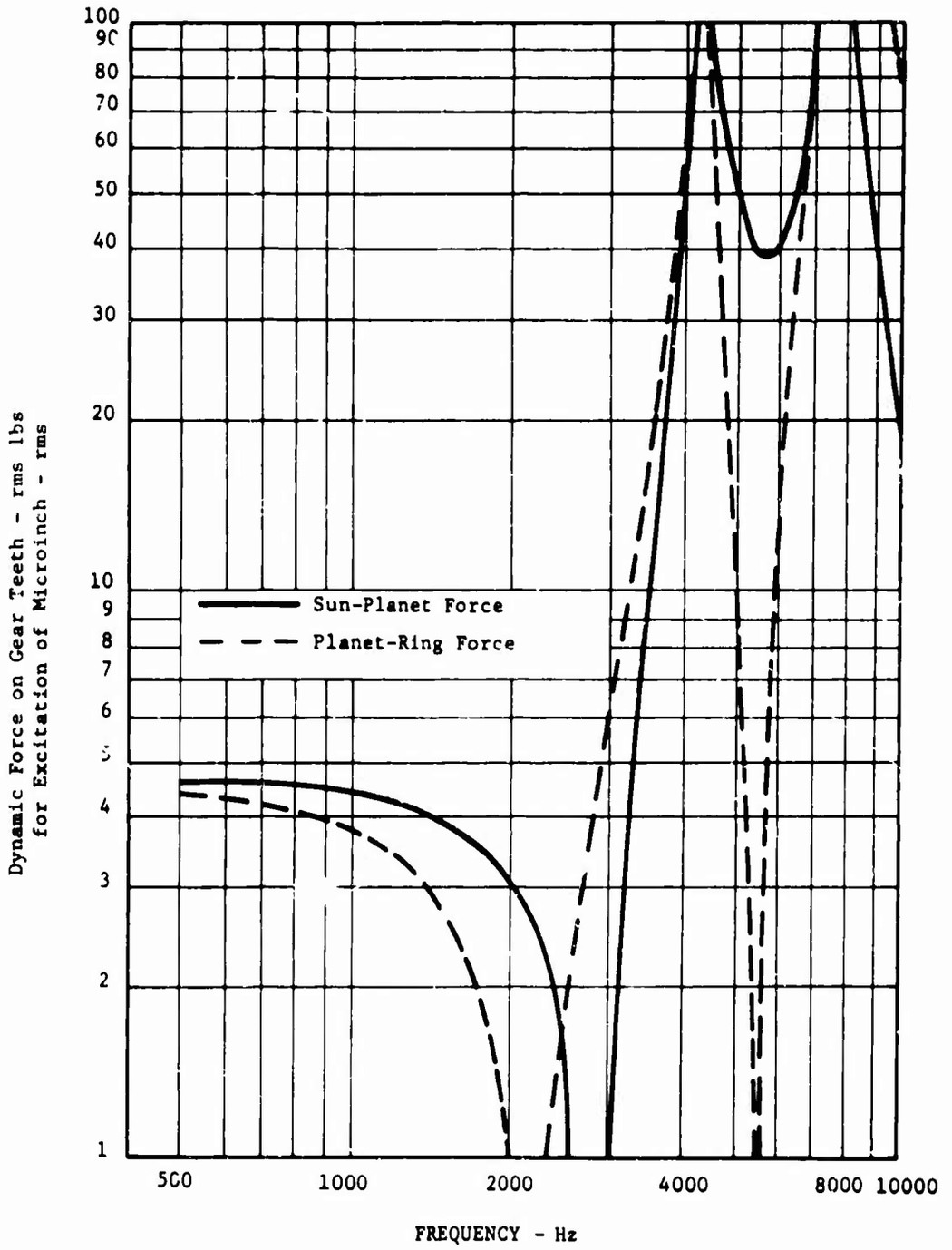

Figure 39. Dynamic Forces at Lower Planetary Gear Teeth for Excitation at Planet-Ring Gear Mesh.

TABLE VIII. COMPUTED GEAR TOOTH DYNAMIC FORCES - CRUISE FLIGHT CONDITION

Engine Speed 6600 rpm - 85% Rated Power
All Forces Tangential to Pitch Circles - LBS

Gear Stage	Static Force	Order of Harmonic	Frequency-Hz	Force at Bevel Gear Mesh	Force at Sun-Planet Mesh	Force at Planet-Ring Mesh
Bevel	4300	Fund.	3190	910		
Upper Planetary	2500	Fund.	644		234	234
		2nd Harm.	1288		83	87
		3rd Harm.	1932		20	25
Lower Planetary	1610	Fund.	1982		73	73
		2nd Harm	3964		870	707
		3rd Harm	5846		217	340

quite well substantiated by the noise measurements. The direct relationship between the vibration of the casing and the noise levels adjacent to the gearbox has been confirmed by the in-flight vibration measurements. The almost uniform casing response characteristics, except at the lower gear excitation frequencies, were demonstrated by the casing resonance tests. Other simplifying assumptions in the noise level analysis have not been individually verified by experiment or observation. Hence, justification for this new analytical tool must rest largely on a comparison of the final predicted noise levels and those measured in the aircraft.

The excitation and dynamic force values listed in Tables VII and VIII were combined with the relevant factors as explained and illustrated in Appendix VI. This gave predicted noise levels for each of the gear excitation frequencies studied. These frequencies fell in the range of about 600 to 6000 Hz. The higher harmonics of the bevel gear excitation had to be omitted because of the limitations in the analytical tools in their present state of development. The resulting noise levels have been plotted in Figure 40, which, like most of the noise level plots in this report, is on a third-octave band frequency scale. Of the eleven bands in the range of frequencies shown, the six "peak" bands contain at least one of the excitation frequencies. These discrete frequency noise components, as explained earlier,would establish the third-octave band levels even in an actual system with lower level random noise present. The five "valleys" in the plot were derived from the characteristics of a typical third-octave noise level analyzer. If it is assumed that the only noise present is at the gear excitation frequencies, and if such an analyzer were set at a band which did not contain any of these excitation frequencies, it would nevertheless record some low noise level. As explained in an earlier description of noise level plots, the imperfect signal filters in the analyzer would simply pass some of the signal from the noise frequencies in the adjoining bands. Under the actual conditions of random noise, these "valleys" would be raised, but would tend to stay below the adjacent peaks. Therefore, in interpreting the noise level plot in Figure 40, the "valleys" should be recognized as an artificial means of helping to show the "peaks", and attention should be directed only at these "peaks".

The measured noise levels shown in Figure 40 are in the form of two curves giving the maximum and minimum levels measured at each frequency for the three aircraft studied. The double curve is really an envelope of the three individual noise level curves of Figures 5, 6, and 7. This envelope conveys a measure of the variability of noise levels among aircraft and permits consideration of this variability in evaluating the comparison with the calculated results.

The two sets of results, measured and calculated, show rather good correlation. The three items of difference which do appear readily suggest explanations. The most apparent difference is the high calculated noise level in the 640 Hz band. The analytical procedure assumed uniform gearbox casing response for all gear excitation frequencies, but the measured response was actually uniform only at frequencies above about 2000 Hz and was decidedly lower at 640 Hz. This discrepancy at the lowest frequency therefore indicates that a more advanced analysis should give some

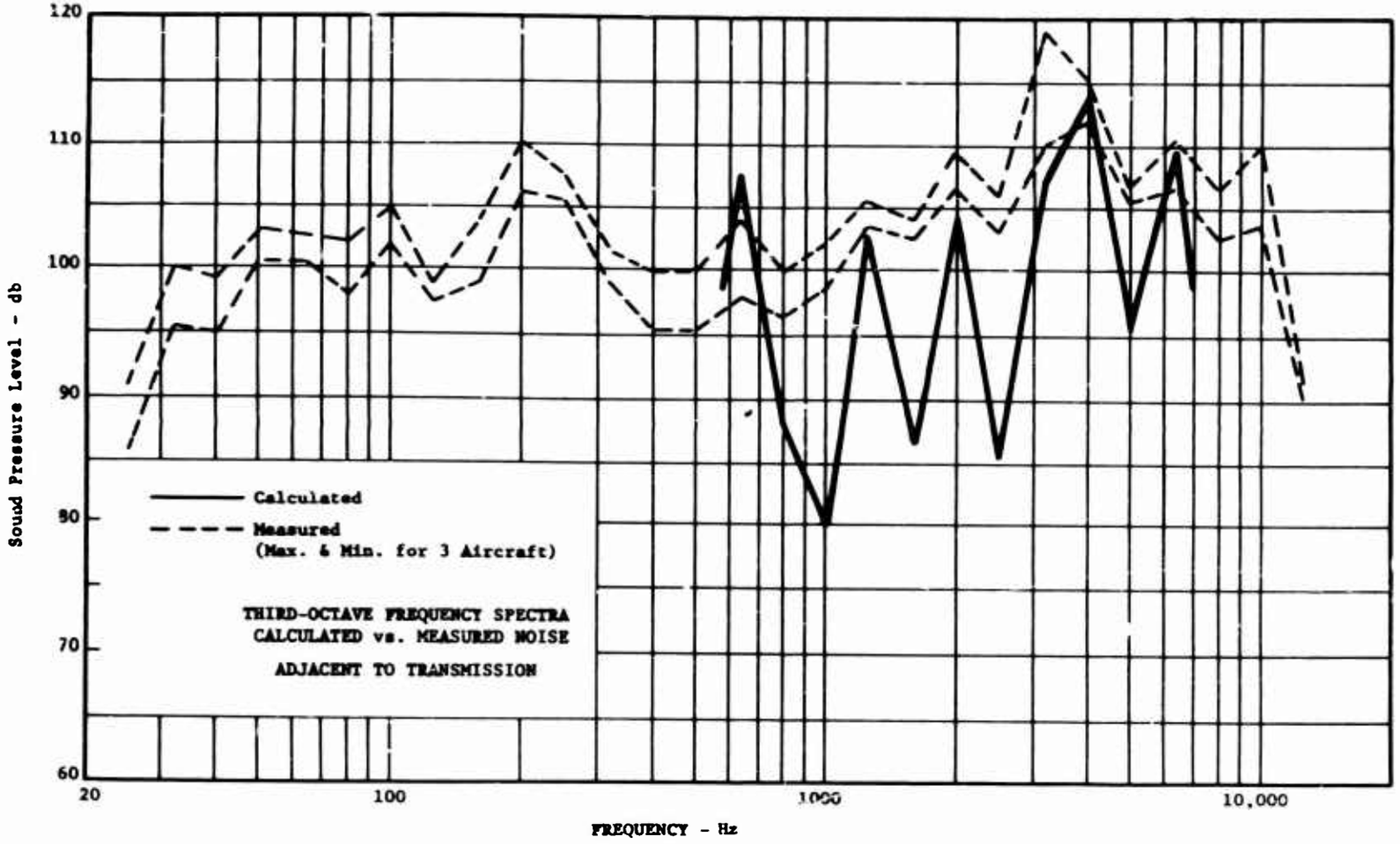

Figure 40. Comparison of Calculated and Measured Noise Levels Adjacent to the Gearbox, Cruise Condition.

consideration to this varying casing response. The second discrepancy worth noting is the somewhat lower overall level of the calculated values as compared to the measured values. This may be attributed to the sound reinforcement or reverberations in the enclosure surrounding the gearbox. The noise analysis assumes a "free field" noise radiation. This overall difference between the two curves is almost independent of frequency; therefore, it appears possible that this environmental factor can be accommodated in the analysis by an additional constant factor. The third item which attracts attention is more the difference between the two measured noise curves than it is the difference between measured and calculated curves. The noise levels in the 3200 Hz band resulted from the fundamental component of the bevel gear excitation. The unusually wide range between the maximum and minimum measured noise levels indicates that this excitation component is particularly variable, which is not too surprising for spiral bevel gears with all their additional elements of variability. The calculated level for this excitation, it should also be recalled, is based on an approximation necessitated by the limitations of the present gear excitation analysis. Since this bevel gear excitation may in some cases be an overriding factor in gear noise, an extended analysis which would better treat this source would be expecially valuable.

These differences between measured and calculated noise levels do not weaken the validity of the new analytical tools. Instead, they demonstrate how the analysis developed in this study can serve as a foundation on which to build more comprehensive and more detailed analytical methods for noise study.

MODIFICATIONS FOR NOISE REDUCTION

INTRODUCTION

The primary effort in this study has been directed toward developing and testing analytical tools for investigating the elements which contribute to helicopter gearbox noise. These tools have been made sufficiently general that they can be used for analytically evaluating a wide range of noise reduction measures. This includes most of the proposed design changes described in the noise control literature (References 6, 7 and 10), which up to now could be evaluated only experimentally. These changes which may be evaluated by the new analytical methods include:

- Increase of contact ratio
- Reduction of pitch
- Reduction of pressure angle
- Modification of tooth profile
- Improvement of tooth profile accuracy
- Increase of recess action
- Tooth impulse phasing
- Introduction of torsional discs
- Torsional isolation of ring gear

A comprehensive evaluation of all these noise reduction concepts, even if limited to a single set of operating conditions, would require an effort beyond the limits of this program. In place of a complete study, a few of these have been subjected to some investigation, as much for the purpose of illustrating the special capabilities of the new analytical tools as for the purpose of demonstrating the promise these items hold as noise reduction measures. It must be emphasized, however, that none of the modifications studied, even those that showed the greatest promise, were thoroughly pursued to bring out the full potential in them. (This will have to be part of a separate, and more systematic, investigation.)

The modifications considered fell within both the gear excitation and the dynamic force areas of noise production. These are described along with sufficient calculated results to give a quantitative character to the predicted benefits. Because the program, both experimentally and analytically, took into account the role of the gearbox casing, some consideration was also given to possible modifications in this area. The empirical nature of that portion of the analysis dealing with these factors prevented any kind of quantitative evaluation of possible noise reduction. Therefore, when this area is discussed, the suggestions will be presented without data, which will have to come from experimental work or, perhaps even better, from more extensive analytical studies.

GEAR TOOTH MODIFICATIONS

Examination of gear mesh pulsation curves, such as in Figure 27, reveals that the steps in the curves are the major culprits in producing all the gear excitation components from any pair of gears. The ideal curve would

be a horizontal straight line signifying no pulsations and, hence, no excitation. There appears to be no practical way to achieve this ultimate, but there are ways to make substantial improvement. The two to be described involve means of "smoothing out" the abrupt steps in the curves and means of bringing the high and low points in the curves closer together.

An often-suggested method is the use of modified profiles. Theoretically, it should be possible to add material to the tooth profile to compensate exactly for the displacement of the profile that takes place because of the deflection of the tooth under a specific load. But since the displacement characteristic has the rather abrupt step at two points, it would take a profile with a corresponding pair of steps to provide exact compensation. Unless these profile steps were perfectly positioned to synchronize with the load transfer positions, they could introduce a worse excitation characteristic. Other practical problems associated with such profile steps could come up in their manufacture and in their effect on the lubrication process between the teeth. For these reasons, another type of profile modification is proposed, one which will smooth out the step rather than eliminate it.

The dotted lines on the lower scales of Figures 28 and 29 show a first attempt at designing such a new profile modification for upper sun-planet mesh and upper planet-ring mesh respectively. These curves, in greatly exaggerated scale, show a ramp effect which acts to smoothen out the load transfer and thereby reduce the abruptness of the pulsation curve. The figures imply a double "hump" on each tooth flank, one inside and one outside the pitch circle. However, it may also be possible to divide this modification between the planet and its mating gear so that each has only one of the humps.

Before the potential benefit to be gained by such profile modifications is examined, it is necessary to consider also the role of profile manufacturing error. Any modification which gave improvement only when made without error would be of no value. To simulate the error which might be associated with such a profile, the measured point-by-point deviations from the design profile of each of the two gears, sun and ring, were simply added to the proposed modified profiles. The resulting "as-manufactured" modified profiles are also shown in Figures 28 and 29. In Figure 30, the effect of these profiles in the upper sun-planet mesh is shown. The pulsation curve is considerably smoother than the other profiles shown. The benefit of the modification is more effectively shown in the load transfer curve in Figure 30. An almost smooth transition of load is demonstrated. Because the degree of modification was not exactly matched to the load condition used, some abruptness still remains in both curves. The quantitative differences in excitation values and resulting noise levels between the present measured profiles and the proposed modified profiles are given in Table IX. The specific modifications under the particular load conditions do not benefit the fundamental noise components; in fact, in one case, the level is increased. The real benefits show up in the second and even in the third harmonics. More careful design of the modifications would likely give even greater benefits.

TABLE IX. COMPARISON OF GEAR EXCITATION - EFFECT OF NEW MODIFIED PROFILE

	Fundamental	Second Harmonic	Third Harmonic
Upper Sun Driving Planet at 85% Rated Load			
Excitation with Measured Profile - mil (Case 103) - with manufacturing error	.174	.088	.057
Excitation with New Modified Profile - mil (Case 110) - with Manufacturing error superimposed	.189	.013	.043
Effect of New Profile Modification on Noise	+.7 db	-16.6 db	-2.4 db
Upper Planet Driving Ring at 85% Rated Load			
Excitation with Measured Profile - mil (Case 303) - with manufacturing error	.156	.054	.048
Excitation with New Modified Profile - mil (Case 310) - with manufacturing error superimposed	.218	.015	.016
Effect of New Profile Modification on Noise	+2.9 db	-11.1 db	-9.6 db

Note: The excitation amplitudes given in this table are the resultants of the sine and cosine components for each harmonic. These resultants do not reflect the phase shift for each harmonic which may accompany the changed profile.

The noise level changes are based on the assumption that each excitation component acts alone to excite dynamic forces and noise. In the planetary stages, excitation from sun and ring gear meshes interact and effective noise changes may not correspond to those shown in the table.

Since the degree of profile modification is based on the gear tooth deflection, which is in turn based on the load transmitted, the effect of load on the modification benefits must be examined. Results of such load variations are shown in Table X. This may be compared with Table VI, where similar load variations and their effect on excitation levels in the case of the design profiles are given. The modified profile, very much like the standard profile, has a reduction in fundamental and third harmonic excitation as load is reduced. However, in the case of the second harmonic, the new modified profiles give excitation level reductions, and major reductions at that, when the load is increased, in contract to the opposite for the standard profile. This comparison demonstrates some of the promise to be found in this profile modification approach. Furthermore, this investigation of changing profiles shows the usefulness of the gear excitation program.

The second approach to gear excitation reduction to be mentioned is one which brings together the high and low points in the pulsation curve and at the same time provides some smoothing of abrupt steps in the curve. These benefits will be realized as the number of pairs of teeth in contact is increased from the present one and two to a preferable two and three. This can only be accomplished if helical gears are used in place of spur gears. Although the existing gear excitation program does not treat helical gears, some estimate of improvement can be made, particularly for the case of the fundamental noise component. In the case of spur gears, the pulsation curve has steps which correspond to the difference between the tooth deflection under full load and tooth deflection under half load, or what might be called one-half load tooth deflection. In the case of helical gears with two and three pairs stressing load, the pulsation curve would have steps corresponding to the difference between a one-half load tooth deflection and a one-third load tooth deflection, or a one-sixth load tooth deflection. This improvement from one-half for the spur to one-sixth for the helical gives a ratio of one to three, or a change of 9.5 db. A suitable design of the helical gear would go far in making the gear mesh pulsation curve resemble a sine wave more than the square-wave of the spur gear. Such a change in wave shape would materially reduce the second harmonic over and above the 9.5 db associated with the compressed pulsation amplitude.

The benefits inherent in the helical gear approach emphasize the need for, and value of, extending the gear excitation analysis to helical gears. Not only could the exact improvement be evaluated, but the optimum design would be more easily arrived at.

DRIVE SYSTEM MODIFICATION

There are two ways in which the drive system can influence the level of dynamic forces resulting from a particular set of gear excitations. When there is more than one point at which excitation of a certain frequency is introduced, the system design can determine the extent to which the several excitations combine or cancel each other. This is commonly referred to as tooth impulse phasing. The other system influence is through the vibration response or degree of vibration amplification which results from the

TABLE X. COMPARISON OF GEAR EXCITATION - EFFECT OF OPERATING LOAD WITH NEW MODIFIED PROFILE

	Fundamental		Second Harmonic		Third Harmonic	
	Amplitude	Relative Noise Level	Amplitude	Relative Noise Level	Amplitude	Relative Noise Level
Upper Sun Driving Planet - new mod. prof. with mfg. error						
45% rated load (Case 111)	.127 mil	-3.3 db	.043 mil	+10.4db	.035mil	-1.8db
65% rated load (Case 112)	.155	-1.7	.026	+ 6.0	.037	-1.3
85% rated load (Case 110)	.189	0	.013	0	.043	0
105% rated load (Case 113)	.222	+1.4	.005	- 8.3	.049	+1.2
Upper Planet Driving Ring - new mod. prof. with mfg. error						
45% rated load (Case 311)	.147 mil	-3.4 db	.033 mil	+ 6.4db	.013mil	+1.2db
65% rated load (Case 312)	.182	-1.6	.023	+ 3.7	009	-5.0
85% rated load (Case 310)	.218	0	.015	0	.016	0
105% rated load (Case 313)	.254	+1.3	.009	- 4.2	.026	+2.1

Note: The excitation amplitudes given in this table are the resultants of the sine and cosine components for each harmonic. These resultants do not reflect the phase shift for each harmonic which may accompany the changed load.

The noise level changes are based on the assumption that each excitation component acts alone to excite dynamic forces and noise. In the planetary stages, excitation from sun and ring gear meshes interact and effective noise changes may not correspond to those shown in the table.

resonance conditions in the system. Vibration and noise reduction then becomes possible by control of these two influences. An illustration of reduction in each of these respects is given below.

Each planetary stage consists of several vibrational subsystems, each made up of the sun gear, a single planet gear, the ring gear, and the planet support in the carrier. The flexible connections between the inertias are fairly well concentrated in the two gear meshes and in the bearing supporting the planet. Each of these subsystems has two points of gear excitation: at the sun-planet mesh and at the planet-ring mesh. It is the sum of these excitations which tends to vibrate the planet in its support, and it is the reaction to this vibration which sets up the dynamic forces in the meshing gear teeth. It is the phasing of these two excitations which is to be considered.

In the gearbox under study, the planet gears have been designed with an odd number of teeth. The effect of this on the excitation phasing is shown with the aid of Figure 41. The planet with odd-numbered teeth, on the left, has been drawn with the sun-planet mesh at the pitch points of the two gear tooth surfaces. The pulsation curve of this mesh, referenced to the pitch point, in the same manner as in Figure 27, is given below the gear sketch. Because the mesh at the ring gear uses the reverse side of the tooth, as shown, this mesh will also be at a pitch point, neglecting the effect of backlash. The planet-ring mesh pulsation curve is also referenced from the pitch point and is very similar in timing to that of the sun-planet. The stepped portions of both curves come fairly close to each other, making the combined excitation very close to the sum of the two individual excitations. If each of the pulsation curves is resolved into its separate former components, the corresponding components for both curves are nearly in phase and are additive.

If the planet gears were changed to have an even number of teeth, the mesh conditions would be as shown on the right side of Figure 41. The sun-planet mesh is again shown at the pitch point, but the planet-ring mesh is now displaced to a position corresponding to the midpoint between successive pitch points. The pulsation curves now are related in a new manner. The steps in the two curves are approximately opposite each other, and the effect tends to be one of cancellation between the two excitations. When the two curves are now resolved into their separate former components, the odd harmonics only see the 180-degree phase shift and experience cancellation, while the even harmonics still have the original phase relationship and remain cumulative.

The effectiveness of the cancellation is therefore seen to be determined by both the shapes and the amplitudes at the two pulsation curves. A further factor in the cancellation effect comes from the dynamics of the system. As seen in a comparison of Figures 36 and 37, for example, the response of the planetary subsystem is not identical for the excitations at the two different meshes. The cancellation effect at the two odd harmonics, the fundamental and third harmonic, is therefore influenced by their particular frequencies in relation to the subsystem resonances.

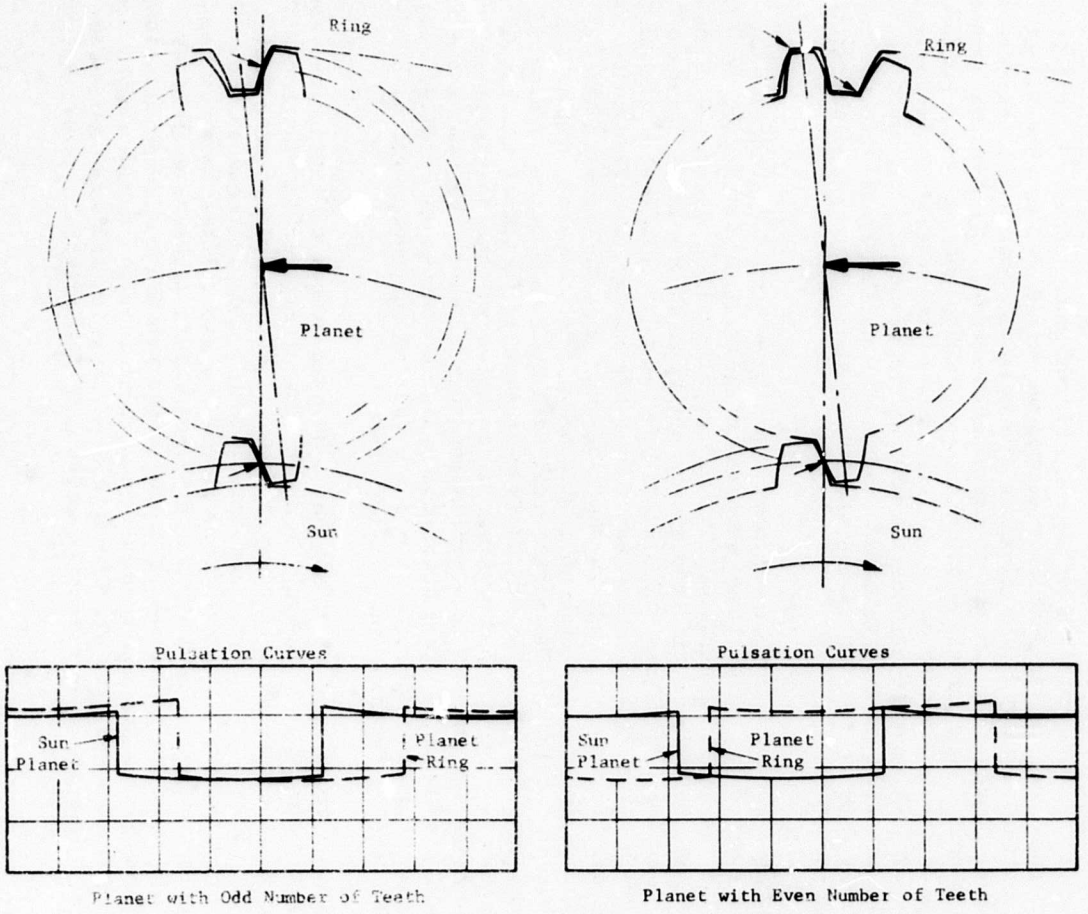

Figure 41. Planet Gear Design and Sun-Ring Excitation Phasing.

The combined effect of all of these influences for the gearbox study is given in Table XI. The data presented have resulted from first introducing the standard excitations into their respective planetary systems and computing the resulting dynamic forces at each meshing point, and then repeating this with the planet-ring excitations reversed in the fundamental and third harmonics. The total of the forces at both meshes are compared on a db scale to give an indication of the effect on predicted noise level. Improvement by phasing shows up only in the fundamental components and is fairly modest. The third harmonic shows an even greater increase in noise level. These first-try indications, however, should not be interpreted as showing the limited benefits to be expected from this sun-ring excitation phasing. The significant point, rather, is that careful design of the gears is first required to give pulsation curves which will best lend themselves to cancellation by reversed phasing. The parameters which will have to be varied in such design are the relative addenda and face widths.

The second illustration of noise reduction by drive system modification concerns a reduction in vibration response or free amplication. Figure 35 shows response characteristics for the bevel set; Figures 36 through 39, for the planetary stages. Any shift in resonance locations relative to the exciting frequencies which will bring the excitation frequencies further from resonant frequencies will have the effect of reducing dynamic forces and hence the noise levels. One difficulty which becomes apparent is that a change which helps at one of the noise components will not necessarily help as much, or at all, at the other noise components. This can be true if the change is made by changing the excitation frequencies, as by going to a different pitch with a proportionate change in the number of teeth and hence the gear meshing frequency. It can also be true if the change is made by changing an individual system inertia or stiffness to reposition the resonance locations or the frequency scale of the response curves.

An example of the latter has been calculated, with results shown in Table XII. For each of the planetary systems, the planet support compliance has been varied over a range from approximately one-third to ten times the present design value. The figures in the table show that the effect of the compliance change is uneven among the various harmonics. In the upper planetary system, a three-times increase in compliance reduces the predicted noise level of all three harmonics, but in amounts varying from 1.6 to 7.0 db. In the lower planetary stage, a corresponding change in compliance has a very different result. There is practically no change at the fundamental and third harmonics, and a moderate increase at the second harmonic.

This attempt by no means exhausts the possibilities of noise reduction by drive system modifications. There are many other points of system response modification which must be tried, individually and in combination.

GEARBOX CASING MODIFICATIONS

The experimental work performed on measuring gearbox casing vibration response showed appreciable amplification over most of the range of frequencies associated above 2000 Hz in contrast with the response at the lower frequency of 640 Hz. This suggests that there are elements

TABLE XI. COMPARISON OF PLANETARY DYNAMIC FORCES - EFFECT OF SUN-RING EXCITATION PHASING

Engine Speed 6600 rpm - 85% Rated Power - All Forces Tangential to Pitch Circles

Gear Stage	Order of Harmonic	Frequency Hz	Teeth in Planet	Sun-Ring Excitation Phasing	Force at Sun-Planet Mesh - lbs	Force at Planet-Ring Mesh - lbs	Change in Noise Level - db
Upper Planetary	Fund.	644	Odd number	As Designed	234	234	0
			Even number	Reversed	140	141	-2.2
	2nd Harm	1288	Odd	As Designed	83	87	0
			Even	Reversed	83	87	0
	3rd Harm	1932	Odd	As Designed	20	25	0
			Even	Reversed	52	53	+3.6
Lower Planetary	Fund.	1982	Odd	As Designed	73	63	0
			Even	Reversed	53	51	-1.2
	2nd Harm	3964	Odd	As Designed	87	50	0
			Even	Reversed	87	50	0
	3rd Harm	5946	Odd	As Designed	217	73	0
			Even	Reversed	389	227	+3.4

TABLE XII. COMPARISON OF PLANETARY DYNAMIC FORCES - EFFECT OF PLANET SUPPORT COMPLIANCE

Engine Speed 6600 rpm - 85% Rated Power - All Forces Tangential to Pitch Circles

Gear Stage	Order of Harmonic	Frequency - Hz	Planet Support Compliance 10^{-6} rad/in-lb	Force at Sun-Planet Mesh	Force at Planet-Ring Mesh	Mean Change in Noise Level db
Upper Planetary	Fund	644	.06	467	468	+3.0
			.20 present design	234	234	0
			.60	88	88	-4.2
			2.00	16	16	-11.6
	2nd Harm	1288	.06	188	192	+3.5
			.20 present design	83	87	0
			.60	15	19	-7.0
			2.00	21	16	-6.6
	3rd Harm	1932	.06	53	58	+3.9
			.20 present design	20	25	0
			.60	17	14	-1.6
			2.00	27	22	+ .4
Lower Planetary	Fund	1982	.075	284	274	+5.7
			.25 present design	73	73	0
			.75	92	92	+1.0
			2.5	186	181	+4.0
	2nd Harm	3964	.075	70	88	-10.1
			.25 present design	870	707	0
			.75	1704	1487	+3.0
			2.5	217	332	+5.2
	3rd Harm	5946	.075	479	525	+2.6
			.25 present design	217	340	0
			.75	217	340	0
			2.5	217	333	0

contributing to this differential level of response which might be exploited as a means of noise control. No attempt was made to investigate this because it lay outside the scope of the program. However, one possible approach is suggested by the test results. In Figures 22, 23, and 24, it may be noted that the vibration at each of the non-drive portions of the casing has a frequency characteristic that is generally similar to the vibration at the drive point. This confirms that excitation of vibration at one point on the casing travels, as it were, to the large areas of the casing, exciting them to similar vibration. Any barrier to such a transmitted effect would materially reduce the vibration of the casing and the noise it generates The reported benefits or ring gear isolation (References 7 and 10) might well be more a result of reducing the transmission of vibration energy generated at the ring gear to other parts of the casing than a result of any reduction in dynamic forces developed in the drive system itself.

Another aspect of gearbox casing design which should be considered is the mechanism whereby the mechanical energy of vibration of the casing is converted into acoustic energy. The factor representing this conversion in the analysis considers only the energy transfer to air from an uncoated metal body. This leaves open consideration of surface coatings or other surface treatments as possible means of reducing the sound generated by the casing vibration. A more thorough and quantitive understanding of this mechanism could well lead to effective means of gearbox noise reduction.

CONCLUSIONS

HELICOPTER GEARBOX NOISE

1. High noise levels result predominantly from the meshing action of the gear teeth. Most of the excitation is due to the periodic variation in deflection of the gear teeth as load transfers from tooth to tooth. Noise component frequencies correspond to the first three harmonics of the teeth meshing rates. Manufacturing imperfections in tooth profiles add to the excitation, but only to a small degree when the gears are highly loaded. Other gear manufacturing imperfections such as tooth spacing errors and runout are not significant contributors. Similarly, the bearings do not make a direct recognizable contribution to the high noise levels.

2. The overall power transmission system contains resonances in the general range of gear excitation frequencies. One excitation frequency in the gearbox falls close to such a resonance, leading to a higher noise level at that frequency. The gearbox casing has many structural resonances, but these tend to combine to give a fairly uniform response over most of the gear excitation frequency range.

3. The gearbox housing mounts are effective in attenuating vibration from the gearbox. The lift link is a relatively effective transmitter of vibration to the aircraft structure. There is a direct relation between housing vibration, and indirect indications point to a significant airborne mode of noise transmittal from gearbox to cabin.

4. A calculation procedure has been developed for predicting noise levels from design and operating data. The procedure includes calculation of gear excitation, dynamic gear forces, and acoustic power.

5. Noise measurements on three UH-1D helicopters show a high degree of uniformity. The calculated noise levels for the cruise condition shows good agreement with the measured levels.

MODIFICATIONS FOR NOISE REDUCTION

1. The new noise calculation procedure may be used to evaluate many of the widely proposed methods of noise reduction.

2. Individual design modifications generally affect each of the gear noise components to varying degrees and sometimes increase one while reducing another. The selection of optimum modifications therefore requires careful balancing of these effects.

3. Some of the more promising modifications and some measure of their expected improvements in noise level for the test gearbox are:

   Tooth profile modifications will be effective in reducing the second harmonic noise components by more than 10 db. With somewhat closer manufacturing tolerances, the third harmonic can be

reduced almost as much.

Reversing the sun-ring excitation phasing by going from odd- to even-numbered teeth on the planets will reduce the fundamental noise components by 2 db on the gears as presently designed. Greater improvement is possible if the gear tooth addenda are revised concurrently.

Shifting the relationship between the excitation and the resonant frequencies can reduce many of the noise components. For example, tripling the upper planet support compliance will reduce the upper planetary noise components by up to 7 db.

LITERATURE CITED

1. Sternfeld, H., Jr., Spencer, R.H., and Schaeffer, E.G., "Study To Establish Realistic Accoustic Design Criteria for Future Army Use", TREC Technical Report 61-72, June 1961.

2. Bell Helicopter Co., "UH-1A Internal Noise Survey", Report No. 204-099-278, 21 August 1961.

3. Harris, C.M., "Handbook of Noise Control", Chapter 2, McGraw-Hill Book Company, Inc., 1957.

4. Scanlan, R.H., "Noise in Rolling Element Bearings", ASME Paper No. 65-WA/MD-6, 1965.

5. Dudley, Darle W., "Principles of Acoustical Engineering of Gear Transmissions", presented at the American Institute of Aeronautics and Astronautics, Torpedo Propulsion Conference, U.S. Naval Underwater Ordnance Station, Newport, R.I., July 25, 1963.

6. Schlegel, Ronald G., King, Robert J., and Mull, Harold R., "Gear Noise", Machine Design, February 27, 1964.

7. Harris, C.M., "Handbook of Noise Control", Chapter 23.

8. Bell Helicopter Co., "Torsional Vibration Analysis of the AH-1G Helicopter Drive System", Report No. 209-099-043, 6 January 1967.

9. Schlegel, Ronald G., and Mard, Kenneth C., "Transmission Noise Control - Approaches in Helicopter Design", ASME Paper No. 67-DF-58, 1967.

10. O'Donnel, W.J., "Stress and Reflection in Built-in Beams", ASME Paper No. 62-WA-16, 1962.

11. Palmgren, Arvid, "Ball and Roller Bearing Engineering", 3rd Edition, SKF Industries, Inc., p. 46.

APPENDIX I

NOISE AND VIBRATION MEASUREMENTS

Two series of noise and vibration measurements were made on helicopters in operation. The first series was performed to obtain some data early in the program for preliminary analysis and to check out the installation and performance of the transducers and recording equipment in the helicopter. These measurements were performed on one UH-1D helicopter (Aircraft No. 65-9960) operating in level flight (6600 rpm engine speed, 75-80 knots airspeed, about 85 percent power). The second series of measurements was obtained on three UH-1D helicopters (Aircraft Nos. 66-1038, 66-1039 and 66-1043)* operating both in level flight (same conditions as above) and in the "flight-idle" condition on the ground (4,000-4,400 rpm, power estimated at 20-25 percent of full power).

In addition, limited data were obtained during takeoff and landing for the same engine speed and power settings as were used for level flight.

In this appendix, the instrumentation used in making the sound and vibration measurements and procedures for its calibration are described. Then, the results of the measurements are presented in graphical and tabular form. In general, there is no discussion of the results since the discussion using selected parts of the data is included in the main body of the report.

DESCRIPTION OF INSTRUMENTATION AND CALIBRATION PROCEDURES

The arrangements of instrumentation used to obtain, analyze, and record sound and vibration data are shown schematically in Figure 42. Specifics on the types and model numbers of the various components are given below:

Accelerometers (5) - Bruel & Kjaer (B & K) 4313
Microphones (3) - B & K 4133 - 1/2-inch condenser microphone, with B & K type 2630 battery-powered cathode followers.
Switch - Kistler 562 - 8-position
Sound Level Meter (SLM) - B & K 2203
Frequency Analyzers - B & K 2107 narrow band. B & K 1612-1/3 octave and octave band pass.
Microphone Amplifier - B & K 2603
Level Recorder - B & K 2305
Tape Recorder - Nagra III

The accelerometers have a mounted resonant frequency of 45 kHz, indicating an error of less than 1 db for an operating frequency range to 15 kHz. The condenser microphones have a flat frequency response over the range from 20 to 20,000 Hz. The sound level meter, which was used as the indicating amplifier, has an operating frequency range of from 10 to 20,000 Hz. The Nagra III recorders have a frequency range of from 30 to 15,000 Hz, flat within 1.5 db.

---

* The gearbox serial numbers on the three machines were A12-1386, A12-1388 and A12-1390 respectively.

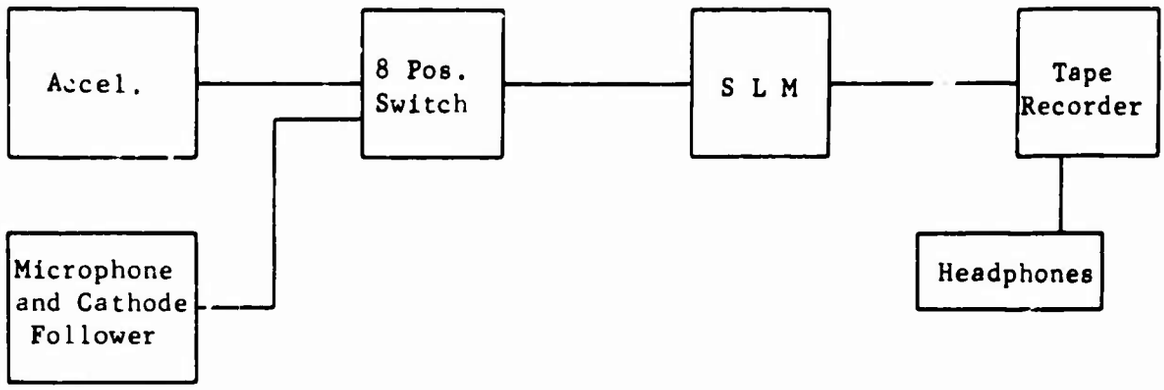

(a) Recording

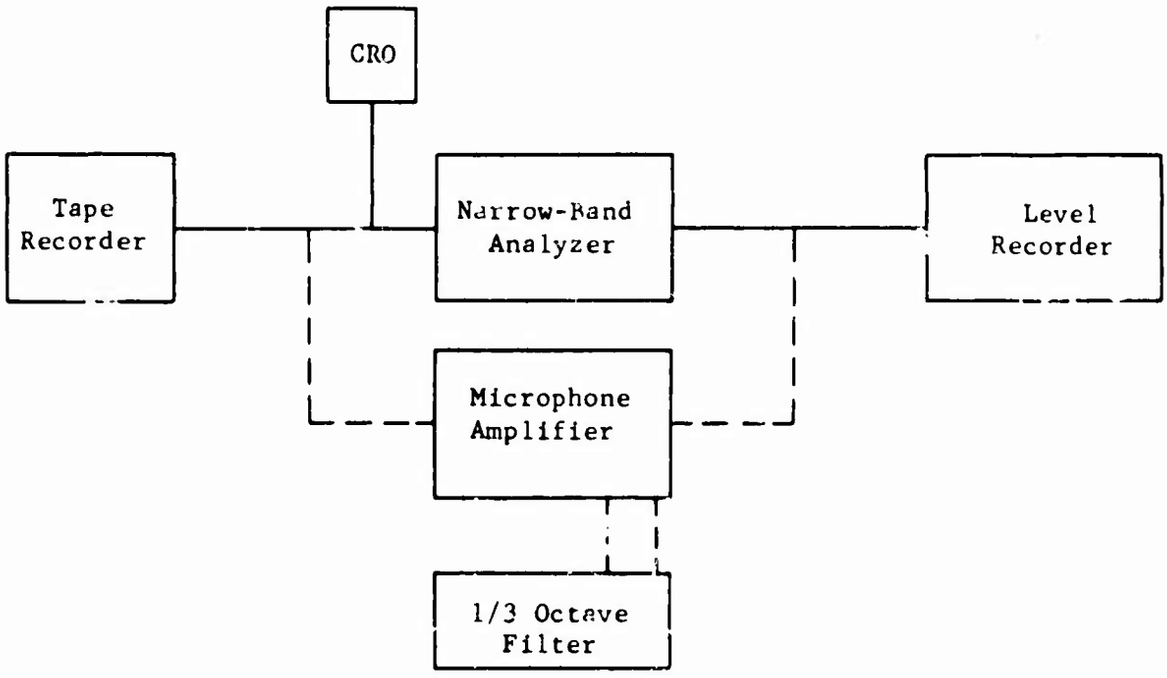

(b) Frequency Spectrum Analysis

Figure 42. Instrumentation Arrangements for Recording and Analyzing Sound and Vibration Data.

The equipment for readout and recording the accelerometer and microphone outputs was installed in the rear of the helicopter cabin. The leads to the accelerometers mounted on and around the gearbox were passed through a small hatch in the bulkhead which encloses the gearbox and separates it from the cabin. The installation of the readout and record equipment in the helicopter is shown in Figure 43.

One-third octave band and narrow-band frequency spectrum analyses were performed in the laboratory from the recorded signals. The selectivity characteristics of the one-third octave and narrow-band analyzers are illustrated in Figure 44. The bandwidth of the filters is determined by the ratio of the frequencies at the filter 3-db down points. For the one-third octave filter, this ratio is two-thirds; for the narrow-band filter, it is 6 percent of the center frequency. However, all of the "energy" under the filter curve is reflected in the filter output, even that part which is beyond the 3-db down points. During recording, the signals were monitored by earphones from the tape, on the sound level meter display and on the recorder VU meter.

The arrangements for calibration of the sound and vibration measurement systems were as follows:

1) Initial calibration of accelerometers - the accelerometers, leads, selector switch, and sound level meter were assembled in the same arrangement as was subsequently used for measurements on the helicopters. Each of the accelerometers was mounted in turn on an electromagnetic vibration exciter along with a reference calibration accelerometer. The reference accelerometer was connected to a Fluke 873A differential voltmeter using only the lead supplied with the accelerometer. The vibration exciter was adjusted for about 1 g peak acceleration at 100 and at 1,000 Hz, and readings were taken on both the differential voltmeter and the sound level meter (including both the meter reading and the recorder jack output). The calibration constant (in mv/g) of each of the measurement accelerometers with its leads, and including the selector switch, was obtained using the reference accelerometer and differential voltmeter as the standard. The differential voltmeter had recently been calibrated and was in use as a laboratory standard.

2) Calibration of the sound measuring system - a B & K type 4220 pistonphone was used for absolute calibration of the sound measuring system. When mounted properly on the microphone, the pistonphone produces a pure tone sound pressure of 124 db (re 2×10^{-4} μ bar) $\pm$ 0.2 db at 250 Hz. This signal was used to calibrate the sound level meter and was recorded on the tape recorder prior to each series of measurements in order to provide a calibration signal for setting up the analysis and level recording equipment.

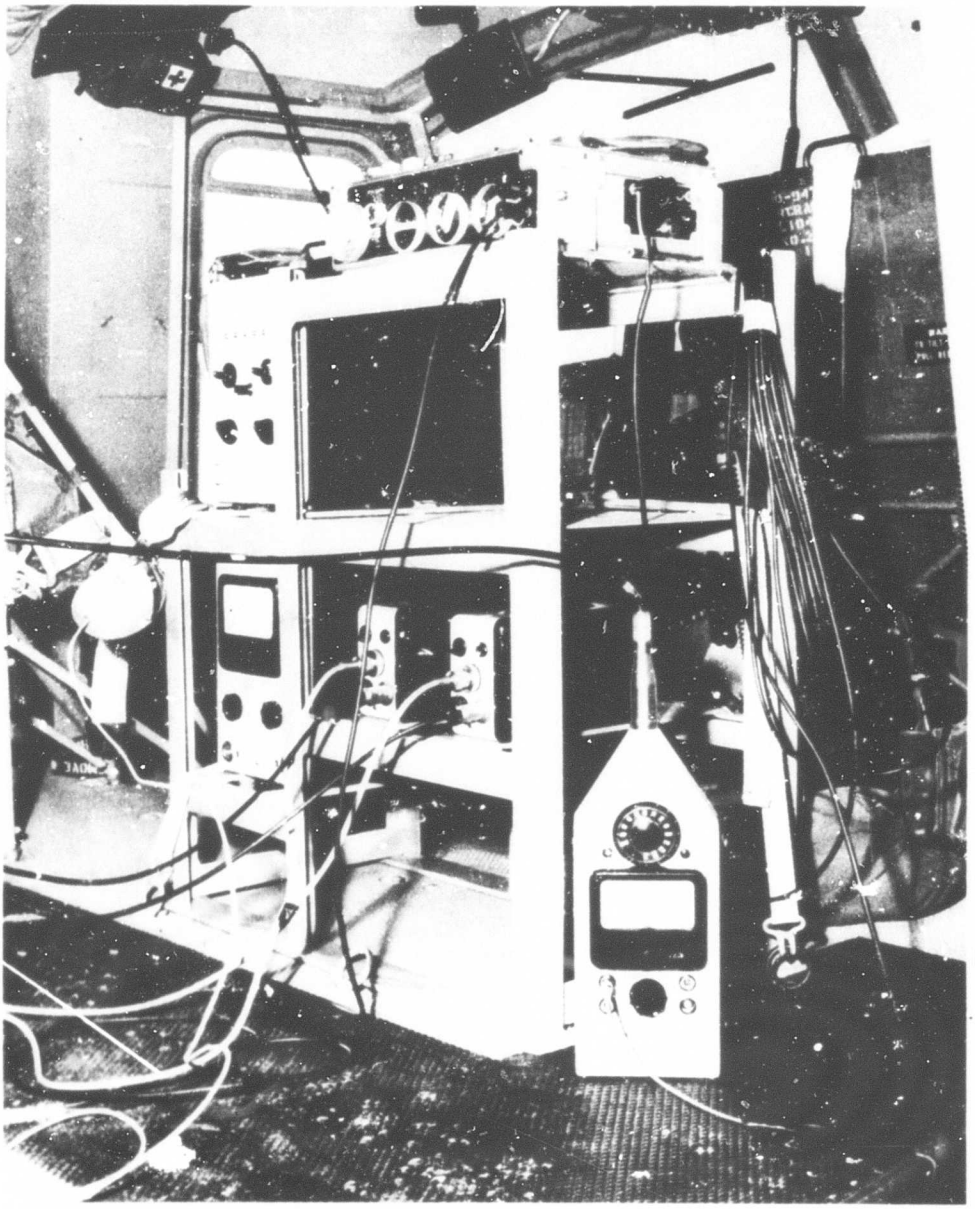

Figure 43. Installation of Recording and Readout Equipment in Helicopter.

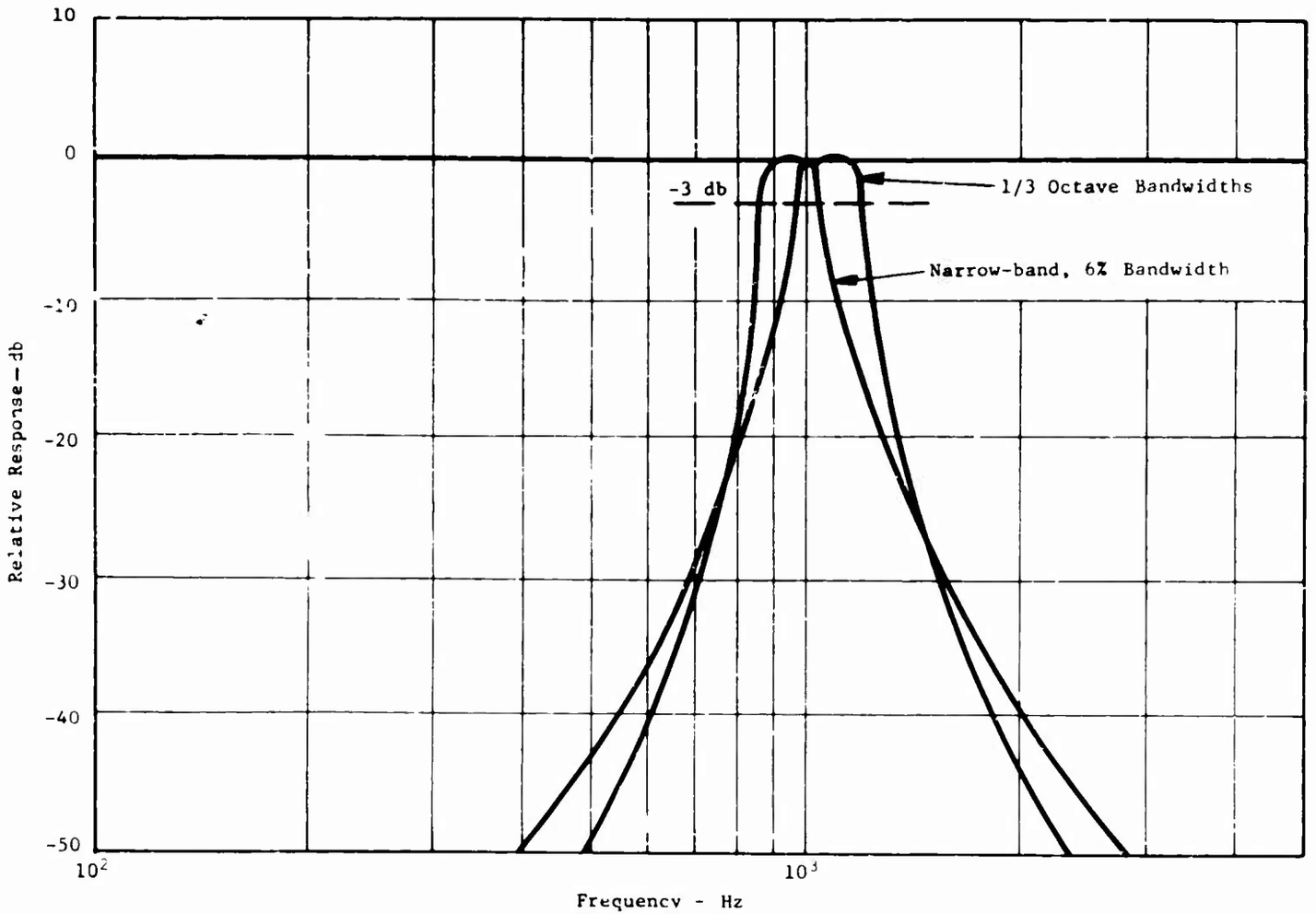

Figure 44. Typical Filter Frequency Selectivity Characteristics.

SOUND PRESSURE LEVEL MEASUREMENTS

The microphone locations for sound pressure level (SPL) measurements for both the first and second series of measurements are shown on a cabin layout schematic in Figure 45. In all cases, the microphones were positioned at about head level for a seated person. The location at the rear by the right side bulkhead of the gearbox compartment was at an open hatch in the bulkhead. When measurements were being made at the other positions, this hatch was blocked.

Overall SPL levels (linear response) for each measurement position and for all four machines are given in Table XIII.

One-third-octave frequency analyses of the SPL measurements for the second series of measurements are given in Tables XIV, XV, and XVI, for flight-idle operation, and Tables XVII, XVIII, and XIX, for cruise operation. The results of the narrow-band analysis of the measurements for cruise operation are given in Tables XX, XXI, and XXII. The center frequencies at which there are identifiable peaks or maxima, in the SPL spectrum, are listed with the amplitudes of SPL at those frequencies.

VIBRATION MEASUREMENTS

The locations of the accelerometers on the gearbox and its support structure for the first, preliminary series of measurements are shown in Figure 46. The accelerometers were mounted by cementing (using Eastman 910 adhesive) small steel blocks (5/8-inch square by 3/16-inch thick) to the gearbox or structure surface after removing the paint and thoroughly cleaning the surface with abrasive paper and solvent. Permanent magnet mounting blocks, supplied with the accelerometers, were used to attach the accelerometers to the steel blocks. The surfaces of the steel blocks were ground flat and smooth, except the one used at the ring gear housing location was shaped to fit the housing contour. At the conclusion of the flight test, the magnetic mounting blocks at the ring gear flange and upper lift link clevis positions were shifted slightly from their original positions on the steel blocks. It was resolved to use other, more positive, mounting methods for the final series of measurements.

Results of the first series of measurements are given in Table XXIII. These results are overall vibration levels at each measurement point with the instrumentation set for linear response from 20 to 20,000 Hz. The number of points for vibration measurement was reduced to five for the second series of measurements. The accelerometer locations for these tests were (referring to Figure 46):

1. Ring Gear Housing
2. Base - Front Corner
3. Base - Aft Corner
4. Upper Lift Link Clevis
5. Lower Lift Link Clevis

The method for attaching the accelerometer was changed by cementing

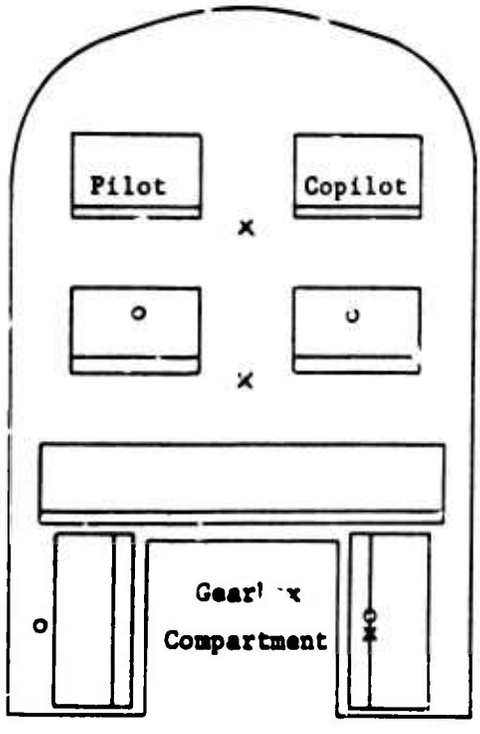

o Initial Series

×Second Series

Figure 45. Microphone Locations for Sound Pressure Level Measurements.

TABLE XIII. OVERALL SOUND PRESSURE LEVELS
(db, rms, re 0.0002 dyne/cm^2)

Aircraft No.	Microphone Position			
First Series	Main Cabin		Cabin Rear	
	Left	Right	Left	Right (open hatch)
Cruise				
65-9960	107.5	107	107	115.5

Second Series	Cabin Forward	Cabin Rear	At Open Hatch
Cruise			
66-1038	105.8	105.5	121.2
66-1039	105.2	105.7	120.8
66-1043	105	105.7	119
Flight Idle			
66-1038	101.5	100	117
66-1039	100.5	100	120.5
66-1043	97	97.2	117

TABLE XIV. TABULATED ONE-THIRD-OCTAVE FREQUENCY ANALYSIS OF SOUND MEASUREMENTS, FLIGHT IDLE OPERATION AIRCRAFT NO. 66-1038

SPL, db re 0.0002 dyne/cm^2

Center Frequency Hz	Measurement Position		
	At Gearbox Compt. Hatch	Behind Pilot	Rear of Cabin
20	<74	<67	<64
25	81.5	90.5	84
32	84	85.5	86
40	87	82	85
50	89.5	84	84
64	92.5	93.5	86
80	88.5	90.5	78
100	90.7	84	84
125	91	85	83.5
160	94.5	88.5	86
200	93.7	87	84.5
250	103.5	95	90.5
320	90.5	86.8	81.5
400	94	89.6	91.5
500	89	81.5	82
640	94	80.8	81
800	96.3	79.8	82
1000	101	80	78.5
1250	106	83.5	82.2
1600	102.1	80	78.6
2000	112.5	82.8	88.2
2500	106	83.5	80.5
3200	105.2	83.2	79.7
4000	105.2	82.2	78.1
5000	103.8	80.8	77.6
6400	111.2	91	86.3
8000	111.5	87	82.5
10,000	96	75.9	73
12,500	100	74.2	70.5
16,000	84	<67	64
Lin	117	101.5	100

TABLE XV. TABULATED ONE-THIRD-OCTAVE FREQUENCY ANALYSIS OF SOUND MEASUREMENTS, FLIGHT IDLE OPERATION AIRCRAFT NO. 66-1039

SPL, db re 0.0002 dyne/cm^2

Center Frequency Hz	Measurement Position		
	At Gearbox Compt. Hatch	Behind Pilot	Rear of Cabin
20	<74	<64	<64
25	78	76	80
32	82.5	83	83.5
40	96	91	89.5
50	94	89.5	89.5
64	90	83.5	82.5
80	94	91	85
100	89	78.5	84.5
125	88.5	81.5	84
160	95.5	85.5	84
200	97.5	93.5	89.5
250	105.5	89.4	88.4
320	95.5	83	81.5
400	97.5	86.5	85.8
500	96	84.5	82.5
640	93	77.5	81.4
800	102	83.5	83.5
1000	96.5	80.5	80.2
1250	109.2	82	85.8
1600	102.2	77.8	79.2
2000	111.8	83.5	80.8
2500	109.5	83	81.3
3200	105.5	81	80.5
4000	107.5	81.5	81
5000	106.5	81	79.5
6400	105.5	83.2	84
8000	104.5	84	84.5
10,000	97	75.5	75
12,500	96	71	72
16,000	90	66	65.5
Lin.	120.5	100.5	100

TABLE XVI. TABULATED ONE-THIRD-OCTAVE FREQUENCY ANALYSIS OF SOUND MEASUREMENTS, FLIGHT IDLE OPERATION AIRCRAFT NO. 66-1043

SPL, db re 0.0002 dyne/cm^2

Center Frequency Hz	Measurement Position		
	At Gearbox Compt. Hatch	Behind Pilot	Rear of Cabin
20	< 74	< 54	< 64
25	78	80	72
32	78.5	79.5	82.5
40	82	84	82
50	85.5	76	80
64	93	83.5	85.5
80	85	79	76
100	84	75	81
125	91	79.5	80.5
160	94	85.5	85.5
200	93.5	87.5	78.5
250	91	78	79.5
320	89.5	79	84.5
400	92	84	84.5
500	92	84	84.5
640	94	77	81
800	95	79.4	86
1000	101	78	82
1250	104.5	78	81.5
1600	104	77.5	79.5
2000	110.5	80	81
2500	104.5	80	80.6
3200	105.5	80	81.7
4000	106.5	80	80
5000	102.8	78.[illegible]	79
6400	112.5	85.5	90.7
8000	105	82.5	89.8
10,000	93	72	74.5
12,500	97.5	70	72.4
16,000	84.5	59.5	64
Lin.	117	97	97.2

TABLE XVII. TABULATED ONE-THIRD-OCTAVE FREQUENCY ANALYSIS OF SOUND MEASUREMENTS - CRUISE OPERATION AIRCRAFT NO. 66-1038

SPL, db re 0.0002 dyne/cm^2

Center Frequency Hz	Measurement Position		
	At Gearbox Compt. Hatch	Behind Pilot	Rear of Cabin
20	<74	<64	<64
25	91	84	87
32	95.5	98.5	92
40	95	89	87.5
50	101.5	89	96.8
64	101.3	91	92.5
80	98	92	89.5
100	102.5	92.5	93.5
125	97.5	92.5	96
160	99	95.5	94.5
200	107.5	95.5	96
250	105.5	93.5	97.5
320	99	95.7	91
400	95.5	91.5	88.5
500	95.5	85.7	87
640	99	85.7	86.7
800	96.5	82	83.5
1000	100.5	82	82
1250	105.5	80	81.5
1600	102.3	79.5	79.5
2000	106.3	84.2	83.5
2500	104	77.4	78
3200	118	85.5	87.2
4000	113	85.5	83.3
5000	105.8	78.3	78.3
6400	110.8	80	78.8
10,000	105	79	81
12,500	88	66.5	66.5
16,000	78.5	<64	< 64
Lin.	121.2	105.8	105.5

TABLE XVIII. TABULATED ONE-THIRD-OCTAVE FREQUENCY ANALYSIS OF SOUND MEASUREMENTS - CRUISE OPERATION AIRCRAFT NO. 66-1039

SPL, db re 0.0002 dyne/cm^2

Center Frequency Hz	Measurement Position		
	At Gearbox Compt. Hatch	Behind Pilot	Rear of Cabin
20	<74	< 64	< 64
25	86.5	83.5	87
32	98.5	98	90
40	97.5	91	93.5
50	103	91	97
64	102.5	90.5	91.5
80	99	88.5	87
100	105	95	99
125	99	91	94
160	101.5	96.5	92.5
200	110	95.5	95.5
250	107.4	95	95.5
320	101.5	92.5	91.5
400	100	89	89
500	96.5	90.5	86
640	101.5	86.5	88.5
800	98	81.5	84
1000	98.5	81.5	81.5
1250	103.5	81.5	82.5
1600	102.7	78.5	78.8
2000	108.7	80	80.5
2500	103	78.5	79
3200	110.5	85.2	80.5
4000	115.5	89.4	89.5
5000	106	79.3	78.4
6400	110	81	79.7
8000	106.4	79.5	78.5
10,000	110	82	83.5
12,500	92.5	68	67.2
16,000	81.5	< 64	< 64
Lin.	120.8	105.2	105.7

TABLE XIX. TABULATED ONE-THIRD-OCTAVE FREQUENCY ANALYSIS OF SOUND MEASUREMENTS - CRUISE OPERATION AIRCRAFT NO. 66-1043

SPL, db re 0.0002 dyne/cm^2

Center Frequency Hz	Measurement Position		
	At Gearbox Compt. Hatch	Behind Pilot	Rear of Cabin
20	< 84	< 64	< 74
25	90	82	68
32	99.5	96	88.5
40	99	88.5	88.5
50	103	89	95
64	101	92.5	93.5
80	102	90	88.5
100	102	91	91.5
125	99	91.3	91
160	104	95	93
200	106	93.5	97.3
250	106	93	93
320	99.5	90.8	81.5
400	99	86.5	88
500	100	88	94
640	104	94.5	93.5
800	100	84	83
1000	102	84.3	82.5
1250	105.5	81.2	83
1600	104	81.2	80
2000	109.5	84.4	83
2500	106	80.5	81
3200	110	86	83.5
4000	112	85	84.5
5000	105.6	80	79
6400	106.5	80.5	81.5
8000	104.5	80	79
10,000	103.5	80	81
12,500	90.5	67	< 74
16,000	< 84	< 64	< 74
Lin.	119	105	105.7

TABLE XX. NARROW-BAND FREQUENCY ANALYSIS OF SPL MEASUREMENTS FOR CRUISE OPERATION, AIRCRAFT NO. 66-1038

Measurement at Hatch to Gearbox Compartment		Measurement Behind Pilot		Measurement At Rear of Cabin	
Frequency Hz	SPL db re 0.0002 dyne/cm^2	Frequency Hz	SPL db re 0.0002 dyne/cm^2	Frequency Hz	SPL db re 0.0002 dyne/cm^2
22	96	21.5	97	22	96
26	86	27	83	26	83
33	94	33	98	27	85
44	96.5	44	88	28	84
54	101	55	87	32	89
73	85	73	92	44	84
83	86	100	5	54	94
97	88	142	90	73	87
110	89	165	93.5	110	91
165	87	220	88	140	94
220	108	265	91	163	92
270	101	280	94	195	91
285	101	300	93	220	95
300	94	320	92	230	94
320	93	670	83	240	91
360	94	800	79	270	94
440	91	1100	79	290	93
670	96	2000	83	300	89
1100	100	3250	84	320	88
1300	105	4000	82	360	87
1950	105	6000	78	540	83
3200	117	9200	82	1320	77
4000	113			1900	80.5
6000	110			3200	84
9200	94			4000	79
				6000	76
				9200	77
				9700	78

TABLE XXI. NARROW-BAND FREQUENCY ANALYSIS OF SPL MEASUREMENTS FOR CRUISE OPERATION, AIRCRAFT NO. 66-1039

Measurement at Hatch To Gearbox Compartment		Measurement Behind Pilot		Measure[illegible]t Rear c[illegible]	
Frequency Hz	SPL db re 0.0002 dyne/cm^2	Frequency Hz	SPL db re 0.0002 dyne/cm^2	Frequency Hz	SPL db re 0.0002 dyne/cm^2
21.5	96	21.7	92	21.5	96
32	100.5	27	79	27	82
44	96	32.2	98.5	32	89
56	102	43	88.5	43	93.5
65	98	55	91	55	96
72	97	64	90	64	80
110	104	72	88	72	85
132	97	98	85	88	83.5
165	98	112	92	98	92.5
220	110.5	140	87	112	99
250	107	166	95.5	165	89.4
270	104	195	92	200	92
290	105.5	260	92.5	255	92
360	102	275	97	270	94
450	95	330	88	280	93
650	103	360	89	295	87
740	97	400	87	360	91
780	95.5	450	85	550	83
870	96	650	85	645	86
1100	97.5	1020	78	1100	79
1300	105	1060	78	1300	84
1900	109.5	1300	82	1900	80
2230	100	1900	78	2100	77
3200	110.2	2700	77	2800	79.5
4000	115.5	3200	87	3200	82
6000	109	4000	87	4000	84
8000	102	6000	81.5	6000	8[illegible]
9500	113.5	8300	81.5	9500	86.5
		9600	87		

TABLE XXII. NARROW-BAND FREQUENCY ANALYSIS OF SPL MEASUREMENTS FOR CRUISE OPERATION, AIRCRAFT NO. 66-1043

Measurement at Hatch To Gearbox Compartment		Measurement Behind Pilot		Measurement At Rear of Cabin	
Frequency Hz	SPL db re 0.0002 dyne/cm^2	Frequency Hz	SPL db re 0.0002 dyne/cm^2	Frequency Hz	SPL db re 0.0002 dyne/cm^2
21.5	94	21.5	93	21.5	96
27	86	32	98	32	86
32	97	44	83	44	88
44	98	55	88.5	55	95.5
54	102	64	87	64	88
72	99	72	88	72	92
85	96	97	86.5	85	77
110	105	110	90	98	92
140	94	150	91.5	110	96
165	98	165	92.5	125	88
200	101	190	90.5	135	91
220	110	218	94	165	92
270	102	255	89	220	98
320	94	275	92	265	90
500	98	320	88	280	90
640	103	500	84.5	300	89
1100	104	640	94.5	320	89
1300	104.5	800	80	440	86
1900	107	1100	82	520	94
2800	106	1300	79.5	640	92
3200	106	1600	77	840	80
4000	111.5	1850	84	1100	84
6000	105	2750	79.5	1300	83
8000	100	3200	82.5	1850	84
9200	109	4000	87	2800	82
		4800	75	3200	90
		6000	80	4000	85
		9300	81	6000	80
		10,200	74	9200	87

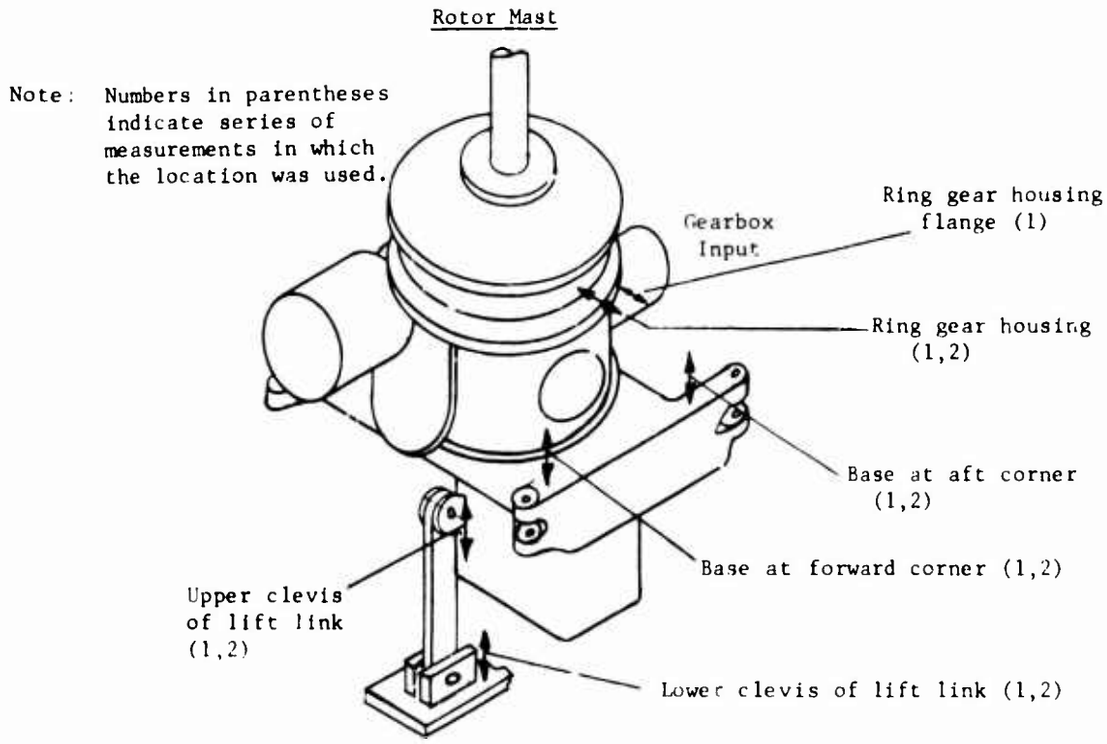

(a) Entire gearbox with lift link.

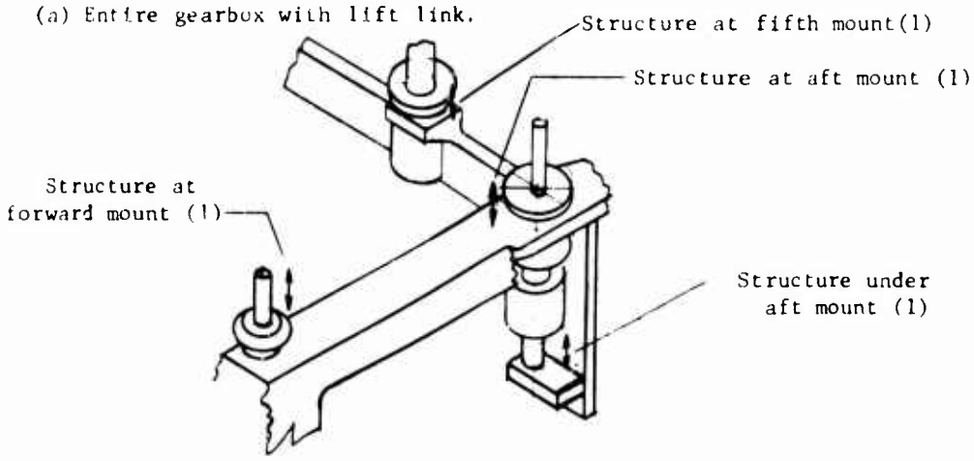

(b) Enlarged detail of aircraft structure, showing corner mount and damper.

Figure 46. Accelerometer Locations for Vibration Measurements in the First and Second Flight Series.

TABLE XXIII. VIBRATION LEVELS MEASURED ON GEARBOX AND SUPPORTING STRUCTURE DURING INITIAL SERIES OF MEASUREMENTS

Location	Acceleration, g, rms (Lin.)
Ring Gear Housing	13.5
Ring Gear Housing Flange	30.0
Base - Front Corner	2.6
Structure at Forward Mount	1.6
Base - Aft Corner	7.8
Structure at Aft Mount	2.2
Structure Below Aft Damper	1.7
Structure at Fifth Mount	4.4
Upper Lift Link Clevis	16.
Lower Lift Link Clevis	21.5

aluminum blocks (5/8-inch square by 3/8-inch thick) to the gearbox surface (Eastman 910 adhesive) and attaching the accelerometers to the blocks with mounting studs. This arrangement was entirely satisfactory.

Overall levels of vibration (linear response) are tabulated in Table XXIV for all measurement points and both flight conditions. One measurement point, the ring gear housing location for aircraft No. 66-1039, cruise operation, was not obtained due to damage to the connecting lead at some time after the installation was completed and checked out.

The results of one-third-octave frequency analysis for all of the vibration measurement points, including cruise and flight-idle operation of all three aircraft, are given in Tables XXV, XXVI, XXVII, XXVIII, XXIX, and XXX.

MEASUREMENTS ON CABIN SURFACES

During cruise operation with aircraft No. 66-1039, a hand-held accelerometer probe was used to obtain vibration measurements at a number of locations on the cabin deck, side, and gearbox compartment bulkhead surfaces. The locations of the measurement points are identified on a schematic of the cabin layout in Figure 19 in the Discussion section of this report. Overall acceleration levels recorded at each of the 16 measurement positions are tabulated under the schematic layout.

Narrow-band analysis was performed on the data from the center of the gearbox compartment bulkhead (position 16), and results of this are shown also in Figure 19. These results are presented as the frequencies and surface vibration velocity amplitudes of identifiable maxima in the narrow-band spectrum.

TABLE XXIV. VIBRATION LEVELS MEASURED ON GEARBOX DURING FINAL SERIES OF TESTS

Accelerometer Location	Acceleration, g, rms (Lin.) Aircraft No.		
	66-1038	66-1039	66-1043
Cruise Operation			
Ring Gear Housing	78.0	-	33.0
Base - Fwd. Corner	33.0	22.0	27.0
Base - Aft Corner	12.4	29.0	12.5
Above Lift Link	16.3	25.0	16.5
Below Lift Link	11.5	8.7	7.5
Flight - Idle Operation			
Ring Gear Housing	22.0	35.0	24.0
Base - Fwd. Corner	10.5	13.5	11.2
Base - Aft Corner	7.5	12.5	9.8
Above Lift Link	8.5	11.5	11.7
Below Lift Link	3.4	7.7	3.3

TABLE XXV. TABULATED ONE-THIRD-OCTAVE FREQUENCY ANALYSIS OF VIBRATION DATA, AIRCRAFT NO. 66-1038 - CRUISE OPERATION

Center Frequency	Acceleration, g (rms)				
	Ring Gear Housing	Base Fwd.	Base Aft	Below Lift Link	Above Lift Link
20	<.50	<.19	<.06	<.05	<.165
25	<.50	.23	.085	.36	<.165
32	<.50	<.19	.095	.085	<.165
40	.90	.23	.135	.175	<.165
50	.53	<.19	.09	.165	<.165
64	1.90	.80	.30	.40	.24
80	.67	.42	.29	.37	.23
100	.57	.28	.24	.2	.17
125	1.13	.45	.14	.15	<.165
160	.73	.21	.13	.13	<.165
200	2.1	.19	.19	.11	<.165
250	1.8	.215	.21	.085	<.165
320	.85	.21	.25	.075	<.165
400	.90	.235	.30	.13	<.165
500	.85	<.19	.25	.80	.18
640	.80	.75	.43	.12	.25
800	.85	.35	.34	.14	.23
1000	1.0	1.05	.74	.40	.42
1250	1.9	1.35	.90	.49	.62
1600	3.02	1.30	.95	.47	.99
2000	10.3	4.5	2.70	1.55	2.40
2500	5.8	3.0	1.01	1.10	2.40
3200	9.5	14.0	4.40	3.60	14.50
4000	53.0	27.0	5.50	10.50	5.20
5000	23.5	6.4	5.40	2.18	1.80
6400	45.0	9.2	7.40	.95	1.55
8000	34.0	4.9	3.50	.32	.70
10,000	10.2	2.0	1.70	.38	.58
12,500	5.6	.95	1.01	.185	.76
16,000	1.5	.255	.27	<.05	.24
Lin.	78.0	33.0	12.4	11.5	16.3

TABLE XXVI. TABULATED ONE-THIRD-OCTAVE FREQUENCY ANALYSIS OF VIBRATION DATA, AIRCRAFT NO. 66-1039 - CRUISE OPERATION

Center Frequency	Acceleration, g (rms)				
	Ring Gear Housing	Base Fwd.	Base Aft	Below Lift Link	Above Lift Link
20	NO DATA OBTAINED	<.19	<.18	<.05	.165
25		<.19	.36	.165	.26
32		.225	.34	.09	.22
40		<.19	.21	.085	.22
50		<.19	.21	.08	.22
64		.52	.47	.11	.44
80		.20	.21	.11	.26
100		<.19	.21	.115	.22
125		.20	.21	.105	.245
160		<.19	<.18	.07	.185
200		.215	<.18	.07	.185
250		.215	.21	.085	.175
320		<.19	<.18	.055	.165
400		.19	.195	.065	.165
500		.215	.21	.08	.165
640		.47	.38	.125	.28
800		.40	.26	.155	.195
1000		.85	.60	.46	.26
1250		2.0	1.35	.50	.92
1600		1.05	.75	.62	1.20
2000		2.40	1.90	1.60	2.50
2500		1.95	1.05	1.10	2.15
3200		6.40	3.40	1.65	9.70
4000		15.0	21.0	7.30	22.0
5000		6.8	9.0	3.30	5.40
6400		14.0	18.0	1.95	2.80
8000		4.2	5.30	.54	1.45
10000		2.90	2.30	1.01	1.15
12500		2.15	1.45	.21	.54
16000		.40	.38	<.05	.28
Lin.		22.0	29.0	8.7	25.0

TABLE XXVII. TABULATED ONE-THIRD-OCTAVE FREQUENCY ANALYSIS OF VIBRATION DATA, AIRCRAFT NO. 66-1043 - CRUISE OPERATION

Center Frequency	Acceleration, g (rms)				
	Ring Gear Housing	Base Fwd.	Base Aft	Below Lift Link	Above Lift Link
20	<.16	<.19	<.18	<.05	<.05
25	.18	.215	<.18	.105	.09
32	<.16	.205	<.18	<.05	<.05
40	.21	.19	<.18	<.05	<.05
50	.18	<.19	<.18	.07	<.05
64	1.22	.65	.20	.47	.53
80	1.22	.42	<.18	.43	.46
100	.24	.215	<.18	.06	<.05
125	.28	<.19	<.18	.06	<.05
160	.31	<.19	<.18	<.05	<.05
200	.42	<.19	<.18	<.05	<.05
250	.29	<.19	<.18	<.05	<.05
320	.29	<.19	<.18	<.05	<.05
400	.50	.23	<.18	.155	<.05
500	.28	.43	.295	.26	.45
640	.25	1.50	1.20	.14	.46
800	.62	.44	.21	.22	.07
1000	.29	.80	.55	.43	.09
1250	.43	1.15	.84	.37	.64
1600	.82	1.10	.70	.37	.81
2000	2.40	2.55	1.80	1.25	2.[illegible]
2500	1.75	3.40	1.25	.95	2.85
3200	2.50	12.8	3.50	1.42	8.70
4000	13.8	21.0	5.30	5.50	13.0
5000	12.0	6.0	6.70	3.50	3.40
6400	24.0	8.0	6.70	2.60	4.70
8000	12.0	3.1	3.10	[illegible]5	1.35
10000	7.0	1.55	2.00	.26	.80
12500	3.9	.85	1.10	.33	.50
16000	1.1	.19	.28	<.05	.055
Lin.	33.0	27.0	12.5	7.50	16.5

TABLE XXVIII. TABULATED ONE-THIRD-OCTAVE FREQUENCY ANALYSIS OF VIBRATION DATA, AIRCRAFT NO. 66-1038 (FLIGHT-IDLE OPERATION)

Center Frequency	Acceleration, g (rms)				
	Ring Gear Housing	Base Fwd.	Base Aft	Below Lift Link	Above Lift Link
20	<.11	<.06	<.055	<.017	<.05
25	<.11	<.06	.06	.03	.08
32	<.11	.08	.07	.02	.06
40	.70	.40	.55	.34	.28
50	.32	.32	.44	.27	.21
64	<.11	.075	<.055	.04	.09
80	<.11	<.06	.06	.045	.07
100	<.11	.075	<.055	.035	.075
125	.13	.065	<.055	.035	.065
160	<.11	.08	.07	.035	.06
200	<.11	.085	.065	.035	.06
250	<.11	.085	.06	.03	.055
320	<.11	.14	.115	.035	.055
400	.28	1.35	.57	.18	.15
500	.13	.20	.135	.045	.07
640	.33	.54	.47	.075	.09
800	.31	.35	.18	.165	.15
1000	.37	.75	.47	.35	.19
1250	1.40	1.75	1.45	.80	.50
1600	2.10	.91	.75	.31	.80
2000	5.80	4.00	3.70	.72	3.50
2500	5.00	4.00	1.45	1.02	3.10
3200	4.70	3.50	1.45	1.75	5.70
4000	10.5	5.00	3.20	2.40	4.30
5000	10.5	4.70	4.80	1.08	1.30
6400	10.5	4.00	2.10	.28	.63
8000	10.5	1.40	1.65	.145	.33
10000	2.10	.70	2.50	.09	.33
12500	.80	.27	.45	.08	.08
16000	.26	.90	.14	.04	.105
Lin.	22.0	10.5	7.50	3.4	8.50

TABLE XXIX. TABULATED ONE-THIRD-OCTAVE FREQUENCY ANALYSIS OF VIBRATION DATA, AIRCRAFT NO. 66-1039 (FLIGHT-IDLE OPERATION)

Center Frequency	Acceleration, g (rms)				
	Ring Gear Housing	Base Fwd.	Base Aft	Below Lift Link	Above Lift Link
20	<.54	<.19	<.18	<.165	<.05
25	<.54	<.19	<.18	<.165	.07
32	<.54	<.19	<.18	<.165	.105
40	.60	.34	.26	.35	.31
50	1.35	1.15	.85	1.30	1.10
64	<.54	.19	.20	<.165	.25
80	.56	<.19	<.18	<.165	.10
100	.64	<.19	<.18	<.165	.11
125	.64	<.19	<.18	<.165	.11
160	.60	<.19	<.18	<.165	.105
200	.64	<.19	<.18	<.165	.105
250	<.54	<.19	<.18	<.165	.11
320	<.54	<.19	<.18	<.165	.105
400	.54	.90	.67	.79	.47
500	<.54	.52	.33	.165	.145
640	<.54	.23	<.18	<.165	.11
800	.67	.70	.65	.22	.25
1000	.67	.65	.52	.22	.23
1250	1.80	1.30	1.30	.79	1.10
1600	2.40	.90	.86	.33	.70
2000	5.50	5.80	3.30	1.30	2.00
2500	13.0	4.00	2.40	2.15	3.00
3200	5.50	2.80	1.60	1.11	3.60
4000	19.0	9.00	5.50	7.00	9.60
5000	21.0	5.80	9.00	2.40	4.30
6400	11.2	3.50	4.80	.55	1.25
8000	8.50	1.60	2.40	.20	.60
10000	5.00	.90	.92	<.165	.42
12500	1.35	.60	.36	<.165	.165
16000	.54	<.19	<.18	<.165	.10
Lin.	35.0	13.5	12.5	7.70	11.5

TABLE XXX. TABULATED ONE-THIRD-OCTAVE FREQUENCY ANALYSIS OF VIBRATION DATA, AIRCRAFT NO. 66-1043 (FLIGHT-IDLE OPERATION)

Center Frequency	Acceleration, g (rms)				
	Ring Gear Housing	Base Fwd.	Base Aft	Below Lift Link	Above Lift Link
20	<.54	<.19	<.18	<.05	<.165
25	<.54	<.19	<.18	<.05	.175
32	<.54	<.19	<.18	<.05	.21
40	1.60	2.1	.95	.63	.62
50	1.00	1.12	.46	.295	.30
64	<.54	<.19	<.18	.06	.165
80	<.54	<.19	<.18	<.05	.165
100	<.54	<.19	<.18	<.05	<.165
125	<.54	<.19	<.18	<.05	<.165
160	<.54	<.19	<.18	<.05	<.165
200	<.54	<.19	<.18	<.05	<.165
250	<.54	<.19	<.18	< 05	<.165
320	<.54	.25	.18	<.05	<.165
400	.67	1.45	.60	.23	.23
500	<.54	.20	.18	.06	<.165
640	<.54	.27	.30	.085	<.165
800	<.54	.28	.24	22	.23
1000	<.54	.80	.57	.62	.35
1250	.95	1.20	.85	.62	.53
1600	1.80	1.60	1.32	.24	.65
2000	4.30	8.00	7.20	.88	2.20
2500	5.40	3.20	1.45	.88	2.30
3200	6.40	3.80	2.00	1.40	7.50
4000	13.2	3.80	3.00	1.65	7.50
5000	16.0	3.80	4.70	2.20	1.50
6400	10.0	3.20	2.10	.40	1.55
8000	6.00	1.20	1.08	.19	.43
10000	2.70	.56	.60	.085	.31
12500	.75	.28	.36	.065	.165
16000	<.54	<.19	<.18	<.05	<.165
Lin.	24.0	11.2	9.80	3.30	11.7

APPENDIX II

MEASUREMENT OF GEARBOX HOUSING STRUCTURAL RESPONSE

The procedure was to apply cyclic force at one of several points on the gearbox structure while measuring the response at the point of force application and at a number of other points on the structure. The locations of the points of force application and of the accelerometers are shown in Figure 47. The selected drive points were the ring gear housing and those locations of input shaft and mast support bearings which were accessible without disassembling the gearbox. Prior to affixing the accelerometers, various points on the housing were probed with a hand-held accelerometer while driving at the mast upper bearing support. There were no points of especially high level response, so the accelerometers were mounted mostly at the same locations as were used to obtain vibration data in the helicopter.

For these measurements, the gearbox was supported on the soft mounts which normally hold it in its shipping container. These are located at the four corner positions normally used for mounting in the aircraft. The lift link was not connected and the mast was removed. The procedure was to drive with a small electromagnetic shaker at a series of discrete frequencies from 200 to 10,000 Hz. The shaker excitation was adjusted to give a constant input force of 3.165 lb peak-to-peak at all frequencies as measured by a piezoelectric force cell inserted in the drive connection under compressive preload. The fixtures for attaching the drive rod to the gearbox were designed so that the rod end was in direct contact with the gearbox surface under substantial preload. The accelerometers were mounted by studs on aluminum blocks which were cemented to the gearbox surface.

Figure 48 shows the gearbox with the shaker connected to drive at the ring gear housing. The accelerometers mounted on the ring gear housing, lower housing, and base after corner (Nos. 1, 2, and 3 in Figure 47) are visible. The mounting bracket for the drive rod at the input shaft bearing housing is also visible.

Complete results of the measurements are given in Table XXXI as acceleration in db, with slightly different reference levels for the different measurement points depending on the accelerometer sensitivity.

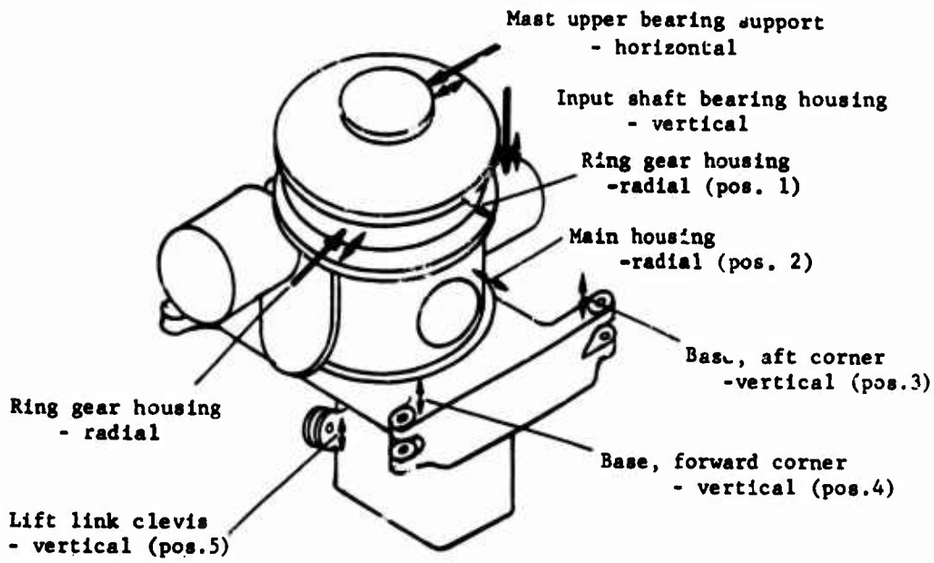

Legend:

Location and orientation of excitation force

Location and orientation of accelerometer

Notes:

Accelerometers in positions 1 through 5 remained in position shown for all excitations.

Accelerometers shown alongside excitation force changed positions with change of excitation. Data for each of these positions are listed under position 6 in the data tables.

Figure 47. Location of Excitation and Accelerometers for Gearbox Housing Structural Response Measurements.

TABLE XXXI. MEASURED CASING RESPONSE

Excitation(1) Applied to Mast Upper Bearing Support

Acceleration, db (rms)(2)

Frequency Hz	POSITION(3)					
	1	2	3	4	5	6
200	50.0	50.0	53.2	49.0	49.5	57.0
300	52.0	50.0	49.5	49.5	50.0	58.7
500	52.5	50.0	49.5	49.0	50.5	58.0
700	57.8	50.0	50.5	49.0	52.0	68.3
750	63.8	52.0	57.0	54.3	52.5	76.3
800	69.9	54.2	62.0	59.0	54.5	76.4
900	73.8	56.0	54.2	66.8	57.7	82.0
1000	75	60.0	67.4	56.0	60.0	85.6
1050	80	63.7	71.0	61.5	66.2	91.0
1100	86.8	64.5	71.2	65.4	72.0	95.5
1200	83	53.5	69.2	54.0	64.3	90.0
1400	77.3	52.5	57.7	55.4	59.8	80.0
1500	78.5	60.0	66.5	56.7	55.5	78.0
1570	80	61.7	54.2	50.5	57.5	77.7
1700	82.5	68.5	65.0	64.2	65.5	62.5
1900	81.8	66.5	68.0	69.5	77.5	89.0
2000	72.0	68.4	67.2	64.0	76.0	91.0
2250	84.0	74.5	76.5	70.0	72.5	94.6
2500	88.2	75.0	80.0	74.0	76.0	110.0
2750	91.0	65.5	89.3	73.8	90.5	111.2
3000	96.0	76.3	79.0	85.5	94.0	113.2
3500	85.3	78.7	87.9	80.2	85.7	118.6
4000	91.0	76.3	74.5	74.5	71.5	105.7
4500	86.5	77.0	93.0	97.4	71.0	106.5
5000	86.4	75.5	79.6	75.7	64.5	106.2
5500	82.2	70.5	72.2	70.0	77.0	98.0
5800	82.5	74.0	71.0	77.8	81.5	104.4
6000	83.9	67.0	75.4	75.0	66.5	103.3
6270	73.0	63.5	74.3	74.7	70.0	98.3
7000	82.5	72.0	78.5	67.5	72.5	95.0
7500	83.3	77.5	64.8	77.5	64.7	89.7
8000	77.2	80.0	61.0	70.0	61.0	95.0
8500	77.7	76.7	71.5	71.5	66.0	96.8
9000	77.7	75.2	70.5	71.0	70.0	93.6
10000	59.8	76.0	75.3	60.0	61.0	96.0

(1) Drive force was 3.165 lb p-p.

(2) Reference values depend on accelerometer sensitivites and were as follows:

2 (5.8×10^{-5}g), 3(5.7×10^{-5}g), 4(5.2×10^{-5}g), 5(5.2×10^{-5}g), 6(4.9×10^{-5}g)

(3) Accelerometer positions are identified on Figure 47.

TABLE XXXI. - Continued

Excitation(1) Applied at Input Shaft Bearing Support Acceleration, db (rms)(2)

Frequency Hz	POSITION(3)					
	1	2	3	4	5	6
200	50.0	49.5	49.4	50.5	49.3	51.7
300	50.8	49.7	52.0	54.5	49.5	56.0
400	50.5	49.2	49.5	49.5	49.5	58.0
475	50.9	49.5	50.0	49.5	50.0	72.0
500	50.6	49.5	49.7	49.8	50.8	70.0
600	49.5	49.5	49.5	49.5	50.0	63.0
700	50.5	49.3	52.3	53.0	49.4	64.7
800	51.0	49.7	55.0	53.2	50.0	64.7
900	50.2	49.8	49.8	59.0	50.0	64.0
970	55.9	51.5	55.8	53.5	50.0	73.5
1000	55.9	49.7	54.8	52.0	50.0	50.0
1050	55.8	50.0	51.5	51.0	49.5	63.5
1100	53.0	52.6	51.0	50.5	51.0	61.5
1150	57.0	50.0	50.0	52.7	49.5	69.4
1200	58.5	51.8	49.8	50.0	50.7	61.0
1300	58.7	52.0	49.5	52.0	51.4	65.3
1500	57.0	52.0	52.0	54.2	50.7	65.2
1750	58.0	60.7	59.3	60.3	60.0	87.0
2000	81.8	75.0	77.3	77.0	75.5	103.7
2100	81.3	32.0	82.6	80.4	79.8	103.0
2250	78.0	82.5	84.0	73.7	81.5	106.5
2500	77.0	74.2	71.7	67.5	79.0	98.0
2750	76.5	78.3	83.2	74.0	87.5	91.0
3000	66.3	79.7	79.3	70.0	81.5	95.0
3250	73.0	78.7	73.0	70.0	92.0	91.2
3500	80.6	76.0	75.7	67.2	78.7	86.0
4000	73.3	68.5	59.5	59.5	57.0	93.8
4500	61.0	60.5	77.7	78.8	57.0	88.5
5000	55.6	65.0	64.7	60.2	51.0	86.0
5500	66.8	70.8	62.0	71.2	56.4	88.8
6000	63.8	65.3	77.0	70.4	63.2	95.0
6100	58.5	66.4	74.8	66.2	60.0	95.7
6500	73.9	79.7	68.4	76.0	72.0	96.4
7000	70.1	73.5	72.4	73.2	63.7	96.4
8000	67.3	72.5	70.7	64.5	61.0	82.7
9000	61.0	65.5	58.8	73.5	50.0	87.4
9500	63.5	77.8	73.8	60.2	51.5	88.0
9800	80.0	64.2	82.0	83.2	80.7	83.4
10000	81.7	77.6	65.2	73.6	75.8	98.0

(1) Drive force was 3.165 lb p-p.

(2) Reference values depend on accelerometer sensitivites and were as follows: 2(5.8×10^{-5}g), 3(5.7×10^{-5}g), 4(5.2×10^{-5}g), 5(5.2×10^{-5}g), 6(4.9×10^{-5}g)

(3) Accelerometer positions are identified on Figure 47.

TABLE XXXI. - Continued

Excitation(1) Applied to Ring Gear Housing

Acceleration, db (rms)(2)

Frequency Hz	POSITION(3) 1	2	3	4	5	6
200	49.0	49.0	49.2	57.2	49.0	59.0
300	50.0	49.4	51.0	53.0	49.7	54.6
400	50.7	49.3	49.7	50.0	53.8	56.0
500	51.0	49.8	49.3	49.3	50.6	61.2
600	51.0	49.5	49.8	50.5	51.0	64.4
800	60.2	50.4	58.8	57.2	50.0	71.3
900	63.3	55.4	50.0	49.2	50.0	74.8
1000	69.5	54.1	57.6	56.2	54.0	77.7
1050	72.8	55.0	[illegible]	53.5	51.8	79.6
1100	82.0	54.8	63.2	56.7	61.2	84.4
1150	76.5	57.2	56.2	62.0	70.0	75.4
1200	70.0	50.4	56.3	61.0	53.0	77.2
1300	70.8	56.0	53.1	52.5	57.8	77.4
1350	69.1	53.3	55.0	49.5	58.2	79.7
1400	69.0	53.2	55.0	51.8	61.8	82.0
1450	71.3	49.5	60.6	58.0	65.4	83.0
1500	73.2	50.8	57.3	58.8	66.2	84.0
1550	75.0	54.6	57.0	59.0	64.5	85.4
1600	75.0	60.4	58.8	54.5	66.2	86.7
1750	75.0	68.5	58.2	63.2	63.4	90.5
1900	90.2	69.5	70.7	69.3	73.7	104.1
2000	89.1	75.7	76.6	76.0	73.2	100.0
2100	91.8	78.9	77.1	73.7	78.4	100.1
2150	93.0	75.8	71.4	62.0	73.1	95.8
2250	96.0	76.8	78.9	69.3	76.7	96.7
2400	99.0	72.5	71.1	72.0	86.0	101.3
2500	97.1	67.6	64.0	63.1	77.2	95.0
2750	97.9	81.2	79.8	84.0	89.4	98.4
3000	96.8	83.3	82.6	76.3	91.4	97.8
3250	101.2	90.5	80.4	84.0	98.5	104.4
3500	97.8	85.9	81.0	80.8	77.0	105.4
3750	102.1	97.4	80.8	81.5	79.5	107.4
4000	97.0	78.6	86.2	73.4	69.8	110.4
4250	95.0	82.7	88.7	84.8	71.0	106.4
4500	96.0	76.5	92.2	90.2	76.2	99.4
4750	96.0	90.0	90.8	83.1	75.4	101.6
5000	90.3	81.4	82.4	71.6	63.2	94.6
5250	88.7	80.4	84.3	89.2	77.8	100.2
5500	79.3	76.7	65.0	74.8	64.6	90.1
6000	85.7	80.7	89.2	86.7	68.4	94.6
6400	88.0	70.0	53.8	81.8	66.8	93.2
7000	81.8	74.3	74.8	63.4	66.5	84.4
8000	89.2	71.8	63.6	73.6	62.0	87.7
9000	86.	72.0	66.0	70.9	62.0	95.6
9800	90.5	67.8	64.5	70.3	60.7	90.8
10000	90.0	73.3	59.4	68.3	67.0	90.0

(1) Drive Force was 3.165 lb p-p.

(2) Reference values depend on accelerometer sensitivities and were as follows: 2(5.8 x 10^{-5}g), 3(5.7 x 10^{-5}g), 4(5.4 x 10^{-5}g), 5(5.2 x 10^{-5}g), 6(4.9 x 10^{-5}g)

(3) Accelerometer positions are identified on Figure 47.

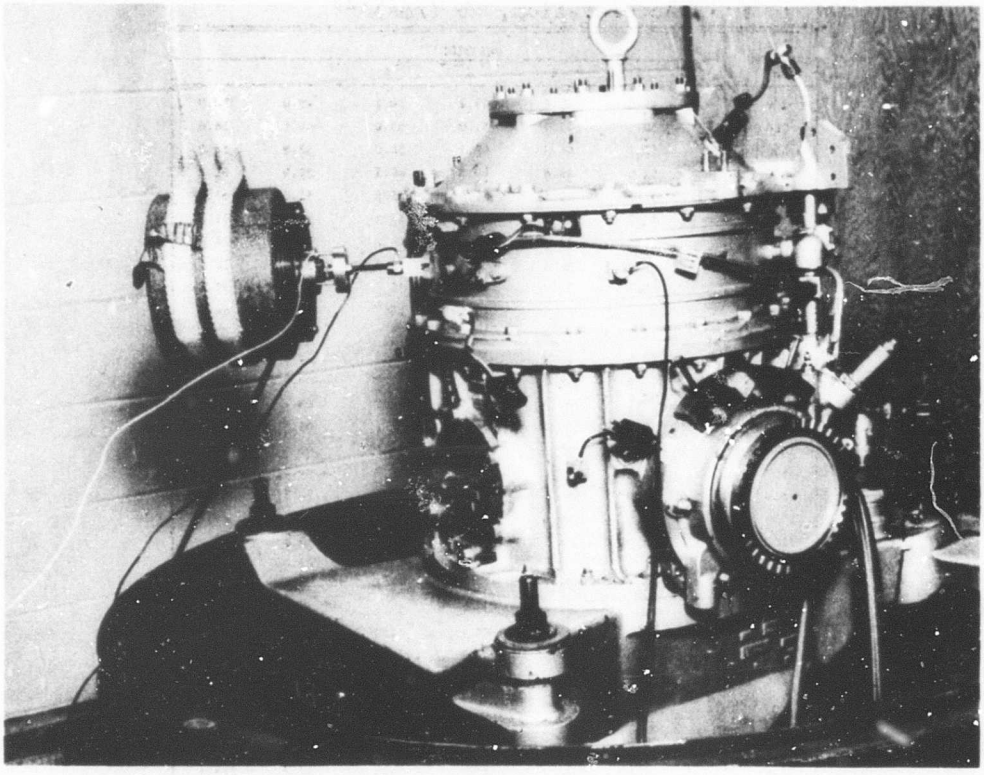

Figure 48. Gearbox Housing With Electromagnetic Shaker and Accelerometers for Structural Response Measurements.

APPENDIX III

GEAR MEASUREMENTS

GENERAL METHODS OF GEAR INSPECTION

The techniques that have been used to inspect gears for commercial purposes fall into two classes: analytical and composite. These techniques have been developed as a result of the needs of industry. Virtually all gears in commerce are bought and sold on the basis of their quality as well as their geometric and metallurgical features. Gear inspection techniques have evolved as a simple means of assuring that contractual obligations pertaining to the quality of the gear manufacturer have been met. As a result, the more conventional "analytical" inspection techniques measure specific geometric features of gear teeth by methods that are both reasonably accurate and convenient. However, these measurements do not necessarily reflect the degree to which the individual features of the teeth contribute to noise or vibration.

A large number of gears are evaluated commercially on the basis of a composite test. This test is one in which the gear to be evaluated is run very slowly in tight mesh with a "master" gear on a gear rolling checker. This machine holds the gears together under spring tension and displays or charts variations in tight mesh center distance as the gear under inspection is turned through one revolution. This method of inspection evaluates certain geometric features of the teeth as they are "seen" by another gear. Since the teeth must be in tight (no backlash) mesh and since the measurement of errors is made radially or at right angles to the path along which the teeth drive, this method also does not evaluate geometric errors directly in terms of their dynamic characteristics.

A new innovation in gear measurement has been introduced by Buckingham Associates of Springfield, Vermont. This method of measurement is still a laboratory technique. It is not in general industrial use. It does, however, measure the running qualities of the gears under inspection. Of all the gear measuring techniques available, this technique comes closest to providing data on gear quality that are applicable to the evaluation of the noise or vibration levels that will be produced by a gear after it is assembled.

A shortcoming in common with all composite inspection techniques, however, is the lack of means of applying the design load to the gear while being measured. In many high-quality gear designs, a feature leading to the success of the unit is profile modification. The tip, and in some cases the flank of the tooth near the root, is modified away from an exact involute curve. Since the teeth will deflect under load, the modification is intended to be such that when the teeth are loaded, the portion of the teeth contacted by the mating gear will appear to the mating gear to be involute. Under light or no load conditions, the teeth with such modification will not run in the same way as when deflected under load. Thus, a composite-type check of relatively accurate gears designed for heavy loads is not an adequate indicator of full load performance.

GEAR ERRORS AND ANALYTICAL MEASUREMENT TECHNIQUES

The analytical characteristics most commonly measured are the following:

1. Runout (also: Out-of-Roundness)
2. Pitch (also: Tooth Spacing)
3. Profile
4. Lead

All of these are associated with the active profile of gear teeth. By the active profile is meant that portion of the tooth surface that makes actual contact with the active profile of the mating tooth during some portion of the meshing cycle. The active profile is bounded lengthwise by the end rounds of the tooth, if such are present, or by the faces of the gear blank. Its inner boundary is the minor form diameter, and its outer boundary is either the outside diameter of the blank or the beginning of the tip round.

Runout

In an ideal gear, the teeth are assumed to be located on the surface of a perfect cylinder, itself rotating about its true axis. The runout is the departure from this ideal geometry. Each of the measurement techniques used has its own way of finding or expressing this departure. The interpretation of the inspection data is generally an attempt to account for the errors in terms of the gear cutting process. This approach is acceptable since most gear inspectors are familiar with gear manufacturing techniques, and since inspection is concerned with controlling the process as well as the product. The drawback of this approach, however, is that it becomes very difficult to obtain measurements from gear inspections that can be used to predict the kinematic qualities of the gears.

Typical measuring techniques for runout are

1. Over wires measurement - A pin is placed in successive tooth spaces of a gear mounted on bench centers and free to turn. A dial indicator is placed over the pin so as to make radial readings. Variations in tooth space widths will allow the pin to lie at different radii relative to the axis of rotation. This test compares the widths of successive tooth spaces as defined by a chordal dimension on a measuring pin which is essentially constant.

2. Span measurements - A pair of fingers having parallel cylinders or balls at their tips may be used to contact the driving and coast sides of the gears. These fingers are preset at a specific separation. The fingers can contact both sides of either one tooth space or one tooth at a time. The fingers are driven into the tooth space radially, and the variations in depth where they contact the active profiles are recorded.

Pitch

Pitch is the distance between corresponding points on adjacent teeth. Errors in pitch are measures of the inconsistency of these distances and are expressed in several different ways.

1. Pitch error, also known as tooth-to-tooth spacing error, is the maximum difference in the arc (or the chordal distance) from a point on one tooth profile to a corresponding point on an adjacent profile. Usually the measurements are taken at or near the standard pitch circle, although there are some occasions wherein the measurement is taken along the line of action.

2. Pitch range, also known as total error, is the difference between the minimum and the maximum pitch error noted in an entire gear.

3. Index error, sometimes called accumulated spacing, is the largest angular error between any two teeth on a gear.

Profile

In spur and helical gears of involute tooth form, the profile measurement is made in the plane of rotation to determine how closely the active profile measured from root to tip corresponds to the theoretical or specified profile. To measure profile, special gear tooth measuring machines are required. Most of these operate on the principle of generating a theoretical involute curve of the correct base diameter and of using this to tram an indicator or stylus along the active profile. Involute errors are the departures from the theoretical curve measured normal to the gear tooth surface.

There is no practical way in which to measure the profiles of bevel gears. These profiles vary continuously from the inner (toe) end of the tooth to the large outer (heel) end. Moreover, the profiles of bevel gears are not involute. They may be of any of a large number of profiles. Bevel gear profile is generally checked by tooth bearing pattern checks. These give only a qualitative indication.

Lead

Gear teeth have length, and in order to carry load and to mesh smoothly, the contacting surfaces must be parallel. In the case of spur gear teeth, the elements of the contacting faces must be parallel to the axis of rotation. In helical gears, the elements must make a constant angle at any given diameter with the plane of rotation. Any departure from the correct angle between the tooth elements and the plane of rotation is called a lead error.

Lead is measured by moving an indicator or recording stylus along the length of the tooth on a theoretically correct path and by recording the surface departures from this path. Spur gears are measured on equipment that is little more than bench centers. Helical gears require a

specialized inspection machine that can move the stylus along a very precise helix.

Lead is usually checked on or near a pitch line element of the tooth. It should be checked from one face of the gear blank to the other. A small allowance is often made for the effects of edge round on the teeth.

There is no convenient method of measuring the equivalent of "lead" in spiral bevel gears. This characteristic of the gear is measured in the same bearing pattern check mentioned in connection with bevel gear profiles. As with the profile, this technique does not yield numerical results.

COMPOSITE MEASURING TECHNIQUES

The most common composite measuring technique is the gear rolling check. In this technique, the gear to be inspected is held by spring force in tight mesh (double flank) contact with a master gear on a gear rolling fixture. The gear rolling fixture supports the axes of the gears in mesh such that they remain parallel (for spur and helical gears) while one axis is free to move closer or farther from the other. A dial indicator or a recording system makes observable the motion of the movable shaft axis while the gear being inspected is rotated through one complete revolution. This device is shown schematically in Figure 49. As the work gear is slowly turned, changes in the thickness of the teeth going through mesh cause changes in center distance. The features of the gear teeth that can be sensed by the mating master gear and that can be translated into variations in center distance are presented in composite form, as in the example shown in Figure 50. Three elements of the composite form are used as measures of quality.

1. Tooth-to-tooth action - composite error - As an individual tooth goes through mesh, any departures from a perfect lead, profile, or spacing tend to appear to the master gear to be a change in perfect tooth thickness. Thus, a small change in the center distance occurs to accommodate these imperfections. The chart shows small wiggles resulting from the tooth-to-tooth errors going through mesh. The "maximum" tooth-to-tooth composite error is the largest difference found in the peak-to-valley readings over any length of chart equal to 360 degrees/number of teeth in gear.

2. Runout and out-of-round - As the gear is rotated through a full revolution, all departures from perfect concentricity, or out-of-roundness, will be charted. These two features can be seen by smoothing out the tooth-to-tooth action wiggles. Runout will appear as a single sine wave in the interval of one revolution. Out-of-roundness will appear as superimposed distortions in the sine wave or as independent variations, if there is little or no runout.

3. Total composite error - The extremes in variation of center

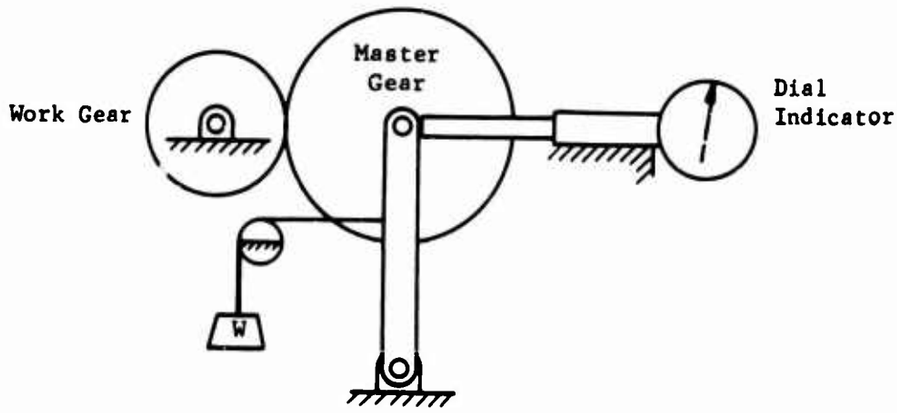

Figure 49. Schematic Diagram of a Gear Rolling Fixture.

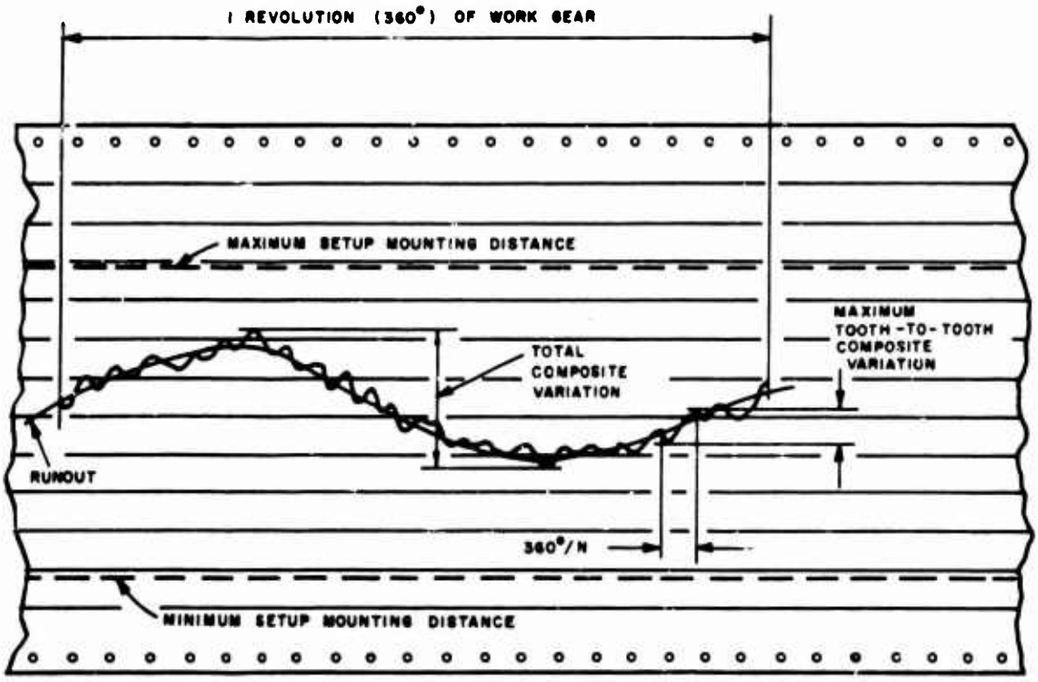

Figure 50. Chart of Gear Tooth Errors of a Typical Gear When Run With a Master Gear on a Gear Rolling Fixture.

distance that appear as a combination of the tooth-to-tooth composite error and the runout establish the total composite error for the gear.

The actual "size" of the gear (large or small) is shown by the relative position of the total composite error trace on the chart. When it is desirable to establish limits to tooth or gear size, this can be done by means of allowable limits on acceptable center distance variation in the gear testing fixture. These limits are shown in Figure 50 as a "Maximum Setup Center Distance" and a "Minimum Setup Center Distance".

It should be emphasized that although gear errors are measured as "seen" by a perfect mating gear (a master gear), this method of testing does not directly measure the kinetic effect of the errors on gears in action. First, all measurements are made normal to the pitch surfaces. This is about a right angle to the direction that the kinetic errors will act. Secondly, the method involves a double flank contact. The master gear teeth detect errors on both sides of a gear tooth simultaneously. As a result, errors on the non-driving side (coast side) of the teeth have an undue influence on the readings.

A second composite measuring technique is the gear cardiograph check. This is a recent development in the field of composite checking. At the present time, this equipment is being used primarily to evaluate the meshing quality of gears on a laboratory basis rather than as a means of production inspection. As yet, it is not in general use in the gear industry.

The cardiograph measures the angular displacement of a work gear relative to its theoretical position as it is driven by a perfect (almost) rack. Any errors on the gear teeth in the plane of measurement tend to displace the work gear behind or ahead of where it should be at that specific instant. These errors are then recorded in chart form, which is a plot of displacement versus angular position of the gear.

Figure 51 shows the gear cardiograph manufactured by the Dover Instrument Corporation. The basic measuring element of the cardiograph is a worm having an involute helicoid. Such a worm will mesh with a spur gear or a helical gear with a straight line contact (line of action). The master worm of the cardiograph is made to an extreme degree of precision. A master worm is used in place of a master gear, since the worm can be made to a somewhat higher degree of accuracy then can a conventional master gear with a similar expenditure of effort. The meshing contact between an involute helicoid and the work gear is the same as the contact between a rack and the work gear. The worm is driven by a synchronous motor through a highly precise change gear train.

The instantaneous angular position of the work gear is measured electronically by light passing through a 16,000-line optical disk which is mounted on the work spindle. This spindle is supported by an air bearing; thus, the effects of stick-slip which would mask small errors are minimized.

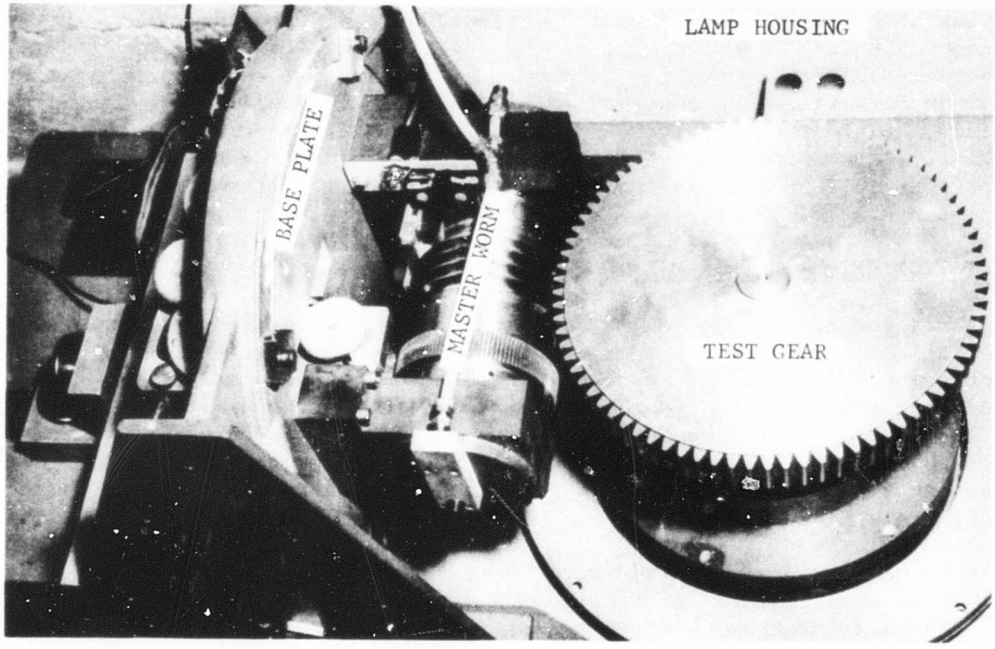

Figure 51. Gear Cardiograph.

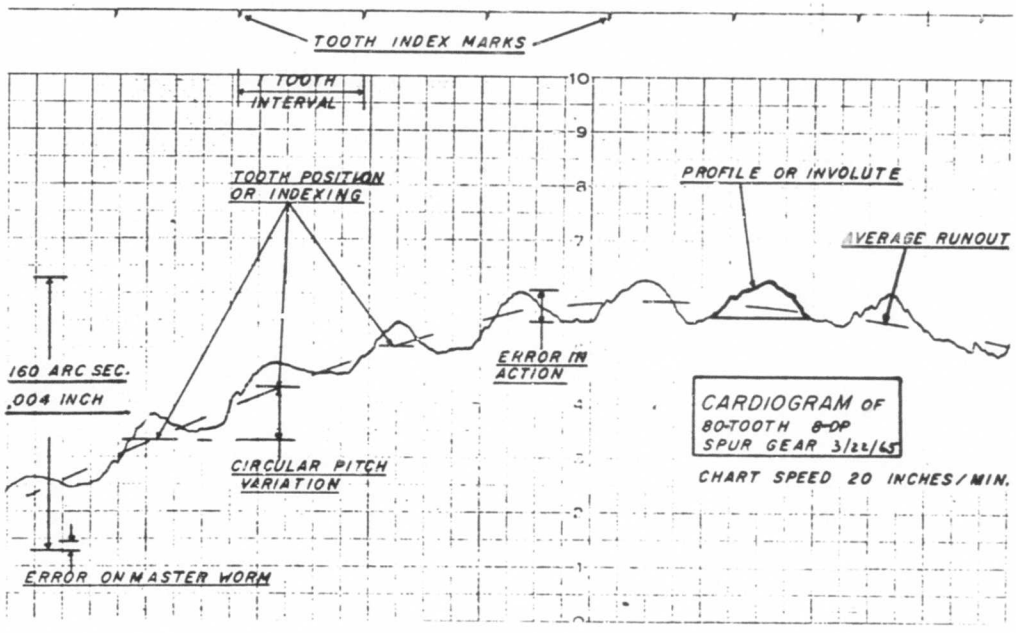

Figure 52. Portion of a Sample Cardiogram

The cardiograph does not segregate errors as is done by analytical checks. The cardiograms show concentricity of the gear as a basic sine wave. The spacing errors appear as a series of plateaus, one for each gear tooth, whose height is a function of both the individual spacing and the effects of out-of-position produced by concentricity. Figure 52 shows a portion of a sample cardiogram and contains identification of some of the errors it reveals. Since the cardiograph measures along the line of action and detects all errors in a plane of rotation (this would exclude effects in variations in lead), it is the best index of manufacturing error contribution to operational noise.

INSPECTION OF UH-1D TRANSMISSION GEARING

The gears inspected included two of each of the main drive gears: input stage spiral bevel pinion and gear, lower planetary stage sun gear, upper planetary sun gear, planet gear common to both planetary stages, and combined ring gear for the two planetary stages. Because working-quality gears could not be released from Government inventories, these gears were selected from rejected production parts but, were insofar as possible, of representative, acceptable quality in those features which related to the measurements planned.

The types of measurements made were those judged to be most commonly used to control gear quality and most commonly associated with noise generation. They included measurement of tooth spacing errors and runout on all gears, tooth profile on all external spur gears, and composite gear errors on all external spur gears.

The measurements of tooth spacing, runout, and profile were performed on the Hofler Gear Measuring Machine. Figures 53 through 60 show some of the gears in the process of being measured on the Hofler Machine. This machine was selected because of its inherent accuracy and because its inspection process is fully automatic. This latter feature is valuable in restricting human error. Measurements were made by the machine manufacturer at his plant in Ettlingen, Germany. This arrangement was chosen in preference to the use of a machine in the United States in order to take advantage of the manufacturer's thorough familiarity with his machine and its use.

The composite gear measurements were performed on the gear cardiograph manufactured by the Dover Instrument Corporation of Waltham, Massachusetts. The measurements were made by Buckingham Associates, Inc., of Springfield, Vermont. Figure 61 shows one of the gears in the process of being measured on the gear cardiograph.

Typical measurements in the form of charts from each of the four inspection processes are given in Figures 62 through 65. The illustrations and the above information on the type of measurement, the equipment used, and the gears measured are summarized in Table XXXII.

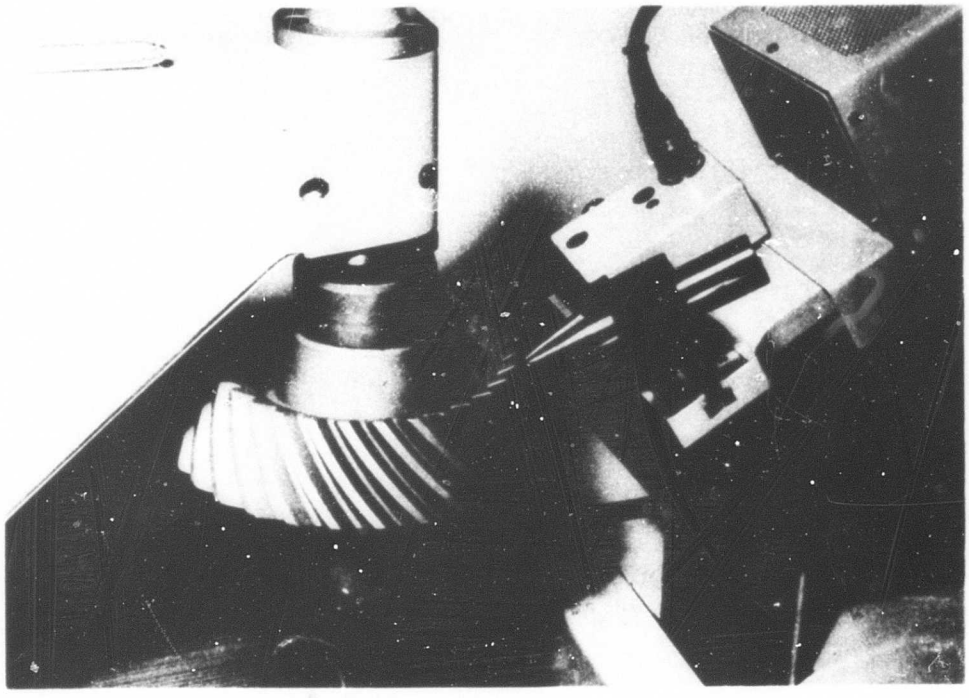

Figure 53. Measurement of Runout on the Input Stage Spiral Bevel Pinion Performed by the Hofler Gear Measuring Machine.

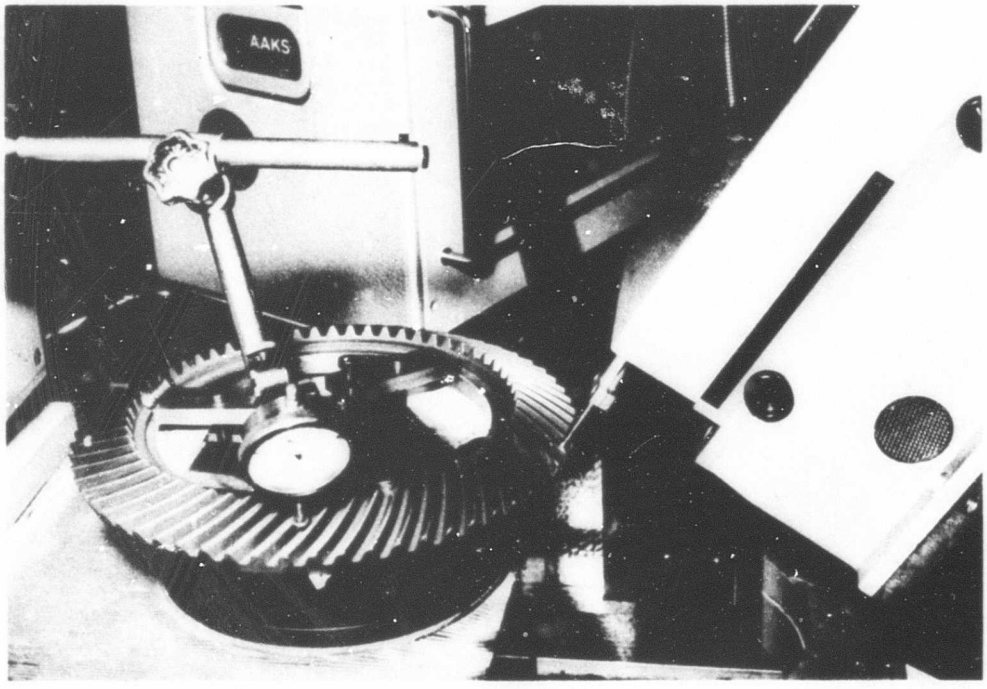

Figure 54. Measurement of Runout on the Input Stage Spiral Bevel Gear Performed by the Hofler Gear Measuring Machine.

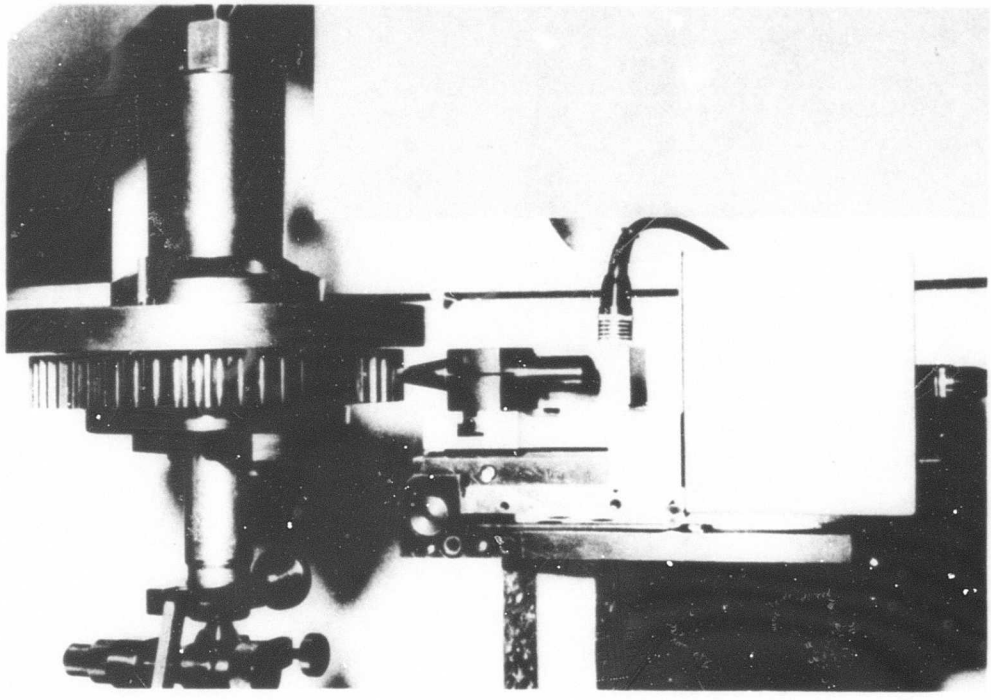

Figure 55. Measurement of Runout on the Lower Stage Planetary Sun Gear Performed by the Hofler Gear Measuring Machine.

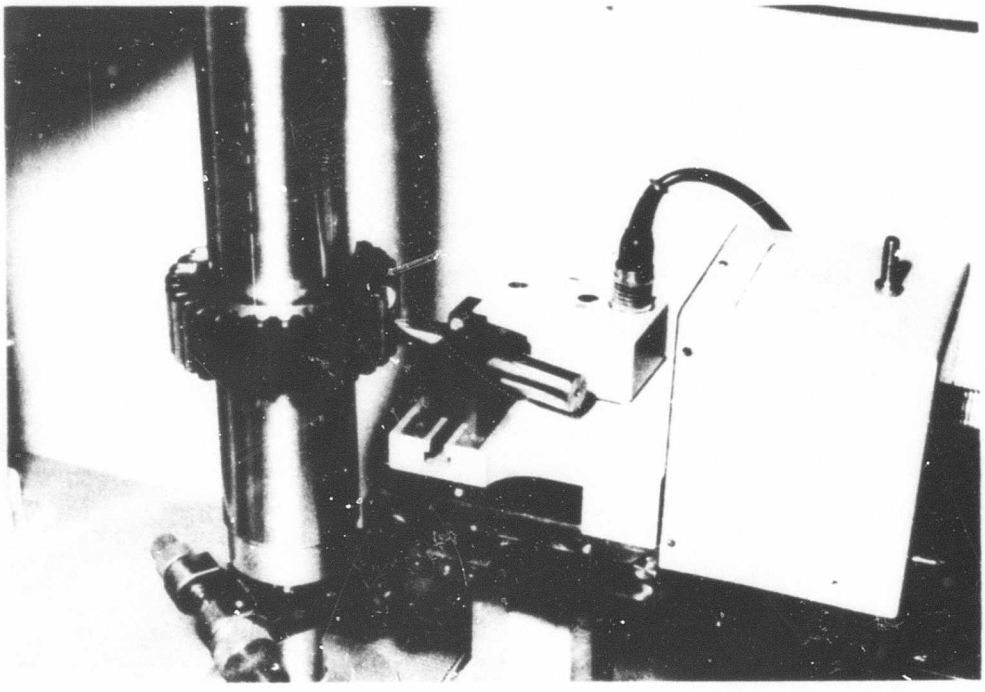

Figure 56. Measurement of Runout on the Planet Gear Performed by the Hofler Gear Measuring Machine.

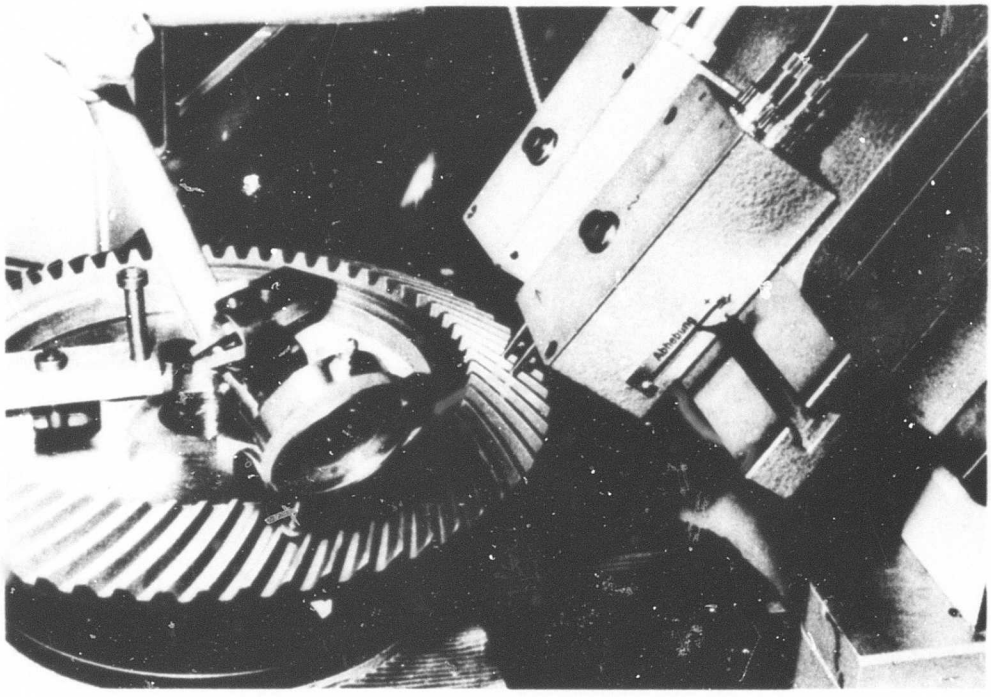

Figure 57. Measurement of Tooth Spacing on the Input Stage Spiral Bevel Gear Performed by the Hofler Gear Measuring Machine.

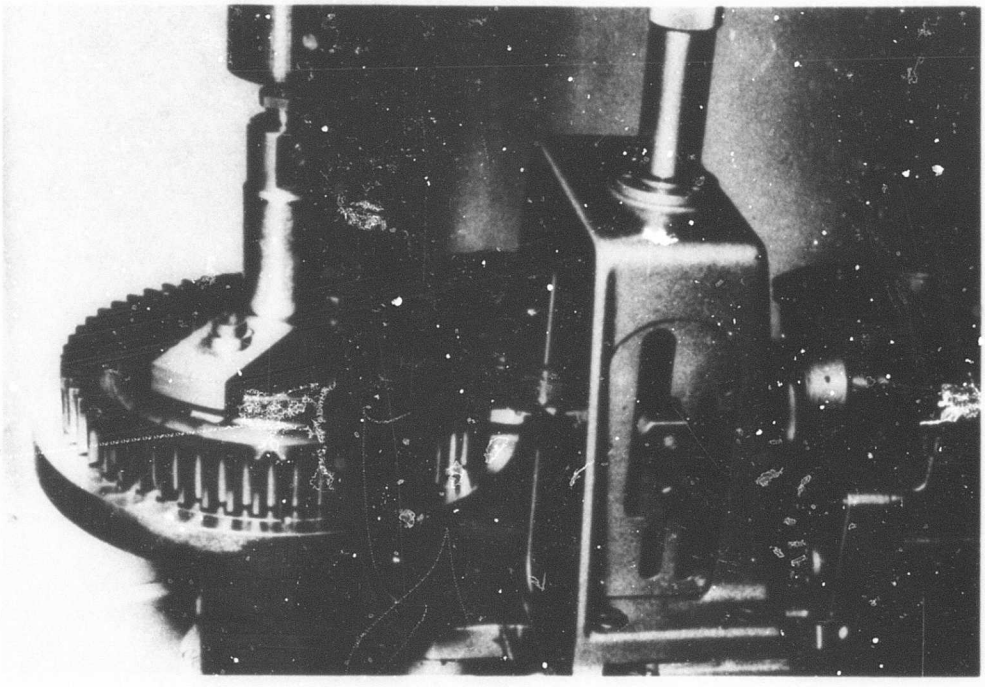

Figure 58. Measurement of Profile on the Lower Stage Planetary Sun Gear Performed by the Hofler Gear Measuring Machine.

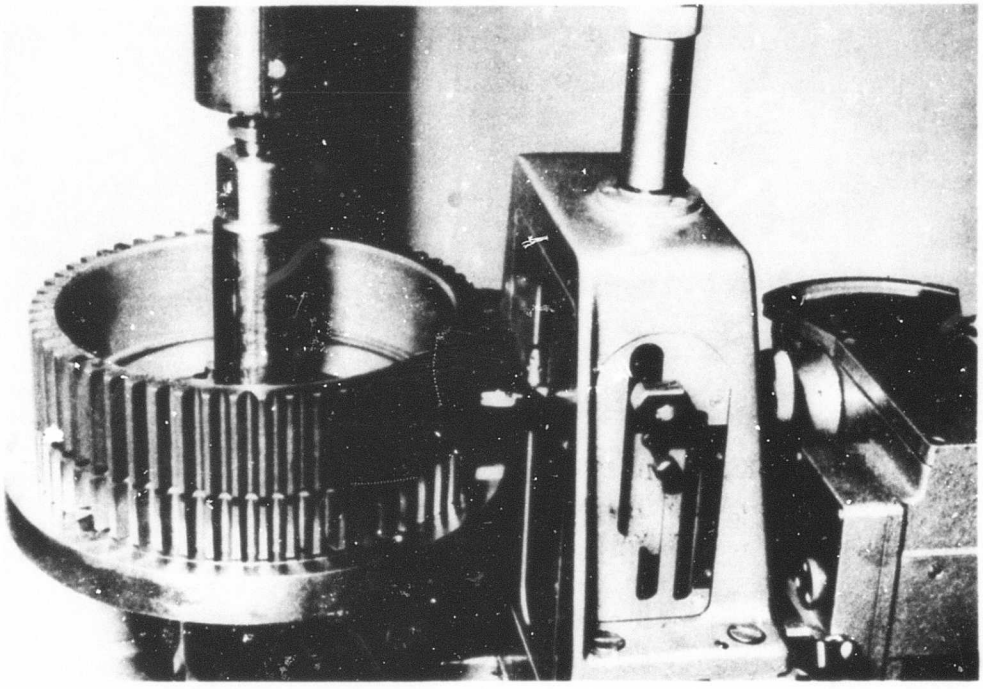

Figure 59. Measurement of Profile on the Upper Stage Planetary Sun Gear Performed by the Hofler Gear Measuring Machine.

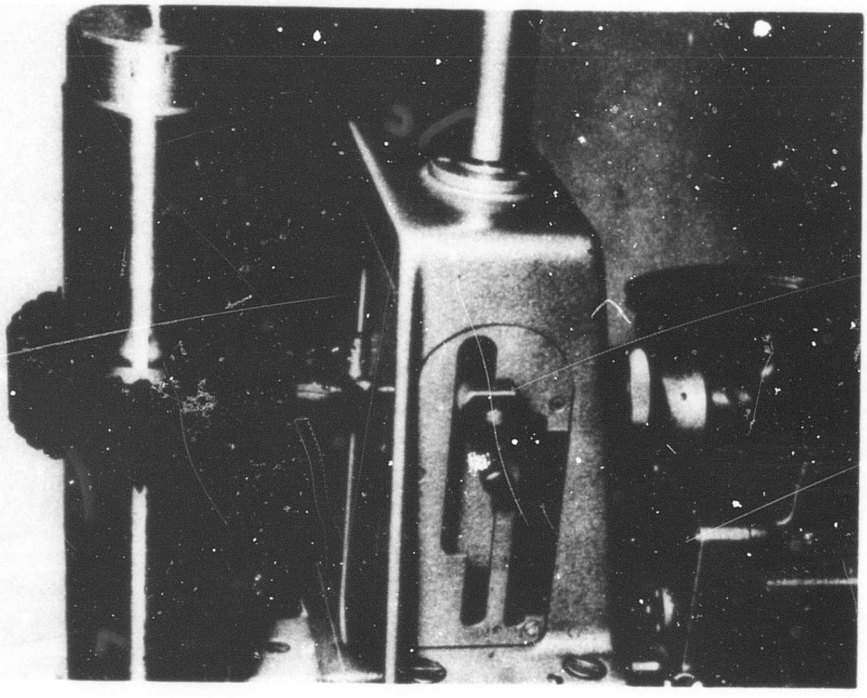

Figure 60. Measurement of Profile on the Planet Gear Performed by the Hofler Gear Measuring Machine.

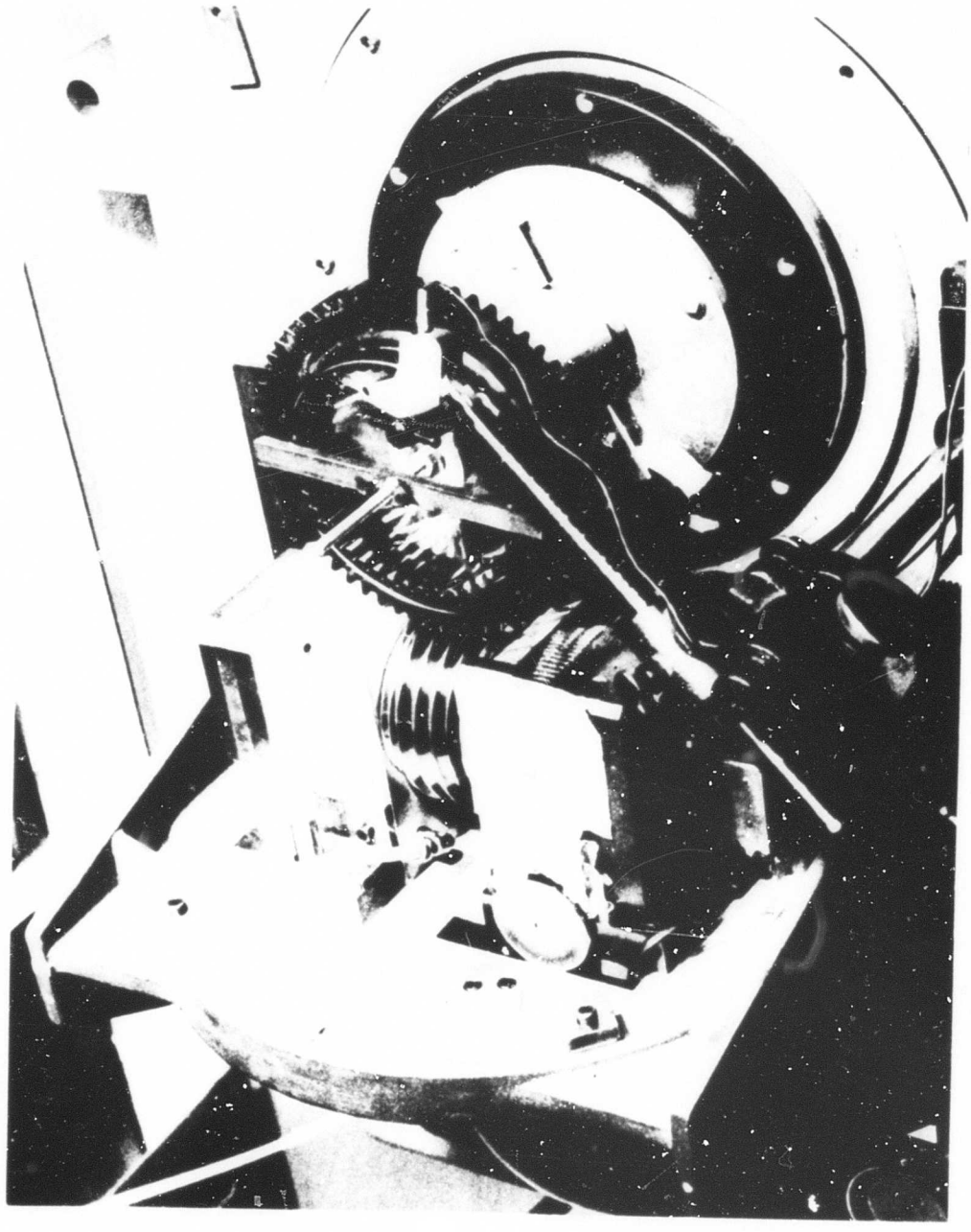

Figure 61. Measurement of the Lower Stage Planetary Sun Gear on the Gear Cardiograph.

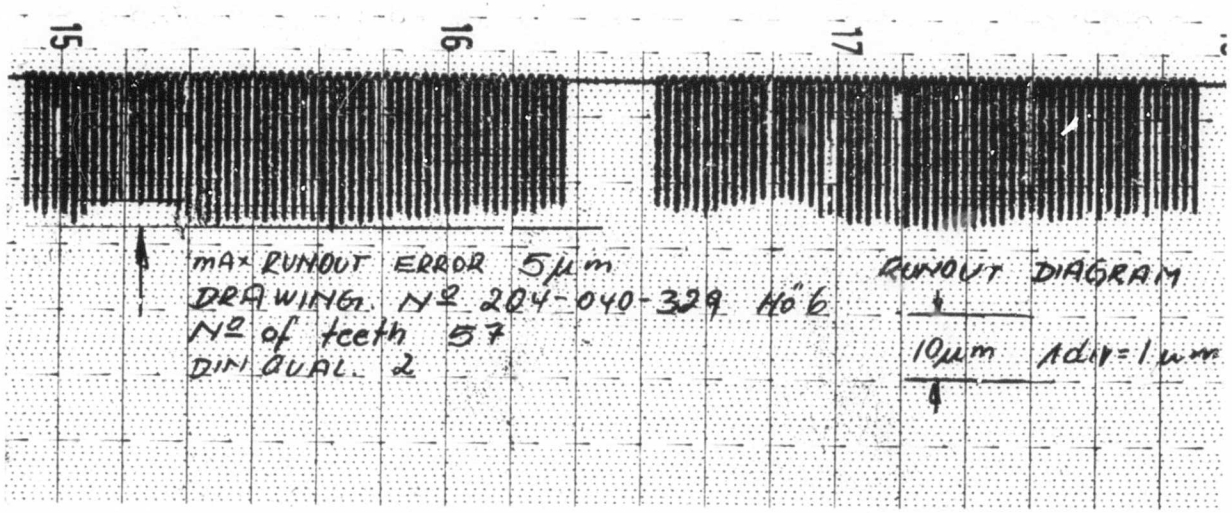

Figure 62. Runout Measurement of the Lower Planetary Stage Sun Gear as Measured on the Hofler Gear Measuring Machine.

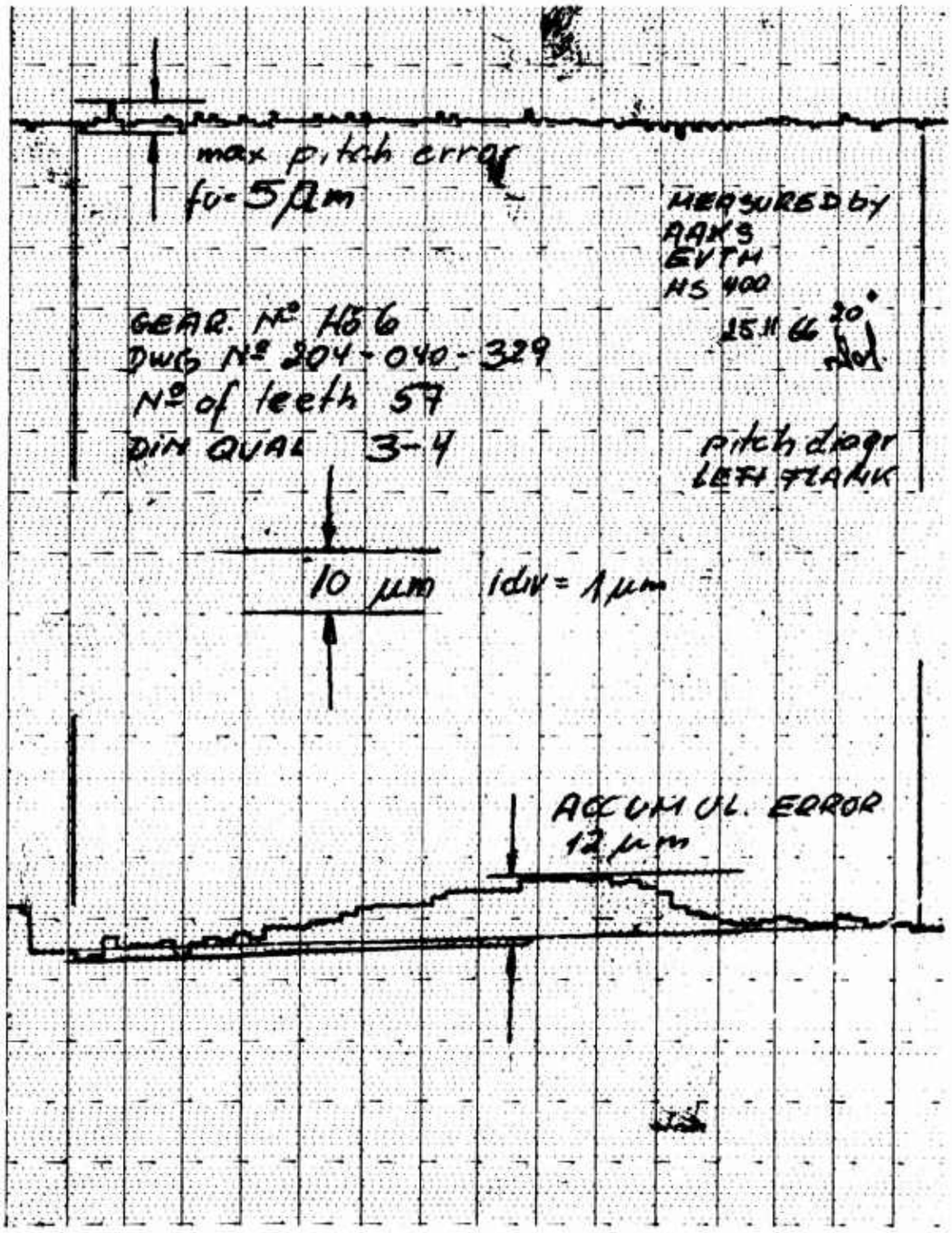

Figure 63. Tooth Spacing Measurement of the Lower Planetary Stage Sun Gear as Measured on the Hofler Gear Measuring Machine.

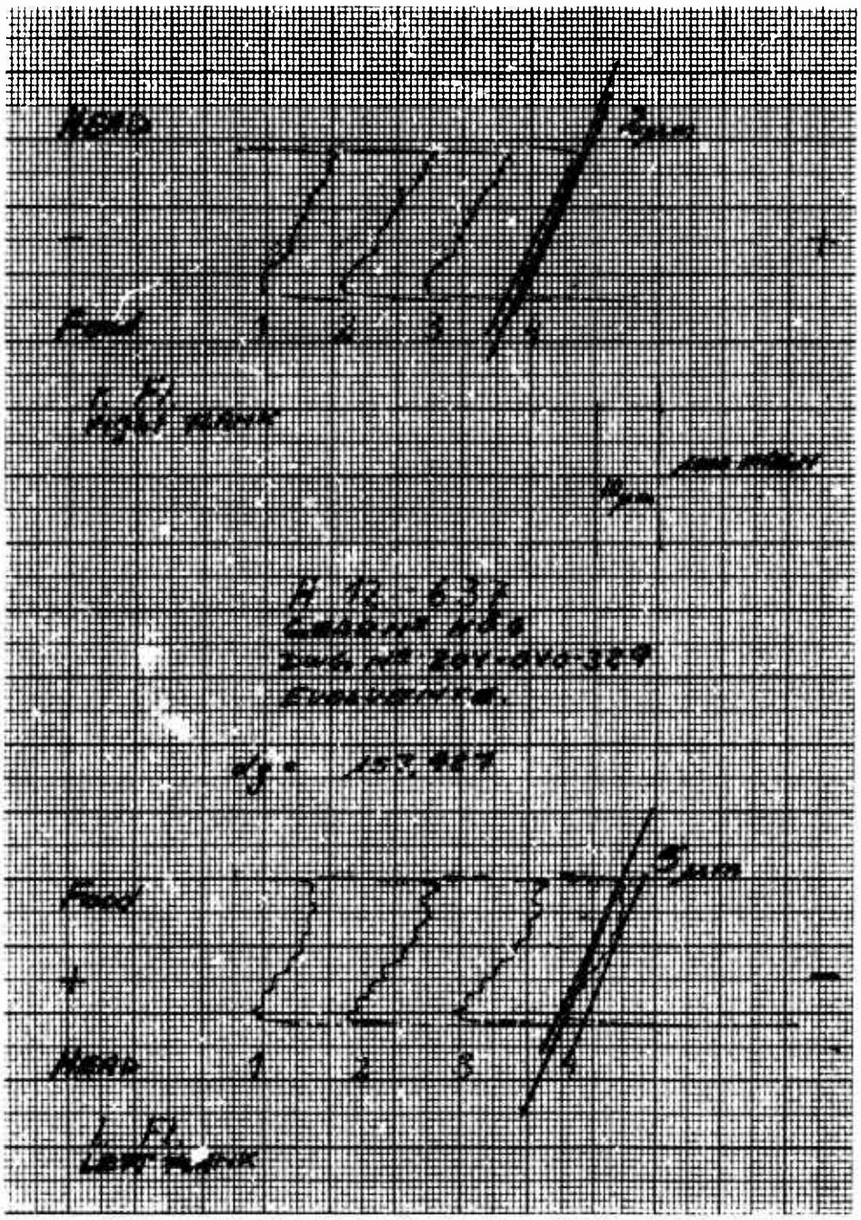

Figure 64. Profile Measurement of the Lower Planetary Stage Sun Gear as Measured on the Hofler Gear Measuring Machine.

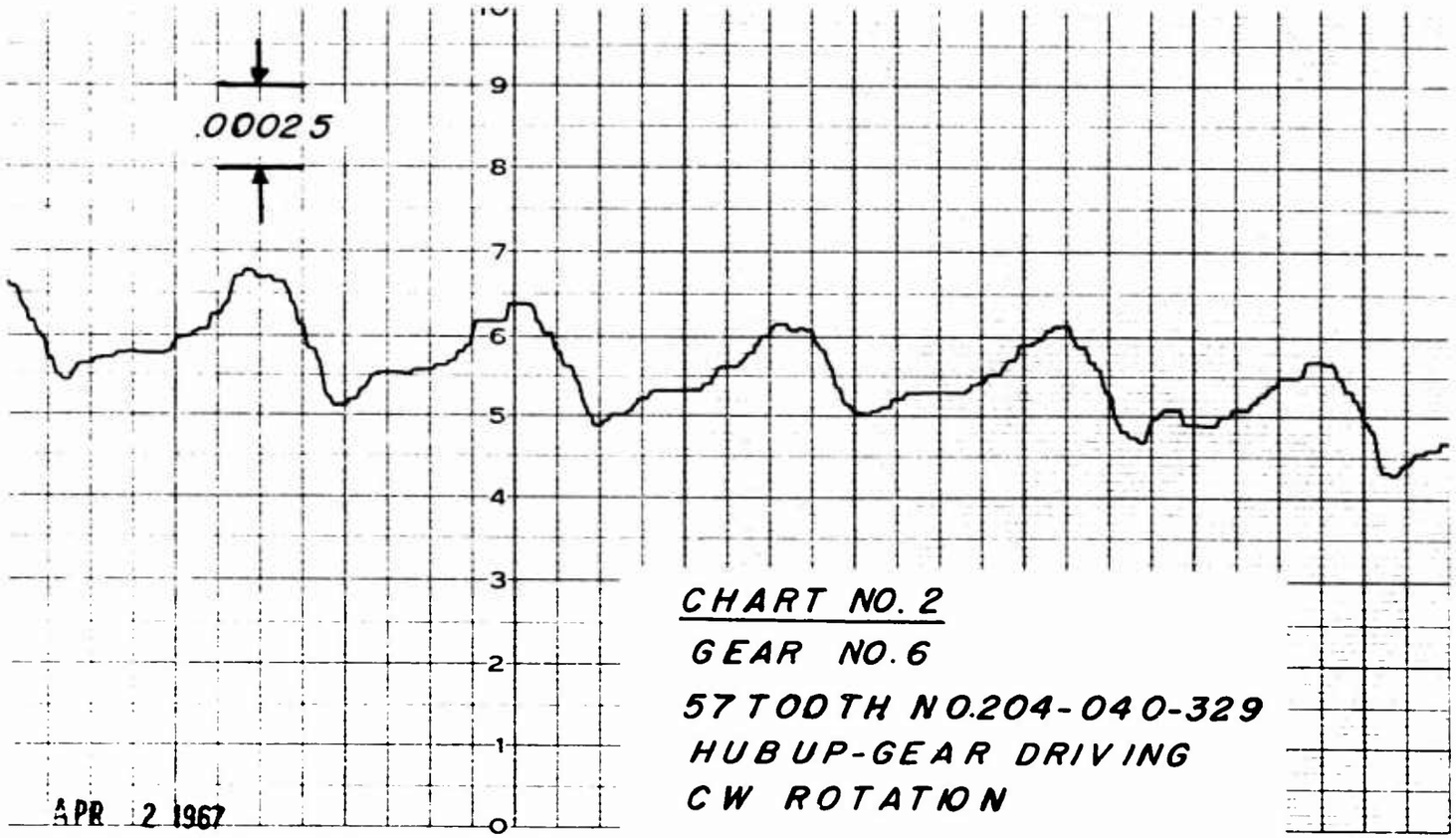

Figure 65. Portion of the Composite Gear Measurement of the Lower Stage Sun Gear as Measured on the Gear Cardiograph.

TABLE XXXII. MEASUREMENTS MADE ON UH-1D TRANSMISSION GEARS

Type of Measurement	Inspection Equipment	Gears Measured*	Illustration of Measurement (Figure Number)	Typical Results (Figure Number)
Runout	Hofler	1,2,3,4,5,6	21,22,23,24	30
Pitch or Tooth Spacing	Hofler	1,2,3,4,5,6	25	31
Tooth Profile	Hofler	3,4,5	26,27,28	32
Composite	Buckingham	3,4,5	29	33

*Identification numbers of gears inspected, 2 samples of each

1. Input stage spiral bevel pinion
2. Input stage spiral bevel gear
3. Lower stage planetary sun gear
4. Upper stage planetary sun gear
5. Planet gear common for both stages
6. Combined ring gear for both stages

APPENDIX IV

GEAR EXCITATION ANALYSIS

INTRODUCTION

One of the desired characteristics of the ideal set of gears is the transfer of motion with an absolutely constant speed ratio. As each pair of teeth goes into and out of engagement, the rotation of the driven gear will follow exactly the motion of the driving gear without any instantaneous changes or errors. In order to achieve this ideal transfer, or conjugate action as it is known, the shape of the gear teeth is designed to match a mathematical curve which is consistent with the requirement. In the case of helicopter transmission gearing, as in most other gearing in general use, the mathematical curve used is the involute of the circle. However, despite the use of the proper mathematical model, actual gears do not give this perfect motion. The departure from the ideal is due to various causes. The two most significant are the nonuniform deflection of the gear teeth and the manufacturing errors in the shape or spacing of the gear teeth. These effects combine to introduce instantaneous changes or irregularities in the transferred motion. In some gearing applications, the deviation from pure conjugate action is undesirable simply as a motion error. In helicopter gearing, the irregularity of motion becomes one of the major sources of excitation of vibration in the drive system, especially of the vibration associated with noise production.

The purpose of this analysis is to make an evaluation of these motion irregularities as deviations from pure conjugate action as a pair of loaded spur gears goes into and out of engagement. It is intended that the analysis will use only conventional gear design data and conventional gear measurement data and that the final results will be in a form suitable for introduction as excitation values in any subsequent vibration analysis.

In the course of fulfilling this purpose, the analysis also provides other useful information about the gear action. Along with the point-by-point values of the difference in motion between driving and driven gears are found the point-by-point values of the load transmitted by each pair of teeth in engagement. A plot of these values portrays the load transfer as one pair of teeth is at first joined and then replaced by the following pair. Another useful outcome of the analysis is the deflection data needed to compute mean tooth stiffness.

LIMITATIONS AND ASSUMPTIONS

The limitations of design and operation and the major assumptions on which the analysis is based are listed below. Other assumptions are given later in the section dealing with the derivations of formulas.

1. Only spur gears are treated, and these are treated only in the two cases of

   a. an external gear driving an external gear and

b. an external gear driving an internal gear.

Straight bevel gears may be treated in an approximate manner by replacing them with equivalent spur gears by Tregold's Approximation.

2. The working portions of the tooth profiles are essentially involute. Design and manufacturing profile deviations are small enough so as not to affect load location, load direction, or tooth stiffness.

3. There is no tip interference, either due to excessive addendum length or due to tooth deflection under load.

4. The spur gear centers are at a fixed spacing, or at a spacing that stays constant under constant load.

5. In any single interval between the pitch points of two successive pairs of teeth, contact and load carrying are limited to the two successive pairs of teeth. In the same interval, there must be at all times at least one pair of teeth in contact and carrying load. This prevents consideration of cases where the contact ratio is less than one or more than two; it may in some unusual designs also eliminate cases where the contact ratio has certain intermediate values.

6. The load is assumed to be transmitted uniformly across the face of the gear except for normal end effects in stress distribution. This excludes any consideration of face crowning, lead modification, lead manufacturing error, gear windup, or nonuniform deflection of gear supports.

7. The total load transmitted is constant in magnitude and direction. This signifies that there is no consideration of secondary effects of dynamic tooth forces developed as a result of the gear excitation. This also signifies that the possible effects of tooth sliding friction are not considered.

8. All variations in tooth deflection as the load point moves along the tooth profile either are confined to elastic effects on the tooth alone or can be supplied as point-by-point compliances as part of the input data. This means that variations such as might result from the deflection of thin rims are not calculated by the analysis; however, if supplied, they will be given proper consideration.

9. Any lubricant film separating the pair of mating teeth is assumed to have a constant thickness which is independent of the magnitude or the location of the transmitted load. The contact deformation is assumed to be independent of the lubricating film.

10. The measured tooth profiles for each set of two adjacent teeth on

the same gear are assumed to be identical.

DESCRIPTION OF ANALYSIS

The analysis contains five phases. The specific equations used and their origin or derivation are given separately in the next section.

The first phase determines the engagement conditions for any single pair of teeth. It starts with the basic design information for the set of gears under study, the kind of information which normally appears on the individual gear drawings. These data include the operating pressure angle and, for each of the gears, the number of teeth and the following radii: pitch circle, outside (or inside on a ring gear), base circle, root circle, and T.I.F. (i.e., radius to beginning of the involute profile). By using this information, the angles of approach and recess for each of the gears are calculated. By using a similar calculation, the rotation angles which are related to two points on the involute profile, at the root radius (for the extended involute) and at the T.I.F. radius, are found. Next, the angular spacing between adjacent gear teeth on each gear is divided into a convenient odd number of equal intervals, using the radial line through the pitch point as the zero reference. By comparing the values of angles associated with each of these subdivisions to the angles of approach and recess, the analysis determines whether the condition of engagement is present at that particular subdivision or calculation point. With the proper matching of such information from the two gears, the analysis determines whether one or two pairs of teeth will be in simultaneous engagement. The other angles mentioned above are also compared to the angles of approach and recess to provide some checks on possible errors or limitations in the original gear designs.

The second phase concerns itself with calculating the coordinates of the involute profile or, more simply, with defining the point-by-point dimensions of each gear tooth. It uses the data supplied or computed in the first phase with the addition of the fillet radius and of the circular tooth thickness measured along the pitch circle. This additional information is also normally specified on the gear drawing. If the latter is not so specified, it can be approximated from the circular pitch and backlash data. For each of the gears, the calculation process considers separately each of the subdivision angles selected in phase one and found to lie within the angles of approach and recess. Each angular position is then associated with a point on the involute profile. The direction of the line of action (or more simply, the load direction) at this point relative to the tooth centerline is found. The calculation goes on to determine the coordinates of these points relative to the same centerline. A separate calculation is used to find the coordinates of a point on the root circle which lies halfway between the tangent point of the fillet radius on the root circle and the point on the involute extended to the root circle. If the root circle lies within the base circle, the limit of the involute profile, the extension is taken as the radial line to the end of the involute. This halfway point at the fillet is considered as the end of the effective thickness of the tooth at its point of support on the gear rim.

The third phase is devoted to calculating the unit elastic compliance of the gear tooth for each load position. In addition to the data used and developed in the previous phases, this phase requires the face widths of the gear teeth, the load transmitted by the gears, and the elastic properties of the materials from which the gears are made. These latter include the tensile and shear moduli of elasticity and Poisson's ratios. The four major contributing elastic deformations are considered. The gear tooth is first treated as a wide, uniformly loaded cantilever in bending. Because of its stubby proportions and tapering outline, this cantilever requires consideration of more than the usual factors. The applied load has a transverse component which acts as an applied concentrated load on this cantilever. The axial component of this load, because it is eccentric from the tooth centerline, acts to apply a moment to the cantilever at the load point. This second load condition tends to oppose the first, and it is the combination of the two which establishes the cantilever beam component of deflection. The tapered outline comes into consideration in connection with the rotation of the transverse section at the load point which accompanies the beam deflection. This rotation shifts a greater tooth thickness over to the fixed point of load application, thus, to some extent, further offsetting the basic cantilever deflection. The nonuniform crosssection of the beam necessitates a summation process for calculation of the net bending deflection. The gear tooth is therefore treated as a composite of uniform "slices", with the slice lines located at the profile calculation points determined in the previous phase. The final slice, at the base of the tooth, lies between the profile calculation point closest to the root and the root section passing through the fillet halfway point, also determined in the previous phase.

The next elastic deformation considered is that due to shear deflection in the gear tooth resulting from the transverse component of the applied load. Because the shear deflection takes place without any rotation of sections, there is no shifting of greater tooth thickness to the point of local application. In calculating the shear deflection, the same slicing into uniform depth sections as described above has been used.

The effect of the axial component of the applied force in compressing the gear tooth, thus adding to the normal displacement at the load point, was found to be small in comparison to the other deformation and was therefore not treated.

The tooth as a cantilever beam undergoes a further significant deflection in that the beam as a rigid member rotates against the supporting restraint in the gear rim. The calculation of this deformation assumes that the rim is sufficiently thick in relation to tooth thickness to justify treatment as a semi-infinite restraint. This calculation requires only the effective thickness of the beam at its support and the net cantilevered moment and therefore is independent of the changing tooth outline. Although this foundation rotation is accompanied by a foundation shear deflection, this latter effect was small enough to be ignored.

The final contributing elastic deformation is that due to the contact or Hertzian deformation at the load point. There are various and conflicting

methods for the evaluation of this deformation. The one selected for this analysis was a modification of an empirical relationship developed for roller contact deflection in roller bearings. This relationship had two special advantages. It was in part based on deformation in the case of a convex surface loaded onto a concave surface, which is true in the case of a pinion loaded onto a ring gear. Also, the empirical relationship took into account the kind of end effects present in the load distribution across the gear face. Since the contact or Hertzian deformation is nonlinear, that is, it is dependent on load, the load becomes a factor in this deformation calculation. At this stage in the analysis, the actual load sharing which might be taking place at each calculation point has still not been determined, so that the actual load values cannot be used. Instead, this deformation calculation uses an average value in recognition of the fact that the nonlinear effect is quite small at other than very low loads, and that any error resulting from this approximation will have little effect on the total deformation calculated.

The four components of deformation are summed up for each gear design into combined unit compliances normal to the gear tooth profiles.

The fourth phase of the analysis determines the rotational displacement of the driven gear body relative to the driving gear body as a deviation from pure conjugate action. Besides the data used and generated in prior phases, the calculation makes use of profile data giving deviation from a true involute, known compliance of the structure supporting the tooth, and also any tooth spacing error (all of these for each of the two gears). The profile and support compliance data are measured along the line of action, or normal to the tooth surface, and are related to the individual calculation points using the pitch point as the zero reference. It is assumed that successive teeth on the same gear have identical profiles and support compliance conditions. The tooth spacing error is measured between pitch points of successive teeth. The calculation treats separately the case where only one pair of teeth is in engagement and the case where two pairs are in engagement. For each of the calculation points with the former case, the total displacement under the applied load is found from the deflection corresponding to the calculated unit compliance, as combined with profile or spacing deviations. For the calculation points at which two pairs of teeth are engaged, load sharing is determined by matching the total displacements, deformations plus deviations. The indication of a negative load required at one pair in order to achieve this matching, means that the full load is taken at the other pair and that the total displacement is reevaluated accordingly. This calculation then results in a value of total displacement at each calculation point, where each calculation point corresponds to a subdivision of the rotational angle between successive teeth. The load sharing present with two-pair engagement also results. These results are changed into the more convenient form of the values as measured tangent to the pitch circle.

The fifth and final phase of the analysis takes the displacement values of the previous phase and, considering them as cyclic in nature, finds the Fourier coefficients of sine and cosine components which will combine to reproduce the cyclic displacement curve. It is this Fourier calculation

which imposed the condition of an odd number of subdivisions in the tooth-to-tooth rotational angle. Although the Fourier calculation will provide coefficients for the sinusoidal functions up to a harmonic number equal to the number of data points or subdivisions, it is possible to limit the printed results to the first few harmonics which will be of special interest. When tooth spacing errors have been introduced, the displacement pattern is not cyclic, and the Fourier analysis should not be used.

The computer programming of this analysis was so prepared that the results of each phase are provided along with the final results. This permits the use of the analysis to find any of the intermediate results which might be useful for gear design and study.

DERIVATION OF ANALYTICAL RELATIONSHIPS

Analytical relationships for four of the five phases of the analysis will be presented. These are the phases that solve for the following:

1. Engagement conditions
2. Profile coordinates
3. Elastic compliance
4. Rotational deviations

The final phase, which solves for the Fourier coefficients of the sinusoidal components of the cyclic rotational deviations, uses the standard mathematical techniques. This requires no special presentation.

The symbols for all four phases are given in one list. There is extensive use of subscripts in the analysis. These are listed separately with explanations about how they restrict the major symbol to which they are attached. The final section of the list contains the major symbols. Some of these are given with their subscripts and the corresponding specific definition. Other major symbols, especially those which appear in the text with various combinations of subscripts, are listed without the subscripts and are defined in general terms only. Combining these definitions with those of the attached subscripts will give the specific definitions.

The numerical subscripts identify the gear:

1 driving gear, always an external gear
2 driven gear, either an external or an internal gear

A group of alphabetic subscripts identify points on the tooth flank:

A point at which the mating gear tooth first makes contact, the point at the beginning of the "approach" action

B point on the base circle met by the involute curve extended

E point on the root circle halfway between points M and F defined below

F point where the fillet radius is tangent to the root circle

G point where the fillet radius is tangent to the involute profile

I point on the inside or the tip diameter on internal gears

J general point on the involute portion of the tooth profile, or on the involute curve extended beyond the tooth profile. This designation is related to rotational positions of the gear or to points of contact with the mating involute

K general point on the tooth profile. This designation is used for the successive segments of the tooth used in calculating its elastic properties.

M point on the root circle and the involute profile extended, on both external and internal gears

O point on the outside diameter on external gears

P point on the pitch circle

R point at which contact is last made with the mating gear tooth, that is, the point at the end of the "recess" action

T point which is the manufacturing limit of the involute profile on its end toward the root circle

Three alphabetic subscripts identify the direction of forces and displacements or their components:

N normal to the involute profile

X parallel to the radial centerline of the tooth

Y perpendicular to the radial centerline of the tooth

A pair of alphabetic subscripts identifies the pair of mating teeth when meshing between two successive pairs is under consideration:

C first pair

D second pair

Four lower case alphabetic subscripts identify the mode of deformation under consideration. One letter is also accompanied by a numerical subscript which identifies the loading condition with which the deformation is associated. These subscripts are placed outside of parentheses enclosing the major symbol.

a bending of the tooth as a cantilevered beam

a_1 bending as a cantilevered beam under a concentrated load

a_2 bending as a cantilevered beam under a moment load

b shear deformation of the tooth as a cantilevered beam

c rotation of the tooth in the supporting structure at its base

d contact or Hertzian deformation

The major symbols are all alphabetic. Greek letters are used for angles and nondimensional ratios. Any set of consistent units may be used even though the program uses inches and pounds. All angles are in radians. The figure numbers after some of the definitions identify the figures in which they first appear.

A area of the indicated cross section of the gear tooth

B deflection at the point of loading, Figure 70

E modulus of elasticity of the gear material

E_ν modulus adjusted to account for wide teeth

F face width of the gear tooth

G shear modulus of the gear material

I moment of inertia of the indicated cross section of the gear tooth

$\bar{I}_K$ mean moment of inertia of the cross-sectional area of the portion of the gear tooth between points K and K-1

L_K length of the portion of the gear tooth between points K and K-1, Figure 70

N number of teeth

N_J number of intervals between two successive teeth, selected to give convenient points for computational purposes

Q compliance of the tooth surface in the direction of load, i.e., the deflection in this direction per unit of load

R radius to point indicated by subscript, Figure 66

R'_F fillet radius, Figure 68

S_{JK} distance between the cross section through point K and that through point J at which the load is applied, Figure 70

T circular tooth thickness at pitch circle

U compliance at the load due to elasticity outside the tooth, or its adjacent supporting material

V tooth spacing error between successive pitch points but adjusted to a line-of-action error, and positive when the second tooth is too close to the first, Figure 72

W_N load applied normal to the involute tooth profile, Figure 70

X,Y abscissa and ordinate of points on the involute profile when the origin is the center of the gear and when the x-axis is the radial centerline of the tooth, Figure 68

Z tooth profile error, normal to the true involute form and positive in the direction of excess material, Figure 72

α angle of rotation of the gear from the position at which contact is at the indicated point to the position at which contact is at the pitch point, Figure 66

ρ ratio of indicated radius to base circle radius

α_A angle of approach; also the angle α for the point of initial contact with the mating gear, Figure 66

α_R angle of recess; also the angle α for the point of final contact with the mating gear, Figure 66

γ_J angle of rotation of the cross section of the tooth at the point J due to the load applied at J, Figure 70

ε deviation in angular position from the theoretical of the driven gear relative to the driving gear, expressed as an angle on the indicated gear, and positive when the driven gear is leading the theoretical position

θ angle between two radial lines: the centerline of the tooth and a line to the indicated point on the profile, Figure 68

ν Poisson's ratio for the gear material

ϕ angle between two radial lines: a line to the indicated point on the involute curve and a perpendicular to the tangent to the base circle from the indicated point on the profile, Figure 67

ϕ_P pressure angle; also the angle ϕ for the pitch point on the involute, Figure 66

ψ angle between two radial lines: the centerline of the tooth and a perpendicular to the tangent to the base circle from the

indicated point on the profile, Figure 67

Engagement Conditions

Figure 66 shows two external gears in engagement. The points of contact on the profiles as the teeth move through engagement fall on the line of action. First contact is at A; as contact moves to the pitch point P, the driving gear rotates through α_{A1}, the angle of approach. The special characteristic of the involute curve is that the distance from its generating point to the point of tangency of the developing line on the base circle is the same whether measured along this line or along the base circle. The angle of approach of the driving gear may be found by tracing the relationships between the arcs and line segments. The minus sign has been introduced to show that a rotation backwards from the pitch-point contact position is required.

$$\alpha_{A1} = \frac{-\widehat{B_{P1}B_{A1}}}{R_{B1}} = \frac{-(\widehat{B_{P1}V_1} - \widehat{B_{A1}V_1})}{R_{B1}} = \frac{-(\overline{PV_1} - \overline{A_1V_1})}{R_{B1}} = \frac{-\overline{PA_1}}{R_{B1}}$$

$$\alpha_{A1} = \frac{-(\overline{V_2A_1} - \overline{V_2P})}{R_{B1}} = \frac{-\sqrt{\overline{C_2A_1}^2 - \overline{C_2V_2}^2} - \overline{C_2V_2}^2 \tan \phi_P}{R_{B1}}$$

$$\alpha_{A1} = -\left[\frac{\sqrt{R_O^2 - R_B^2} - R_{B2} \tan \phi_P}{R_{B1}}\right]$$

$$\alpha_{A1} = -\frac{R_{B2}}{R_{B1}}\left[\sqrt{\left(\frac{R_{02}}{R_{B2}}\right)^2 - 1} - \tan \phi_P\right] \qquad (1)$$

Using the substitutions

$$\frac{N_2}{N_1} = \frac{R_{B2}}{R_{B1}} \qquad (2)$$

and

$$\rho_{02} = \frac{R_{02}}{R_{B2}} \qquad (3)$$

Equation (1) becomes

$$\alpha_{A1} = -\frac{N_2}{N_1}\left[\sqrt{\rho_{02}^2 - 1} - \tan \phi_P\right] \qquad (4)$$

In a similar manner, the angle of recess for the driving gear may be found.

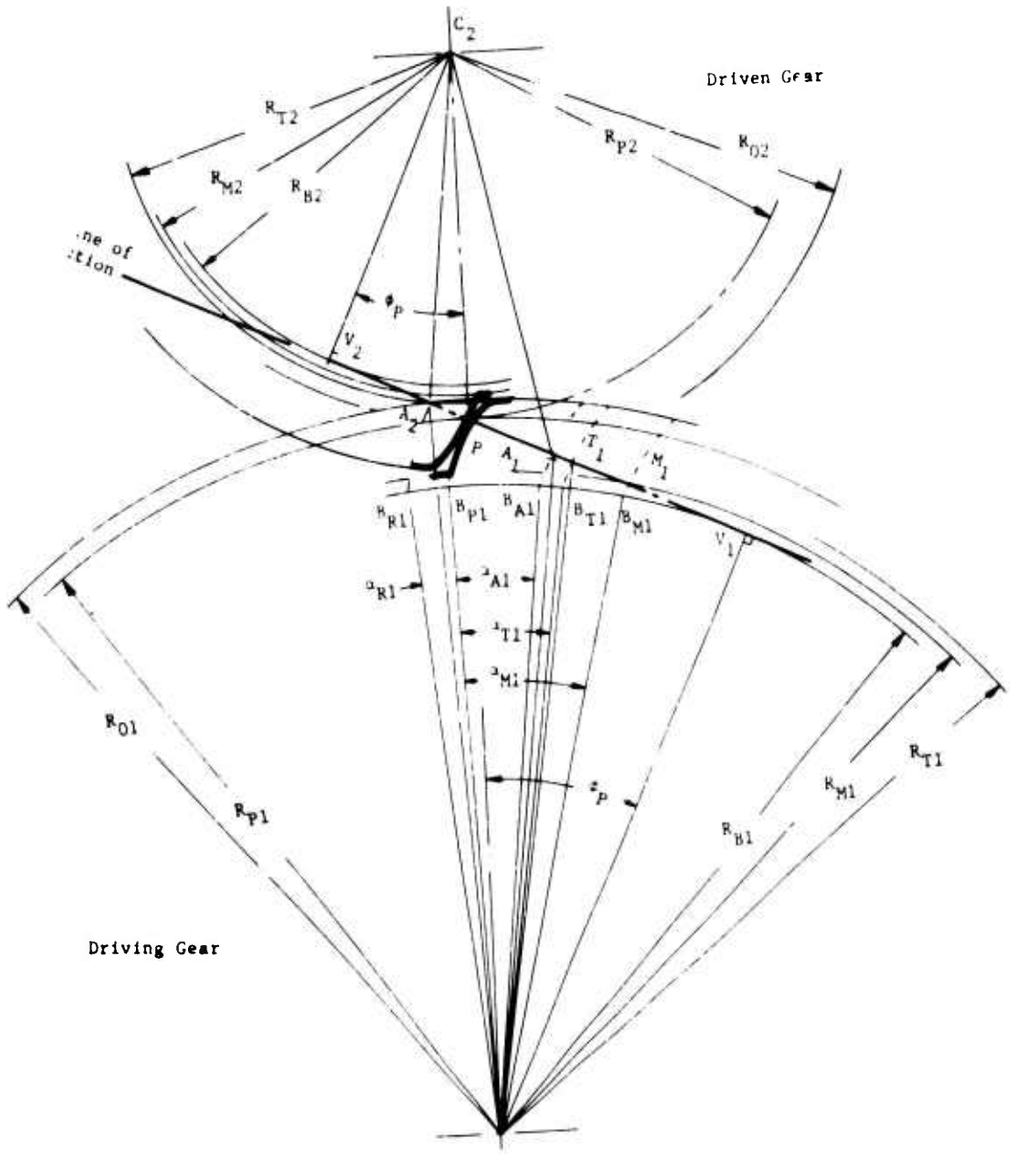

Figure 66. External Gear Tooth Driving External Gear Tooth.

$$\alpha_{R1} = \frac{\widehat{B_{R1}B_{P1}}}{R_{B1}} = \frac{\widehat{B_{R1}V_1} - \widehat{B_{P1}V_1}}{R_{B1}} = \frac{\overline{A_2V_1} - \overline{PV_1}}{R_{B1}}$$

$$\alpha_{R1} = \frac{\sqrt{\overline{C_1A_2}^2 - \overline{C_1V_1}^2} - \overline{C_1V_1} \tan \phi_P}{R_{B1}}$$

$$\alpha_{R1} = \frac{\sqrt{R_{01}^2 - R_{B1}^2} - R_{B1} \tan \phi_P}{R_{B1}}$$

$$\alpha_{R1} = \sqrt{\left(\frac{R_{01}}{R_{B1}}\right)^2 - 1} - \tan \phi_P \qquad (5)$$

Using the substitution

$$\rho_{01} = \frac{R_{01}}{R_{B1}} \qquad (6)$$

Equation (5) becomes

$$\alpha_{R1} = \sqrt{\rho_{01}^2 - 1} - \tan \phi_P \qquad (7)$$

This process may be applied to other points on the involute profile or the involute curve extended. One such point is M_1, where the extended involute intersects the root circle. If the mating tooth were long enough, contact could theoretically take place at this point. The rotation of the gear from the position of contact at the pitch point to the position of contact at M_1 is given by the angle α_{M1}. The same procedure for finding α_{R1} is used, with the minus sign introduced to show the direction of rotation from the pitch-point contact position.

$$\alpha_{M1} = - \left[\sqrt{\rho_{M1}^2 - 1} - \tan \phi_P\right] \qquad (8)$$

In a similar manner, for the point T_1, which is the manufactured starting point of the involute profile,

$$\alpha_{T1} = - \left[\sqrt{\rho_{T1}^2 - 1} - \tan \phi_P\right] \qquad (9)$$

Consideration of the driven gear gives a similar set of equations by simply replacing the subscript 2 for 1 and vice versa; Equations (4) through (7) lead to

$$\alpha_{A2} = - \frac{N_1}{N_2} \left[\sqrt{\rho_{01}^2 - 1} - \tan \phi_P\right] \qquad (10)$$

$$\alpha_{R2} = \sqrt{\rho_{02}^2 - 1} - \tan \phi_P \qquad (11)$$

$$\alpha_{M2} = -\left[\sqrt{\rho_{M2}^2 - 1} - \tan \phi_P\right] \tag{12}$$

$$\alpha_{T2} = -\left[\sqrt{\rho_{T2}^2 - 1} - \tan \phi_P\right] \tag{13}$$

These relationships may be used to check one of the features of the design of each of the gears. When the involute portion of the profile extends far enough toward the root to permit contact with the tip of the mating tooth, the following condition will be met (the direction of the inequality sign recognizes the negative values for the angles):

$$\alpha_{A1} \geq \alpha_{T1} \tag{14}$$

$$\alpha_{A2} \geq \alpha_{T2} \tag{15}$$

For purposes of computational convenience, the angle between successive teeth on the same gear is divided into N_J equal intervals. The angle between teeth is equal to 2π divided by the number of teeth, and the angle of each subdivided interval is $2\pi/N\ N_J$. These intervals form a scale which may be associated with the angle through which the gear rotates as the point of contact moves along the involute profile. Starting from a zero position when contact is at the pitch point, the successive values of J (positive as contact moves outward on the involute and negative as it moves inward) identify the intervals of rotation as follows:

$$\alpha_{J1} = J_1\left(\frac{2\pi}{N_1 N_J}\right) \tag{16}$$

$$\alpha_{J2} = J_2\left(\frac{2\pi}{N_2 N_J}\right) \tag{17}$$

To check for engagement between the teeth of one meshing pair at any rotational position, the particular value of α_{J1} or α_{J2} may be compared to the angles of rotation which limit the range of engagement. Therefore, engagement is possible only when

$$\alpha_{R1} \geq \alpha_{J1} \geq \alpha_{A1} \tag{18}$$

Figure 67 shows an external gear driving an internal gear. The identification of individual points is similar to that of Figure 66, except where the internal gear introduces differences. As in the first case, the point on the tooth profile of the driving gear at which contact initiates is A_1, and the last point is A_2. The angle of approach is found in an almost identical manner. Note that the minus is again introduced to show that rotation backwards from the pitch-point contact position is required.

$$\alpha_{A1} = \frac{-\widehat{B_{P1}B_{A1}}}{R_{B1}} = \frac{-(\widehat{B_{P1}V_1} - \widehat{B_{A1}V_1})}{R_{B1}} = \frac{-(\overline{PV_1} - \overline{A_1V_1})}{R_{B1}} = \frac{-\overline{PA_1}}{R_{B1}}$$

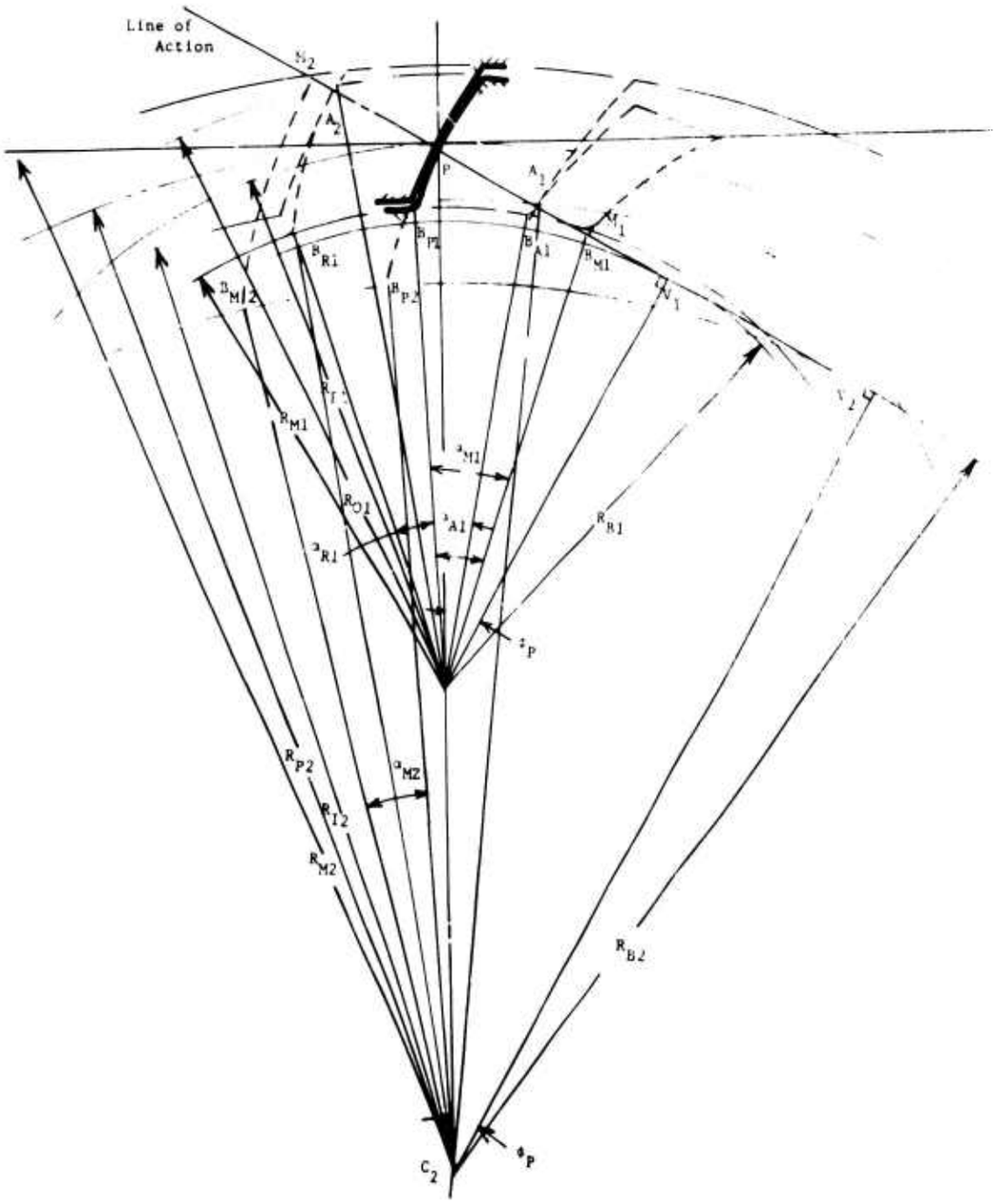

Figure 67. External Gear Tooth Driving Internal Gear Tooth.

$$\alpha_{A1} = \frac{-(\overline{V_2P} - \overline{V_2A_1})}{R_{B1}} = -\left[\frac{\overline{C_2V_2}\tan\phi_P - \sqrt{\overline{C_2A_1}^2 - \overline{C_2V_2}^2}}{R_{B1}}\right]$$

$$\alpha_{A1} = -\left[\frac{R_{B2}\tan\phi_P - \sqrt{R_{I2}^2 - R_{B2}}}{R_{B1}}\right] \tag{19}$$

$$\alpha_{A1} = -\frac{R_{B2}}{R_{B1}}\left[\tan\phi_P - \sqrt{\left(\frac{R_{I2}}{R_{B2}}\right)^2 - 1}\right] \tag{20}$$

With the substitutions

$$\frac{N_2}{N_1} = \frac{R_{B2}}{R_{B1}} \tag{21}$$

and

$$\rho_{I2} = \frac{R_{I2}}{R_{B2}} \tag{22}$$

Equation (20) becomes

$$\alpha_{A1} = -\frac{N_2}{N_1}\left[\tan\phi_P - \sqrt{\rho_{I2}^2 - 1}\right] \tag{23}$$

For the angle of recess, the procedure is identical to the earlier case. Referring to Figure 67, the derivation preceding Equation (7) may be repeated. Therefore, for the case of the driven gear as the internal gear,

$$\alpha_{R1} = \sqrt{\rho_{01}^2 - 1} - \tan\phi_P \tag{24}$$

Equations (8) and (9) are also repeated in unchanged form for this second case.

$$\alpha_{M1} = -\left[\sqrt{\rho_{M1}^2 - 1} - \tan\phi_P\right] \tag{8}$$

$$\alpha_{T1} = -\left[\sqrt{\rho_{T1}^2 - 1} - \tan\phi_P\right] \tag{9}$$

To find the corresponding angles for the driven internal gears, the interchange of subscripts cannot be used. In the case of the angles of approach and recess, another simplification is possible. When one member of the mating gears is internal, the actions of approach and recess are simultaneous. Therefore, these angles for the driven gear are the same as for the driving gear when multiplied by the gear ratio. These angles therefore become

$$\alpha_{A2} = \frac{N_1}{N_2}\alpha_{A1} \tag{25}$$

$$\alpha_{R2} = \frac{N_1}{N_2}\alpha_{R1} \tag{26}$$

When these are combined with Equations (23) and (24), the angles for the driven internal gear become

$$\alpha_{A2} = -\left[\tan\phi_P - \sqrt{\rho_{I2}^2 - 1}\right] \tag{27}$$

$$\alpha_{R2} = \frac{N_1}{N_2}\left[\sqrt{\rho_{01}^2 - 1} - \tan\phi_P\right] \tag{28}$$

An independent derivation is given for the angle associated with point M_2. This is the theoretical point where the involute profile extended intersects the root circle. Note that the root circle of the teeth on the internal gear is the one of greatest diameter.

From Figure 67,

$$\alpha_{M2} = \frac{\widehat{B_{M2}V_2}}{R_{B2}} = \frac{\widehat{B_{M2}V_2} - \widehat{B_{P2}V_2}}{R_{B2}} = \frac{\overline{M_2V_2} - \overline{PV_2}}{R_{B2}}$$

$$\alpha_{M2} = \frac{\sqrt{\overline{C_2M_2}^2 - \overline{C_2V_2}^2} - \overline{C_2V_2}\tan\phi_P}{R_{B2}}$$

$$\alpha_{M2} = \frac{\sqrt{R_{M2}^2 - R_{B2}^2} - R_{B2}\tan\phi_P}{R_{B2}}$$

$$\alpha_{M2} = \sqrt{\left(\frac{R_{M2}}{R_{B2}}\right)^2 - 1} - \tan\phi_P \tag{29}$$

Using the substitution

$$\rho_{M2} = \frac{R_{M2}}{R_{B2}} \tag{30}$$

Equation (29) becomes

$$\alpha_{M2} = \sqrt{\rho_{M2}^2 - 1} - \tan\phi_P \tag{31}$$

In a similar fashion, the equation for the rotation angle corresponding to the manufactured outer end of involute profile (not shown in Figure 67) is

$$\alpha_{T2} = \sqrt{\rho_{T2}^2 - 1} - \tan\phi_P \tag{32}$$

The same kind of design check performed with the two external gears may now be applied. When the involute portion of the tooth profiles extends sufficiently to permit contact with the tip of the mating tooth, the

following condition will be met (the direction of the inequality sign recognizes the proper sign of the angles):

$$\alpha_{A1} \geq \alpha_{T1} \tag{33}$$

$$\alpha_{R2} \geq \alpha_{T2} \tag{34}$$

As with the case of the two external gears, the same kind of subdivision of the angle between successive teeth on the same gear may be introduced. To check for engagement at any of the subdivisions of rotational positions, the same comparison as in Equation (18) is used. Engagement is possible only when

$$\alpha_{R1} \geq \alpha_{J1} \geq \alpha_{A1} \tag{35}$$

Profile Coordinates

Figure 68 shows the outline of an external gear tooth consisting of an involute profile joining the root circle with a circular fillet. The coordinates of points on the tooth outline may be found from the geometry portrayed.

From Figure 68a, for angles associated with the pitch point P,

$$\theta_P = \frac{\widehat{PQ}}{R_P} = \frac{1}{2}\frac{\widehat{PS}}{R_P}$$

$$\theta_P = \frac{T}{2R_P} \tag{36}$$

where T = tooth thickness measured along the pitch circle.

$$\psi_P = \phi_P - \theta_P \tag{37}$$

For any point J along the involute profile,

$$\psi_J = \psi_P + \alpha_J \tag{38}$$

Equations (36), (37), and (38) may be combined as follows:

$$\psi_J = (\phi_P - \frac{T}{2R_P}) + \alpha_J \tag{39}$$

The values of ϕ_P, T, and R_P may be taken from the gear design data. The value of α_J, the angle through which the gear must rotate to move the contact point from P to J, has been assigned to each point J according to Equations (16) and (17) in the previous section.

Again, from Figure 68a,

$$\tan \phi_J = \frac{\overline{JK}}{\overline{CK}} \tag{40}$$

From the properties of the involute curve,

$$\overline{JK} = \overline{PV} + \widehat{JK} \tag{41}$$

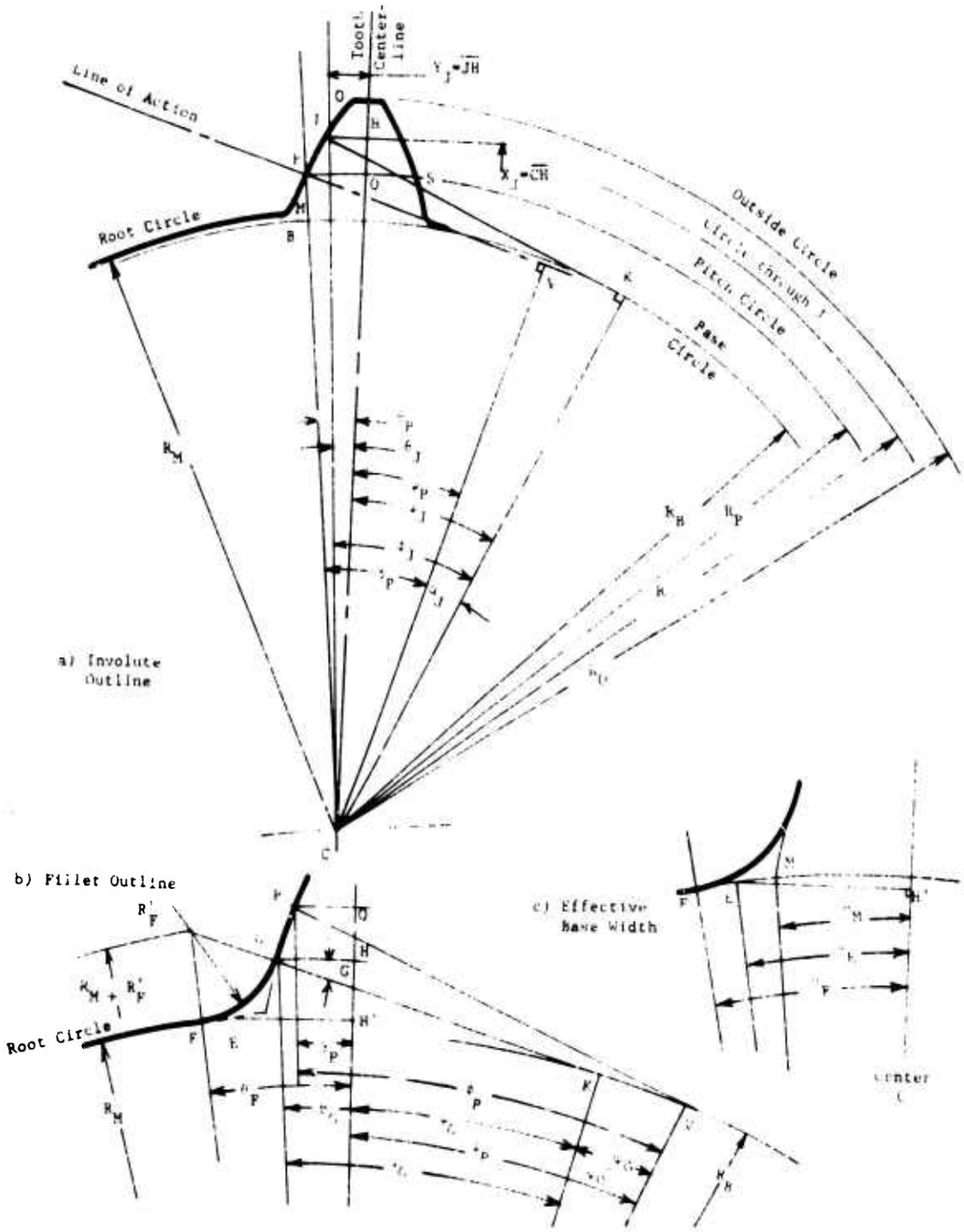

Figure 68. Outline of External Gear Tooth.

Substituting Equation (41) into Equation (42) gives

$$\tan \phi_J = \frac{\overline{PV} + \widehat{JK}}{\overline{CK}} = \frac{\overline{CV} \tan\phi_P + \overline{CK}\alpha_J}{\overline{CK}}$$

$$\tan \phi_J = \frac{R_B \tan \phi_P + R_B\alpha_J}{R_B} = \tan \phi_P + \alpha_J$$

$$\phi_J = \tan^{-1} (\tan \phi_P + \alpha_J) \tag{42}$$

As explained after Equation (39), the two values on the right-hand side are known from the design data and the selection of point J.

From Figure 38a,

$$\theta_J = \phi_J - \psi_J \tag{43}$$

The coordinates of the point J may now be expressed in terms of the angles found in Equations (42) and (43) from Figure 68a;

$$X_J = \overline{CH} = \overline{CJ} \cos \theta_J = \frac{\overline{CK}}{\cos \phi_J} \cdot \cos \theta_J$$

$$X_J = \frac{R_B \cos \theta_J}{\cos \phi_J} \tag{44}$$

$$Y_J = \overline{JH} = \overline{CJ} \sin \theta_J = \frac{\overline{CK}}{\cos\phi_J} \cdot \sin \theta_J$$

$$Y_J = \frac{R_B \sin \theta_J}{\cos \phi_J} \tag{45}$$

Figures 68b and 68c show the circular fillet which blends the involute profile into the root circle. Point G is the tangent point between the fillet and the involute, and point F is the tangent point between the fillet and the root circle. Two other points in the figure are of special interest. Point M locates the intersection of the extended involute on the root circle. Point E is located on the root circle halfway between F and M. It is taken to represent the "effective" tooth thickness at its base.

The angle θ_M, which locates point M, may be found from Equations (39), (42), and (43) which were derived for any point J on the involute profile. Replacing the subscript J by M in these equations gives

$$\psi_M = (\phi_P - \frac{T}{2R_P}) + \alpha_M \tag{46}$$

$$\phi_M = \tan^{-1} (\tan \phi_P + \alpha_M) \tag{47}$$

$$\theta_M = \phi_M - \psi_M \tag{48}$$

Note that the angle α_M may be found according to Equations (8) or (12) of the previous section.

A different procedure is used to find θ_F. First, the point G must be considered. From Figure 68b,

$$\psi_P - \psi_G = \angle KCV = \frac{\widehat{KV}}{\overline{CV}} = \frac{\overline{PV} - \overline{GK}}{\overline{CV}}$$

$$\psi_P - \psi_G = \frac{R_B \tan \phi_P - R_B \tan \phi_G}{R_B}$$

$$\psi_P - \psi_G = \tan \phi_P - \tan \phi_G$$

When rearranged,

$$\psi_G = \psi_P - \tan \phi_P + \tan \phi_G \tag{49}$$

From Figure 68b,

$$\tan \phi_G = \frac{\overline{GK}}{\overline{CK}} = \frac{\overline{DK} - \overline{DG}}{\overline{CK}} = \frac{\overline{CK} \tan (\theta_F + \psi_G) - \overline{DG}}{\overline{CK}}$$

$$\tan \phi_G = \frac{R_B \tan (\theta_F + \psi_G) - R'_F}{R_B}$$

$$\tan \phi_G = \tan (\theta_F + \psi_G) - \rho'_F \tag{50}$$

where

$$\rho'_F = \frac{R'_F}{R_B}$$

Again, from Figure 68b,

$$\tan (\theta_F + \psi_G) = \frac{\overline{DK}}{\overline{CK}} = \frac{\sqrt{\overline{CD}^2 - \overline{CK}^2}}{\overline{CK}}$$

$$\tan (\theta_F + \psi_G) = \frac{\sqrt{(R_M + R'_F)^2 - R_B^2}}{R_B}$$

$$\tan (\theta_F + \psi_G) = \sqrt{(\rho_M + \rho'_F)^2 - 1} \tag{51}$$

where

$$\rho_M = R_M/R_B.$$

Equation (51) may be rearranged to give

$$\theta_F = \tan^{-1} \sqrt{(\rho_M + \rho'_F)^2 - 1} - \psi_G \tag{52}$$

Combining Equations (49), (50), and (52) gives

$$\psi_G = \psi_P - \tan \phi_P + \sqrt{(\rho_M + \rho_F')^2 - 1} - \rho'_F \tag{53}$$

Equation (53) may now be substituted into Equation (52) and

$$\theta_F = \tan^{-1} \sqrt{(\rho_M + \rho_F')^2 - 1} - \sqrt{(\rho_M + \rho_F')^2 - 1} + \rho_F' - \psi_P + \tan \phi_P \tag{54}$$

Point E may now be located. By definition,

$$\theta_E = \frac{1}{2} (\theta_M + \theta_F) \tag{55}$$

The coordinates of point E are

$$X_E = \overline{CH'} = \overline{CE} \cos \theta_E$$

$$X_E = R_M \cos \theta_E \tag{56}$$

$$Y_E = \overline{EH'} = \overline{CF} \sin \theta_E$$

$$Y_E = R_M \sin \theta_E \tag{57}$$

In summary, to find the coordinates X_E and Y_E on the external gear, use Equations (46), (47), and (48) to find θ_M and Equation (54) to θ_F, combine these in Equation (55), and finally use Equations (56) and (57).

The case of the internal gear is treated in the same manner. Figures 69a and 69b use the same letters to label the corresponding points on the internal gear. The derivation for the coordinates of the point J on the involute profile is identical to that for the external gears and leads to identical equations. Equations (39), (42), (43), (44), and (45) are repeated below.

$$\psi_J = (\phi_P - \frac{T}{2R_P}) + \alpha_J \tag{58}$$

$$\phi_J = \tan^{-1} (\tan \phi_P + \alpha_J) \tag{59}$$

$$\theta_J = \phi_J - \psi_J \tag{60}$$

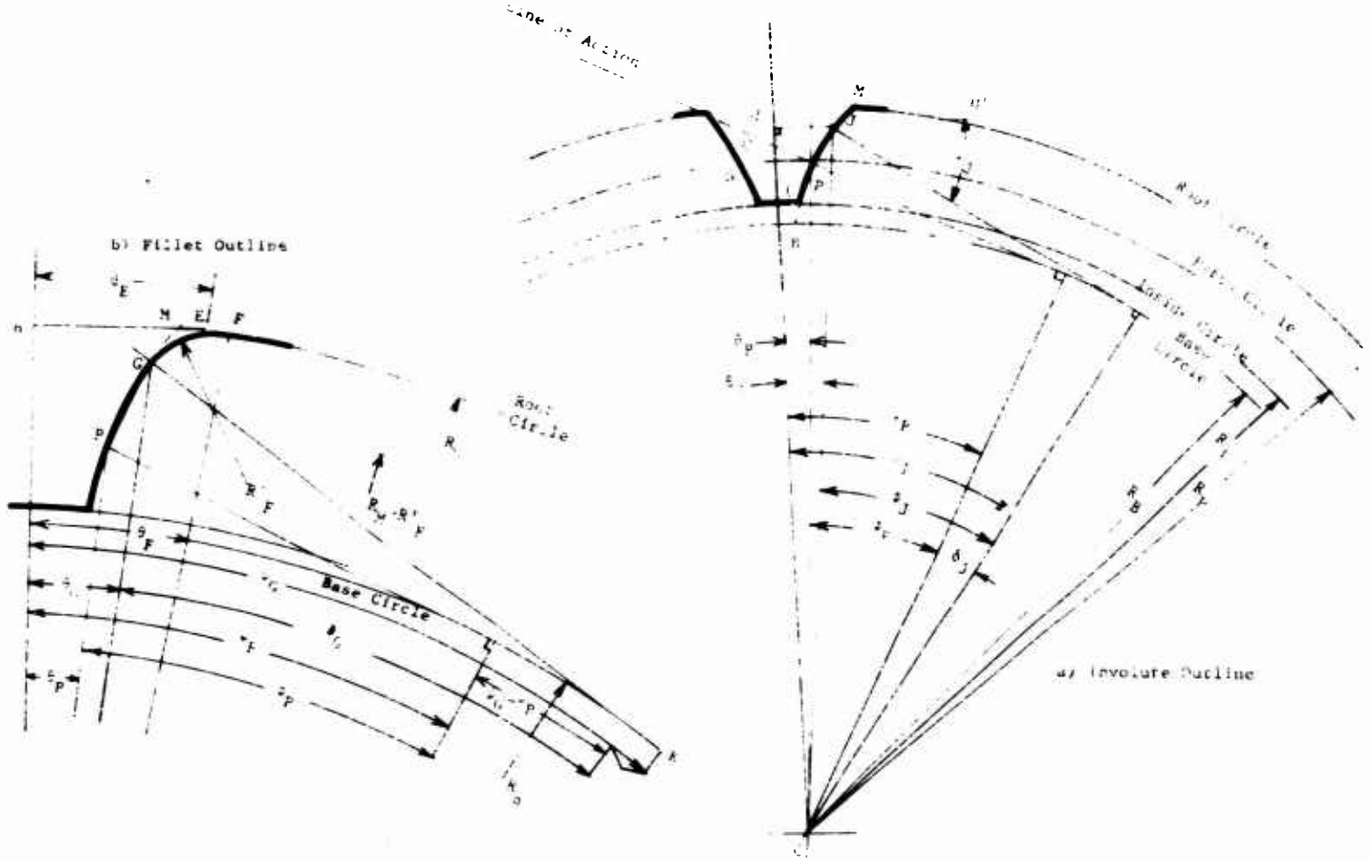

Figure 69. Outline of Internal Gear Tooth.

$$X_J = \frac{R_B \cos \theta_J}{\cos \phi_J} \tag{61}$$

$$Y_J = \frac{R_B \sin \theta_J}{\cos \phi_J} \tag{62}$$

In the same manner, Equations (46), (47), and (48) which solve for θ_M may be repeated for the internal gear.

$$\psi_M = (\phi_P - \frac{T}{2R_P}) + \alpha_M \tag{63}$$

$$\phi_M = \tan^{-1} (\tan \phi_P + \alpha_M) \tag{64}$$

$$\theta_M = \phi_M - \psi_M \tag{65}$$

The equations for finding θ_F are only slightly different. They may be found by following the identical procedure used for the external gear.

From Figure 69b,

$$\psi_G - \psi_P = \angle KCV = \frac{\widehat{VK}}{\overline{CV}} = \frac{\overline{GK} - \overline{PV}}{\overline{CV}}$$

$$\psi_G - \psi_P = \frac{R_B \tan \phi_G - R_B \tan \phi_P}{R_B}$$

$$\psi_G - \psi_P = \tan \phi_G - \tan \phi_P$$

$$\psi_G = \psi_P - \tan \phi_P + \tan \phi_G \tag{66}$$

Equation (66) is identical to Equation (49).

From Figure 69b,

$$\tan \phi_G = \frac{\overline{GK}}{\overline{CK}} = \frac{\overline{DK} + \overline{DG}}{\overline{CK}} = \frac{\overline{CK} \tan (\psi_G - \theta_F) + \overline{DG}}{\overline{CK}}$$

$$\tan \phi_G = \frac{R_B \tan (\psi_G - \theta_F) + R_F'}{R_B}$$

$$\tan \phi_G = \tan (\psi_G - \theta_F) + \rho'_F \tag{67}$$

From Figure 69b

$$\cos (\psi_P - \theta_P) = \frac{\overline{DK}}{\overline{CK}} = \frac{\sqrt{\overline{CD}^2 - \overline{CK}^2}}{\overline{CK}}$$

$$\tan(\psi_G - \theta_F) = \frac{\sqrt{(R_M - R'_F)^2 - R_B^2}}{R_B}$$

$$(\psi_G - \theta_F) = \tan^{-1}\sqrt{(\rho_M - \rho_F')^2 - 1} \tag{68}$$

This may be rearranged to

$$\theta_F = -\tan^{-1}\sqrt{(\rho_M - \rho_F')^2 - 1} + \psi_G \tag{69}$$

Combining Equations (66), (67), and (68) gives

$$\psi_G = \psi_P - \tan\phi_P + \sqrt{(\rho_M - \rho_F')^2 - 1} + \rho_F' \tag{70}$$

Substituting Equation (70) into Equation (69) gives

$$\theta_F = -\tan^{-1}\sqrt{(\rho_M - \rho_F')^2 - 1} + \sqrt{(\rho_M - \rho_F')^2 - 1} + \rho_F' + \psi_P - \tan\phi_P \tag{71}$$

The balance of the derivations for the internal gear are again identical to those for the external gear. Equations (55), (56), and (57) apply also to the internal gear and are repeated below.

$$\Theta_E = \frac{1}{2}(\Theta_M + \Theta_F) \tag{72}$$

$$X_E = R_M \cos\Theta_E \tag{73}$$

$$Y_E = R_M \sin\Theta_E \tag{74}$$

Equations (63), (64), and (65) together with Equations (71), (72), (73), and (74) serve the purpose of evaluating the coordinates X_E and Y_E.

Elastic Compliance of the Gear Teeth

The load acting on the gear tooth develops a pattern of deformation within the tooth and its supporting structure. The effective deflection at the load point is the subject of this portion of the analysis. The total value of this deformation will be derived from the summation of individual contributors, each found by applying a simple deflection analysis. The contributing deformations which will be considered here are given below. Each will be in the form of a displacement of the tooth surface at the load point in the direction of the applied normal load.

$(B_J)_a$ displacement due to the bending of the tooth as a cantilevered beam

$(B_J)_b$ displacement due to the shear deformation of the tooth as a cantilevered beam

$(B_J)_c$ displacement due to the rotation of the tooth in the supporting structure at its base

$(B_J)_d$ displacement due to the contact or Hertzian deformation

There are two other contributing deformations. One is the displacement due to radial compression of the tooth. The other is the displacement due to transverse shear in the supporting structure of the tooth. Both of these have been omitted because in the geometry of gear teeth, they contribute substantially less to the total displacement than the factors included.

In finding the first two deformations, $(B_J)_a$ and $(B_J)_b$, the gear tooth will be treated as a sequence of transverse segments, each of uniform rectangular cross section. The depth of the uniform section will be intermediate to the depths at both ends of the segment. Figure 70 shows an external gear tooth with one such segment. Each segment will be identified by a K value associated with its outer section, and the K value will be increasing as the K section moves out toward the tip of the tooth. The selection of the location of each K section may be made to correspond to the location of each of the J points described in the previous sections, as long as the J points are sufficiently close to each other. Such a selection permits the use of the X and Y coordinates for the points on the tooth outline, as found previously. In Figure 70, J represents the point at which the load is applied. The angle ψ_J gives the direction of this load relative to the tooth centerline, and ψ_J is the same angle as found by Equation (39). The analysis which follows traces the contribution of each K segment to the displacement at the point J, which itself remains fixed. As the mating gears rotate, J moves into successive portions, and the deflection calculations must be repeated for each new position.

The moment of inertia of the rectangular cross-sectional area at K may be expressed in terms of the Y coordinate and the tooth face width F.

$$I_K = \frac{1}{12} F (2Y_K)^3 = \frac{2FY_K^3}{3}$$

At the K-1 cross section, which is the other end of the K segment,

$$I_{K-1} = \frac{2FY_{K-1}^3}{3}$$

For the assumed uniform cross section of the segment between K and K-1, the mean of the two moments of inertia will be used.

$$\bar{I}_K = \frac{I_K + I_{K-1}}{2}$$

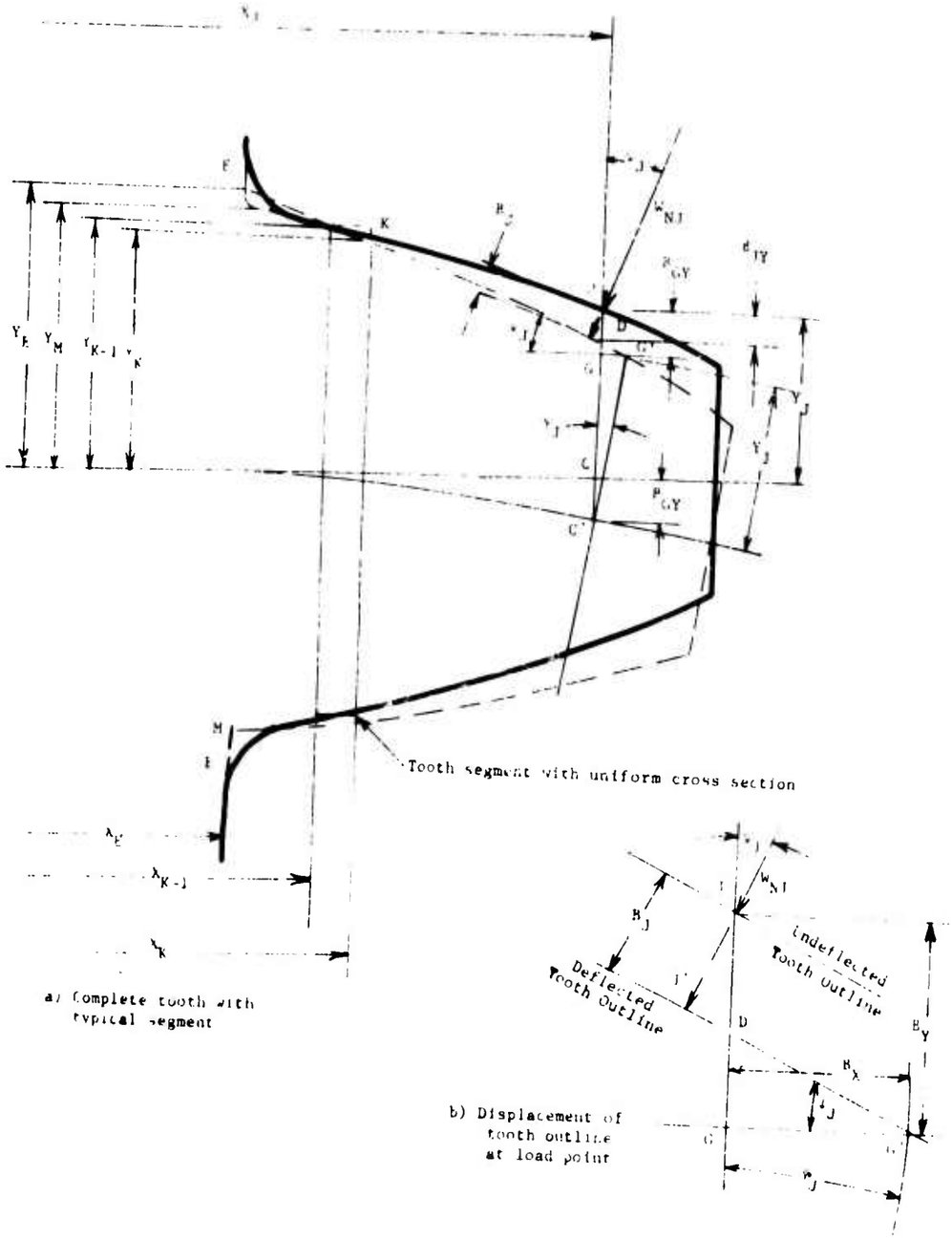

Figure 70. Beam Deflections in the Gear Tooth.

$$\bar{I}_K = \frac{F}{3}(Y_K^3 + Y_{K-1}^3) \tag{75}$$

In the same manner, the mean area for the two cross sections may be found.

$$A_K = F(2Y_K) = 2FY_K$$

$$A_{K-1} = 2FY_{K-1}$$

$$\bar{A}_K = \frac{A_K + A_{K-1}}{2}$$

$$\bar{A}_K = F(Y_K + Y_{K-1}) \tag{76}$$

The length of the K segment may be found from the X coordinates.

$$L_K = X_K - X_{K-1} \tag{77}$$

Each of the above Equations, (75), (76), and (77), will also be applied to the segment of lowest K value, the one situated at the base of the tooth. The K-1 point will not be on the involute curve because of the fillet radius between the involute profile and the root circle. The X and Y coordinates to be used at this K-1 point will therefore be those found for the effective base of the gear tooth, namely, X_E and Y_E, as found, for example, in Equations (56) and (57).

The distance of the K segment, at its outer end, from the point J of load application is similarly found from the X coordinates of the points K and J.

$$S_K = X_J - X_K \tag{78}$$

Another variable which will be used in the deflection calculations is the bending modulus of elasticity E. This will appear in the denominator of the expressions for bending deflections.

Many gears have a face width which is large compared to the tooth thickness. This greater width gives an added stiffening effect which must be included in the bending deflection equation. The necessary factor is $(1-\nu^2)$, which customarily appears in the numerator of the deflection expression. For convenience in writing equations, this factor will here be applied as a correction factor to E, giving a corrected modulus of elasticity

$$E_\nu = \frac{E}{(1-\nu^2)} \tag{79}$$

If the gear tooth is narrow relative to its thickness, the correction factor should be dropped.

In Figure 70a, the normal load at J acts in two ways to load the cantilevered gear tooth:

1. A concentrated load equal to the transverse component of the

applied load, $W_{NJ} \cos \psi_J$.

2. A moment load equal to the axial component of the applied load times one-half the thickness of the tooth at the point of load application, $W_{NJ} \sin \psi_J \cdot Y_J$.

In the bending of the tooth, each of these load conditions causes a transverse displacement and a rotation of the tooth centerline under the point of load application. These two displacements will be evaluated for each of the two load conditions and then combined.

As mentioned earlier, the procedure for finding deflections will treat the gear tooth as a succession of transverse segments of uniform cross section. The contributions of all segments will be found and summed to give the total deflection.

The first case to be considered is that of a tooth segment subjected to a transverse load applied some distance away, with the rest of the gear tooth serving as a rigid support or a rigid extension. This is portrayed in its simplest form in the sketch below.

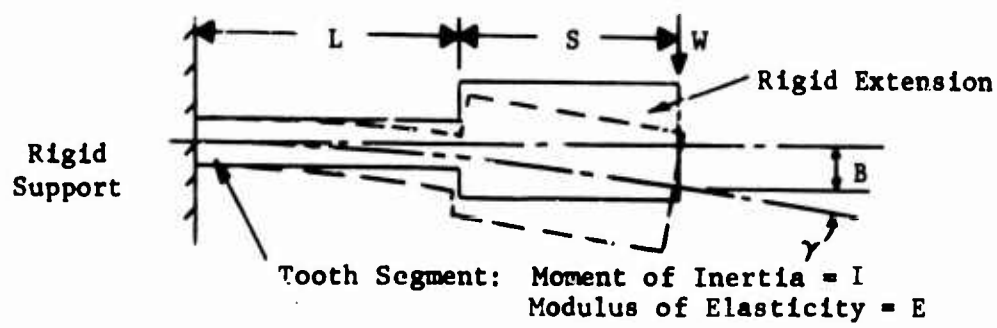

From the standard methods of beam deflection analysis, the transverse deflection at the load is

$$B = \frac{WL}{3EI} (L^2 + 3SL + 3S^2) \tag{80}$$

The centerline rotation at the load is

$$\gamma = \frac{WL}{2EI} (L + 2S) \tag{81}$$

These may be rewritten in the terminology of the main analysis. For the K segment with load applied at J,

B becomes $(B_{YK})_{al}$

E becomes E_ν

I becomes $\bar{I}_K$

L becomes L_K

S becomes S_{JK}

W becomes $W_{NJ} \cos \psi$

γ becomes $(\gamma_{JK})_{al}$

Therefore, the two centerline displacements under the transverse component of the total load are

$$(B_{YK})_{al} = \frac{W_{NJ} \cos \psi_J L_K}{3E_v \bar{I}_K} (L^2_K + 3S_{JK}L_K + 3S^2_{JK}) \tag{82}$$

$$(\gamma_{JK})_{al} = \frac{W_{NK} \cos \psi_J L_K}{2E_v \bar{I}_K} (L_K + 2S_{JK}) \tag{83}$$

The second case to be considered is that of the tooth segment subjected to a moment load applied some distance away, with the rest of the gear tooth acting as a rigid support or a rigid extension. This is portrayed in its simplest form in the sketch below.

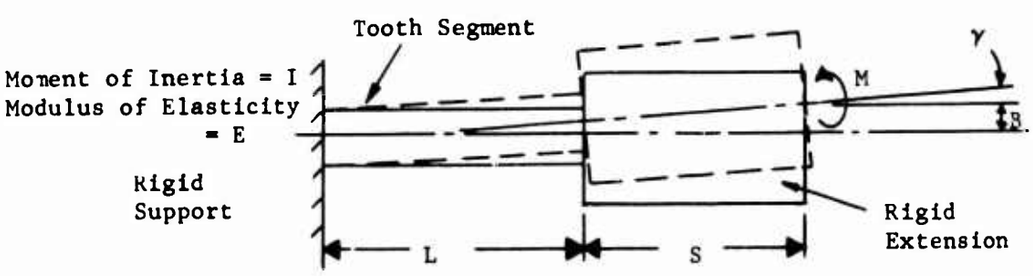

From the standard methods of beam deflection analysis, the transverse deflection at the load is

$$B = -\frac{ML}{2EI}(L + 2S) \tag{84}$$

The centerline rotation at the load is

$$\gamma = -\frac{ML}{EI} \tag{85}$$

The minus sign is included because, with a moment applied in the direction shown, the directions for the deflection are opposite to those in the previous case.

These two equations may be rewritten in the terminology of the main

analysis using the same replacements as listed above, with the addition that

$$M \text{ becomes } W_{NJ}\sin\psi_J \cdot Y_J$$

The new equations

$$(B_{YK})_{a2} = \frac{-W_{NJ}\sin\psi_J \cdot Y_J L_K}{2E_\nu \bar{I}_K}(L_K + 2S_{JK}) \tag{86}$$

$$(\gamma_{JK})_{a2} = \frac{-W_{NJ}\sin\psi_J \cdot Y_J \cdot L_K}{E_\nu \bar{I}_K} \tag{87}$$

The deflections for each tooth segment will be summed next. Equations (82), (83), (86), and (87) are rewritten showing this summation, which is for all K segments from the base of the tooth to the point J of applied load. The factors which do not vary with individual segment are written outside the summation sign.

$$(B_Y)_{a1} = \frac{W_{NJ}\cos\psi_J}{3E_\nu \bar{I}_K} \sum L_K(L_K^2 + 3S_{JK}L_K + 3S_{JK}^2) \tag{88}$$

$$(\gamma_J)_{a1} = \frac{W_{NJ}\cos\psi_J}{2E_\nu \bar{I}_K} \sum L_K(L_K + 2S_{JK}) \tag{89}$$

$$(B_Y)_{a2} = \frac{-W_{NJ}\sin\psi_J \cdot Y_J}{2E_\nu \bar{I}_K} \sum L_K\,(L_K + 2S_{JK}) \tag{90}$$

$$(\gamma_J)_{a2} = \frac{-W_{NJ}\sin\psi_J \cdot Y_J}{E_\nu \bar{I}_K} \sum L_K \tag{91}$$

The combination of these displacements will begin with consideration of each load condition separately. The effect of the combined transverse and rotation displacements associated with each load will be found, and then the two effects will themselves be combined.

Figure 70 shows the manner in which the two types of displacements combine. The transverse displacement is shown as $\overline{CC'}$; the angular rotation, as $\angle JC'G'$. An important result of the rotation is that the deflected tooth outline does not pass through the point G where $\overline{JG} = \overline{CC'}$. Instead, it passes through the axially displaced point G'. The displacement in the direction of the load is therefore from J to J', a lesser distance than would result from no centerline rotation. Described in different terms, the centerline rotation due to bending combines with the inclined outline at the load to "cam up" or to reduce the deflection under the load.

The relationship between these displacements can be found from the

geometry shown in Figure 70b.

$$\overline{JD} = \overline{JG} - \overline{DG} \tag{92}$$

$$\overline{JD} = \frac{\overline{JJ'}}{\cos\psi_J} = \frac{B_J}{\cos\psi_J} \tag{93}$$

where B_J is the displacement of the tooth outline in the direction of the applied force.

$$\overline{JG} = \overline{CC'} = B_Y \tag{94}$$

where B_Y is the transverse displacement described above.

$$\overline{DG} = \overline{GG'} \tan\psi_J \tag{95}$$

$$\overline{GG'} = \overline{GC'} \quad (\angle GC'G') \tag{96}$$

$$\overline{GC'} = \overline{JC} = Y_J \tag{97}$$

where Y_J is one-half the thickness of the tooth at point J.

$$\angle GC'G' = \gamma_J \tag{98}$$

where γ_J is the angular rotation described above.

Combining Equations (92) through (98) gives

$$\frac{B_J}{\cos\ _J} = B_Y - Y_J\psi_J \tan\ _J$$

Multiplying through by $\cos\psi_J$ changes this to

$$B_J = B_Y\cos\psi_J - Y_J\gamma_J \sin\psi_J \tag{99}$$

Equation (99) can now be used to combine the individual displacements. For the two displacements from the concentrated load condition, Equations (88) and (89) are introduced into Equation (99).

$$(B_J)_{al} = \frac{W_{NJ}}{E_v\overline{I}_K}\left[\frac{\cos^2\psi_J}{3}\sum L_K(L_K^{\ 2} + 3S_{JK}L_K + 3S_{JK}^{\ 2} - \frac{\cos\psi_J\sin\psi_J \cdot Y_J}{2}\sum L_K(L_K + 2S_{JK})\right] \tag{100}$$

For the moment load condition, Equations (90) and (91) are introduced into Equation (99).

$$(B_J)_{a2} = \frac{W_{NJ}}{E_v \bar{I}_K} \left[- \frac{\cos\psi_J \sin\psi_J \cdot Y_J}{2} \sum L_K (L_K + 2S_{JK}) + \sin^2\psi_J Y_J \sum L_K \right] \quad (101)$$

The total displacement of the tooth outline in the load direction from the combination of the two load conditions is

$$(B_J)_a = (B_J)_{a1} + (B_J)_{a2} \quad (102)$$

Introducing Equations (100) and (101) into equation (102) gives

$$(B_J)_a = \frac{W_{NJ}}{E_v \bar{I}_K} \left[\frac{\cos^2\psi_J}{3} \sum L_K (L_K^2 + 3S_{JK}L_K + 3S_{JK}^2) - \cos\psi_J \sin\psi_J \cdot Y_J \sum L_K (L_K + 2S_{JK}) + \sin^2\psi_J \cdot Y_J^2 \sum L_K \right] \quad (103)$$

This gives the total deflection from the bending of the tooth loaded as a cantilevered beam.

The shear deflection of the tooth as a cantilevered beam is caused by the same transverse component of the applied load, namely, $W_{NJ}\cos\psi_J$. This deflection takes the form of offsetting the centerline without rotating any transverse section. The deflection at the load point then becomes the sum of the deflections for each of the tooth segments defined previously.

The individual segment subjected to the shear load is represented in the sketch below, with the rest of the gear tooth appearing as a rigid support or a rigid extension.

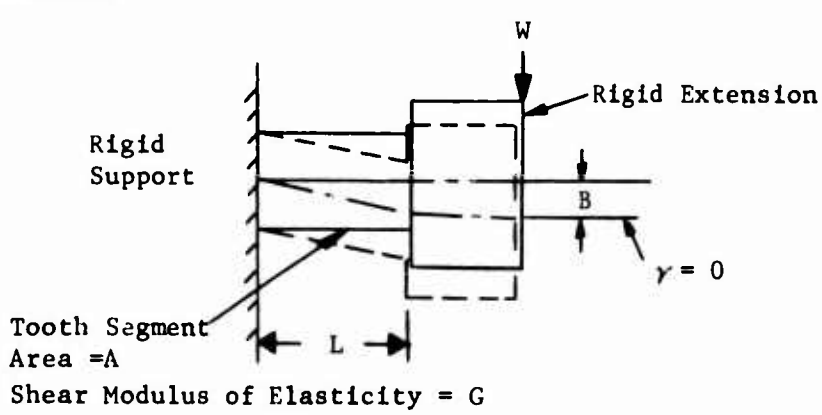

From the standard methods for beam shear deflection analysis, the transverse deflection when the cross section is rectangular is

$$B = \frac{1.2\ WL}{GA} \tag{104}$$

As noted above, the centerline rotation at the load is

$$\gamma = 0 \tag{105}$$

Rewritten in the terminology of the main analysis, for the segment K with the load applied at J,

A becomes $\bar{A}_K$

B becomes $(B_{YK})_b$

G becomes G

L becomes L_K

W becomes $W_{NJ}\cos\psi_J$

γ becomes $(\gamma_{JK})_b$

Making the replacements in Equations (104) and (105) gives

$$(B_{YK})_b = \frac{1.2W_{NJ}\cos\psi_J \cdot L_K}{G\bar{A}_K} \tag{106}$$

$$(\gamma_{JK})_b = 0 \tag{107}$$

Summing the deflection for all segments from the base of the tooth to the point J of the applied load gives

$$(B_Y)_b = \frac{1.2W_{NJ}\cos\psi_J}{G}\sum\frac{L_K}{\bar{A}_K} \tag{108}$$

$$(\gamma_J)_b = 0 \tag{109}$$

To obtain the resulting displacement of the tooth outline in the direction of the load, Equations (108) and (109) are substituted into Equation (99)

$$(B_J)_b = \frac{1.2W_{NJ}\cos^2\psi_J}{G}\sum\frac{L_K}{\bar{A}_K} \tag{110}$$

Equation (110) gives the displacement due to the shear deformation of the tooth as a cantilevered beam.

The third contributor to tooth deformation comes from the rotation of the tooth as a rigid member in its supporting structure at its base. The moment that causes this rotation comes from the applied load. The transverse component of this load $W_{NJ}\cos\psi_J$ will create the moment $W_{NJ}\cos\psi_J \cdot S_J$,

where S_J is the distance from the load point to the base of the tooth. The axial component, as noted previously, will create the moment $W_{NJ}\sin\psi_J \cdot Y_J$ which acts to oppose the first moment.

The sketch below shows this loading and the resulting deflection in simplified form.

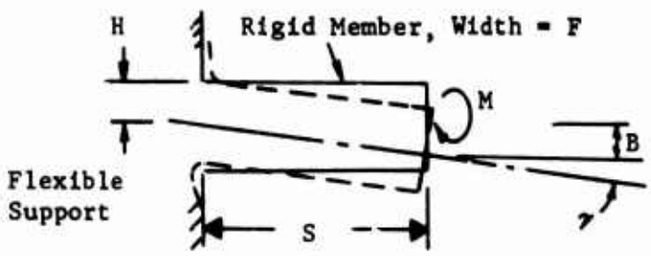

The equations for the displacements at the load are (see Reference 10)

$$\gamma = \frac{1.327\ M}{EH^2F} \tag{111}$$

$$B = \gamma S = \frac{1.327\ MS}{EH^2F} \tag{112}$$

Rewritten in the terminology of the main analysis,

B	becomes	$(B_Y)_c$
E	becomes	E_ν
F	becomes	F
H	becomes	Y_E
M	becomes	$W_{NJ}\cos\psi_J \cdot S_J - W_{NJ}\sin\psi_J \cdot Y_J$
S	becomes	$S_J (= X_J - X_E)$
γ	becomes	$(\gamma_J)_c$

Making the replacements in Equations (111) and (112) gives

$$(B_Y)_c = \frac{1.327W_{NJ}(\cos\psi_J \cdot S_J - \sin\psi_J \cdot Y_J)S_J}{E_\nu Y_E{}^2F} \tag{113}$$

$$(\gamma_J)_c = \frac{1.327\ W_{NJ}(\cos\psi_J \cdot S_J - \sin\psi_J \cdot Y_J)}{E_v Y_E^2 F} \tag{114}$$

To obtain the resulting displacement of the tooth outline in the direction of the load, Equations (113) and (114) are substituted into Equation (99).

$$(B_J)_c = \frac{1.237W_{NJ}(\cos\psi_J \cdot S_J - \sin\psi_J \cdot Y_J)\ (\cos\psi_J \cdot S_J - \sin\psi_J \cdot Y_J)}{E_v Y_E^2 F}$$

$$(B_J)_c = \frac{1.327W_{NJ}\ (\cos\psi_J \cdot S_J - \sin\psi_J \cdot Y_J)^2}{E_v Y_E^2 F} \tag{115}$$

Equation (115) gives the displacement due to the rotation of the tooth in its supporting structure.

Equations (103), (110), and (115) have all been derived with the external gear tooth in mind. However, the same equations apply for the internal gear tooth, as long as the values for L_K, S_{JK}, and S_J are maintained as positive values and as long as the summation of the K segments proceeds between the base of the tooth and the load point.

Each of these three equations may be rewritten to express a compliance, or deflection per unit load, defined as

$$Q_J = \frac{B_J}{W_{NJ}} \tag{116}$$

Equation (103) becomes

$$(Q_J)_a = \frac{1}{E_v I_K}\left[\frac{\cos^2\psi_J}{3}\sum L_K(L_K^2 + 3S_K L_K + 3S_{JK}^2) - \cos\psi_J \sin\psi_J \cdot Y_J \sum L_K(L_K + 2S_{JK}) + \sin^2\psi_J \cdot Y_J^2 \sum LK\right] \tag{117}$$

Equation (110) becomes

$$(Q_J)_b = \frac{1.2\ \cos^2\psi_J}{G}\sum\frac{L_K}{\bar{A}_K} \tag{118}$$

Equation (115) becomes

$$(Q_J)_c = \frac{1.327(\cos\psi_J \cdot S_J - \sin\psi_J \cdot Y_J)^2}{E_v Y_E^2 F} \tag{119}$$

These three compliances combined may be viewed as the total beam compliance

of the gear tooth

$$(Q_J)_{abc} = (Q_J)_a + (Q_J)_b + (Q_J)_c \tag{120}$$

This total compliance can be found independently for each of the mating gear teeth by using the above equation.

The accuracy of these equations has been checked by comparison to some unpublished experimental results. These results came from a test procedure which permitted the separation of the beam deflection of one gear tooth from other deflections. The agreement of calculated results with measured results for the cases analyzed was better than ten percent.

The fourth and final elastic displacement to be considered is that of the contact or Hertzian deformation. The treatment of this deformation which will be used in this analysis is based on a semi-empirical equation developed for contacting cylinders in ordinary roller bearings. This equation, with terminology revised to resemble the terminology of this analysis, is (Reference 11)

$$B_{12} = \frac{3\times10^{-4}\varepsilon_E^{2.7}\, W^{0.9}}{F_{12}^{0.8}} \tag{121}$$

where

$$\varepsilon_E = \sqrt[3]{\frac{11,500(E_{\nu1} + E_{\nu2})}{(E_{\nu1}E_{\nu2})}} \tag{122}$$

This equation treats the general case in which the materials of the two mating surfaces have different properties. Subscripts 1 and 2 are used to refer to the two surfaces. The deflection given by the equation is for the two contacting surfaces combined; hence, the notation of 12 is used in the subscript. Since the face widths of the two surfaces may be unequal, F_{12} refers to the effective face width of the combination. A suitable approximation of this effective face width is the smaller of the two widths.

The notation for a composite modulus of elasticity may be introduced.

$$\frac{1}{E_{\nu12}} = \frac{1}{2}\left(\frac{1}{E_{\nu1}} + \frac{1}{E_{\nu2}}\right. = \frac{(E_{\nu1} + E_{\nu2})}{2(E_{\nu1}E_{\nu2})} \tag{123}$$

After the substitution of Equation (123) is made in Equation (122), the result may be combined with Equation (121). When fully simplified, this becomes

$$B_{12} = \frac{2.55\, W^{0.9}}{E_{\nu12}^{0.9}\, F_{12}^{0.8}} \tag{124}$$

Equation (124) will be revised somewhat to adapt it more closely to the case of contacting gear teeth. This will be done after noting a major difference between the conditions applying to a roller between bearing races and those applying to a loaded gear tooth. Although, in both cases,

contact is between cylindrical surfaces, the nature of the support of the bodies with these cylindrical surfaces is quite different. The force at one contacting surface on the roller is opposed by an equal force located diametrically opposite. As a result, the entire roller is loaded with the full compressive force, and the deflection given by Equation (124) is the deflection at the contact point and throughout the roller. A gear tooth does not provide the full cylindrical cross section of the roller. Furthermore, the applied load is not supported by diametrically opposed force but by the shear forces distributed across the base of the tooth. The first item calls attention to a reduced material cross section available for deformation. The second item points out that, due to the side support, the internal loading in the cross section of the tooth is not constant, but reduces with increased distance from the contact point. These differences make the contact deflection in gear teeth significantly less than that called for by Equation (124). The estimate to be used for this reduction in deflection is 50 percent. This correction gives calculated results which proved to be still somewhat larger than the experimental results to which they were compared. However, the apparent excess in calculated contact deflection will be more than offset in many practical applications by the increase in deflection resulting from slight errors in the contacting surfaces.

With the 50-percent correction, Equation (124) may be rewritten to apply to the case of contacting gear teeth.

$$(B_{J12})_d = \frac{1.275\ W_{NJ}^{0.9}}{E_{\nu 12}^{0.9}\ F_{12}^{0.8}} \tag{125}$$

Converting this to give the mean compliance according to Equation (116),

$$(Q_{J12})_d = \frac{(B_{J12})_d}{W_{NJ}} = \frac{1.275\ W_{NJ}^{0.9}}{E_{\nu 12}^{0.9}\ F_{12}^{0.8}\ W_{NJ}}$$

$$(Q_{J12})_d = \frac{1.275}{E_{\nu 12}^{0.9}\ F_{12}^{0.8}\ W_{NJ}^{0.1}} \tag{126}$$

Equation (126) shows that the compliance is not constant but is somewhat dependent on the value of the actual load. However, since the load appears to the one-tenth power, there will be little variation in compliance over a reasonably wide range of load. Therefore, W_{NJ} may be replaced by an average value covering all conditions of loading without fear of introducing appreciable error. A suitable average value would be one-half the total load carried by the gear teeth. The load on any one tooth will vary from zero to the total load, but the condition of approximately equal sharing between two successive teeth is the condition requiring the best possible estimate of compliance. The substitution to be used is

$$W_{NJ} = .5\ W_N \tag{127}$$

Equation (126) now becomes

$$(Q_{J12})_d = \frac{1.37}{E_{v12}^{0.9} \; F_{12}^{0.8} \; W_N^{0.1}} \tag{128}$$

Because this relationship is independent of surface curvature, it will apply for all load point positions. For the same reason, it will apply for both the case of two external gears and the case of one external and one internal gear. The contact compliance, it should be noted, requires the additional input information of the total transmitted load W_N and, in this respect, differs from the other compliance components.

In summary, the total elastic compliance of the mating gear teeth may be found by applying Equations (117), (118), and (119) for each of the gears, combining the results, and then adding in the contact compliance for the two gears in combination.

$$Q_{J12} = (Q_{J1})_{abc} + (Q_{J2})_{abc} + (Q_{J12})_d \tag{129}$$

Rotational Deviations

Figure 71 shows the general case of two successive pairs of teeth in mesh and transferring load. The points of contact on the two teeth from the same gear have a fixed relationship to each other. If the position of one is known, the other can be found readily. As discussed prior to Equation (16), each point on the profile used as a calculation point is associated with a rotation angle α_J. This angle is also the angle through which the gear will rotate to move the point in question. In Figure 71, α_{JC} is the angle associated with the contact point on the first tooth of the pair, and α_{JD} is the angle associated with the contact point on the second. The combination of the two angles is equal to the tooth spacing angle, or

$$\alpha_{JC} + (-\alpha_{JD}) = \frac{2\pi}{N}$$

The minus sign in front of the second angle provides for its negative direction. In rearranged form, this equation shows how the location of the second contact point is found from the first.

$$\alpha_{JD} = -\left(\frac{2\pi}{N} - \alpha_{JC}\right) \tag{130}$$

The division of transferred tooth load shown in Figure 71 will be determined from a consideration of the gear teeth compliances and the relevant manufacturing errors for the two contact points. These factors are shown in Figure 72, which is a schematic diagram of the meshing condition shown in Figure 71. The gear teeth are represented as slender, spring-like members with deflections (B) caused by their respective loads. Profile errors (Z) at the points of contact are shown as buttons interacting with the deflections of the spring teeth. Tooth spacing errors (V) are pictured as offsets in the projections of the bases of the spring teeth.

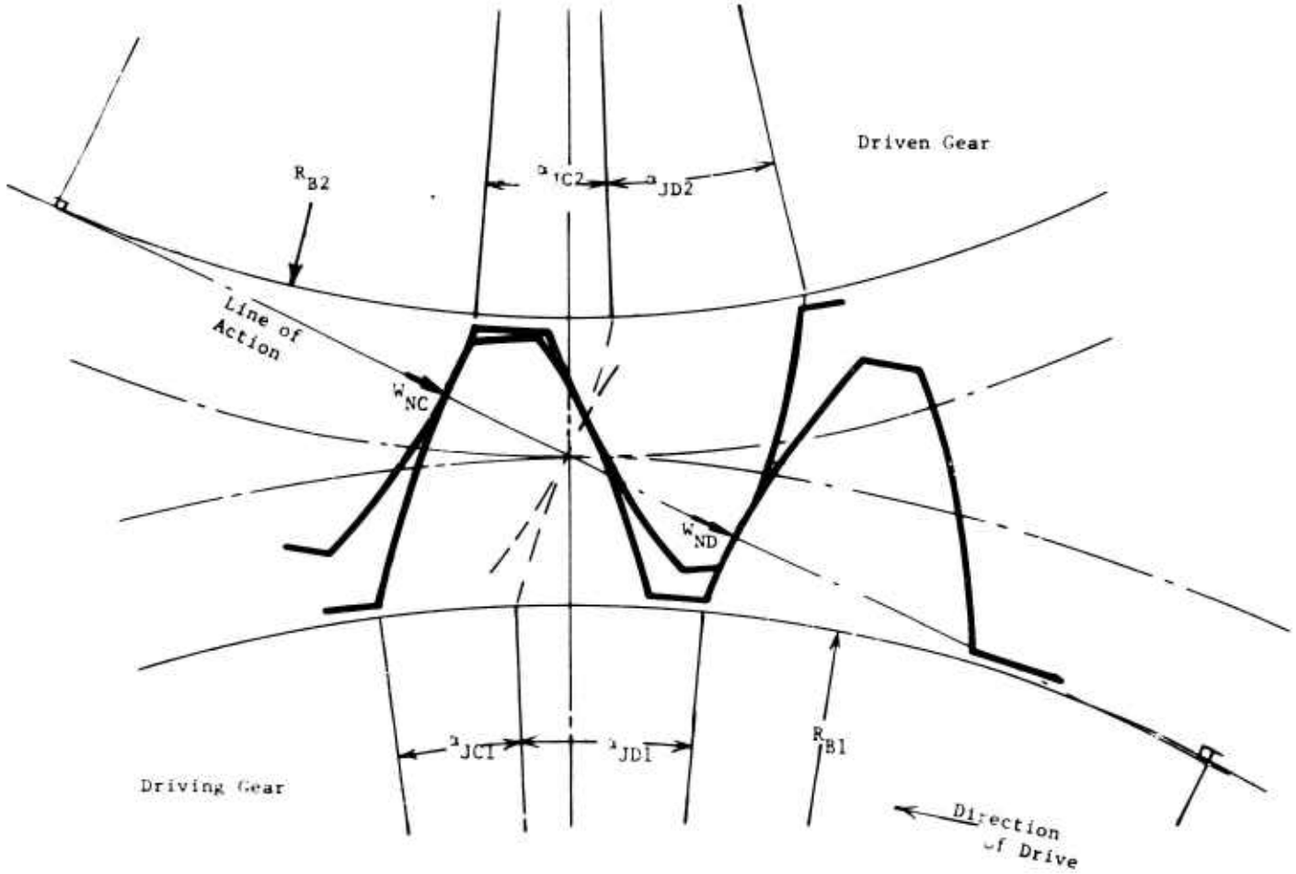

Figure 71. Two Successive Pairs of Teeth in Mesh and the Division of Transferred Tooth Load.

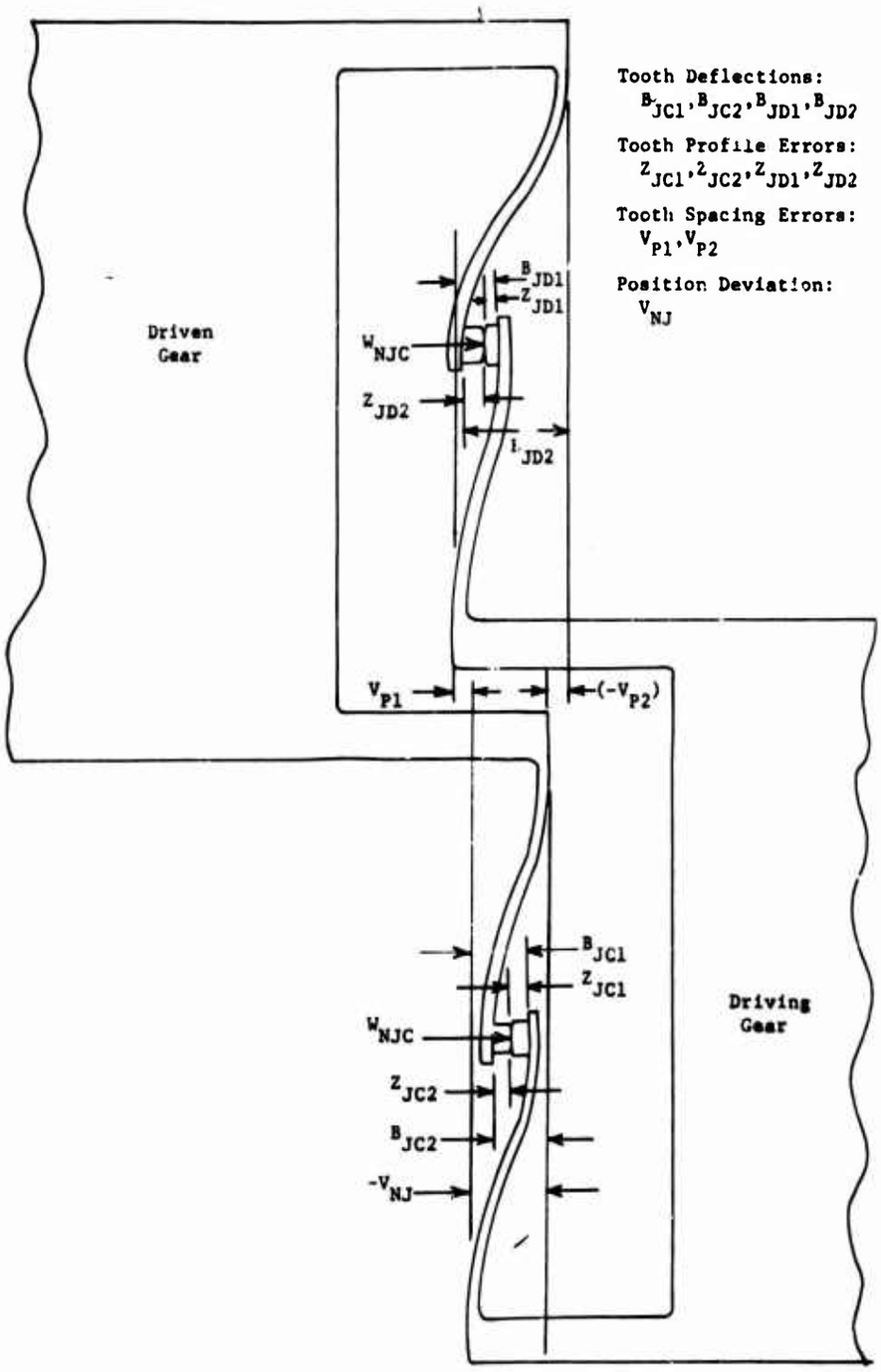

Figure 72. Diagram Representing Two Successive Pairs of Gear Teeth in Mesh.

The deviation (V_{NJ}) in the position of the driven gear relative to the driving gear, which results from the combination of deflections and errors, is shown by the offset between the base of the first spring-tooth on the driving gear and the base of the first spring-tooth on the driven gear.

The profile errors, the tooth spacing errors, and the position deviation are all measured along the line of action or, stated otherwise, as normal to the tooth surface.

To separate the two effects of profile error and tooth spacing, the former will be defined as zero at the pitch point, and the latter will be measured between pitch points of successive teeth. To be consistent with the requirement of direction along the line of action, the tooth spacing error, as measured between pitch points, must be adjusted by the factor $\cos\phi_P$.

The chains of displacements pictured in Figure 72 supply the equations for the case of both teeth transmitting load. For the driving gear,

$$V_{NJ} + B_{JC1} - Z_{JC1} - Z_{JC2} + B_{JC2} = 0 \qquad (131)$$

For the driven gear,

$$V_{NJ} - V_{P1} + B_{JD1} - Z_{JD1} - Z_{JD2} + B_{JD2} - (-V_{P2}) = 0 \qquad (132)$$

These may be rearranged to

$$V_{NJ} + (B_{JC1} + B_{JC2}) = (Z_{JC1} + Z_{JC2}) \qquad (133)$$

$$V_{NJ} + (B_{JD1} + B_{JD2}) = (Z_{JD1} + Z_{JD2}) + (V_{P1} - V_{P2}) \qquad (134)$$

Each pair of the deflections may be replaced by a product; the load causing them times the combined compliances involved. These compliances are the elastic tooth compliances (Q) derived in the previous section and other known compliances (U) of the structure supporting the tooth.

$$W_{NJC}Q_{JC} = W_{NJC}(Q_{JC12} + U_{JC12}) = B_{JC1} + B_{JC2} \qquad (135)$$

$$W_{NJD}Q_{JD} = W_{NJD}(Q_{JD12} + U_{JD12}) = B_{JD1} + B_{JD2} \qquad (136)$$

For simplification, the errors for each tooth may be grouped.

$$Z_{JC} = (Z_{JC1} + Z_{JC2}) \qquad (137)$$

$$Z_{JD} = (Z_{JD1} + Z_{JD2}) + (V_{P1} - V_{P2}) \qquad (138)$$

When Equations (135) and (137) are combined with Equation (133), when Equation (136) and (138) are combined with Equation (134), and when the

sum of the two parts of the transferred load is set equal to the total load,

$$V_{NJ} + W_{NJC}\, Q_{JC} = Z_{JC} \tag{139}$$

$$V_{NJ} + W_{NJD}\, Q_{JD} = Z_{JD} \tag{140}$$

$$W_{NJC} + W_{NJD} = W_N \tag{141}$$

These three simultaneous equations can be solved with the aid of determinants.

$$V_{NJ} = \frac{\begin{vmatrix} Z_{JC} & Q_{JC} & 0 \\ Z_{JD} & 0 & Q_{JD} \\ W_N & 1 & 1 \end{vmatrix}}{\begin{vmatrix} 1 & Q_{JC} & 0 \\ 1 & 0 & Q_{JD} \\ 0 & 1 & 1 \end{vmatrix}} = \frac{Q_{JC}\, Q_{JD}\, W_N - Z_{JC}\, Q_{JD} - Z_{JD}\, Q_{JC}}{-Q_{JD} - Q_{JC}}$$

The position deviation in the direction of the line of action is

$$V_{NJ} = \frac{Q_{JC}\, Z_{JD} + Q_{JD}\, Z_{JC} - Q_{JC}\, Q_{JD} W_N}{Q_{JC} + Q_{JD}} \tag{142}$$

$$W_{NJC} = \frac{\begin{vmatrix} 1 & Z_{JC} & 0 \\ 1 & Z_{JD} & Q_{JD} \\ 0 & W_N & 1 \end{vmatrix}}{\begin{vmatrix} 1 & Q_{JC} & 0 \\ 1 & 0 & Q_{JD} \\ 0 & 1 & 1 \end{vmatrix}} = \frac{Z_{JD} - Q_{JD} W_N - Z_{JC}}{-Q_{ND} - Q_{JC}}$$

The load transmitted by the first pair of teeth is

$$W_{NJC} = \frac{Q_{JD} W_N + Z_{JC} - Z_{JD}}{Q_{JC} + Q_{JD}} \tag{143}$$

$$W_{NJD} = \frac{\begin{vmatrix} 1 & Q_{JC} & Z_{JC} \\ 1 & 0 & Z_{JD} \\ 0 & 1 & W_N \end{vmatrix}}{\begin{vmatrix} 1 & Q_{JC} & 0 \\ 1 & 0 & Q_{JC} \\ 0 & 1 & 1 \end{vmatrix}} = \frac{Z_{JC} - Z_{JD} - Q_{JC}W_N}{-Q_{JD} - Q_{JC}}$$

The load transmitted by the second pair of teeth is

$$W_{NJD} = \frac{Q_{JC}W_N + Z_{JD} - Z_{JC}}{Q_{JC} + Q_{JD}} \tag{144}$$

The results of Equation (143) and (144) may be tested for sign. Since the denominator in both cases will be positive, the test may be confined to the numerators. If the numerator is negative, the indication is that no load is transmitted by that pair and that the other pair carries the full load.

The corrected load relationship must be introduced into the original Equations (139) and (140) in order to find the true position deviation.

If $Q_{JD}W_N + Z_{JC} - Z_{JD} \leq 0$, then $W_{NJC} = 0$, $W_{NJD} = W_N$, and only the D-teeth are in contact.

In this case, Equation (142) becomes

$$V_{NJ} = Z_{ND} - Q_{JD}W_N \tag{145}$$

If $Q_{JC}W_N + Z_{JD} - Z_{JC} \leq 0$, then $W_{NJD} = 0$, $W_{NJC} = W_N$, and only the C-teeth are in contact.

In this case, Equation (142) becomes

$$V_{NJ} = Z_{NC} - Q_{JC}W_N \tag{146}$$

Most gear designs have a range of rotational positions in which engagement takes place between one pair of teeth only. The rotational positions for which this is true have been found through Equation (18). In the cases of engagement of the first pair only, $W_{NJC} = W_N$, $W_{NJD} = 0$, and Equation (146) should be used directly. With engagement of the second pair, $W_{NJC} = 0$, $W_{NJD} = W_N$, and Equation (145) are used.

It may be more convenient to express the loads found by Equations (143) and (144) as tangential or pitch loads instead of the normal loads used in the analysis. The conversion is obtained by setting equal the torques resulting from each of the two alternative load directions. For the total

load,

$$WR_P = W_N R_B$$

$$W = W_N \frac{R_B}{R_P}$$

$$W = W_N \cos \phi_P \tag{147}$$

For the divided loads,

$$W_{JC} = W_{NJC} \cos \phi_P \tag{148}$$

$$W_{JD} = W_{NJD} \cos \phi_P \tag{149}$$

Conversions may also be made for the position deviation. The position deviations may be expressed as an angular deviation of either the driving gear or the driven gear.

$$J1 = \frac{V_{NJ}}{R_{B1}}$$

$$J2 = \frac{V_{NJ}}{R_{B2}} \tag{150}$$

The conversion to a tangential or a pitch line deviation is made by noting that both deviations must result in the same angular deviation.

$$J = \frac{V_{NJ}}{R_B} = \frac{V_J}{R_P}$$

$$V_J = V_{NJ} \frac{R_P}{R_B}$$

$$V_J = \frac{V_{NJ}}{\cos \phi_P} \tag{151}$$

DESCRIPTION OF COMPUTER PROGRAM

Input Variables, Format, and Instructions

Card 1 Title, colums 2 through 72.

Card 2 Control numbers. Format (5I5)

a. NUZ Number of sets of tooth load and spacing error data being submitted with this control card.

Place the last digit of this number in column 5.

b. INT Identification as to whether this control card represents the last complete set of input data being submitted.
If more sets of input data follow, use 0.
If this is the last set, use 1.

Place this digit in column 10.

c. NMZ Number of sets of profile and support compliance data being submitted with this control card.

Place the last digit of this number in column 15.

d. MN Classification of the types of spur gears to be considered.
If both the driving and the driven gears are external gears, use 1.
If the driving gear is an external gear and if the driven gear is an internal (ring) gear, use 0.
(The program will not run properly if the internal gear is submitted as the driving gear.)

Place this digit in column 20.

e. MMM Number of initial terms of the Fourier analysis for which coefficients will be printed, beyond the coefficient for the constant term. This number cannot exceed (2I +1), where I is the input variable submitted on card 4.

Place the last digit of this number in column 25.

Card 3 Gear design data. Format (6E 13.5)

a. FN1 Number of teeth in the driving gear.

Use columns 1 through 13. (Do not omit decimal point.)

b. FN2 Number of teeth in the driven gear.

Use columns 14 through 26. (Do not omit decimal point.)

c. RP1 Radius of the pitch circle of the driving gear, in. This must be the working pitch radius based on the actual center distance, including any substantial spreading under load. If not specified in the gear design data, it may be calculated by multiplying the actual center distance by the ratio of (FN1)

to (FN1 + FN2).

Use columns 27 through 39.

Note: The pitch radius of the driven gear is not included in the input data; instead, it is calculated from the other input data and is printed as a calculated result.

d. THETP Pressure angle, deg. This must be the working pressure angle based on the base circle radii and the actual center distance, including any substantial spreading under load. If not specified in the gear design data, its sine may be calculated by dividing the driving gear base circle radius by its pitch radius, as found for RP1 above.

Use columns 40 through 52.

e. RØ1 Radius to the outside diameter of the driving gear, in. This should be reduced by any radial loss in working surface at the tip of the teeth, as from tip rounding or chamfering.

Use columns 53 through 65.

f. RØ2 or RI2 Radius to the outside diameter of the driven gear, if external, and to the inside diameter, if internal, in. This should be corrected for any radial loss in working surface at the tip of the teeth, as from tip rounding or chamfering. In the case of an internal gear, this radius must be equal to or greater than the base circle radius. No check for this is provided.

Use columns 66 through 78.

Card 4 Gear design data, continued. Format (6E 13.5)

a. RT1 Radius to the beginning (near the base of the tooth) of the involute profile on the driving gear, in.

This is used in the program only in a design check as to whether adequate length of involute has been provided for contact on the teeth of the mating gear up to its tip. If this radius is not specified in the gear design data, this check may be bypassed by substituting the root circle radius.

Use columns 1 through 13.

b. RT2 Radius to the beginning (near the base of the tooth)

of the involute profile on the driven gear, in. See above for substitute when not specified.

Use columns 14 through 26.

c. RM1 Radius to the root circle of the driving gear, in. If the radius submitted is smaller than the computed base circle radius, this is noted in the output, and the input value of root radius is used at some points in the program. If the root radius is sufficiently smaller than the base circle radius so that the root fillet center lies inside the base circle, the tooth outline between the base circle and the fillet is assumed to be a radial line by the program.

Use columns 27 through 39.

d. RM2 Radius to the root circle of the driven gear, in. For the case of an external gear, the same comments as above apply.

Use columns 40 through 52.

e. FI Number which indirectly establishes the number of calculation points. The number of these points will equal one plus twice the value of FI. The calculation points may be viewed as selected contact points on the true involute profile, extended where necessary. These contact points with the mating involute are associated with specific angular positions taken by the gear as it is rotated, where the angular positions correspond to uniform subdivisions of the tooth spacing angle. A greater number of these points will give more closely spaced point-by-point output data. It will also give more accurate calculations of tooth deflections and Fourier coefficients. A value of FI equal to 12 giving 25 calculation points has been found to be convenient.

Use columns 53 through 65. (Do not omit decimal point.)

f. T1 Circular tooth thickness at the pitch circle of the driving gear, in. The radius of the pitch circle is as defined in card 3. If not specified in the gear design data, it may be estimated as one-half of the difference between the actual circular pitch and the working backlash.

Use columns 66 through 78.

Card 5 Gear design data, continued. Format (5E 13.5)

a. T2 Circular tooth thickness at the pitch circle of the driven gear, in. The comments for T1 also apply here.

Use columns 1 through 13.

b. F1 Effective tooth face width of the driving gear, in. Where the face widths of the two gears are similar, use the actual face width without any reduction for normal end chamfering or rounding. Where one tooth is much wider, use as its effective face width an amount suitably larger than the narrower width to allow for the limited additional support that the greater width provides.

Use columns 14 through 26.

c. F2 Effective tooth face width of the driven gear, in. The comments for F1 also apply here.

Use columns 27 through 39.

d. RF1 Fillet radius on the driving gear, in.

Use columns 40 through 52.

e. RF2 Fillet radius on the driven gear, in.

Use columns 53 through 65.

Card 6 Gear material properties. Format (6E 13.5)

a. YE1 Young's modulus (in bending) for the material of the driving gear, $lb/in.^2$

Use columns 1 through 13.

b. YE2 Young's modulus (in bending) for the material of the driven gear, $lb/in.^2$

Use columns 14 through 26.

c. GE1 Shear modulus for the material of the driving gear, $lb/in.^2$

Use columns 27 through 39.

d. GE2 Shear modulus for the material of the driven gear, $lb/in.^2$

Use columns 40 through 52.

e. PØS1 Poisson's ratio for the material of the driving gear. Since this ratio is used only in the alllowance for the "wide beam effect", it should be reduced for the cases where tooth face width is not much greater than tooth thickness, with a limiting value of zero when the teeth have a width smaller than the thickness.

Use columns 53 through 65.

f. PØS2 Poisson's ratio for the material of the driven gear. Comments for PØS1 also apply here.

Use columns 66 through 78.

Cards 7-1 to 7-2N Point-by-point data. Format (4E 13.5)

Total number of cards equal to twice the number of calculation points (N_J) between pitch points of adjacent teeth, or the same as two plus four times the value of F1 (see card 4). This specifies that cards must be introduced even if it is known that there is no contact at the particular calculation point or even if the tooth profile does not actually extend to the calculation point. As explained below, a blank card may be used for these points.

For the driving gear, the first card is for the calculation point located (N_J-1) points preceding before the pitch point (or inside the pitch circle); the (N_J)th card is for the pitch point; the last or ($2N_J$)th card is for the calculation point located (N_J) points after the pitch point (or outside the pitch circle). This last point may also be described as the point of contact on one meshing tooth when the pitch point is the point of contact on the next meshing tooth.

For the driven gear which is an external gear, the first card is for the calculation point located (N_J) points before the pitch point (or inside the pitch circle); the (N_J+1)th card is for the pitch point; the last or ($2N_J$)th card is for the calculation point located (N_J-1) points after the pitch point (or outside the pitch circle). The point for the first card may also be described as the point of contact on one meshing tooth when the pitch point is the point of contact on the previous meshing tooth.

For the driven gear which is an internal gear, the first card is for the calculation point located (N_J) points following the pitch point (or outside the pitch circle); the (N_J+1)th card is for the pitch point; the last or ($2N_J$)th card is for the calculation point located (N_J-1) points before the pitch point (or inside the pitch circle). The point for the first card may also be described as the point of contact on the meshing tooth when the pitch point is the point of contact on the next meshing tooth.

a. ZJ1 Deviation of the point on the actual tooth profile on the driving gear from the true involute (as defined by the gear design data), in. This true involute is positioned relative to the actual profile so that its deviation at the pitch point is zero. Where the deviation represents material added to the true involute, it is positive; where it represents material subtracted, it is negative. The deviation is measured normal to the involute profile. If the profile does not extend to the particular calculation point or if it is known that the mating gear will not contact at this point, the deviation may be noted as zero.

Use columns 1 through 13.

b. UJ1 Tooth support compliance, or any compliance supplementary to the tooth compliance included in the analysis, on the driving gear, in./lb. This compliance is the deflection under unit load at the calculation point on the profile in the direction of the load (or normal to the profile). A uniform compliance for all calculation points, such as would result from a uniform gear shaft compliance, would not affect the final results as far as motion irregularities or load transfer are concerned; it would only increase the mean deviation in transmitted motion.

Use columns 14 through 26.

c. ZJ2 Deviation of the point on the actual tooth profile on the driven gear from the true involute, in. The comments under ZJ1 also apply here.

Use columns 27 through 39.

d. UJ2 Tooth support compliance, etc., on the driven gear, in./lb. The comments under UJ1 also apply here.

Use columns 40 through 52.

Cards 8-1 to 8-NUZ Tooth load and spacing error data. Format (3E 13.5)

The number of cards is equal to NUZ in card 2, and each represents a case for which an individual set of motion and load data will be computed.

a. WT Total load, tangent to the pitch circle, transmitted by the gear teeth, lb.

Use columns 1 through 13.

b. VPT1 Tooth spacing error on the driving gear, in. This error is based on the distance between the pitch points of successive teeth, but the error is adjusted to apply to the direction of the line of action. This adjustment is accomplished by multiplying the pitch line error by the cosine of the pressure angle. The error is positive if the measured spacing is smaller than the desired spacing.

Use columns 14 through 26.

c. VPT2 Tooth spacing error on the driven gear, in. The comments under VPT1 also apply here.

Use columns 27 through 39.

Output Variables and Explanations

Tabulation of Input Data

Title

Control numbers - NUZ, INT, NMZ, MN, MMM, as in input card 2

Design data - FI(=I), FN1(=N1), RP1, RO1, RT1, RM1
THETP, FNZ(=N2), blank, Roz or RI2, RT2, RM2
T1, F1, RF1, YE1, CE1, PØS1
T2, Fw, RF2, YE2, GEZ, PØS2
all as in input cards 2 through 6.

Calculated Data

Incidental data - blank, RB1, BA1, BR1, AT1
RP2, RB2, BA2, BR2, AT2

where: RP2 - Pitch circle radius of driven gear, in.
RB1 - Base circle radius of driving gear, in.
RB2 - Base circle radius of driven gear, in.
BA1 - Arc of approach of driving gear, rad.

BA2 - Arc of approach of driven gear, rad. (negative on internal gears)
BR1 - Arc of recess of driven gear, rad.
BR2 - Arc of recess of driving gear, rad. (negative on internal gears)
AT1 - Angle of rotation of driving gear from the position at which the line of action intersects the involute at the start of the involute profile to the position at which the line of action intersects the involute at the pitch point, rad.
AT2 - Similar angle of rotation of driven gear, rad.

Check statement when part of the profile extends within the base circle.

Program will continue in any case, and, where necessary, the root radius will be set equal to the base circle radius. However, in calculating the tooth profile and the tooth deflections, the original root circle radius will be used with the specified fillet radius. If the root circle lies inside the base circle by more than this fillet radius, a radial line is assumed to connect fillet and involute.

Driving gear date - J1, CJ1, AJ1, QJ1ABC, XJ1, XME1(=X), YME1(=Y), YJ1, J1, QJ1A, QJ1B, QJ1C

where: J1 - Identification number for calculation points (see under F1 of card 4 in the input data). Listed for values of (-2I) to (2I+1).
CJ1 - Condition of engagement if equal to 1 and no engagement if equal to zero.
AJ1 - Angle of rotation from the position of contact at the pitch point to the position of contact at the calculation point - negative for points inside the pitch circle, rad.
XJ1 and YJ1 - Coordinates of the calculation point on the involute profile with the origin at the gear center and with the X-axis as the centerline of the tooth, given only for the points at which contact will take place with the mating gear, in.
XME1 and YME1 - Coordinates of the point on the root circle midway between the tangent point of the fillet radius and the involute profile extended (and radial inside the base circle), in. This point is considered to be the end

of the effective base of the tooth for deflection purposes.

QJ1A- Elastic compliance of the gear tooth acting as a cantilever beam in bending only, normal to the profile at the calculation point, in./lb.

QJ1B- Elastic compliance of the gear tooth as a cantilever beam in shear only; otherwise as above.

QJ1C- Elastic compliance of the gear tooth as a rigid member rotating in its supporting structure; otherwise as above.

QJ1ABC - Combined compliance of the three above, in./lb.

Driven gear data - J2, blank, AJ2, QJ2ABC, XJ2, YJ2, XME2, YME2 J2, QJ2A, QJ2B, QJ2C

where: J2 - Identification number for the calculation points. For external gears, J2 is listed for values of (-2I-1) to (2I). For this case, contact takes place between points of the two gears for which J1 = -J2. For internal gears, J2 is listed for values of (2I+1) to (-2I). For this case, contact takes place between points of the two gears for which J1 = J2.

All other variables are similar to their counterparts for the driving gear.

Additional input data - WT, VPT1, VPT2, as in input card 8.

Data based on input load WN - QJD

where: WN - Total normal load transmitted by the teeth, lb.

QJD - Contact or Hertzian compliance combined for both teeth at the contact point, in./lb.

Tooth meshing errors and loads - JC1, AJC1, EJT, WTC, WTD

where: JC1 - Identification number for the calculation point on the first tooth of the driving gear, starting with the first point after the pitch point and ending with the point corresponding to the pitch point of the next tooth.

AJC1 - Angle of rotation of the driving gear

from its position with contact at the pitch point to the position with contact at the calculation point, rad. The last angle is the tooth spacing angle.

EJT - Tooth meshing error or deviation from pure conjugate action, as a pitch line linear measurement of the motion of the driven gear leading the driving gear, in. A negative value indicates that the driven gear is lagging the driving gear, as might be caused by deflection of the teeth.

WTC - Tangential load carried by the first pair of teeth, lb.

WTD - Tangential load carried by the second pair of teeth, lb.

Fourier Coefficients - I, A, B.

where: I - Order of the harmonic to which the coefficients apply. The zero order refers to the constant component.

A - The Fourier coefficient of the cosine or real component for that harmonic of the meshing error, in. The value for I = 0 is twice the constant component or mean value of the meshing error.

B - The Fourier coefficient of the sine or imaginary component for that harmonic of the meshing error, in.

Program Listing of Source Deck

This program was written in FORTRAN II - Extended and may be compiled with FORTRAN IV. It was developed on the IBM 1800 Computer. In the source deck listing which follows, the READ and WRITE statements are written with the variable NR to specify the reading unit and with the variable NW to specify the writing unit. To recompile the program for the IBM 7090, introduce the required unit numbers by making the necessary changes on the cards as noted in the listing.

In addition to the controlling portion of this gear calculation program, named GEARO, there are three subroutines. The first, AJCDH, in turn calls the second, CALCJ. Both of these are used in the gear calculation proper. The third subroutine, FOUR, performs the Fourier analysis.

Running time on IBM 1800 was approximately

3 minutes for a first case with 25 calculation points and one set of load and profile data

1.2 minutes additional for each similar case with new design data

1 minute additional for each new set of load or profile data.

GEARO - Gear Tooth Meshing Deviations

```
      DIMENSION      UJC1(25),UJD1(25),UJ2(50),UJC2(25),UJD2(25),ZJ1(50)
     1,ZJC1(25),ZJD1(25),ZJ2(50),ZJC2(25),ZJD2(25),QJ1(50),QJC1(25),QJD1
     2(25),QJ2(50),QJC2(25),                    FJ1(50),UJ1(50),        CJC1(2
     35),CJD1(25),          AJ1(50),AJ2(50),QJC(50),QJD(50),ZJC(50),ZJD(50
     4),VJ(50),EJ1(50),FJ2(50),AJC1(25),AJC2(25),FJC1(25), QJD2(25),ZM2(
     550),UM2(50)
      COMMON PJ(50),CJ(50),QJ(50),AJ(50),XJ(50),YJ(50),A(25),B(25),G(50)
      COMMON DD,BR,BA,FJ,CC,YM,NN,N,FNJ,EP,TAN,RB,GM,F,XM,MN,II,M
      COMMON QA(50),QB(50),QC(50),QA1(50),QB1(50),QC1(50),QA2(50),QB2(50
     1),QC2(50) ,IH,IP
C SPECIFY AND INITIALIZE   READING AND WRITING UNITS FOR IBM 1800
      NR = 2
      NW= 3
  196 READ(NR,100)
      READ(NR,117)NUZ,INT,NMZ,MN,MMM
      READ(NR,112)FN1,FN2,RP1,THETP,RO1,RO2
      READ(NR,112)RT1,RT2,RM1,RM2,FI,T1
      READ(NR,112)T2,F1,F2,RF1,RF2
      READ(NR,112)YE1,YE2,GE1,GE2,POS1,POS2
      WRITE(NW,100)
      WRITE(NW,101)
      WRITE(NW,108)
      WRITE(NW,109)NUZ,INT,NMZ,MN,MMM
      WRITE(NW,104)
      WRITE(NW,102)FI,FN1,RP1,RO1,RT1,RM1
      IF(MN) 511,510,511
  510 WRITE(NW,103)
      GO TO 512
  511 WRITE(NW,160)
  512 WRITE(NW,158)THETP,FN2,RO2,RT2,RM2
      WRITE(NW,105)
      WRITE(NW,102)T1,F1,RF1,YE1,GE1,POS1
      WRITE(NW,107)
      WRITE(NW,102)T2,F2,RF2,YE2,GE2,POS2
      WRITE(NW,164)
      IF(F1-F2) 320,320,321
  321 FF2=F2
      GO TO 322
  320 FF2=F1
  322 FF2=FF2**0.8
      THETP=0.017453239*THETP
      IF(MN) 304,303,304
  303 T2=-T2
  304 DD1=-T1/2.0/RP1+THETP
      F12=FN1/FN2
      RP2=RP1/F12
      DD2=-T2/2.0/RP2+THETP
      FNJ=2.0*FI+1.0
      N=FNJ
      NN=N+N
      CS=COS (THETP)
      SS=SIN (THETP)
      TAN=SS/CS
      EP1=1.0-POS1*POS1
      EP1=YE1/EP1
```

```
      EP2=1.0-POS2*POS2
      EP2=YE2/EP2
      EP12=(1.0/EP1+1.0/EP2)*0.5
      EP12=EP12**0.9
      RB1=RP1*CS
      RB2=RP2*CS
      C1=RO1/RB1
      C2=RO2/RB2
      BR2=(SQRT (C2*C2-1.0)-TAN)
      BR1=(SQRT (C1*C1-1.0)-TAN)
      C3=TAN/F12
      IF(BR1-C3) 403,403,404
  404 BR1=C3
      WRITE(NW,126)BR1
  403 BA1=BR2/F12
      BA2=BR1*F12
      IF(MN) 440,450,440
  450 BA1=-BA1
      BA2=-BA2
  440 IF(BA1-TAN) 401,401,402
  402 BA1=TAN
      WRITE(NW,125)BA1
  401 C1=6.2831845/FN1
      IF(BA1-C1) 213,213,611
  611 WRITE(NW,174)
  213 IF(BR1-C1) 215,612,612
  612 WRITE(NW,175)
  215 C1=RT1/RB1
      C2=RT2/RB2
      C1 =SQRT (C1*C1-1.0)-TAN
      AT1=ABS (C1)
      C2 =SQRT (C2*C2-1.0)-TAN
      AT2=ABS (C2)
      WRITE(NW,122)
      WRITE(NW,159)RB1,BA1,BR1,AT1
      WRITE(NW,162)
      WRITE(NW,102)RP2,RB2,BA2,BR2,AT2
      IF(AT1-BA1) 311,215,216
  311 WRITE(NW,176)
  216 IF(AT2-BA2) 309,217,217
  309 IF(MN) 620,621,620
  621 WRITE(NW,178)
      GO TO 217
  620 WRITE(NW,179)
  217 IF(RM1-RB1) 191,192,192
  191 RM1=RB1
      WRITE(NW,118)RM1
  192 AM1=RM1/RB1
      C1=AM1
      AM1=SQRT (AM1*AM1-1.0)-TAN
      C2=RF1/RB1
      PF1=C2
      C3=(C1+C2)**2-1.0
      IF(C3) 406,406,407
  406 PD1=0.0
      TPD1=0.0
      WRITE(NW,156)PD1
      GO TO 408
  407 PD1=SQRT (C3)
      TPD1=ATAN (PD1)
  408 IF(RM2-RB2) 193,194,194
```

```
193 RM2=RB2
    WRITE(NW,119)RM2
194 AM2=RM2/RB2
    C1=AM2
    AM2=SQRT (AM2*AM2-1.0)-TAN
    C2=RF2/RB2
    PF2=C2
    IF(MN) 456,455,456
455 C2=-C2
456 C3=(C1+C2)**2-1.0
    IF(C3) 409,409,410
409 PD2=0.0
    TPD2=0.0
    WRITE(NW,155)PD2
    GO TO 411
410 PD2=SQRT (C3)
    TPD2=ATAN (PD2)
411 K1=1
    E1=PF1
    E2=PD1
    E3=TPD1
    E4=RM1
    DD=DD1
    C1=AM1
201 C2=DD+C1
    C1=ATAN (TAN+C1)
    C4=C1-C2
    C3=E3-E2-DD+TAN
    IF(K1-1) 422,422,425
425 IF(MN) 422,421,422
421 C3=-C3
    C4=-C4
422 C1=C3+E1
    C4=(C1+C4)*0.5
    Y=E4*SIN (C4)
    X=E4*COS (C4)
    IF(K1-1) 202,202,203
202 XM1=X
    YM1=Y
    K1=K1+1
    DD=DD2
    C1=AM2
    E1=PF2
    E2=PD2
    E3=TPD2
    E4=RM2
    GO TO 20.
203 XM2=X
    YM2=Y
    EE=6.2831854/FNJ
    CC=EE/FN1
    FJ =-FNJ+1.0
    RB=RB1
    BR=BR1
    BA=BA1
    DD=DD1
    XM=XM1
    YM=YM1
    GM=GE1
    F=F1
    II=1
```

```
      EP=EP1
      WRITE(NW,151)
      CALL AJCDH
      DO 221 I=1,NN
      C1     =XJ(I)
      C2     =YJ(I)
      FJ1(I)=PJ(I)
      C3=CJ(I)
      AJ1(I)=AJ(I)
      QJ1(I)=QJ(I)
      IH1=IH
      IP1=IP
      QA1(I)=QA(I)
      QB1(I)=QB(I)
      QC1(I)=QC(I)
      IF(C3) 515,515,516
  515 WRITE(NW,102)FJ1(I),C3,AJ1(I)
      GO TO 221
  516 WRITE(NW,102)FJ1(I),C3,AJ1(I),QJ1(I),C1,C2
  221 CONTINUE
      WRITE(NW,120)XM1,YM1
      WRITE(NW,161)
      DO 517 I=IH1,IP1
  517 WRITE(NW,102)FJ1(I),QA1(I),QB1(I),QC1(I)
      DD=DD2
      RB=RB2
      XM=XM2
      YM=YM2
      IF(MN) 302,301,302
  301 FJ=FNJ
      GO TO 310
  302 FJ=-FNJ
  310 F=F2
      EP=EP2
      GM=GE2
      CC=EE/FN2
      II=2
      WRITE(NW,152)
      CALL AJCDH
      L=NN
      DO 222 I=1,NN
      C4     =XJ(I)
      C5     =YJ(I)
      IH2=IH
      IP2=IP
      QA2(I)=QA(I)
      QB2(I)=QB(I)
      QC2(I)=QC(I)
      FJ2(I)=PJ(I)
      C1=AJ(I)
      AJ2(L)=C1
      C2=QJ(I)
      QJ2(L)=C2
      IF(C2) 519,518,519
  518 WRITE(NW,132)FJ2(I),C1
      GO TO 520
  519 WRITE(NW,132)FJ2(I),C1,C2,C4,C5
  520 IF(L-1) 222,222,226
  226 L=L-1
  222 CONTINUE
      WRITE(NW,120)XM2,YM2
```

```
      WRITE(NW,163)
      DO 521 I=IH2,IP2
  521 WRITE(NW,102)FJ2(I),QA2(I),GB2(I),QC2(I)
      DO 251 I=1,N
      IN=I+N
      FJC1(I)=FJ1(IN)
      AJC1(I)=AJ1(IN)
      AJC2(I)=AJ2(IN)
      QJD1(I)=QJ1(I)
      QJC1(I)=QJ1(IN)
      QJC2(I)=QJ2(IN)
      QJD2(I)=QJ2(I)
      CJD1(I)=CJ (I)
  251 CJC1(I)=CJ (IN)
      MUZ=1
      MMZ=1
  197 WRITE(NW,110)
      L=NN
      DO 209 I=1,NN
      READ(NR,112)ZJ1(I),UJ1(I),ZJ2(I),UJ2(I)
      WRITE(NW,102)ZJ1(I),UJ1(I),ZJ2(I),UJ2(I)
      ZM2(L)=ZJ2(I)
      UM2(L)=UJ2(I)
      IF(L-1) 209,209,225
  225 L=L-1
  209 CONTINUE
      DO 415 I=1,N
      IN=I+N
      UJD1(I)=UJ1(I)
      UJC1(I)=UJ1(IN)
      UJC2(I)=UM2(IN)
      UJD2(I)=UM2(I)
      ZJD1(I)=ZJ1(I)
      ZJC1(I)=ZJ1(IN)
      ZJC2(I)=ZM2(IN)
      ZJD2(I)=ZM2(I)
      QJC(I)=QJC1(I)+UJC1(I)+QJC2(I)+UJC2(I)
      QJD(I)=QJD1(I)+UJD1(I)+QJD2(I)+UJD2(I)
  415 ZJC(I)=ZJC1(I)+ZJC2(I)
  199 READ(NR,112)WT,VPT1,VPT2
      WRITE(NW,106)
      WRITE(NW,102)WT,VPT1,VPT2
      WN=WT/CS
      VP1=VPT1/CS
      VP2=VPT2/CS
      WRITE(NW,171)WN
      IF(WN) 214,214,418
  418 C1=WN**0.1
      QD=1.37/FF2*EP12/C1
      WRITE(NW,172)QD
      WRITE(NW,115)
      DO 501 I=1,N
      ZJD(I)=ZJD1(I)+ZJD2(I)+VP1-VP2
      CCC    =QJC(I)+QD
      DDD    =QJD(I)+QD
      C1=CJC1(I)
      C2=CJD1(I)
      IF(C1) 256,256,257
  256 IF(C2) 501,501,258
  257 IF(C2) 259,259,260
  259 VJ(I)=ZJC(I)-CCC    *WN
```

```
      WTC=WN*CS
      WTD=0.0
      GO TO 261
  258 VJ(I)=ZJD(I)-DDD    *WN
      WTC=0.0
      WTD=WN*CS
      GO TO 261
  260 C3=CCC    *WN+ZJD(I)-ZJC(I)
      C4=DDD    *WN+ZJC(I)-ZJD(I)
      IF(C3) 259,259,262
  262 IF(C4) 258,258,263
  263 C1=CCC+DDD
      C2=CCC    *ZJD(I)+DDD    *ZJC(I)-CCC*DDD*WN
      VJ(I)=C2/C1
      C1=CS/C1
      WTC=(DDD*WN+ZJC(I)-ZJD(I))*C1
      WTD=(CCC*WN+ZJD(I)-ZJC(I))*C1
  261 EJ1(I)=VJ(I)/CS
      WRITE(NW,102)FJC1(I),AJC1(I),EJ1(I),WTC,WTD
  501 CONTINUE
      M=FI
      WRITE(NW,128)
      DO 20 I=1,N
   20 G(I)=EJ1(I)
   22 CALL FOUR
      LL=MMM+1
      DO 21 I=1,LL
      LP=I-1
   21 WRITE(NW,129)LP,A(I),B(I)
   24 IF(NUZ-MUZ) 504,504,502
  502 MUZ=MUZ+1
      GO TO 199
  504 MUZ=1
      IF(NMZ-MMZ) 214,214,506
  506 MMZ=MMZ+1
      GO TO 197
  214 IF(INT) 503,198,503
  503 CALL EXIT
  100 FORMAT(72H1
     1                    )
  101 FORMAT(72H0  PN0335=COMPUTATIONS OF GEAR TOOTH MESHING ERRORS
     1  3-22-1966      )
  102 FORMAT(6E13.5)
  103 FORMAT(12H0  PRE.ANGLE7X2HN224X3HRI210X3HRT210X3HRM2)
  104 FORMAT(/7X1HI111X2HN111X3HRP110X3HRC110X3HRT110X3HRM1)
  105 FORMAT(/6X2HT111X2HF111X3HRF15X12HYOUNGS MOD-12X11HSHEAR MOD-12X11
     1HPOS.RATIO-1)
  106 FORMAT(//54H INPUT DATA ON TANGENTIAL LOAD AND TOOTH SPACING ERROR
     1/6X2HWT10X4HVPT19X4HVPT2)
  107 FORMAT(/6X2HT211X2HF211X3HRF25X12HYOUNGS MOD-22X11HSHEAR MOD-22X11
     1HPOS.RATIO-2)
  108 FORMAT(62H0 SETS OF VP      INPUT     SETS OF U,Z  DIFF.GEAR N.OF HA
     1RMONIC)
  109 FORMAT(4XI4,4(8XI4))
  110 FORMAT(60H0INPUT LISTING OF PROFILE ERROR AND SUPPLEMENTARY COMPLI
     1ANCE/6X2HZ111X2HU111X2HZ211X2HU2)
  112 FORMAT(6E13.5)
  115 FORMAT(42H0CALCULATED TOOTH MESHING ERRORS AND LOADS//6X3HJC19X4HA
     1JC16X11HTANG. ERROR6X3HWTC10X3HWTD)
  117 FORMAT(5I5)
  118 FORMAT(74H0DRIVING GEAR INPUT ROOT RADIUS SMALLER THAN BASE CIRCLE
```

```
    1 RADIUS-CHANGED TO//6H  RM1=,  E13.6)
119 FORMAT(74H0DRIVEN  GEAR INPUT ROOT RADIUS SMALLER THAN BASE CIRCLE
    1 RADIUS-CHANGED TO//6H  RM2=,  E13.6)
120 FORMAT(48H0COOD. OF EFFECTIVE TOOTH PROFILE AT ROOT CIRCLE11X1HX13
    1X1HY/52X,2E13.6)
122 FORMAT(/19X3HRB110X3HBA110X3HBR110X3HAT1)
125 FORMAT(66H0 DRIVEN GEAR TEETH ENGAGE UNDER CUT PORTION OF DRIVING
    1GEAR TEETH//6H  BA1=,  E13.6)
126 FORMAT(66H0 DRIVING GEAR TEETH ENGAGE UNDER CUT PORTION OF DRIVEN
    1GEAR TEETH//6H  BR1=,  E13.6)
128 FORMAT(43H0CALCULATED FOURIER COEFFICIENTS FOR ERRORS//7H      13X
    15HA(I) 13X4HB(I))
129 FORMAT(I7,2(4X  E14.7))
132 FORMAT(  E13.5,13X,4E13.5)
151 FORMAT(/6X2HJ111X3HCJ110X3HAJ18X6HQJ1ABC9X3HXJ110X3HYJ1)
152 FORMAT(/6X2HJ224X3HAJ28X6HQJ2ABC9X3HXJ210X3HYJ2)
155 FORMAT(75H0DRIVEN  GEAR INPUT RADIUS TO FILLET CENTER INCREASED TO
    1 BASE CIRCLE RADIUS//6H  PD1=,  E13.6)
156 FORMAT(75H0DRIVING GEAR INPUT RADIUS TO FILLET CENTER INCREASED TO
    1 BASE CIRCLE RADIUS//6H  PD2=,  E13.6)
158 FORMAT(2E13.5,13X,3E13.5)
159 FORMAT(13X,4E13.5)
160 FORMAT(12H0  PRE.ANGLE7X2HN224X2HRO210X3HRT210X3HRM2)
161 FORMAT(/6X2HJ110X4HQJ1A9X4HQJ1B9X4HQJ1C)
162 FORMAT(/6X3HRP210X3HRB210X3HBA210X3HBR210X3HAT2)
163 FORMAT(/6X2HJ210X4HQJ2A9X4HQJ2B9X4HQJ2C)
164 FORMAT(//16H CALCULATED DATA)
170 FORMAT(43H0CALCULATED TOTAL CONTACT COMPLIANCE   QJD=,E13.6)
171 FORMAT(23H0CALCULATED NORMAL  WN=,  F13.6)
174 FORMAT(80H0 ANGLE OF APPROACH ON DRIVING GEAR IS GREATER THAN TOOT
    1H SPACING ANGLE. PROGRAM/25HCONTINUED WITHOUT OVERLAP)
175 FORMAT(75H0 ANGLE OF RECESS ON DRIVING GEAR IS NOT SMALLER THAN TO
    1OTH SPACING ANGLE. /34H PROGRAM CONTINUED WITHOUT OVERLAP.
176 FORMAT(80H0 DRIVING GEAR TEETH MESHING ON PROFILE INSIDE OF TIP DI
    1AMETER. PROGRAM CONTINU-/21HED WITHOUT CORRECTION)
178 FORMAT(80H0 DRIVEN  GEAR TEETH MESHING ON PROFILE OUTSIDE OF TIP D
    1IAMETER. PROGRAM CONTIN-/22HUED WITHOUT CORRECTION)
179 FORMAT(80H0 DRIVEN  GEAR TEETH MESHING ON PROFILE INSIDE OF TIP DI
    1AMETER. PROGRAM CONTINU-/21HED WITHOUT CORRECTION)
    END
// FOR AJCDH
```

Subroutine AJCDH

```
      SUBROUTINE AJCDH
      DIMENSION SD(50),CD(50),BIK(50),AIK(50),FLK(50) ,CDC(50)
      COMMON PJ(50),CJ(50),QJ(50),AJ(50),XJ(50),YJ(50),A(25),B(25),G(50)
      COMMON DD,BR,BA,FJ,CC,YM,NN,N,FNJ,EP,TAN,RB,GM,F,XM,MN,II,M
      COMMON QA(50),QB(50),QC(50),QA1(50),QB1(50),QC1(50),QA2(50),QB2(50
     1),QC2(50),IH,IP
      DO 106 I=1,NN
      QA(I)=0.0
      QB(I)=0.0
      QC(I)=0.0
      QJ(I)=0.0
      XJ(I)=0.0
  106 YJ(I)=0.0
      IF(II-1) 405,405,403
  405 MM=1.0
      GO TO 404
```

```
403 MM=MN
404 K=1
    DO 501 I=1,NN
    AJ(I)=FJ*CC
    PJ(I)=FJ
    IF(II-1) 412,412,413
412 CALL CALCJ(AJ(I),BR,BA,XY)
    CJ(I)=XY
    GO TO 414
413 XY=CDC(I)
414 IF(XY) 503,503,101
101 IF(K-1) 102,102,103
102 IH=I
103 AX=AJ(I)
    DJ=DD+AX
    SD(I)=SIN (DJ)
    CD(I)=COS (DJ)
    C1=ATAN (TAN+AX)
    C3=COS (C1)
    C4=C1-DJ
    IF(MM) 402,401,402
401 C4=-C4
402 C5=SIN (C4)
    C6=COS (C4)
    C1=RB/C3
    XJ(I)=C1*C6
    YJ(I)=C1*C5
    IF(K-1) 242,242,243
242 BIK(I)=(YJ(I)**3+YM**3)/3.0*F
    AIK(I)=(YJ(I)+YM)*F
    FLK(I)=XJ(I)-XM
    GO TO 504
243 BIK(I)=(YJ(I)**3+YJ(I-1)**3)/3.0*F
    AIK(I)=(YJ(I)+YJ(I-1))*F
    FLK(I)=XJ(I)-XJ(I-1)
504 K=K+1
503 IF(I-NN) 502,501,501
502 IF(MM) 506,505,506
505 FJ=FJ-1.
    GO TO 501
506 FJ=FJ+1.0
501 CONTINUE
    IF(II-1) 301,301,302
301 IF(MM) 601,302,601
601 LL=NN
    DO 303 I=1,NN
    CDC(I)=CJ(LL)
    IF(LL-1) 303,303,305
305 LL=LL-1
303 CONTINUE
302 IP=K+IH-2
410 DO 246 L=IH,IP
    E1=0.0
    E2=0.0
    E3=0.0
    E4=0.0
    EE=XJ(L)-XM
    IM=L
    IF(MM) 202,203,202
203 EE=-EE
202 DO 245 I=IH,IM
```

```
      C1        =XJ(L)-XJ(I)
      C5=FLK(I)
      IF(MM) 207,208,207
  208 C1=-C1
      C5=-C5
  207 C2=C5/BIK(I)
      C3=(C5+3.0*C1)*C5+3.0*C1*C1
      E4=E4+C2
      C4=2.0*C1+C5
      E1=E1+C3*C2
      E2=E2+C4*C2
  245 E3=E3+C5/AIK(I)
      IF(MM) 206,205,206
  205 IM=IM-1
  206 C1=CD(L)*CD(L)
      C2=SD(L)*YJ(L)
      QA(L) =C1/3.0*E1/EP+(C2*E4-CD(L)*E2)/EP*C2
      QB(L) =C1/GM*E3*1.2
      C1=(EE*CD(L)-YJ(L)*SD(L))/YM
      QC(L)=C1/EP*1.327/F*C1
  246 QJ(L)=QA(L)+QB(L)+QC(L)
      RETURN
      END
```

Subroutine FOUR

```
      SUBROUTINE FOUR
      COMMON PJ(50),CJ(50),QJ(50),AJ(50),XJ(50),YJ(50),A(25),B(25),G(50)
      COMMON DD,BR,BA,FJ,CC,YM,NN,N,FNJ,EP,TAN,RB,GM,F,XM,MN,II,M
      C=1.0
      S=0.0
      N1=M+1
      AN=M
      N2=M*2
      T1=2.0/(2.0*AN+1.0)
      T2=T1*3.1415927
      C1=COS (T2)
      S1=SIN (T2)
      DO 7 IP=1,N1
      U1=0.0
      U2=0.0
      DO 3 I=1,N2
      J=N2-I+2
      U3=G(J)+2.0*C*U1-U2
      U2=U1
    3 U1=U3
      A(IP)=T1*(G(1)+C*U1-U2)
      B(IP)=T1*S*U1
      Q=C1*C-S1*S
      S=C1*S+S1*C
    7 C=Q
      RETURN
      END
```

Subroutine CALCJ

```
      SUBROUTINE CALCJ(C1,C2,C3,C4)
      IF(C3) 240,231,241
  241 IF(C1) 230,218,218
  230 IF(ABS (C1)-C3)  220,220,219
  231 IF(C1) 219,218,218
```

```
240 IF(C1) 219,219,242
242 C3=-C3
    IF(C1-C3) 219,218,218
218 IF(C2-C1) 219,220,220
220 C4=1.0
    GO TO 221
219 C4=0.0
221 RETURN
    END
```

Input Listing of Sample Case

```
UPPER SUN DRIVING PLANET - CASES 108, 8-14-67
  1   0   1   1   6
57.          31.          3.3530       22.          3.4398       1.9405
3.2535       1.7430       3.199        1.6825       12.          .175
.1896        1.54         1.333        .056         .056
30000000.    30000000.    11600000.    11600000.    .3           .3
.0
.0
.0
.0
.0
.0
.00003
.00006
.00009
.00012
.00015
.00018
.00022
.00026
.0003
.0003
.00026
.00022
.00018
.00015
.00012
.00009
.00006
.00003
.0
.00005
.0001
.00015
.0002
.00025
.00025
.00023
.00021
.00018
.00015
.00012
.00009
.00006
.00003
.0
.0
.0
.0
.0
.0
.0
.0
.0
.0
2500.
```

Output Listing of Sample Case

CLB, GEARO LD XQ

UPPER SUN DRIVING PLANET - CASES 108, 8-14-67

PN0335=COMPUTATIONS OF GEAR TOOTH MESHING ERRORS 3-22-1966

SETS OF VP	INPUT	SETS OF U,Z	DIFF.GEAR	N.OF HARMONIC	
1	0	1	1	6	
I	N1	RP1	RO1	RT1	RM1
0.12000E 02	0.57000E 02	0.33530E 01	0.34398E 01	0.32535E 01	0.31990E 01
PRE.ANGLE	N2		RO2	RT2	RM2
0.22000E 02	0.31000E 02		0.19405E 01	0.17430E 01	0.16825E 01
T1	F1	RF1	YOUNGS MOD-1	SHEAR MOD-1	POS.RATIO-1
0.17500E 00	0.15400E 01	0.56000E-01	0.30000E 08	0.11600E 08	0.30000E 00
T2	F2	RF2	YOUNGS MOD-2	SHEAR MOD-2	POS.RATIO-2
0.18960E 00	0.13330E 01	0.56000E-01	0.30000E 08	0.11600E 08	0.30000E 00

CALCULATED DATA

RB1	BA1	BR1	AT1
0.[illegible]1088E 01	0.86575E-01	0.69517E-01	0.95442E-01

RP2	RB2	BA2	BR2	AT2
0.18235E 01	0.16907E 01	0.12782E 00	0.15918E 00	0.15357E 00

DRIVEN GEAR INPUT ROOT RADIUS SMALLER THAN BASE CIRCLE RADIUS-CHANGED TO

RM2= 0.169077E 01

J1	CJ1	AJ1	QJ1ABC	XJ1	YJ1
-0.24000E 02	0.00000E 00	-0.10582E 00			
-0.23000E 02	0.00000E 00	-0.10141E 00			
-0.22000E 02	0.00000E 00	-0.97003E-01			
-0.21000E 02	0.00000E 00	-0.92594E-01			
-0.20000E 02	0.00000E 00	-0.88185E-01			
-0.19000E 02	0.10000E 01	-0.83775E-01	0.16844E-07	0.32622E 01	0.11693E 00
-0.18000E 02	0.10000E 01	-0.79366E-01	0.18320E-07	0.32665E 01	0.11572E 00
-0.17000E 02	0.10000E 01	-0.74957E-01	0.19863E-07	0.32708E 01	0.11448E 00
-0.16000E 02	0.10000E 01	-0.70548E-01	0.21479E-07	0.32751E 01	0.11321E 00
-0.15000E 02	0.10000E 01	-0.66138E-01	0.23171E-07	0.32796E 01	0.11189E 00
-0.14000E 02	0.10000E 01	-0.61729E-01	0.24945E-07	0.32840E 01	0.11054E 00
-0.13000E 02	0.10000E 01	-0.57320E-01	0.26807E-07	0.32885E 01	0.10915E 00
-0.12000E 02	0.10000E 01	-0.52911E-01	0.28762E-07	0.32931E 01	0.10773E 00
-0.11000E 02	0.10000E 01	-0.48501E-01	0.30817E-07	0.32977E 01	0.10626E 00
-0.10000E 02	0.10000E 01	-0.44092E-01	0.32978E-07	0.33024E 01	0.10476E 00
-0.90000E 01	0.10000E 01	-0.39683E-01	0.35254E-07	0.33071E 01	0.10322E 00
-0.80000E 01	0.10000E 01	-0.35274E-01	0.37651E-07	0.33119E 01	0.10163E 00
-0.70000E 01	0.10000E 01	-0.30864E-01	0.40179E-07	0.33167E 01	0.10001E 00
-0.60000E 01	0.10000E 01	-0.26455E-01	0.42848E-07	0.33216E 01	0.98353E-01
-0.50000E 01	0.10000E 01	-0.22046E-01	0.45665E-07	0.33265E 01	0.96648E-01
-0.40000E 01	0.10000E 01	-0.17637E-01	0.48643E-07	0.33314E 01	0.94902E-01
-0.30000E 01	0.10000E 01	-0.13227E-01	0.51792E-07	0.33365E 01	0.93113E-01
-0.20000E 01	0.10000E 01	-0.88185E-02	0.55127E-07	0.33415E 01	0.91282E-01

-0.10000E 01	0.10000E 01	-0.44092E-02	0.58659E-07	0.33466E 01	0.89407E-01
0.00000E 00	0.10000E 01	0.00000E 00	0.62406E-07	0.33518E 01	0.87489E-01
0.10000E 01	0.10000E 01	0.44092E-02	0.66380E-07	0.33570E 01	0.85527E-01
0.20000E 01	0.10000E 01	0.88185E-02	0.70602E-07	0.33623E 01	0.83521E-01
0.30000E 01	0.10000E 01	0.13227E-01	0.75090E-07	0.33676E 01	0.81469E-01
0.40000E 01	0.10000E 01	0.17637E-01	0.79865E-07	0.33729E 01	0.79372E-01
0.50000E 01	0.10000E 01	0.22046E-01	0.84951E-07	0.33783E 01	0.77229E-01
0.60000E 01	0.10000E 01	0.26455E-01	0.90373E-07	0.33838E 01	0.75040E-01
0.70000E 01	0.10000E 01	0.30864E-01	0.96160E-07	0.33893E 01	0.72804E-01
0.80000E 01	0.10000E 01	0.35274E-01	0.10234E-06	0.33948E 01	0.70521E-01
0.90000E 01	0.10000E 01	0.39683E-01	0.10895E-06	0.34004E 01	0.68190E-01
0.10000E 02	0.10000E 01	0.44092E-01	0.11604E-06	0.34060E 01	0.65811E-01
0.11000E 02	0.10000E 01	0.48501E-01	0.12364E-06	0.34117E 01	0.63384E-01
0.12000E 02	0.10000E 01	0.52911E-01	0.13180E-06	0.34174E 01	0.60907E-01
0.13000E 02	0.10000E 01	0.57320E-01	0.14059E-06	0.34232E 01	0.58381E-01
0.14000E 02	0.10000E 01	0.61729E-01	0.15007E-06	0.34290E 01	0.55805E-01
0.15000E 02	0.10000E 01	0.66138E-01	0.16031E-06	0.34349E 01	0.53179E-01
0.16000E 02	0.00000E 00	0.70548E-01			
0.17000E 02	0.00000E 00	0.74957E-01			
0.18000E 02	0.00000E 00	0.79366E-01			
0.19000E 02	0.00000E 00	0.83775E-01			
0.20000E 02	0.00000E 00	0.88185E-01			
0.21000E 02	0.00000E 00	0.92594E-01			
0.22000E 02	0.00000E 00	0.97003E-01			
0.23000E 02	0.00000E 00	0.10141E 00			
0.24000E 02	0.00000E 00	0.10582E 00			
0.25000E 02	0.00000E 00	0.11023E 00			

COOD. OF EFFECTIVE TOOTH PROFILE AT ROOT CIRCLE	X	Y
	0.319529E 01	0.153977E 00

JI	QJIA	QJIB	QJIC
-0.19000E 02	0.26161E-09	0.15393E-07	0.11888E-08
-0.18000E 02	0.34664E-09	0.16490E-07	0.14833E-08
-0.17000E 02	0.44130E-09	0.17606E-07	0.18158E-08
-0.16000E 02	0.54799E-09	0.18743E-07	0.21878E-08
-0.15000E 02	0.66937E-09	0.19901E-07	0.26006E-08
-0.14000E 02	0.80844E-09	0.21081E-07	0.30562E-08
-0.13000E 02	0.96840E-09	0.22283E-07	0.35559E-08
-0.12000E 02	0.11528E-08	0.23508E-07	0.41013E-08
-0.11000E 02	0.13656E-08	0.24757E-07	0.46943E-08
-0.10000E 02	0.16112E-08	0.26031E-07	0.53363E-08
-0.90000E 01	0.18942E-08	0.27331E-07	0.60290E-08
-0.80000E 01	0.22199E-08	0.28657E-07	0.67742E-08
-0.70000E 01	0.25939E-08	0.30012E-07	0.75735E-08
-0.60000E 01	0.30225E-08	0.31396E-07	0.84290E-08
-0.50000E 01	0.35124E-08	0.32810E-07	0.93418E-08
-0.40000E 01	0.40712E-08	0.34257E-07	0.10314E-07
-0.30000E 01	0.47070E-08	0.35738E-07	0.11347E-07
-0.20000E 01	0.54289E-08	0.37254E-07	0.12444E-07
-0.10000E 01	0.62464E-08	0.38807E-07	0.13606E-07
0.00000E 00	0.71708E-08	0.40400E-07	0.14834E-07
0.10000E 01	0.82135E-08	0.42035E-07	0.16131E-07
0.20000E 01	0.93880E-08	0.43715E-07	0.17498E-07
0.30000E 01	0.10708E-07	0.45443E-07	0.18938E-07
0.40000E 01	0.12191E-07	0.47222E-07	0.20452E-07
0.50000E 01	0.13853E-07	0.49055E-07	0.22042E-07
0.60000E 01	0.15715E-07	0.50946E-07	0.23710E-07
0.70000E 01	0.17798E-07	0.52901E-07	0.25459E-07
0.80000E 01	0.20127E-07	0.54925E-07	0.27290E-07

0.90000E 01	0.22729E-07	0.57022E-07	0.29204E-07
0.10000E 02	0.25634E-07	0.59200E-07	0.31205E-07
0.11000E 02	0.28878E-07	0.61467E-07	0.33294E-07
0.12000E 02	0.32500E-07	0.63832E-07	0.35474E-07
0.13000E 02	0.36545E-07	0.66303E-07	0.37745E-07
0.14000E 02	0.41066E-07	0.68895E-07	0.40112E-07
0.15000E 02	0.46121E-07	0.71619E-07	0.42574E-07

J2	AJ2	QJ2ABC	XJ2	YJ2
-0.25000E 02	-0.20268E 00			
-0.24000E 02	-0.19457E 00			
-0.23000E 02	-0.18646E 00			
-0.22000E 02	-0.17836E 00			
-0.21000E 02	-0.17025E 00			
-0.20000E 02	-0.16214E 00			
-0.19000E 02	-0.15403E 00			
-0.18000E 02	-0.14593E 00			
-0.17000E 02	-0.13782E 00			
-0.16000E 02	-0.12971E 00			
-0.15000E 02	-0.12161E 00	0.22884E-07	0.17532E 01	0.11389E 00
-0.14000E 02	-0.11350E 00	0.24554E-07	0.17570E 01	0.11305E 00
-0.13000E 02	-0.10539E 00	0.26309E-07	0.17609E 01	0.11216E 00
-0.12000E 02	-0.97288E-01	0.28156E-07	0.17650E 01	0.11121E 00
-0.11000E 02	-0.89180E-01	0.30100E-07	0.17691E 01	0.11021E 00
-0.10000E 02	-0.81073E-01	0.32147E-07	0.17734E 01	0.10914E 00
-0.90000E 01	-0.72966E-01	0.34306E-07	0.17777E 01	0.10801E 00
-0.80000E 01	-0.64858E-01	0.36584E-07	0.17821E 01	0.10681E 00
-0.70000E 01	-0.56751E-01	0.38988E-07	0.17867E 01	0.10555E 00
-0.60000E 01	-0.48644E-01	0.41530E-07	0.17913E 01	0.10422E 00
-0.50000E 01	-0.40536E-01	0.44218E-07	0.17960E 01	0.10283E 00
-0.40000E 01	-0.32429E-01	0.47065E-07	0.18008E 01	0.10136E 00
-0.30000E 01	-0.24322E-01	0.50081E-07	0.18058E 01	0.99825E-01
-0.20000E 01	-0.16214E-01	0.53281E-07	0.18108E 01	0.98212E-01
-0.10000E 01	-0.81073E-02	0.56680E-07	0.18159E 01	0.96523E-01
0.00000E 00	0.00000E 00	0.60292E-07	0.18210E 01	0.94757E-01
0.10000E 01	0.81073E-02	0.64137E-07	0.18263E 01	0.92912E-01
0.20000E 01	0.16214E-01	0.68232E-07	0.18317E 01	0.90987E-01
0.30000E 01	0.24322E-01	0.72600E-07	0.18372E 01	0.88980E-01
0.40000E 01	0.32429E-01	0.77264E-07	0.18427E 01	0.86890E-01
0.50000E 01	0.40536E-01	0.82251E-07	0.18483E 01	0.84715E-01
0.60000E 01	0.48644E-01	0.87589E-07	0.18541E 01	0.82454E-01
0.70000E 01	0.56751E-01	0.93310E-07	0.18599E 01	0.80105E-01
0.80000E 01	0.64858E-01	0.99451E-07	0.18657E 01	0.77666E-01
0.90000E 01	0.72966E-01	0.10605E-06	0.18717E 01	0.75136E-01
0.10000E 02	0.81073E-01	0.11316E-06	0.18778E 01	0.72513E-01
0.11000E 02	0.89180E-01	0.12082E-06	0.18839E 01	0.69797E-01
0.12000E 02	0.97288E-01	0.12910E-06	0.18901E 01	0.66985E-01
0.13000E 02	0.10539E 00	0.13808E-06	0.18964E 01	0.64076E-01
0.14000E 02	0.11350E 00	0.14781E-06	0.19028E 01	0.61069E-01
0.15000E 02	0.12161E 00	0.15841E-06	0.19092E 01	0.57962E-01
0.16000E 02	0.12971E 00	0.16997E-06	0.19157E 01	0.54754E-01
0.17000E 02	0.13782E 00	0.18264E-06	0.19223E 01	0.51443E-01
0.18000E 02	0.14593E 00	0.19656E-06	0.19290E 01	0.48028E-01
0.19000E 02	0.15403E 00	0.21195E-06	0.19357E 01	0.44508E-01
0.20000E 02	0.16214E 00			
0.21000E 02	0.17025E 00			
0.22000E 02	0.17836E 00			
0.23000E 02	0.18646E 00			
0.24000E 02	0.19457E 00			

COOD. OF EFFECTIVE TOOTH PROFILE AT ROOT CIRCLE

X	Y
0.168455E 01	0.144890E 00

J2	QJ2A	QJ2B	QJ2C
-0.15000E 02	0.48899E-09	0.19691E-07	0.27042E-08
-0.14000E 02	0.60297E-09	0.20872E-07	0.30789E-08
-0.13000E 02	0.73199E-09	0.22084E-07	0.34931E-08
-0.12000E 02	0.87857E-09	0.23327E-07	0.39497E-08
-0.11000E 02	0.10456E-08	0.24602E-07	0.44516E-08
-0.10000E 02	0.12363E-08	0.25909E-07	0.50017E-08
-0.90000E 01	0.14544E-08	0.27248E-07	0.56031E-08
-0.80000E 01	0.17041E-08	0.28620E-07	0.62590E-08
-0.70000E 01	0.19902E-08	0.30026E-07	0.69725E-08
-0.60000E 01	0.23178E-08	0.31465E-07	0.77470E-08
-0.50000E 01	0.26931E-08	0.32939E-07	0.85858E-08
-0.40000E 01	0.31227E-08	0.34449E-07	0.94925E-08
-0.30000E 01	0.36141E-08	0.35996E-07	0.10470E-07
-0.20000E 01	0.41757E-08	0.37582E-07	0.11524E-07
-0.10000E 01	0.48168E-08	0.39207E-07	0.12656E-07
0.00000E 00	0.55480E-08	0.40873E-07	0.13871E-07
0.10000E 01	0.63810E-08	0.42583E-07	0.15172E-07
0.20000E 01	0.73289E-08	0.44339E-07	0.16564E-07
0.30000E 01	0.84062E-08	0.46143E-07	0.18050E-07
0.40000E 01	0.96297E-08	0.47998E-07	0.19636E-07
0.50000E 01	0.11017E-07	0.49909E-07	0.21324E-07
0.60000E 01	0.12590E-07	0.51878E-07	0.23120E-07
0.70000E 01	0.14371E-07	0.53911E-07	0.25027E-07
0.80000E 01	0.16387E-07	0.56013E-07	0.27050E-07
0.90000E 01	0.18668E-07	0.58190E-07	0.29193E-07
0.10000E 02	0.21247E-07	0.60450E-07	0.31461E-07
0.11000E 02	0.24164E-07	0.62802E-07	0.33860E-07
0.12000E 02	0.27462E-07	0.65255E-07	0.36392E-07
0.13000E 02	0.31194E-07	0.67822E-07	0.39063E-07
0.14000E 02	0.35419E-07	0.70518E-07	0.41878E-07
0.15000E 02	0.40208E-07	0.73360E-07	0.44842E-07
0.16000E 02	0.45643E-07	0.76371E-07	0.47960E-07
0.17000E 02	0.51825E-07	0.79578E-07	0.51236E-07
0.18000E 02	0.58875E-07	0.83015E-07	0.54675E-07
0.19000E 02	0.66942E-07	0.86726E-07	0.58284E-07

INPUT LISTING OF PROFILE ERROR AND SUPPLEMENTARY COMPLIANCE

Z1	U1	Z2	U2
0.00000E 00	0.00000E 00	0.00000E 00	0.00000E 00
0.00000E 00	0.00000E 00	0.00000E 00	0.00000E 00
0.00000E 00	0.00000E 00	0.00000E 00	0.00000E 00
0.00000E 00	0.00000E 00	0.00000E 00	0.00000E 00
0.00000E 00	0.00000E 00	0.00000E 00	0.00000E 00
0.00000E 00	0.00000E 00	0.00000E 00	0.00000E 00
0.30000E-04	0.00000E 00	0.00000E 00	0.00000E 00
0.60000E-04	0.00000E 00	0.00000E 00	0.00000E 00
0.90000E-04	0.00000E 00	0.00000E 00	0.00000E 00
0.12000E-03	0.00000E 00	0.00000E 00	0.00000E 00
0.15000E-03	0.00000E 00	0.00000E 00	0.00000E 00
0.18000E-03	0.00000E 00	0.00000E 00	0.00000E 00
0.22000E-03	0.00000E 00	0.00000E 00	0.00000E 00
0.26000E-03	0.00000E 00	0.00000E 00	0.00000E 00
0.30000E-03	0.00000E 00	0.00000E 00	0.00000E 00
0.30000E-03	0.00000E 00	0.00000E 00	0.00000E 00
0.26000E-03	0.00000E 00	0.00000E 00	0.00000E 00
0.22000E-03	0.00000E 00	0.00000E 00	0.00000E 00

0.18000E-03	0.00000E 00	0.00000E 00	0.00000E 00
0.15000E-03	0.00000E 00	0.00000E 00	0.00000E 00
0.12000E-03	0.00000E 00	0.00000E 00	0.00000E 00
0.90000E-04	0.00000E 00	0.00000E 00	0.00000E 00
0.60000E-04	0.00000E 00	0.00000E 00	0.00000E 00
0.30000E-04	0.00000E 00	0.00000E 00	0.00000E 00
0.00000E 00	0.00000E 00	0.00000E 00	0.00000E 00
0.50000E-04	0.00000E 00	0.00000E 00	0.00000E 00
0.10000E-03	0.00000E 00	0.00000E 00	0.00000E 00
0.15000E-03	0.00000E 00	0.00000E 00	0.00000E 00
0.20000E-03	0.00000E 00	0.00000E 00	0.00000E 00
0.25000E-03	0.00000E 00	0.00000E 00	0.00000E 00
0.25000E-03	0.00000E 00	0.00000E 00	0.00000E 00
0.23000E-03	0.00000E 00	0.00000E 00	0.00000E 00
0.21000E-03	0.00000E 00	0.00000E 00	0.00000E 00
0.18000E-03	0.00000E 00	0.00000E 00	0.00000E 00
0.15000E-03	0.00000E 00	0.00000E 00	0.00000E 00
0.12000E-03	0.00000E 00	0.00000E 00	0.00000E 00
0.90000E-04	0.00000E 00	0.00000E 00	0.00000E 00
0.60000E-04	0.00000E 00	0.00000E 00	0.00000E 00
0.30000E-04	0.00000E 00	0.00000E 00	0.00000E 00
0.00000E 00	0.00000E 00	0.00000E 00	0.00000E 00
0.00000E 00	0.00000E 00	0.00000E 00	0.00000E 00
0.00000E 00	0.00000E 00	0.00000E 00	0.00000E 00
0.00000E 00	0.00000E 00	0.00000E 00	0.00000E 00
0.00000E 00	0.00000E 00	0.00000E 00	0.00000E 00
0.00000E 00	0.00000E 00	0.00000E 00	0.00000E 00
0.00000E 00	0.00000E 00	0.00000E 00	0.00000E 00
0.00000E 00	0.00000E 00	0.00000E 00	0.00000E 00
0.00000E 00	0.00000E 00	0.00000E 00	0.00000E 00
0.00000E 00	0.00000E 00	0.00000E 00	0.00000E 00
0.00000E 00	0.00000E 00	0.00000E 00	0.00000E 00

INPUT DATA ON TANGENTIAL LOAD AND TOOTH SPACING ERROR

WT	VPT1	VPT2
0.25000E 04	0.00000E 00	0.00000E 00

CALCULATED NORMAL WN= 0.269633E 04

CALCULATED TOTAL CONTACT COMPLIANCE QJD= 0.846269E-07

CALCULATED TOOTH MESHING ERRORS AND LOADS

JC1	AJC1	TANG. ERROR	WTC	WTD
0.10000E 01	0.44092E-02	-0.55004E-03	0.25000E 04	0.00000E 00
0.20000E 01	0.88185E-02	-0.49851E-03	0.25000E 04	0.00000E 00
0.30000E 01	0.13227E-01	-0.44833E-03	0.25000E 04	0.00000E 00
0.40000E 01	0.17637E-01	-0.39952E-03	0.25000E 04	0.00000E 00
0.50000E 01	0.22046E-01	-0.35210E-03	0.25000E 04	0.00000E 00
0.60000E 01	0.26455E-01	-0.21294E-03	0.19159E 04	0.58406E 03
0.70000E 01	0.30864E-01	-0.21186E-03	0.17990E 04	0.70096E 03
0.80000E 01	0.35274E-01	-0.20985E-03	0.16779E 04	0.82204E 03
0.90000E 01	0.39683E-01	-0.21280E-03	0.15351E 04	0.96489E 03
0.10000E 02	0.44092E-01	-0.21449E-03	0.13893E 04	0.11106E 04
0.11000E 02	0.48501E-01	-0.21491E-03	0.12418E 04	0.12581E 04
0.12000E 02	0.52911E-01	-0.21407E-03	0.10935E 04	0.14064E 04
0.13000E 02	0.57320E-01	-0.20647E-03	0.92686E 03	0.15731E 04
0.14000E 02	0.61729E-01	-0.19734E-03	0.76166E 03	0.17383E 04
0.15000E 02	0.66138E-01	-0.18668E-03	0.59920E 03	0.19007E 04

0.16000E 02	0.70548E-01	-0.33347E-03	0.00000E 00	0.25000E 04
0.17000E 02	0.74957E-01	-0.36439E-03	0.00000E 00	0.25000E 04
0.18000E 02	0.79366E-01	-0.39702E-03	0.00000E 00	0.25000E 04
0.19000E 02	0.83775E-01	-0.43128E-03	0.00000E 00	0.25000E 04
0.20000E 02	0.88185E-01	-0.45631E-03	0.00000E 00	0.25000E 04
0.21000E 02	0.92594E-01	-0.48283E-03	0.00000E 00	0.25000E 04
0.22000E 02	0.97003E-01	-0.51078E-03	0.00000E 00	0.25000E 04
0.23000E 02	0.10141E 00	-0.54013E-03	0.00000E 00	0.25000E 04
0.24000E 02	0.10582E 00	-0.57085E-03	0.00000E 00	0.25000E 04
0.25000E 02	0.11023E 00	-0.60292E-03	0.00000E 00	0.25000E 04

CALCULATED FOURIER COEFFICIENTS FOR ERRORS

I	A(I)	B(I)
0	-0.7215917E-03	0.0000000E 00
1	-0.1558903E-03	0.1099209E-03
2	-0.2292671E-04	0.1315865E-04
3	-0.2709452E-04	-0.1221881E-04
4	0.1308417E-04	0.1013418E-04
5	0.1045603E-05	0.1450376E-05
6	-0.2270080E-05	0.1785091E-04

DATA REDUCTION

Profile Input Data From Profile Measurement Trace

For the particular profile measurement equipment, determine

1. the end of the trace corresponding to the tip of the tooth
2. the direction of trace deviation from the longitudinal line corresponding to excess material (with respect to a true involute), or the direction of positive profile deviation
3. the longitudinal scale of roll angle
4. the transverse scale of profile deviation

From the gear design data, determine

5. the angle corresponding to each of the calculation points

$$\alpha_J = \frac{360° \; J}{N \; N_J}$$

where. J = identification number of calculation point
N = number of teeth
N_J = number of calculation points

6. the angle of recess for an external gear (taken as the driving gear)

$$\alpha_R = \sqrt{\frac{R_O{}^2}{R_B{}^2} - 1} - \tan \phi_P$$

where: R_O = outside radius
R_B = base circle radius
ϕ_P = pressure angle

or the angle of recess for an internal gear taken as the driving gear (which is the same as its angle of approach when taken as the driven gear).

$$\alpha_R = - \left(\tan \phi_P - \sqrt{\frac{R_I{}^2}{R_B{}^2} - 1} \right)$$

where: R_I = inside radius

On the profile measurement trace (see Figures 31 and 32), locate the pitch point in the following manner:

7. measure back from the tip a distance corresponding to the recess angle

8. locate the true involute reference line by drawing a longitudinal line through the pitch point

9. measure off from the pitch point distances corresponding to the angles for each of the calculation points, with positive calculation points between pitch point and tip on external gears and with negative points on internal gears

10. at the calculation point distances, measure off the deviations from the longitudinal, true involute line.

Sample calculations:

The data from one of the traces in Figure 31 are plotted as the measured profile, case 103, in Figure 28.

The data from one of the traces in Figure 32 are plotted as the measured profile, case 303, in Figure 29.

Mean Gear Mesh Compliance From Computed Results

Approximate method

1. Submit the computer case of the gear designs with true involute profiles, any supplementary compliances which apply, and a suitable load.

2. Calculate the approximate mean mesh compliance

$$Q_O = \frac{A_O}{2W_T}$$

where: A_O = computed constant Fourier coefficient

W_T = tangential load

Sample calculation, for the case of the upper sun driving the planet at 85% of rated load

$$A_O = 1.03 \times 10^{-3} \text{ in.}$$

$$W_T = 2500 \text{ lb}$$

$$Q_O = \frac{A_O}{2W_T} = \frac{1.03 \times 10^{-3}}{2 \times 2500}$$

$$Q_O = .206 \times 10^{-6} \text{ in./lb}$$

Accurate method

1. Submit two computer cases, both with the same set of gear designs and with the same applicable profile and supplementary compliance data, but with two loads.

2. Calculate the mean mesh compliance

$$Q_O = \frac{A_{O1} - A_{O2}}{2\ (W_{T1} - W_{T2})}$$

where the added subscripts refer to the data from the two cases submitted.

Sample calculation, for the case of the sun driving the planet with design profile

At 105% rated load, $W_{T1} = 3085$ lb

and $A_{O1} = 1.303 \times 10^{-3}$

At 65% rated load, $W_{T2} = 1910$ lb

and $A_{O2} = .836 \times 10^{-3}$

$$Q_O = \frac{A_{O1} - A_{O2}}{2\ (W_{T2} - W_{T1})} = \frac{(1.303 - .836)10^{-3}}{2(3085 - 1910)} = \frac{.467 \times 10^{-3}}{2(1175)}$$

$$Q_O = .199 \times 10^{-6} \text{ in./lb}$$

APPENDIX V

GEAR TOOTH FORCE ANALYSIS

INTRODUCTION

Any geared system transmitting power is subject to torsional vibration because it contains the necessary elements of rotational inertia, torsional elasticity, and source of excitation. The inertia may be present in concentrated form, as in the body of a gear, or it may be distributed as in the sections of connecting shafting. Similarly, the elasticity or compliance may be concentrated as in a coupling or in the flexing gear teeth, or it may be distributed with the inertia in the shaft sections. As in any other torsionally vibrating system, the excitation may come from externally applied pulsating torques, as from a driving motor or turbine, or from some fluctuating resistance to the steady rotation. However, in geared systems there is also a displacement form of excitation which comes from the imperfect transfer of motion in the meshing gears. This excitation makes the mating teeth at any point of excitation subject to dynamic changes in relative motion. This changing of relative motion can be achieved only if there is generated in turn a dynamic force acting between the teeth to impose the necessary accelerations. This dynamic force, generated in response to the gear displacement excitation, can subject the gear teeth to greater loads than required for the steady transmission of power. In addition, it can become a factor in the generation of noise in the transmission system.

The purpose of this analysis is to evaluate these gear tooth forces. The data required by the analysis to describe the torsionally vibrating system can be in the form of physical dimensions taken directly from design drawings. At the same time, where necessary or where available, the analysis will also accept system data in the form of concentrated inertia or concentrated compliances.

Several features make the analysis sufficiently versatile to deal with a wide range of gear system designs. First, the analysis has provision for branches in the vibrating system. Second, it not only treats multiple cases of the simple gear set involving only one gear driving a second, but it can also treat multiple cases of one type of planetary gear set (the sun gear driving, the ring gear restrained, and the planet carrier transmitting the vibration to the balance of the system). Third, it includes the effects of externally applied damping such as might be developed at the bearings. The analysis presents the resulting dynamic gear tooth forces in a form giving their phase relationships as well as their magnitudes.

LIMITATIONS AND ASSUMPTIONS

The limitations in the gear systems treated and the major assumptions on which the analysis is based are listed below:

1. Excitation is introduced into the system only at the gear meshing points and only in the form of sinusoidal displacements. These

displacements constitute differences in pitch line motion of the mating teeth from the two gears and are introduced in series with any elastic compliances of the teeth themselves.

2. The system is considered linear; that is, all compliances and damping coefficients are assumed to be constant. The varying gear tooth stiffness actually in effect is represented as a constant mean stiffness, while the effect of the variability under a steady load is assumed to have been incorporated in the calculation of the displacement excitation. The linear system also requires that the dynamic tooth forces be smaller than the static forces, so that no separation takes place at a gear mesh.

3. The members of the system are assumed to be compliant only in the torsional mode, with full rigidity in the lateral mode. This means that the kind of interaction between torsional and lateral modes often found in gear systems is not considered in this analysis.

4. The only gearing stages treated are

   a. the simple gear set with one gear driving a second.

   b. the planetary gear set with the sun gear driving, the ring gear elastically restrained, and the planet carrier as the driven member.

5. The system may have simple branches but no loops (that is, branches tied to the system at two or more points).

6. The overall system is one which has no rigid, torsional restraints at its ends or at any other point; neither does it have any externally applied dynamic forces other than those applied at a damping or elastic constraint and due to its own dynamic angular motion. (The rigid restraints, however, can be simulated by introducing very large concentrated inertias at the points in question.)

7. Damping can be applied only between points in the system and ground, and not between points within the system. There is no provision for damping within a planetary set or at the gear mesh in any gear set.

8. In the planetary gear set

   a. all planets are equally spaced.

   b. all excitations from planet to planet are the same in magnitude but differ in phase relation, according to the planet spacing and to the relation between excitation frequency and rotational speeds.

c. all radial forces on the sun or ring are fully balanced, the sun and ring are rigidly supported in the radial direction, or any other set of conditions exists which eliminates lateral modes of vibration.

DESCRIPTION OF ANALYSIS

This analysis is based on a variation of the Holzer analysis commonly used for torsional, critical speed studies. The steps followed in performing the basic analysis are as follows:

1. For each of the portions of the system separated in the input data by station numbers, the properties of its cylindrical section are calculated. This calculation makes use of the outside and inside diameters of the section and the shear modulus and density properties of the material. Where necessary, different outside diameters for the section properties related to inertia and stiffness calculations are considered.

2. A unit angular motion at the specified frequency is tentatively assumed at one end of the system with no independent, externally applied torque at this point. Any concentrated inertia at this end station is viewed as subject to this motion, indicating a torque applied by the connecting system. This torque is calculated, and with it is combined the effect of any external torque due to an elastic or damping restraint applied by ground at the same station. The motion amplitude and the torque requirement are treated as one set of end conditions of the portion of the system between this first section and the next section. Using a relationship which considers that the inertia, where present, is uniformly distributed with compliance along the length of the system segment, the analysis calculates torque at the far end of the system segment. At the second station, the same treatment of concentrated inertia or applied constraints, as described previously, is employed with special provision for tying in the branches, as described later. This process is continued from station to station until the end of the system is reached, generating for each station a torque value just entering the station, an angular motion at the station, and a torque value just leaving the station. This calculation leaves a residual torque after the last station, which may be recognized as a tentative contradiction to the actual boundary condition at this point.

   When a station with a branch is encountered, there is an additional element in the calculation. A unit angular motion is tentatively assumed for the free end of the branch, and the same kind of station-to-station calculation is made until the branching station is reached. The angular motion at this station, as found thus far in the main system calculation, is then compared to the motion found in the branch calculation. The ratio of these is then applied to each value of motion and torque in the branch, in this way matching the branch to the main system. The torque leaving the branched station can then be calculated from the torques applied by both the main and

branch systems, and the calculations for the main system can be carried forward.

At the stations containing simple gear sets, the same procedure is followed, but the motion ratio and the direction reversal associated with the gears are introduced. (This introduction of the gear ratio eliminates the need to change the inertias, compliances, or damping coefficients to effective values at a reference shaft speed, as is commonly required in other calculation procedures.) In this traverse of the system, there is no introduction of excitation at the gear sets.

At any station representing a planetary gear set, the calculation is made using the special relationships between motion and torque going into the planetary system and motion and torque leaving it. This special relationship assumes that the motions of the individual planets inside the system are rotationally in phase; that is, they all act in parallel and together in response to the incoming motions and torques. As in the simple gear sets, no excitation is introduced at the planetary set in this calculation step.

3. The above procedure is repeated with the change that zero angular motion is tentatively assumed for the first station. This leads to zero motion and torque in the system until a station with excitation is reached. At this station, which will be for one of the gear sets, the specified excitation at the same specified frequency introduces a "step" in the motion transmitted. This new motion and any torque requirements it generates at the station where it first has effect, now become the motion and torque inputs to the successive segments of the system. The continuation of the station-by-station calculation, as before, generates at each station values of torque entering the station, motion at the station, and torque leaving the station. Also, as before, the calculation results in a residual torque after the last station. This residual torque is compared to that computed in the previous step. After one complete set of motion and torque data is multiplied by the appropriate ratio of these residual torques, the values are subtracted from their counterparts in the other set. The torque after the last station which results from this operation is now zero, indicating that the original boundary condition has been met. All of the remaining motions and torques therefore represent the response of the system to the particular excitation introduced.

4. The dynamic torque transmitted through the first gear of each simple set of gears is calculated from information now available. This information consists of the torque going into the gear station, on both sides if a branch is connected at this point, of whatever torque is required to supply the computed motion to the concentrated inertia, and of the torque applied by whatever constraints are present. The dynamic force acting on the gears tangent to the pitch circle is found by dividing the gear torque by its pitch radius.

In the case of the planetary set of gears, the individual internal torques, forces, and motions are calculated from the final set of torque and motion results now available for both ends of the station.

5. The three preceding steps are applied simultaneously to both of the two components of the excitation. The components referred to here are the cosine and sine terms, also known as the real and imaginary terms, which together define not only the amplitude of the excitation but also its phase relationship with respect to some reference. In order to treat the two components simultaneously, all calculations are performed with complex numbers.

The excitation conditions in the planetary station require special treatment. There are two excitations at each planet, one at the sun and one at the ring, and the two may be independent of each other. The excitations from planet to planet, however, are assumed to be uniform in amplitude and uniformly spaced in phase relationship, as stated previously. This uniform phasing may be zero, which is to say that all the excitations on either the sun or the ring are exactly in phase rotationally. In this case, the excitations act together in generating the response within the planetary stage and elsewhere in the system. This is the situation treated in the main computer program which embodies the above-described Holzer type of analysis.

The zero phasing condition will occur when the ratio of excitation frequency to the rotational frequency of the carrier is an exact multiple of the number of planets. When this relationship does not hold, the excitations are separated in phase, and each segment of the planetary system with its own planet must be treated as acting separately. Furthermore, under these conditions of complete excitation balancing, the combined effects of the excitations are to generate zero net torques and motions in the input or output members of the planetary system. The planetary system is therefore acting independent of the gear system external to it, and the data of the external system play no role in the response developed within the planetary system. Therefore, in order to calculate this response, a separate analysis is used in an auxiliary program. This separate analysis does not require the Holzer type of analysis but merely uses the solution of the dynamic equations to give the pitch line tooth forces at each mesh. In this auxiliary analysis, as in the main one, excitations at the sun and ring are treated simultaneously. Furthermore, for each of these, the two components of excitation, cosine and sine (or real and imaginary), are treated individually to give separate components in the results.

DERIVATION OF ANALYTICAL RELATIONSHIPS

The relationships used in the analysis are presented in two groups: those that form part of the general Holzer analysis, and those that are specific to the planetary gear stage. Each group is accompanied by its own list of symbols.

Holzer Analysis

The symbols to be used in this portion of the analysis and shown in Figures 73 and 74 are given below. The equations derived are valid for any set of consistent units.

C_n	concentrated torsional damping coefficient acting between stations n and ground
C_{n+1}	concentrated torsional damping coefficient acting between station n+1 and ground
D_{mn}	outside diameter of cylindrical distributed mass after station n, to be used for inertia calculations
D_{qn}	outside diameter of cylindrical distributed mass after station n, to be used for compliance calculations
d_n	inside diameter of distributed mass after station n
f	cycle frequency of excitation
G	shear modulus of elasticity
g	gravitational constant
I_n	concentrated moment of inertia at station n
I_{n+1}	concentrated moment of inertia at station n+1
I'_n	calculated total mass moment of inertia of distributed mass between stations n and n+1
j	mathematical operator which produces a 90° phase rotation
J_n	polar moment of inertia of the cross-sectional area of the distributed mass after station n
L_n	length of distributed mass after station n
n	general station number

Q_n	concentrated torsional compliance* of elastic restraint acting between station n and ground
Q_{n+1}	concentrated torsional compliance of elastic restraint acting between station n+1 and ground
Q_n'	concentrated total torsional compliance of distributed mass between stations n and n+1
Q_n''	concentrated torsional compliance between stations n and n+1, when there is no distributed mass
T_n	torque acting at station n on the side toward the previous station
T_{n+1}	torque acting at the end of the distributed mass after the station; also, the torque acting at station n-1 on the side toward station n
T_n'	torque acting at station n on the side toward the next station; also, the torque acting at the start of the distributed mass after station n
T_{n+1}'	torque acting at station n+1 on the side toward the next station.
T_x'	torque acting at the x location along the distributed mass
x	variable distance along the distributed mass, measured from station n
γ	weight density
θ_n	angular motion at station n
θ_x	angular motion at x location after station n
θ_{n+1}	angular motion at station n+1
ρ	mass density
ω	angular frequency of excitation ($=2\pi f$)

There are two subscripts which may be joined to the subscripts used in the major symbols listed above. These identify the phase component of the variable.

I	imaginary or right angle phase component
R	real or in-phase component

*Compliance is defined as the reciprocal of stiffness.

The objective of this portion of the analysis is to derive the relationships of angular motion and torque between successive stations and at each station in the torsional system (see Figures 73 and 74). Two sets of relationships are required: one set to cover the transferred motion and torque between stations and the other set to cover the torque changes, from that going into to that leaving each station. The first set is derived for the general case where there is distributed mass and compliance in the form of a cylindrical bar between stations, starting from the dimensions of this bar. The case of a concentrated compliance in place of the distributed mass is also treated. The second set considers the effect of concentrated inertia and elastic and damping constants at each station.

Some of the properties of the cylindrical distributed mass between station n and station n+1 will be used in the later derivations. There are:

the section polar moment of inertia

$$J_n = \frac{\pi}{32} (D_{qn}^4 - d_n^4) \tag{152}$$

the total torsional compliance

$$Q_n' = \frac{L}{GJ_n} \tag{153}$$

the mass density

$$\rho = \frac{\gamma}{g} \tag{154}$$

the total moment of inertia

$$I'_n = \frac{\pi}{32} (D_{mn}^4 - d_n^4) \rho L_n \tag{155}$$

If a bar of uniform cross section, Figure 73, is subjected to a sinusoidal torsional vibration of frequency ω, the sinusoidal motion and torque at a section x distance from one end may be expressed in terms of the motion and torque acting at that end and in terms of the properties of the bar, as follows:

$$\theta_x = \theta_n \cos(\omega\sqrt{I_n'Q_n'} \cdot x/L) + T_n' \frac{\sin(\omega\sqrt{I_n'Q_n'} \cdot x/L)}{\omega\sqrt{I'_n/Q_n'}} \tag{156}$$

$$T_x = -\theta_n \omega\sqrt{I'_n/Q_n'} \sin(\omega\sqrt{I'_n Q_n'} \cdot x/L)$$

$$+T_n' \cos(\omega\sqrt{I_n'Q_n'} \cdot x/L) \tag{157}$$

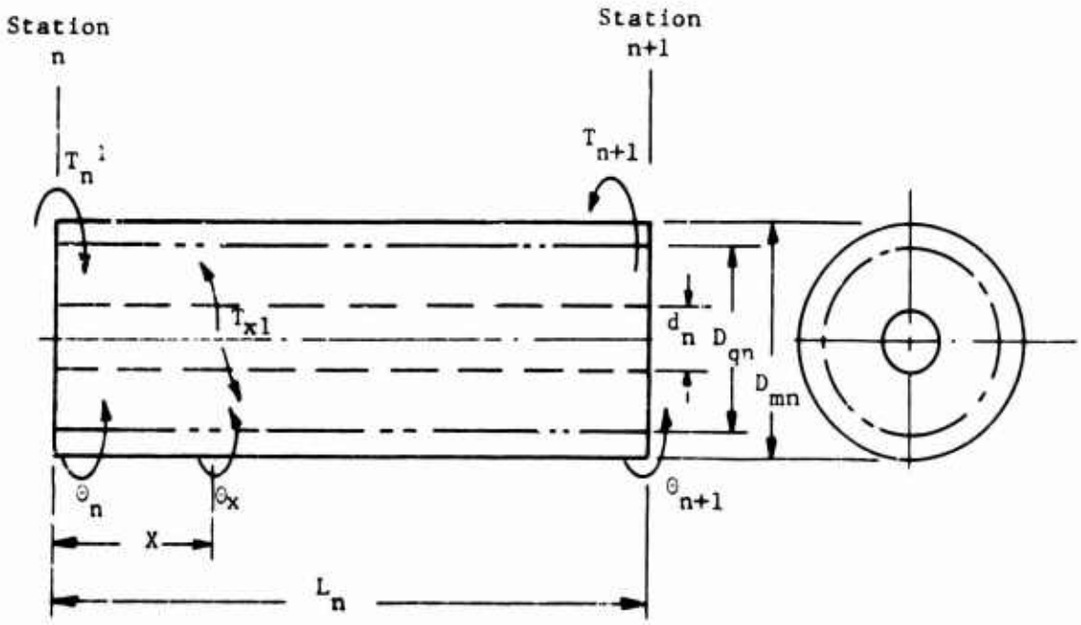

Figure 73. General Case of Distributed Mass Between Stations

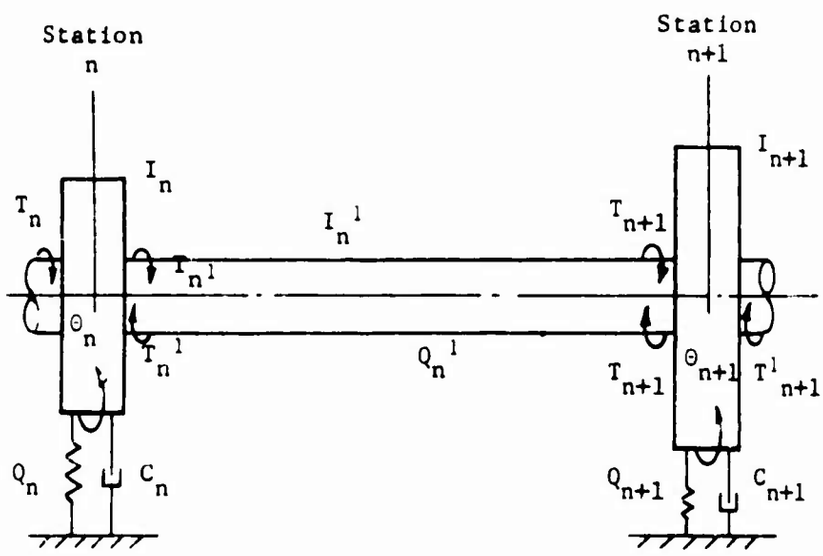

Figure 74. General Portion of the Torsional System.

The values of motion and torque at the far end of the bar, or in this case, the cylindrical distributed mass, may be found by replacing x by L. Equations (156) and (157) then become

$$\theta_{n+1} = \theta_n \cos(\omega\sqrt{I_n'Q_n'}) + T_n' \left[\frac{Q_n'}{\omega\sqrt{I_n'Q_n'}}\right] \sin(\omega\sqrt{I_n'Q_n'}) \tag{158}$$

$$T_{n+1} = -\theta_n \left[\frac{\omega\sqrt{I_n'Q_n'}}{Q_n'}\right] \sin(\omega\sqrt{I_n'Q_n'}) + T_n' \cos(\omega\sqrt{I_n'Q_n'}) \tag{159}$$

These expressions relate the motion and torque at or going into station n+1 to the motion and torque at or leaving station n.

The variables of motion and torque may also be expressed in complex form, where the sets of rectangular components preserve phase relationship as well as magnitude. Each variable is replaced by its real (or in-phase) component and its imaginary (or right angle phase) component. When the right angle operator j is used, the replacements may be expressed as

$$\theta_n = \theta_{nR} + j\theta_{nI} \tag{160}$$

$$T'_n = T'_{nR} + jT'_{nI} \tag{161}$$

$$\theta_{n+1} = \theta_{(n+1)R} + j\theta_{(n+1)I} \tag{162}$$

$$T_{n+1} = T_{(n+1)R} + jT_{(n+1)I} \tag{163}$$

After substituting these replacements in Equations (157) and (158), the real and imaginary terms are segregated. The equations for the real components are

$$\theta_{(n+1)R} = \theta_{nR} \cos(\omega\sqrt{I_n'Q_n'}) + T_{nR}' \left[\frac{Q_n'}{\omega\sqrt{I_n'Q_n'}}\right] \sin(\omega\sqrt{I_n'Q_n'}) \tag{164}$$

$$T_{(n+1)R} = -\theta_{nR} \left[\frac{\omega\sqrt{I_n'Q_n'}}{Q_n'}\right] \sin(\omega\sqrt{I_n'Q_n'}) + T'_{nR} \cos(\omega\sqrt{I_n'Q_n'}) \tag{165}$$

The equations for the imaginary components are

$$\theta_{(n+1)I} = \theta_{nI} \cos(\omega\sqrt{I_n'Q_n'}) + T_{nI}' \left[\frac{Q_n'}{\omega\sqrt{I_n'Q_n'}}\right] \sin(\omega\sqrt{I_n'Q_n'}) \tag{166}$$

$$T_{(n+1)I} = -\theta_{nI}\left[\frac{\omega\sqrt{I_n'Q_n'}}{Q_n'}\right]\sin(\omega\sqrt{I_n'Q_n'}) + T_{nI}'\cos(\omega\sqrt{I_n'Q_n'}) \quad (167)$$

In the case where there is no distributed mass between stations but only a concentrated compliance Q_n'', the applicable equations are found from Equations (164), (165), (166), and (167) by making $I_n' = 0$, and by replacing Q_n' by Q_n''. In simplifying, note that

$$\lim_{a \to o} \frac{\sin a}{a} = 1 \quad (168)$$

The equations for the real components become

$$\theta_{(n+1)R} = \theta_{nR} + T'_{nR}Q_n'' \quad (169)$$

$$T_{(n+1)R} = T'_{nR} \quad (170)$$

For the imaginary components, they become

$$\theta_{(n+1)I} = \theta_{nI} + T'_{nI}Q_n'' \quad (171)$$

$$T_{(n+1)I} = T'_{nI} \quad (172)$$

At station n, the relationship between the torques entering and those leaving the station is found from Figure 74 as

$$T_n' = T_n + Q_n\theta_n + j\omega C_n\theta_n + j^2\omega^2 I_n\theta_n \quad (173)$$

This may be simplified to

$$T_n' = \theta_n(Q_n - \omega^2 I_n + j\omega C_n) + T_n \quad (174)$$

The variables may now be introduced in their complex form, using Equations (49) and (50), and also

$$T_n = T_{nR} + jT_nI \quad (175)$$

The complete equation becomes

$$T'_{nR} + jT'_{nI} = (\theta_{nR} + j\theta_{nI})(Q_n - \omega^2 I_n + j\omega C_n) + (T_{nR} + jI_nI) \quad (176)$$

This simplifies to

$$T'_{nR} + jT'_{nI} = \theta_{nR}(Q_n - \omega^2 I_n) + j^2\theta_{nI}\omega C_n + J_{nR}$$

$$+ j\theta_{nI}(Q_n - \omega^2 I_n) + j\theta_{nR}\omega C_n + jT_{nI} \qquad (177)$$

After separating the real and imaginery terms into separate equations,

$$T'_{nR} = \theta_{nR}(Q_n - \omega^2 I_n) - \theta_{nI}\omega C_n + T_{nR} \qquad (178)$$

$$T'_{nI} = \theta_{nI}(Q_n - \omega^2 I_n) + \theta_{nR}\omega C_n + T_{nI} \qquad (179)$$

Dynamic Analysis of the Planetary Gear Stage

The assumptions made in this analysis are

1. The system is infinitely rigid in the radial direction, and all motions are torsional or tangential in direction. This assumption eliminates from consideration any lateral mode of vibration which would interact with the torsional mode.

2. All compliances are constant, including those at the gear teeth.

3. There is no damping in the system.

4. All the planets are uniformly spaced around the sun gear.

5. The excitations at the sun-planet mesh are identical in amplitude at all planets and have uniformly spaced phase relationships. The same is true of the excitations at the planet-ring mesh.

The nomenclature used in this portion of the analysis and shown in Figure 75 is given below. The equations derived are valid for any set of consistent units.

F_{Ci} force transmitted between the carrier and the ith planet, tangent to the planet orbit

F_{Ri} tangential force transmitted between the ring gear and the ith planet gear

F_{Si} tangential force transmitted between the sun gear and the ith planet gear

I_P mass moment of inertia of each planet about its own center

I_R	mass moment of inertia of the ring gear
I_S	mass moment of inertia of the sun gear
M_P	mass of each planet gear
N_P	number of uniformly spaced and identical planets
q_C	linear compliance between the planet and the carrier, effective value tangent to the planet orbit
Q_G	angular compliance between the ring gear and the ground
q_R	linear compliance between the planet and the ring gears, effective value tangent to the pitch circles
q_S	linear compliance between the sun and the planet gears, effective value tangent to the pitch circles
R_C	radius of the planet orbit
R_P	pitch radius of the planet gears
R_R	pitch radius of the ring gear
R_S	pitch radius of the sun gear
T_C	transmitted torque acting at the hub of the planet carrier
T_R	torque applied to ring gear through its torsionally resilient support
T_S	applied torque acting at the hub of the sun gear
ε_{Ri}	sinusoidal excitation introduced at the planet-ring mesh of the ith planet gears expressed as a linear displacement tangent to the pitch circle
ε_{Si}	sinusoidal excitation introduced at the sun-planet mesh of the ith planet gears, expressed as a linear displacement tangent to the pitch circle
θ_{Bi}	angular position of common centerline of the sun gear and the ith planet gear, relative to ground
θ_C	angular position of the planet carrier, relative to ground
θ_{Pi}	angular position of the ith planet gear, relative to ground
θ_R	angular position of the ring gear, relative to ground

θ_S angular position of the sun gear, relative to ground

ω angular frequency of all the excitations

For each of the gears, equations may be written for the sum of the applied torques equal to the moment of inertia times the angular acceleration. From Figure 75, these are

for the sun gear,

$$T_S - \Sigma F_{Si} \cdot R_S = I_S(-\ddot{\theta}_S) \tag{180}$$

for each planet gear,

$$F_{Si} \cdot R_P - F_{Ri} \cdot R_P = I_P(-\ddot{\theta}_{Pi}) \tag{181}$$

for the ring gear,

$$\Sigma F_{Ri} \cdot R_R - T_R = I_R(-\ddot{\theta}_R) \tag{182}$$

for the carrier,

$$\Sigma F_{Ci} \cdot R_C - T_C = I_C(-\ddot{\theta}_C) \tag{183}$$

For each of the planet gears, the equation may be written for the sum of the applied forces equal to the mass times the linear acceleration, or

$$F_{Si} + F_{Ri} - F_{Ci} = M_P(-\ddot{\theta}_{Bi}) \cdot R_C \tag{184}$$

If the linear system described by these equations is subjected to sinusoidal excitation of angular frequency ω, the resulting motions and forces will also be sinusoidal and of the same frequency Therefore, if each of the variables is understood to now represent the peak values of the resulting sinusoidal variations, then the angular accelerations may each be replaced as follows:

$$\ddot{\theta}_S = -\omega^2\theta_S \tag{185}$$

$$\ddot{\theta}_{Pi} = -\omega^2\theta_{Pi} \tag{186}$$

$$\ddot{\theta}_R = -\omega^2\theta_R \tag{187}$$

$$\ddot{\theta}_C = -\omega^2\theta_C \tag{188}$$

$$\ddot{\theta}_{Bi} = -\omega^2\theta_{Bi} \tag{189}$$

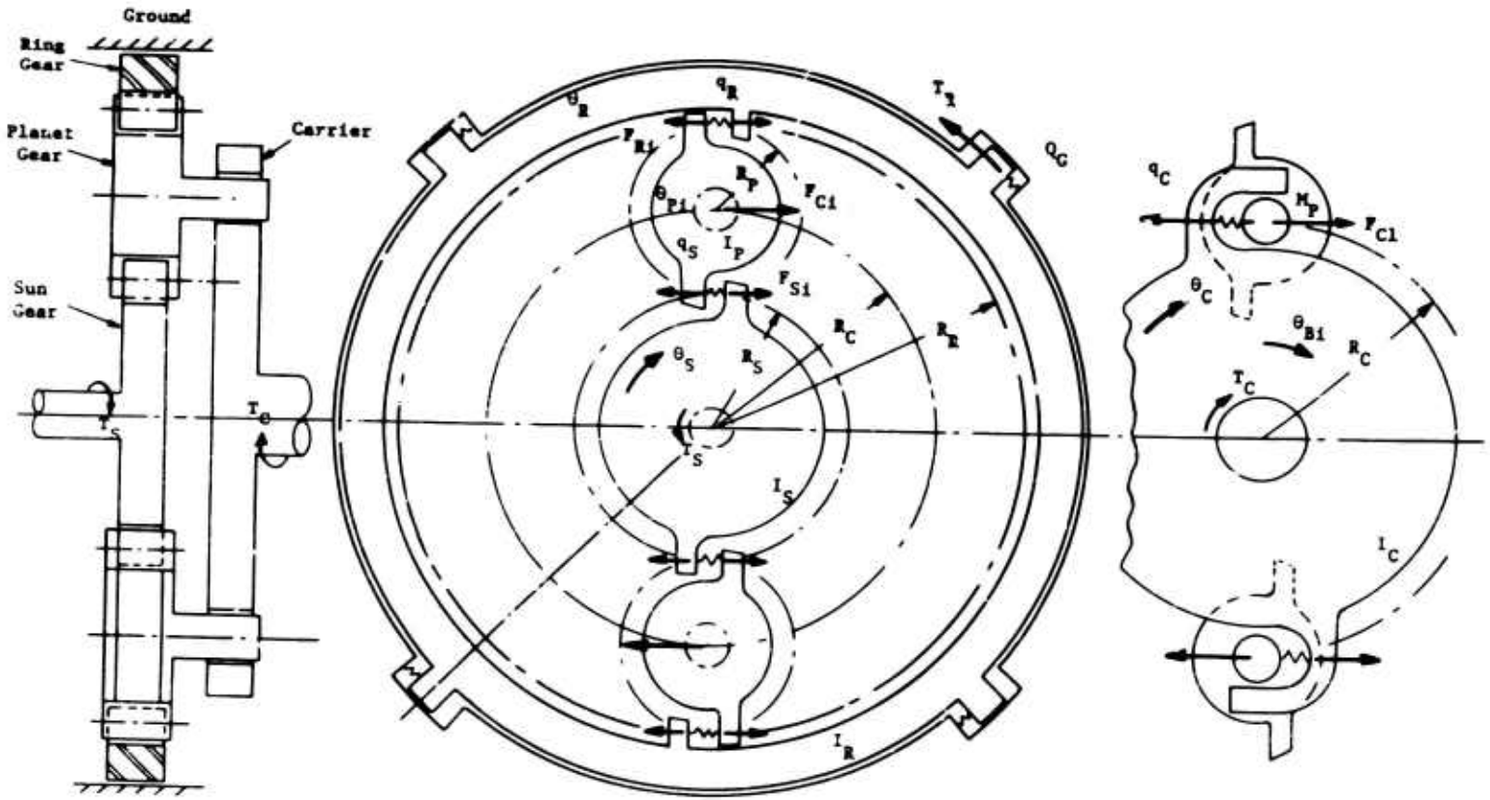

Note: The directions shown for the angular displacements were selected to be consistent with those used in the Holfer analysis. They are opposite to the directions which would result if the torques shown were steady torques.

Figure 75. Schematic Diagram of Planetary Gearing Station.

Equations (180) through (184) may now be written in the following manner, in which the arrangement of terms has also been changed in order to keep T_S and θ_S or the F_{Si} terms on the right-hand side.

From Equations (180) and (185),

$$\Sigma F_{Si} = \frac{1}{R_S}\left[T_S - I_S\omega^2\theta_S\right] \tag{190}$$

From Equations (181) and (186),

$$R_P \cdot F_{Ri} + I_P\omega^2\theta_{Pi} = R_P \cdot F_{Si} \tag{191}$$

When all planets are summed, this becomes

$$R_P\Sigma F_{Ri} + I_P\omega^2\Sigma\theta_{Pi} = R_P\Sigma F_{Si} \tag{192}$$

From Equations (182) and (187),

$$R_R\Sigma F_{Ri} - T_R - \omega^2 I_R\theta_R = 0 \tag{193}$$

From Equations (183) and (188),

$$R_C\Sigma F_{Ci} - \omega^2 I_C\theta_C - T_C = 0 \tag{194}$$

From Equations (184) and (189),

$$F_{Ri} - F_{Ci} - \omega^2 M_P R_C\theta_{Bi} = -F_{Si} \tag{195}$$

When all planets are summed, this becomes

$$\Sigma F_{Ri} - \Sigma F_{Ci} - \omega^2 M_P R_C\Sigma\theta_{Bi} = -\Sigma F_{Si} \tag{196}$$

The next set of equations relates the displacements and the rotations. Note that the displacement at each of the flexible members is equal to the force transmitted times the compliance of that member.

The motion of each planet center in terms of the rotation of the carrier is

$$(-\theta_{Bi})R_C = (-\theta_C)R_C + F_{Ci} \cdot q_C \tag{197}$$

Summed for all planets and rearranged, this becomes

$$q_C\Sigma F_{Ci} - N_P R_C\theta_C + R_C\Sigma\theta_{Bi} = 0 \tag{198}$$

The total motion of the planet at the sun-planet mesh in terms of the rotation of the sun, with the introduction of the sun-planet mesh excitation, becomes

$$(-\theta_{Bi})R_C + (-\theta_{Pi})R_P = (-\theta_S)R_S - F_{Si} \cdot q_S + \varepsilon_{Si} \tag{199}$$

Summed for all planets and rearranged, this becomes

$$-R_C\Sigma\theta_{Bi} - R_P\Sigma\theta_{Pi} = -N_P R_S \Theta_S - q_S\Sigma F_{Si} + \Sigma\varepsilon_{Si} \tag{200}$$

The total motion of the planet at the planet-ring mesh in terms of the rotation of the ring, with the introduction of the planet-ring excitation, becomes

$$(-\theta_{Bi})R_C - (-\theta_{Pi})R_P = -(-\theta_R)R_R - F_{Ri} \cdot q_R + \varepsilon_{Ri} \tag{201}$$

Summed for all planets and rearranged, this becomes

$$-R_C\Sigma\theta_{Bi} + R_P\Sigma\theta_{Pi} - N_P R_R \theta_R + q_R\Sigma F_{Ri} = \Sigma\varepsilon_{Ri} \tag{202}$$

The motion of the ring relative to ground is

$$(-\theta_R) = T_R Q_G \tag{203}$$

Equation (203) may now be substituted into Equation (193) to give

$$R_R\Sigma F_{Ri} + (\omega^2 I_R Q_G - 1)T_R = 0 \tag{204}$$

Similarly, Equation (203) may be substituted into Equation (202) to give

$$-R_C\Sigma\theta_{Bi} + R_P\Sigma\theta_{Pi} + N_P R_R Q_G T_R + q_R\Sigma F_{Ri} = \Sigma\varepsilon_{Ri} \tag{205}$$

These quations relate the transmitted torque T_C and angular motion θ_C to the applied torque T_S and angular motion θ_S, including also the effect of the excitations.

Assumption number 5, stated at the beginning of the dynamic analysis of the planetary gear stage, imposes important restrictions on the excitation summation terms in Equations (200) and (205). If each set of excitations is of the same amplitude with non-zero, uniformly spaced phase relationships, each summation is equal to zero. This may best be demonstrated with the aid of an illustration. If the number of planets is four, the phase separation would be 90° or $\pi/2$ radians. The individual excitations would then be

$$\varepsilon_1 = \varepsilon_o \sin(\omega t)$$

$$\varepsilon_2 = \varepsilon_o \sin(\omega t + \pi/2)$$

$$\varepsilon_3 = \varepsilon_o \sin(\omega t + \pi)$$

$$\varepsilon_4 = \varepsilon_o \sin(\omega t + 3\pi/2)$$

The summation of these is then

$$\Sigma\varepsilon_i = \varepsilon_o + \varepsilon_2 + \varepsilon_3 + \varepsilon_4$$

$$\Sigma\varepsilon_i = \varepsilon_o \sin(\omega t) + \varepsilon_o \sin(\omega t + \pi/2) + \varepsilon_o \sin(\omega t + \pi) + \varepsilon_o \sin(\omega t + 3\pi/2)$$

$$\Sigma\varepsilon_i = \varepsilon_o \sin\omega t + \varepsilon_o \cos\omega t - \varepsilon_o \sin\omega t - \varepsilon_o \cos\omega t$$

$$\Sigma\varepsilon_i = 0$$

If the two excitation summations are equal to zero, the excitations disappear from Equations (200) and (205). This indicates that under these conditions of excitation, there is no excitation influence on the relationship between applied and transmitted torque or angular motion. This does not mean that the effect of these fully balanced excitations is not felt within the planetary gear stage but, rather, that this effect is completely internal and does not play any role in the dynamics of the external system. (The internal dynamics will be discussed later in the analysis.)

There is one special case where there is no balancing of excitations and where the excitations do act on the system dynamics. This case occurs when there is a zero phase relationship between the individual excitations at the sun-planet mesh and, similarly, between the excitations at the planet-ring mesh.

Under these conditions,

$$\Sigma(\varepsilon_{Si})_0 = N_P \varepsilon_{SO} \tag{206}$$

$$\Sigma(\varepsilon_{Ri})_0 = N_P \varepsilon_{RO} \tag{207}$$

At the same time, the symmetry imposed by the equal and synchronized excitations requires that all the unknown forces and motions associated with the planets also be equal and synchronized. Therefore,

$$\Sigma F_{Si} = N_P F_S \tag{208}$$

$$\Sigma F_{Ri} = N_P F_R \tag{209}$$

$$\Sigma F_{Ci} = N_P F_C \tag{210}$$

$$\Sigma\theta_{Pi} = N_P \; P \tag{211}$$

$$\Sigma\theta_{Bi} = N_P \; B \tag{212}$$

With the substitutions of Equations (206) through (212), Equations (190), (192), (194), (196), (198), (200), (204), and (205) become

$$N_P F_S = (T_S - I_S \omega^2 \theta_S)/R_S \tag{213}$$

$$R_P N_P F_R + I_P \omega^2 N_P \theta_P = R_P N_P F_S \tag{214}$$

$$R_R N_P F_R + (I_R \omega^2 Q_G - 1) T_R = 0 \tag{215}$$

$$R_C N_P F_C - I_C \omega^2 \theta_C - T_C = 0 \tag{216}$$

$$N_P F_R - N_P F_C - M_P R_C \omega^2 N_P \; B = -N_P F_S \tag{217}$$

$$q_C N_P F_C - R_C N_P \theta_C + R_C N_P \theta_B = 0 \tag{218}$$

$$-R_C N_P \theta_B - R_P N_P \theta_P = -R_S N_P \theta_S - q_S N_P F_S + N_P \varepsilon_{SO} \tag{219}$$

$$-R_C N_P \theta_B + R_P N_P \theta_P + R_R Q_G N_P T_R + q_R N_P F_R = N_P \varepsilon_{RO} \tag{220}$$

Note that Equations (214) through (220) have all the unknown variables on the left-hand side and the known variables F_S, θ_S, ε_{SO}, and ε_{RO} on the right-hand side. F_S is included among the known torque T_S and motion θ_S applied at the start of the planetary stage.

Equations (214) through (220) are listed in tabular form in Table XXXIII. The solution of these simultaneous equations will give the transmitted torque T_C and motion θ_C, as well as the individual gear tooth forces.

In relating these equations to the Holzer analysis, if the planetary gear stage is located at station n, the following equivalences apply:

$$T_S = T'_n = T_n \tag{221}$$

$$\theta_S = \theta_n \tag{222}$$

$$T_C = T_{n+1} \tag{223}$$

$$\theta_C = \theta_{n+1} \tag{224}$$

It should be noted that Equations (214) through (220) and their solution may also apply when there is no internal excitation; that is, when the excitation is completely external and is introduced by means of the dynamic applied torque T_S and motion θ_S. The only condition implied is that in transmitting the dynamic effects, the planets undergo motions and sustain forces which are all equal and synchronized in phase relationship. This

TABLE XXXIII. DYNAMIC EQUATIONS FOR PLANETARY GEAR STAGE WITH EQUAL, SYNCHRONIZED EXCITATION AMONG PLANETS

Equation No.	Coefficients for Unknowns							
	$N_P F_R$	$N_P F_C$	$N_P \theta_P$	$N_P \theta_B$	θ_C	T_R	T_C	Right-Hand Side
214	R_P		$I_P \omega^2$					$R_P N_P F_S$
215	R_R					$(I_R \omega^2 Q_G - 1)$		0
216		R_C			$-I_C \omega^2$		-1	0
217	1	-1		$-M_P R_C \omega^2$				$-N_P F_S$
218		q_C		$+R_C$	$-R_C N_P$			0
219			$-R_P$	$-R_C$				$-q_S N_P F_S - R_S N_P \theta_S + N_P \epsilon_{SO}$
220	q_R		$+R_P$	$-R_C$		$R_R Q_G N_P$		$N_P \epsilon_{RO}$

Note: $R_C = R_S + R_P = R_R - R_P$

condition may be considered as a realistic one if only because there is no reason to expect that more complex forms of dynamic response will be generated.

The case when the excitations have non-zero, uniformly spaced phase relationships will now be considered. As pointed out previously, the effect of these excitations is completely internal to the planetary gear stage.

For the case when the only excitation at the particular frequency is within the planetary system, the external dynamic torques and motions, whether applied at the sun, T_S and θ_S, transmitted by the carrier, T_C and θ_C, or experienced by the ring gear, T_R and θ_R, are all equal to zero. The same conditions of excitation impose a symmetry that dictates that not only are the summations of excitation equal to zero, but also the summations of all planet forces and motions are equal to zero. Therefore, equations with summations, Equations (190), (192), (193), (194), (196), (198), (200), (202), and their derivatives, all degenerate into identities of 0 = 0. Only the equations written for individual planets still apply. When one planet is selected as typical, [illegible] it is recognized that the other will be identical except for a [illegible] form phase shift in all its forces and motions, the remaining equations, (191), (195), (197), (199), and (201), now become

$$R_P F_R + I_P \omega^2 \theta_P - R_P F_S = 0 \qquad (225)$$

$$F_R - F_C - M_P R_C \omega^2 \theta_B + F_S = 0 \qquad (226)$$

$$-R_C \theta_B - q_C F_C = 0 \qquad (227)$$

$$-R_C \theta_B - R_P \theta_P + q_S F_S = \varepsilon_S \qquad (228)$$

$$-R_C \theta_B + R_P \theta_P + q_R F_R = \varepsilon_R \qquad (229)$$

These five equations are listed in Table XXXIV and may be solved simultaneously to find the five unknowns. This solution, which is independent of external system data, has no links with the Holzer analysis and need not be part of the overall system calculation. Instead, the necessary calculation is provided by an auxiliary program which treats each planetary gear stage by itself. In the special case where excitations of the same frequency occur inside the planetary system and also in the main system, the only treatment possible is to find the two sets of solutions and to combine them by superposition. In making this combination, note that the results from the auxiliary calculation described immediately above must be staggered in phase for the individual planets before being combined with the results of the main calculation described earlier.

TABLE XXXIV. DYNAMIC EQUATIONS FOR SINGLE PLANET OF PLANETARY GEAR STAGE WITH EQUAL EXCITATIONS AMONG PLANETS OF NON-ZERO, UNIFORMLY SPACED PHASE RELATIONSHIP

Equation No.	Coefficients for Unknowns					
	F_S	F_R	F_C	θ_P^*	θ_E^*	Right-Hand Side
225	$-R_P$	R_P		$I_P\omega^2$		0
226	1	1	-1		$-M_P R_C \omega^2$	0
227			$-q_C$		$-R_C$	0
228	q_S			$-R_P$	$-R_C$	ε_S
229		q_R		R_P	$-R_C$	ε_R

Note: $R_C = R_S + R_P = R_R - R_P$

* The signs in front of these coefficients will be reversed if the directions of these angular motions are taken as the reverse of those shown in Figure 75.

DESCRIPTION OF MAIN COMPUTER PROGRAM

Organization of Stations

Selection of Stations

Stations are established where one or more of the following descriptions apply:

a. The free end of any portion of the system, including the end and beginning of the main system and the end of any branch.

b. The point at which a concentrated inertia is acting. By concentrated inertia is meant an inertia which is not calculated by the program from given cylindrical dimensions.

c. The point at which a concentrated compliance is connected to the inertia which precedes or follows it. This inertia may be either concentrated or of the distributed type calculated by the program.

d. The point at which external constraints are applied to the system in the form of an elastic restraint or in the form of damping.

e. Each member of a simple gear set, but without any stations between these two.

f. The start and end of a planetary gear stage.

g. Where inertias and compliances are to be computed by the program, at any point where there are changes in any of the diameters used to define the cylindrical portions of the system. Any non-cylindrical portion, such as a tapered portion, may be approximated by converting it into a series of stepped diameters.

Numbering of Stations

The stations are numbered in accordance with the following procedure. Refer also to Figure 76.

a. Select a "main system" which begins at a free end and trace a path through the system components until it reaches another free end. This path has the restriction that any branches which remain may not have further branching on themselves. Also, the path must enter each planetary stage through the sun gear. In Figure 76, the main system selected consists of the paths 1-4, 9, 15-20, and 25-40. The main system might also have been selected as 1-4, 9, 15-20, and 25-21 (which would of course require changes in station numbers).

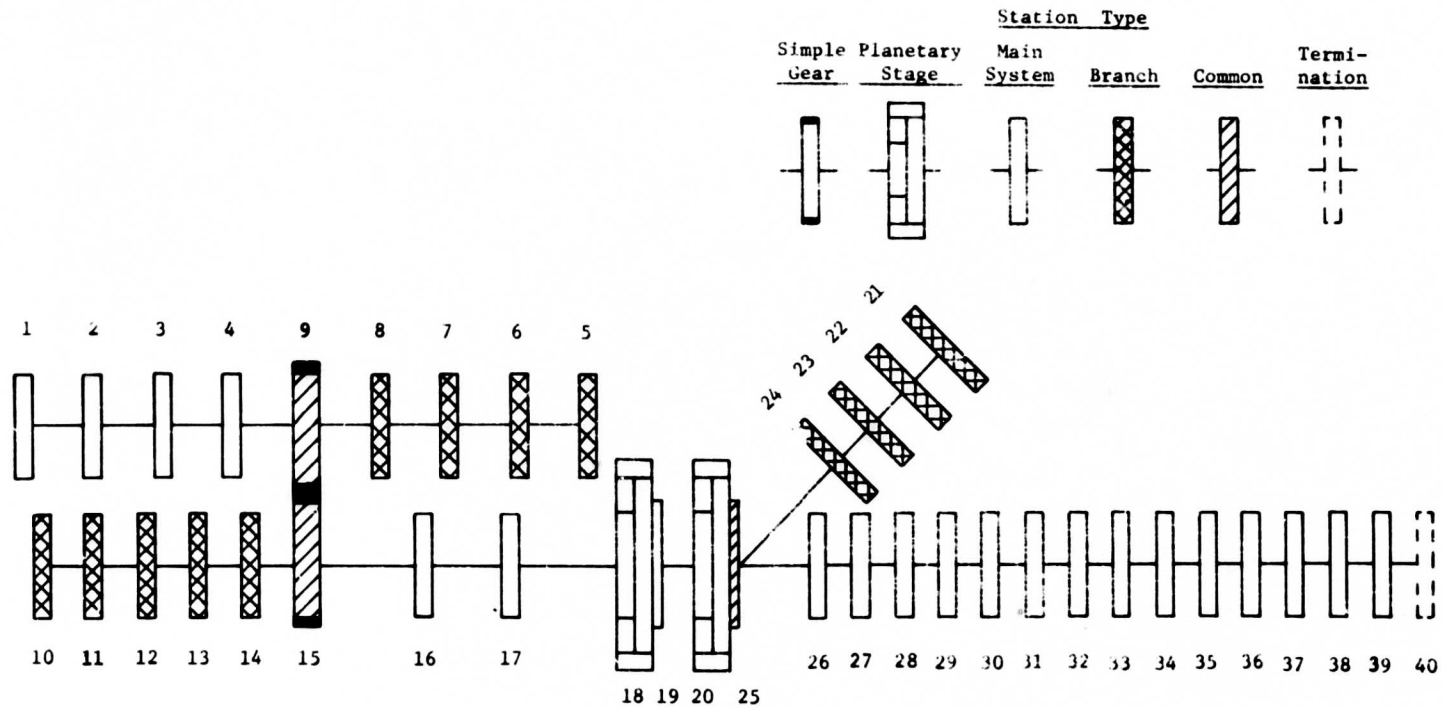

Note: See text for identification of stations.

Figure 76. Schematic Diagram of Torsional Vibrations System for the UH-1D Drive System.

However, a main system with the path 10-20, and 25-40 would not be permissible, because the branch of 5-9 would then have the branch of 1-4 on itself. Also, a main system with the path 40-25, 20-15, 9 and 4-1 would not be permissible, because it enters the planetary stages from the carrier side.

b. Start numbering the stations beginning with 1 at the starting free end, continuing in sequence until a common station with a branch is reached. Do not give the common station the next number. Instead, go to the free, far end of the branch, continuing the numbering sequence at this far end and numbering along the branch until the common is reached. The common then receives the next number, and numbering is continued along the main system. The same procedure is followed whenever another branch is encountered. The end of the main system receives the highest station number.

Input Variables, Format, and Instructions

Card 1 Title, Format (72H). This card precedes each set of input data.

a. Printing instructions, column 1.
For printer to skip a line, use 0.
For printer to go to next sheet, use 1.

b. Title, columns 2 through 72.

Card 2 Control numbers. Format (7I5)

a. NS Total number of stations. (NS $\leq$ 200)
Specification for selection of stations given in earlier section.

Place last digit of this number in column 5.

b. NB Number of stations with external constraints, in the form of elastic restraint or damping, both with respect to ground. (NB $\leq$ NS)

Place last digit of this number in column 10.

c. NBR Number of branches, without including main system. (NBR $\leq$ 20)

Place last digit of this number in column 15.

d. NMPG Total number of cases of gear excitation. A change in station number, frequency, or magnitude of either component constitutes a separate case. In the planetary stations, one pair of sun and ring excitations of the same frequency constitutes one case. Individual solutions are found for each case. Except in the planetary stages, when there are multiple excitations of the same frequency at different points in the system, the solutions for the individual excitations must be combined outside the program.

Place last digit of this number in column 20.

e. INP Identification as to whether this control card represents the last complete set of input data being submitted.
If more sets of input data follow, use 0.
If this is the last set, use 1.

Place this digit in column 25.

f. NSRG Number at simple gear sets. ($0 < NSRG \leq 20$) Each set consists of two gears. If an idler is used between two gears, the combination must be represented by two simple gear sets, where the idler is replaced by two connected gears with no compliance between them and with a total inertia equal to that of the idler. Where one gear drives two or more gears, each leading off to separate branches, a similar conversion must be made. If one gear drives through multiple gears back into the main system, in a so-called star arrangement, the only treatment possible in this program is to combine the multiple intermediate gears into one composite gear, assuming that the excitations, if any, are torsionally synchronous.

Place the last digit of this number in column 30.

g. NPLG Number of planetary gear stages. ($NPLG \leq 2$)

Place this digit in column 35.

Card 3 Rotor material properties. Format (5X, 2E 12.4)

a. GM Shear modulus of elasticity, lb-in.^{2}. May be zero only if all values of RL in the rotor data are zero.

Use columns 6 through 17.

b. DENST Weight density, lb/in.^{3}. May be zero only if all values of RL in the rotor data are zero.

Use columns 18 through 29.

Cards 4-1 to 4-NS Rotor data. Format (I5, 6E 12.4)

a. NSTA Station number at or after which the rotor data apply. There must be given in numerical sequence with no omissions.

Place the last digit of this number in column 5.

b. RIP Moment of inertia concentrated at station, lb-in.^{2}. This includes any inertia in the system which is not to be calculated by the program from dimensional data. At the stations for simple gear sets, list the inertias of both members in the rotor data. All planetary inertias are included only in the separate planetary data cards. The station which immediately follows the planetary may have its own inertia.

Use columns 6 through 17.

c. RL Length of uniform cylindrical shaft section between this station and the adjoining, higher-numbered station, in. At the station for the first member of a simple gear set and at the station for a planetary gear stage, use 0.0. At the terminating or last station, use 0.0 or 1.0.

Use columns 18 through 29.

d. DST Outer diameter for stiffness calculation of the cylindrical shaft section, in. This diameter measures the section which transmits torque. If the actual shaft section is reduced as by a keyway, a diameter which approximates the reduced section should be used. At the station for the first member of a simple gear set and at the station for a planetary gear stage, use 0.0. At the terminating station, use 0.0.

Use columns 30 through 41.

e. DMS Outer diameter for mass calculation of the cylindrical shaft section, in. This diameter measures the section which contributes inertia. It may include any assembled sleeves or hubs which extend the full distance and which rotate with the shaft. Use 0.0 for the special stations as described under DST.

Use columns 42 through 53.

f. DIN Inner diameter for both stiffness and mass calculation of the shaft section, in. If the shaft section is solid, use 0.0. Use 0.0 for the special stations as described under DST.

Use columns 54 through 65.

g. CCOM Concentrated compliance acting between this station and the adjoining, higher-numbered station, rad/in.-lb. This compliance is separate from that calculated by the program from the dimensional data, and it can be used only when there are no such dimensional data between the same two stations. Any value listed as a concentrated compliance will enter into the computations only if RL = 0 for the same station. Use 0.0 for the special stations as described under DST. Concentrated compliances associated with any of the gears are included only in the special data cards for the particular type of gear stage.

Use columns 66 through 77.

Cards 5-1 to 5-NB External constraints. Format (I5, 2E 12.4)
(These cards are omitted in NB =0)

a. LB Station number at which the constraints are acting. These must be given in numerical sequence.

Place last digit of this number in column 5.

b. BK External, torsional, elastic restraint acting at the station, expressed as a torsional stiffness, in.-lb/rad. In an actual system which has steady rotation, the stiffness must be 0 if the restraint is to ground. If in such a rotating system the restraint is to an "infinite" but rotating mass, the stiffness may have any finite value.

Use columns 6 through 17.

c. BCE Coefficient of the external damping constraint acting at the station, in.-lb-sec/rad.

Use columns 18 through 29.

Cards 6-1 to 6-NSRG Simple gear set data. Format (I5, 4E 12.4)
(At least one card must be submitted.)

a. LS Station number at which the first, or lower-numbered, member of the gear set is located. (The second member of the gear set is understood to be at the station LS+1, unless it serves as a common station to a branch. In this case, the second member has the number which completes the branch.) The simple gear set station numbers must be given in numerical sequence.

Place the last digit of this number in column 5.

b. RP Pitch radius of the first member of the gear set at station LS, in.

Use columns 6 through 17.

c. RG Pitch radius of the second member of the gear set, in.

Use columns 18 through 29.

d. SG Combined linear compliance of the two gears, tangential to their pitc circles, in./lb.

Use columns 30 through 41.

Cards 7-1-A,B,C to 7-NPLG-A,B,C Planetary gear stage data.
(These cards are omitted if NPLG = 0. When they are included, they must appear in sets of three, and each set must be arranged in the order given.)

First card of set -A Planetary geometry. Format (I5, 3E 12.4)

a. LEC Station number at the start of the planetary stage. This location of the station is at the connecting point to the sun gear, but the station does not include the sun gear. The sun gear and other planetary components, including the planet carrier, lie between this station and the one following it.

Place the last digit of this number in column 5

b. PN Number of planet gears in the planetary stage.

Use columns 6 through 17. Do not omit decimal point.

c. RS Pitch radius of the sun gear, in.

Use columns 18 through 29.

d. RW Pitch radius of the planet gear, in. The pitch radius of the ring gear will be calculated within the program by adding double the planet radius to the sun radius.

Use columns 30 through 41.

Second card of set -B Planetary inertias. Format (I5, 5E 12.4)

a. IPL Station number of the planetary stage, the same as LEC.

Place the last digit of this number in column 5.

b. PMS Weight on one planet gear, lb. This includes all components which rotate with the planet - everything between bearing surface and gear teeth. One-half the weight of any rolling elements in the bearing should be included.

Use columns 6 through 17.

c. PSP Moment of inertia of the sun gear, lb.in.^{2}. This includes all components between the point of connection to the outside system and the gear teeth.

Use columns 18 through 29.

d. PIP Moment of inertia of each planet gear, lb-in.^{2}. This includes all components used in computing the weight. PMS.

Use columns 30 through 41.

e. PRP Moment of inertia of the ring gear, lb-in.^{2}. This includes all components between the gear teeth and the point of elastic connection to ground. If the connection to ground is rigid, with zero compliance, any finite inertia may be used for the ring gear.

Use columns 42 through 53.

f. PCP Moment of inertia of the planet carrier, lb-in.^{2}. This includes all components between the bearing surfaces in the planet gears and the point of connection to the outside system.

Use columns 54 through 65.

Third card of set -C Planetary compliances. Format (I5, 5E 12.4)

a. IPL Station number of the planetary stage, a repetition of the value in the previous card.

Place the last digit of this number in column 5.

b. SS Combined linear compliance of each sun-planet gear mesh, tangential to its pitch circle, in.-lb. If the sun gear construction is such that there is a significant compliance between the hub and the rim, the starting connection point to the sun gear should be redefined as located at the rim. The hub would then be associated with the outside system as a separate station, with the structural compliance of the sun gear as a connecting concentrated compliance. In this case, the mesh compliance still appears under SS, but the sun gear inertia under PSP would be limited to that of the rim construction.

Use columns 6 through 17.

c. SR Combined linear compliance of each planet-ring gear mesh, tangential to its pitch circle, in.-lb.

Use columns 18 through 29.

d. SW Linear compliance of the planet support in the planet carrier, tangential to the path of planet centers, in.-lb. This compliance is the combination of the compliance of the planet bearing and the compliance of any portion of the carrier which will deflect with the individual planet. If the carrier construction is such that there is a compliance between a hub and a rim-type member which supports all the planets collectively, this structural compliance may be combined with the others to give a total planet carrier compliance. Alternatively, the system may be changed so that the end of the planetary stage, that is, its connection to the external system, is taken at the rim-type member. In this case, the hub becomes associated with the outside system as a separate station. The compliance between hub and rim then appears as a separate concentrated compliance between the station at the close of the planetary stage and the new station for the hub. With this change, the compliance used under SW is the combination of only the first two compliances mentioned above; namely, those associated with the individual planet.

Use columns 30 through 41.

e. Blank Columns 42 through 53 are not read in this main computer program. The auxiliary program used in conjunction with this main program will take the same input planetary data on the same cards, except for one item for which this field has been reserved.

f. ST Angular compliance of the support between the ring and ground, rad/in.-lb. If the ring is rigidly connected to ground, set this compliance equal to zero.

Use columns 54 through 65.

Cards 8-1 to 8-BR Branch data. Format (2I5)
These cards are omitted if BR = 0,)

a. LBR Number of the first or free end station of the branch.

Place the last digit of this number in column 5.

b. LBS Number of the common station of the branch at which it is connected to the main system.

Place the last digit of this number in column 10.

Cards 9-1 to 9-NMPG Gear excitation data. Format (I5, 6E 12.4)
(These cards may be submitted in any order.)

a. IT — Station number which identifies the gears at which the excitation is introduced. For simple gear sets, the number of the first member is used, as for LS in card 6. For planetary gear stages, the station number at the start of the planetary is used, as for LEC in card 7-A.

Place the last digit of this number in column 5.

b. FFQ (TE1) — Frequency of the excitation, cps. (TE1 is used for temporary storage.)

Use columns 6 through 17.

c. AXY or AXY1 (TE2) — The real or cosine component of the linear excitation in the simple gear set (AXY) or in the sun-planet mesh of the planetary gear stage (AXY1), in. This excitation is introduced at the gear mesh tangential to the pitch circles. (TE2 is used for temporary storage.)

Use columns 18 through 29.

d. BXY or BXY1 (TE3) — The imaginary or sine component of the linear excitation described above, in.

Use columns 30 through 41.

e. AXY2 (TE4) — The real or cosine component of the linear excitation in the planet-ring mesh of the planetary gear stage, in. This excitation is introduced at the gear mesh tangential to the pitch circles. On a card with excitation for a simple gear set, this field is left blank. (TE4 is used for temporary storage.)

Use columns 42 through 53.

f. BXY2 (TE5) — The imaginary or sine component of the linear excitation described just above, in.

Use columns 54 through 65.

Output Variables and Explanations

Tabulation of Input Data

Title - as in input card 1

Control numbers - NS, NB, NBR, NMPG, INP, NSRG, NPLG, as in input card 2.

Rotor material properties - GM, DENST, as in input card 3.

Rotor data - NSTA, RIP, RL, DST, DMS, DIN, CCOM, as in input card 4.

External constraint data - LB, BK, BCB, as in input card 5.

Simple gear set data-LS, RP, RG, SG, as in input card 6.

Planetary gear stage data - LEC, PN, RS, RW) all as in
IPL, PMS, PSP, PID, PRP, PCP) input
IPL, SS, SR, SW, Blank, ST) cards 7.

Branch data - LBR, LBS, as in input card 8.

Excitation data-IT,FFQ,AXY or AXYL, BXY or BXY1, AXY2, BXY2, as in input cards 9. Each set of excitation data is given separately followed by its own calculated response.

Calculated Data

Computed response at each simple gear set - LS, TTFR, TTFE

where: LS - Station number identifying the simple gear set.

TTFR - Real or cosine component of the dynamic tangential tooth force developed at the gear mesh, lb.

TTFE - Imaginary or sine component of the same force, lb.

Computed response at each planetary gear stage - LEC, C1, C2, C3, C4

where: LEC - Station number identifying the planetary gear stage.

C1 - Real component of the dynamic tangential tooth force developed at the sun-planet gear mesh, lb.

C2 - Imaginary component of the same force, lb.

C3 - Real components of the dynamic tangential tooth force developed at the planet-ring gear mesh, lb.

C4 - Imaginary component of the same force, lb.

Program Listing of Source Deck

This program was written in FORTRAN II - Extended and may be compiled with FORTRAN IV. It was developed on the IBM 1800 computer. In the source deck listing which follows, the READ and WRITE statements are written with the variable NR to specify the reading unit and with the variable NW to specify the writing unit. To recompile the program for the IBM 7090, introduce the required unit numbers by making the necessary changes on the cards as noted in the listing.

In addition to the controlling portion of this torsional response program, named TORRP, there are two subroutines. The first, named PLNST, treats the planetary stage. The second, named MATIN, performs the matrix inversion that solves the simultaneous equations of the PLNST subroutine.

Running time on IBM 1800 was approximately

4 minutes for a first case of 40 stations and one excitation

.7 minute additional for each similar case with new design data

.3 minute additional for each new excitation.

TORRP **Torsional Response Forces of System With Gears, Planetary Gears, and Branches**

```
      COMMON TBR(2,2),TBE(2,2),TPR(2,2),TPE(2,2),TFSPR(2,2),TFSPE(2,2),
     1 TFPRR(2,2),TFPRE(2,2),TTPCR(2,2),TTPCE(2,2),TTGRR(2,2),TTGRE(2,2)
      COMMON RIP(200),DST(200),DMS(200),DIN(200),BCB(50),LB(50),DDT(200)
     1,BK(50),LEC(2),RS(2),RW(2),PIP(2),PMS(2),PN(2),SS(2),SW(2),SR(2),
     2 ST(2),LBR(20),LBS(20),CCOM(200),AXY1,AXY2,BXY1,BXY2,TLR(200),
     3 TLE(200),THR(200),THE(200),TRR(200),TRE(200),TRR1(200)
      COMMON A(7,7),B(7,2),LS(20),RP(20),RG(20),SG(20),TRR2(200),
     1 TRE1(200),THE1(200),TLE1(200),TRE2(200),TTFR(20),TTFE(20),
     2 PSP(7),THR1(200),TLR1(200),THR2(200),TLR2(200),THE2(200),
     3 TLE2(200),RL(200),PCP(2),PRP(2)
      COMMON IT, K4,L4,MDIAG,FRQ2,ANGR,ANGE,TQR,TQE ,J,NS ,MI,NW,NR,NPLG
C CORRECTIONS PN336  11/67
C SET UP FOR EITHER IBM 1800 OR GE 635
C INITIALIZE NR AND NW FOR 1800
      NR=2
      NW=3
  200 READ(NR,100)
      READ(NR,101)NS,NB,NBR,NMPG,INP,NSRG,NPLG,MDIAG
C NPLG= NO. OF PLANETARY GEARS  (NPLG=0,1 OR 2)
C NSRG = NO. OF SINGLE REDUCTION GEARS (NSRG = 1 TO 10 )
      READ(NR,102)GM,DENST
      WRITE(NW,100)
      WRITE(NW,103)
      IF (MDIAG) 2021,2019,2021
 2019 WRITE (NW,106) NS,NB,NBR,NMPG,INP,NSRG,NPLG
      GO TO 2022
 2021 WRITE (NW,117)
      WRITE(NW,104)NS,NB,NBR,NMPG,INP,NSRG,NPLG,MDIAG
 2022 WRITE (NW,135) GM,DENST
      DENST=DENST/386.069
      WRITE(NW,107)
      DO 201 J=1,NS
CHANGE INPUT TO READ CONCENTRATED COMPLIANCE
      READ(NR,190)NSTA,RIP(J),RL(J),DST(J),DMS(J),DIN(J),CCOM(J)
CHECK STATION NUMBER
      IF(NSTA-J) 2000,2001,2000
 2000 WRITE(NW,191)
C PRINT OUT CONCENTRATED COMPLIANCE
 2001 WRITE(NW,108)NSTA,RIP(J),RL(J),DST(J),DMS(J),DIN(J),CCOM(J)
  201 RIP(J)=RIP(J)/386.069
      LB(1)=NS+2
      LEC(1)=NS+2
      LBR(1)=NS+2
      LBS(1)=NS+2
      LS(1) =NS+2
      IF(NB) 202,202,203
  203 WRITE(NW,109)
      DO 204 J=1,NB
      READ(NR,190)LB(J),BK(J),BCB(J)
```

```
  204 WRITE(NW,108)LB(J),BK(J),BCB(J)
  202 WRITE(NW,112)
      WRITE(NW,113)
      DO 205 I=1,NSRG
      READ(NR,190)LS(I),RP(I),RG(I),SG(I)
  205 WRITE(NW,108)LS(I),RP(I),RG(I),SG(I)
C TEST NO. OF PLANETARY GEARS
      IF(NPLG) 210,210,209
C I OR 2 PLANETARY GEARS
  209 WRITE(NW,114)
      DO 212 J=1,NPLG
      READ (NR,190) LEC(J),PN(J),RS(J),RW(J)
      WRITE(NW,127)
      WRITE (NW,108) LEC(J),PN(J),RS(J),RW(J)
      READ (NR,190) IPL,PMS(J),PSP(J),PIP(J),PRP(J),PCP(J)
      WRITE (NW,128)
      WRITE (NW,108) IPL,PMS(J),PSP(J),PIP(J),PRP(J),PCP(J)
      READ (NR,130) IPL,SS(J),SR(J),SW(J),ST(J)
      WRITE (NW,129)
      WRITE (NW,131) IPL,SS(J),SR(J),SW(J),ST(J)
      PSP(J) =PSP(J)/386.069
      PCP(J)=PCP(J)/386.069
      PRP(J)=PRP(J)/386.069
      PIP(J)=PIP(J)/386.069
  212 PMS(J)=PMS(J)/386.069
  210 IF(NBR) 213,213,214
  214 WRITE(NW,118)
      DO 215 J=1,NBR
      READ (NR,101) LBR(J),LBS(J)
  215 WRITE(NW,119) LBR(J),LBS(J)
  213 K5=NS-1
      DO 216 J=1,K5
      C1=RL(J)
      C2=DST(J)
      IF(C1) 217,216,217
  217 IF(C2) 218,216,218
  218 C5=DIN(J)*DIN(J)
      C4=C5*C5
      C6=DMS(J)*DMS(J)
      C8=0.09817477*(C2**4-C4)
      C3=C8*GM
      C4=0.09817477*DENST*(C6*C6-C4)
      DDT(J)=C1/C3
      DMS(J)=C1*SQRT (C4/C3)
      DIN(J)=SQRT(C3*C4)
  216 CONTINUE
C READ IN FREQUENCY, ONE AT A TIME
C SET UP FOR TOTAL NO. OF GEAR ERRORS
      DO 501 IERR =1,NMPG
C SET STORGES FOR GEAR ERRORS =0
      FFQ=0.0
      AXY=0.0
      BXY=0.0
      AXY1=0.0
      BXY1=0.0
      AXY2=0.0
      BXY2=0.0
C READ IN GEAR ERRORS
      READ(NR,190)IT,TE1,TE2,TE3,TE4,TE5
C TEST FOR S.R. GEAR
      DO 2011 I=1,NSRG
```

```
      IF(IT-LS(I)) 2011,2010,2011
C STORE VALUES FOR SR GEAR
 2010 AXY=TE2
      BXY=TE3
      WRITE(NW,194)
      WRITE(NW,108)IT,TE1,TE2,TE3
      GO TO 2020
 2011 CONTINUE
C TEST FOR PLAN. GEAR
      IF(NPLG) 2018,2018,2013
 2013 DO 2017 I=1,NPLG
      IF(IT-LEC(I)) 2017,2014,2017
 2014 WRITE(NW,195)
      AXY1=TE2
      BXY1=TE3
      AXY2=TE4
      BXY2=TE5
      WRITE(NW,108)IT,TE1,TE2,TE3,TE4,TE5
      GO TO 2020
 2017 CONTINUE
 2018 WRITE(NW,192)
      CALL EXIT
 2020 FFQ=TE1
C CORRECTIONS FOR FREQUENCY AT A TIME
      FRQ=6.2831853*FFQ
      IF(FRQ) 501,501,599
  599 FRQ2=FRQ*FRQ
      M1=1
  502 ANGR=0.0
      ANGE=0.0
      TQR=0.0
      TQE=0.0
      A13R=0.0
      A13E=0.0
      K1=1
      K2=1
      K4=1
      K5=NS+2
      L1=LBR(1)
      L2=LB(1)
C INITIALIZE FOR NO. OF SINGLE RED. GEARS
      NG=1
CORRECTION FOR MORE THAN I SR GEAR
      L3=LS(1)
C TO SET UP FOR NO PLANETARY GEARS , AFTER STATEMENT 502
      L4 =LEC(1)
      GO TO (227,228),M1
  227 ANGR=1.0
  228 DO 503 J=1,NS
      IF(J-L1) 231,230,231
  230 IF(M1-1) 232,232,234
  232 TL1R=TQR
      AL1R=ANGR
      TL1E=TQE
      AL1E=ANGE
  562 ANGR=1.0
      ANGE=0.0
      TQR=0.0
      TQE=0.0
      A13R=0.0
      A13E=0.0
```

```
      GO TO 235
  234 TL2R=TQR
      TL2E=TQE
      AL2R=ANGR
      AL2E=ANGE
  564 ANGR=0.
      ANGE=0.
      TQR=0.
      TQE=0.
      A13R=0.
      A13E=0.
  235 K5=LBS(K1)
      K6=L1
      K1=K1+1
      IF(NBR-K1) 237,236,236
  236 L1=LBR(K1)
      GO TO 249
  237 L1=NS+2
      GO TO 249
  231 IF(J-K5) 249,238,249
  238 IF(M1-1) 248,248,4[illegible]
C FIND AMPLITUDES
  248 AA1 =(ANGR*ANGR+ANGE*ANGE)
      AA2 = SQRT (AA1)
      AA5 =AL1R*ANGR +AL1E*ANGE
      AA3 =(AL1R*AL1R +AL1E*AL1E)
      AA4 = SQRT (AA3)
      IF (AA2-1.0E-7*AA4) 242,241,241
  241 AAR =AA5/AA1
      AAE = (ANGR*AL1E - ANGE*AL1R) /AA1
      TE1 = TQR
      TE2 = TL1R
      TE3 = TQE
      TE4 = TL1E
      ANGR= AL1R
      ANGE = AL1E
      K7=K6
      K8=K5-1
      GO TO 4000
  242 AAR = AA5/ AA3
      AAE = ( AL1R*ANGE - AL1E*ANGR) / AA3
      TE1 = TL1R
      TE2 = TQR
      TE3 =TL1E
      TE4 = TQE
      K7=1
      K8=K6-1
 4000 TQR = AAR* TE1 -AAE* TE3 +TE2
      TQE = AAE *TE1 + AAR*TE3 + TE4
  243 DO 244 L=K7,K8
      C1 = TLR(L)
      C2 = TLE(L)
      C3 = THR(L)
      C4 = THE(L)
      C5 = TRR(L)
      C6 = TRE(L)
      TLR(L) = AAR*C1-AAE*C2
      THR(L) = AAR*C3-AAE*C4
      TRR(L) = AAR*C5-AAE*C6
      TLE(L) = AAE*C1+ AAR* C2
      THE(L) = AAE*C3+ AAR* C4
```

```
  244 TRE(L) = AAE*C5+ AAR* C6
      GO TO 249
  421 TQR=TQR+TL2R
      TQE=TQE+TL2E
      ANGR=ANGR+AL2R
      ANGE=ANGE+AL2E
  249 THE(J)=ANGE
      TLE(J)=TQE
      THR(J)=ANGR
      TLR(J)=TQR
      IF(J-L2) 284,283,284
  283 C1=BK(K2)
      C2=BCB(K2)
      K2=K2+1
      IF(NB-K2) 261,260,260
  260 L2=LB(K2)
      GO TO 285
  261 L2=NS+2
      GO TO 285
  284 C1=0.0
      C2=0.0
  285 C1=C1-FRQ2*RIP(J)
      C2=FRQ*C2
      TQE=TQE+C1*ANGE  +C2*ANGR
      TRE(J)=TQE
      TQR=TQR+C1*ANGR -C2*ANGE
      TRR(J)=TQR
      IF(J-NS) 286,287,287
  287 IF(M1-1) 401,401,402
  286 IF(J-L3) 288,289,289
CHANGE TO SUBSCRIPT VARIABLES FOR MORE THAN ONE SR GEAR
  289 C1=RP(NG)
      C2=RG(NG)
      A11=-C1/C2
      A22=1.0/A11
      A21=0.0
      A12 = -SG(NG)
      NG=NG+1
      IF(N: NSRG) 1019,1019,1020
 1019 L3=LS(NG)
      GO TO 1021
 1020 L3=NS+2
 1021 IF (M1-1) 351,351,251
C TEST FOR EXCITATION
  251 IF(II-J) 351,290,351
C CORRECTION FOR LINEAR EXCITATION
  290 A13R=-AXY
      A13E=-BXY
      GO TO 351
  288 IF(J-L4) 255,254,255
  254 IF (MDIAG) 1092,1095,1095
 1092 IF (K4-1) 1095,1096,1095
 1096 IF (M1-1) 1093,1093,1094
 1093 WRITE (NW,181)
      GO TO 1095
 1094 WRITE (NW,182)
 1095 CALL PLNST
      GO TO 503
  255 C1=RL(J)
      IF(C1) 257,256,257
  256 A11=1.0
```

```
C CORRECTION FOR CONCENTRATED COMPLIANCE
      A12 =CCOM(J)
      A21=0.0
      A22=1.0
      GO TO 351
  257 C3=FRQ*DMS(J)
      IF(C3-0.0003) 258,258,259
  258 C4=C3*C3
      A11=1.0-0.5*C4
      A22=A11
      A12=DDT(J)
      A21=-C3*DIN(J) *FRQ
      GO TO 351
  259 A11=COS (C3)
      A22=A11
      C5=DIN(J)*FRQ
      C4=SIN (C3)
      A12=C4/C5
      A21=-C4*C5
  351 C1=ANGE
      ANGE=A11*ANGE+A12*TQE+A13 E
      TQE=A21*C1  +A22*TQE
      C1=ANGR
      ANGR=A11*ANGR+A12*TQR+A13R
      TQR=A21*C1  +A22*TQR
C RESET EXCITATION TO ZERO
      A13R=0.0
      A13E=0.0
  503 CONTINUE
  401 IF(MDIAG) 410,411,411
  410 IF (NPLG) 1090,1090,1091
 1090 WRITE(NW,181)
 1091 WRITE(NW,126)
  411 DO 403 J=1,NS
      TRR1(J)=TRR(J)
      THR1(J)=THR(J)
      TLR1(J)=TLR(J)
      TRE1(J)=TRE(J)
      THE1(J)=THE(J)
      TLE1(J)=TLE(J)
CHANGE FOR DIAGNOSTIC
      IF (MDIAG) 1030,403,403
 1030 WRITE(NW,108)J,THR1(J),THE1(J),TLR1(J),TLE1(J),TRR1(J),TRE1(J)
  403 CONTINUE
      MI=MI+1
      GO TO 502
  402 IF(MDIAG) 412,413,413
  412 IF(NPLG) 414,414,415
  414 WRITE(NW,182)
  415 WRITE(NW,126)
  413 DO 404 J=1,NS
      TLR2(J)=TLR(J)
      THE2(J)=THE(J)
      TLE2(J)=TLE(J)
      TRR2(J)=TRR(J)
      TRE2(J)=TRE(J)
      THR2(J)=THR(J)
      IF (MDIAG) 1040,404,404
 1040 WRITE(NW,108)J,THR2(J),THE2(J),TLR2(J),TLE2(J),TRR2(J),TRE2(J)
  404 CONTINUE
      C1=TRR2(NS)
```

```
      C2=TRE2(NS)
      C3=TRR1(NS)
      C4=TREI(NS)
      C5=C3*C3+C4*C4
      Q1R=-(C1*C3+C2*C4)/C5
      Q1E=(C1*C4-C2*C3)/C5
      WRITE(NW,120)FFQ
      IF(MDIAG) 1050,1051,1050
 1050 WRITE(NW,183)
      WRITE(NW,126)
C INITIALIZE FOR FIRST SINGLE REDUCTION GEAR SET
 1051 L=1
C CALCULATE       NTIAL TOOTH FORCE
C S1 RE TAN.  .L TOOTH FORCE, REAL AND IMAGINARY PARTS IN TTFR AND TTF
C        ARRAYS RESPECTIVELY
      DO 407 J=1,NS
      C1=THR1(J)*Q1R+THR2(J) -Q1E*THE1(J)
      C2=THR1(J)*Q1E+THE2(J)+Q1R*THE1(J)
      C3=TLR1(J)*Q1R+TLR2(J) -Q1E*TLE1(J)
      C4=TLR1(J)*Q1E+TLE2(J)+TLE1(J)*Q1R
      C5     =TRR1(J)*Q1R-Q1E*TRE1(J)+TRR2(J)
      C6     =TRR1(J)*Q1E+Q1R*TRE1(J)+TRE2(J)
      NGS =LS(L)
      IF(J-NGS) 1054,1100,1054
 1100 TTFR(L) =C5/RP(L)
      TTFE(L) =C6/RP(L)
      L =L+1
 1054 IF(MDIAG) 1055,407,1055
 1055 WRITE(3,108)J,C1,C2,C3,C4,C5,C6
  407 CONTINUE
      IF (NPLG) 1201,1201,1199
 1199 IF (MDIAG) 1057,1201,1057
 1057 WRITE (NW,120) FFQ
      DO 1200 J =1,NPLG
      C7 =PN(J) *RS(J)
      C8 =( RS(J) +  *RW(J))*PN(J)
      C1 =TBR(1,J)*Q1R+TBR(2,J)-Q1E*TBE(1,J)
      C2 =TBR(1,J)*Q1E+TBE(2,J)+Q1R*TBE(1,J)
      C3 =C7*(TFSPR(1,J)*Q1R+TFSPR(2,J)-Q1E*TFSPE(1,J))
      C4 =C7*(TFSPR(1,J)*Q1E+TFSPE(2,J)+Q1R*TFSPE(1,J))
      C5 =TTPCR(1,J)*Q1R+TTPCR(2,J)-Q1E*TTPCE(1,J)
      C6 =TTPCR(1,J)*Q1E+TTPCE(2,J)+Q1R*TTPCE(1,J)
      WRITE(NW,700)
      WRITE (NW,701) LEC(J),C1,C2,C3,C4,C5,C6
      C1 =TPR(1,J)*Q1R+TPR(2,J)-Q1E*TPE(1,J)
      C2 =TPR(1,J)*Q1E+TPE(2,J)+Q1R*TPE(1,J)
      C3 =C8*(TFPRR(1,J)*Q1R+TFPRR(2,J)-Q1E*TFPRE(1,J))
      C4 =C8*(TFPRR(1,J)*Q1E+TFPRE(2,J)+Q1R*TFPRE(1,J))
      C5 =TTGRR(1,J)*Q1R+TTGRR(2,J)-Q1E*TTGRE(1,J)
      C6 =TTGRR(1,J)*Q1E+TTGRE(2,J)+Q1R*TTGRE(1,J)
      WRITE(NW,702)
 1200 WRITE (NW,701) LEC(J),C1,C2,C3,C4,C5,C6
 1201 WRITE (NW,130)
      DO 1070 J=1,NSRG
 1070 WRITE (NW,108) LS(J),TTFR(J),TTFE(J)
      IF(NPLG) 501,501,1079
CALCULATE TANGENTIAL TOOTH FORCE FOR EACH PLANETARY GEAR SET
 1079 WRITE(NW,122)
      DO 1080 J=1,NPLG
      TE1=TFSPR(1,J)
      TE2=TFSPR(2,J)
```

```
      TE3=TFSPE(1,J)
      TE4=TFSPE(2,J)
C CALCULATE REAL PART TAN. TOOTH FORCE SUN-PLANET
      C1=TE1*Q1R+TE2-TE3*Q1E
CALCULATE IMAGINARY PART TAN. TOOTH FORCE SUN-PLANET
      C2=TE1*Q1E+TE4+TE3*Q1R
CALCULATE TANGENTIAL TOOTH FORCE PLANET-RING
      TE1=TFPRR(1,J)
      TE2=TFPRR(2,J)
      TE3=TFPRE(1,J)
      TE4=TFPRE(2,J)
CALCULATE REAL PART
      C3=TE1*Q1R+TE2-TE3*Q1E
CALCULATE IMAGINARY PART
      C4=TE1*Q1E+TE4+TE3*Q1R
 1080 WRITE(NW,108)LEC(J),C1,C2,C3,C4
  501 CONTINUE
      IF(INP) 506,200,506
  506 CALL EXIT
  100 FORMAT(72H1
     1                                    )
  101 FORMAT(8I5)
  102 FORMAT(5X,6E12.4)
  103 FORMAT(82H0 TORSIONAL RESPONSE OF THE SYSTEM WITH GEARS,EPICYCLIC
     1GEARS AND BRANCHES  PN03361
  104 FORMAT(I7,6X,I5,2X,6I10)
  105 FORMAT(8X,6E12.5)
  106 FORMAT(1H0,1X,8HSTATIONS,1X,12HBRG+EXT.CON.,2X,8HBRANCHES,1X,
     19HNO.OF FRQ,2X,8HINP SETS,2X,8HSR GEARS,2X,8HPL GEARS/
     2 I7,6X,I5,2X,5I10)
  107 FORMAT(/5X,10HROTOR DATA//4X,3HSTA,1X,12HM.MOM.INERT.,3X,
     16HLENGTH,4X,10HSTIFFN.DIA,3X,8HMASS DIA,3X,9HINNER DIA,2X,
     212HCONC. COMPL./4X3HNO.2X,9HLBS-IN**2,7X,2HIN,10X,2HIN,10X,2HIN,
     310X,2HIN,6X, 9HRAD/IN-LB)
  108 FORMAT(I7,1X,6F12.5)
  109 FORMAT(/1H1,7X,46HBEARING AND EXTERNAL TORSIONAL CONSTRAINT DATA//
     14X,3HSTA,3X,9HSTIFFNESS,4X,7HDAMPING/9X,10HLBS-IN/RAD,1X,
     213HLB-IN SEC/RAD)
  112 FORMAT(/1H1,9X,26HSINGLE REDUCTION GEAR DATA)
  113 FORMAT(/4X,3HSTA,3X,20HGEAR SET RADII (IN.),2X,
     1 31HCOMBINED TANGENTIAL COMPLIANCES//9X,10HFIRST GEAR,2X
     2 ,11HSECOND GEAR,3X,7H(IN/LB))
  114 FORMAT (/15X,18HPLANETARY SET DATA)
  117 FORMAT(1H0,1X,8HSTATIONS,1X,12HBRG+EXT.CON.,2X,8HBRANCHES,1X,
     19HNO.OF FRQ,2X,8HINP SETS,2X,8HSR GEARS,2X,8HPL GEARS,2X,5HMDIAG)
  118 FORMAT(9H0BRANCHES/30H  FIRST BRANCH  COMMON STATION)
  119 FORMAT(3XI5,11XI5)
  120 FORMAT (/1H1,5X,11HFREQUENCY ,E14.6,2X,3HCPS)
  121 FORMAT(/1H1)
  122 FORMAT(/ 8X,40HCOMPUTED RESPONSE AT PLANETARY GEAR SETS//
     1 10X,43HTANGENTIAL TOOTH FORCE AT EACH PLANET (LBS)/
     2 4X,3HSTA,8X,10HSUN-PLANET,13X,11HRING-PLANET/
     3 4X,3HNO.,5X,4HREAL,6X,9HIMAGINARY,5X,4HREAL,6X,9HIMAGINARY)
  126 FORMAT(/4X,3HSTA, 2X,10HANG.DISP-R,2X ,10HANG.DISP-I,2X,10HTORQUE
     1-R1,2X,10HTORQUE -I1,2X,10HTORQUE -R2,2X,10HTORQUE -I2/12X,4HRAD.,
     28X,4HRAD.,7X,6HIN-LBS,6X,6HIN-LBS,6X,6HIN-LBS,6X,6HIN-LBS)
  127 FORMAT(/4X,3HSTA,4X,6HNO. OF,8X,3HSUN,7X,6HPLANET/
     14X,3HNO.,3X,7HPLANETS,4X,10HRADIUS(IN),2X,10HRADIUS(IN))
  128 FORMAT(/4X,3HSTA,2X,10HWEIGHT(LB),4X,41HPOLAR MASS MOMENTS OF INER
     1TIA (LBS-IN**2)/ 4X,3HNO.,4X,6HPLANET,8X,3HSUN,7X,6HPLANET,7X,
     24HRING,7X,7HCARRIER)
```

```
129 FORMAT(/4X,3HSTA,6X,26HCOMPLIANCE- LINEAR(IN./LB),16X,
   1 15HCOM-ANG(RAD/LB)/ 4X,3HNO.,2X,10HSUN-PLANET,2X,11HPLANET-RING,
   2 1X,10HPLAN.-CAR.,14X,11HRING-GROUND)
130 FORMAT (I5,3E12.4,12X,E12.4)
131 FORMAT(I7,1X,3E12.4,12X,E12.4)
135 FORMAT(/9X,10HSHEAR MOD.,2X,11HWT. DENSITY/9X, 9HLBS/IN**2 ,3X,
   1 9HLBS/IN**3/8X,2E12.5)
180 FORMAT (/8X,36HCOMPUTED RESPONSE AT SIMPLE GEAR SET/
   1/4X,3HSTA,2X,28HTANGENTIAL TOOTH FORCE (LBS)/12X,4HREAL,6X,
   2 9HIMAGINARY)
181 FORMAT(12H0DIAGNOSTICS/5X,53HFIRST PASS- UNIT AMPLITUDE AT STATION
   1 1-NO EXCITATION)
182 FORMAT(12H0DIAGNOSTICS/5X,57HSECOND PASS- ZERO AMPLITUDE AT STATIO
   1N 1- WITH EXCITATION)
183 FORMAT(42H0OUTPUT- COMPUTED RESPONSE AT ALL STATIONS/
   110X,63H(TORQUE-1- GOING INTO STATION, TORQUE-2- COMING OUT OF STAT
   2ION))
190 FORMAT(I5,6E12.4)
191 FORMAT(38H0STATION NO. INCORRECT OR OUT OF ORDER)
192 FORMAT( 37H0STATION NO. FOR GEAR ERROR INCORRECT)
194 FORMAT(1H0,14X,46HSINGLE REDUCTION GEAR- LINEAR EXCITATION (IN.)/
   14X,3HSTA,2X,9HFREQUENCY,6X,4HREAL,6X,9HIMAGINARY)
195 FORMAT(1H0,14X,39HPLANETARY GEAR- LINEAR EXCITATION (IN.)/
   14X,3HSTA,2X,9HFREQUENCY,9X, 8HSUN GEAR,17X, 9HRING GEAR/
   224X,4HREAL,6X,9HIMAGINARY,5X,4HREAL,6X,9HIMAGINARY)
700 FORMAT(/4X,3HSTA,1X,24HANG. DISP.-PLANET CENTER,1X,
   1 22HTOT. TORQUE SUN-PLANET,2X,23HTOT TORQUE PLAN-CARRIER)
701 FORMAT( 4X,3HNO.,5X,4HREAL,6X,9HIMAGINARY,5X,4HREAL,6X,9HIMAGINARY
   15X,4HREAL,6X,9HIMAGINARY /I7,1X,6E12.5)
702 FORMAT(/ 4X,3HSTA,2X,22HANG. DISP.-PLANET BODY,2X,
   1 23HTOT. TORQUE PLANET-RING,2X,22HTOT. TORQUE GRND.-RING)
    END
```

Subroutine PLNST

```
      SUBROUTINE PLNST
      COMMON TBR(2,2),TBE(2,2),TPR(2,2),TPE(2,2),TFSPR(2,2),TFSPE(2,2),
     1 TFPRR(2,2),TFPRE(2,2),TTPCR(2,2),TTPCE(2,2),TTGRR(2,2),TTGRE(2,2)
      COMMON RIP(200),DST(200),DMS(200),DIN(200),BCB(50),LB(50),DDT(200)
     1,BK(50),LEC(2),RS(2),RW(2),PIP(2),PMS(2),PN(2),SS(2),SW(2),SR(2),
     2 ST(2),LBR(20),LBS(20),CCOM(200),AXY1,AXY2,BXY1,BXY2,TLR(200),
     3 TLE(200),THR(200),THE(200),TRR(200),TRE(200),TRR1(200)
      COMMON A(7,7),B(7,2),LS(20),RP(20),RG(20),SG(20),TRR2(200),
     1 TRE1(200),THE1(200),TLE1(200),TRE2(200),TTFR(20),TTFE(20),
     2 PSP(2),THR1(200),TLR1(200),THR2(200),TLR2(200),THE2(200),
     3 TLE2(200),RL(200),PCP(2),PRP(2)
      COMMON IT, K4,L4,MDIAG,FRQ2,ANGR,ANGE,TQR,TQE ,J,NS ,M1,NW,NR,NPLG
C SET UP SUBROUTINE FOR PLANETARY CASE
      C1=RS(K4)+RW(K4)
      C2=C1-RW(K4)
      FLNL=PN(K4)
      A(1,1)=RW(K4)
      A(1,2)=0.
      A(1,3)= FRQ2*PIP(K4)
      A(1,4)=0.
      A(1,5)=0.
      A(1,6)=0.
      A(1,7)=0.
      A(2,1)=1.0
      A(2,2)=-1.0
      A(2,3)=0.
      A(2,4)=-FRQ2*PMS(K4)*C1
      A(2,5)=0.
      A(2,6)=0.
      A(2,7)=0.
      A(3,1)=0.
      A(3,2)=C1
      A(3,3)=0.
      A(3,4)=0.
      A(3,5)=-1.0
      A(3,6)=0.
      A(3,7)=-FRQ2*PCP(K4)
      A(4,1)=C2
      A(4,2)=0.
      A(4,3)=0.
      A(4,4)=0.
      A(4,5)=0.
      A(4,6)=FRQ2*PRP(K4)*ST(K4)-1.0
      A(4,7)=0.
      A(5,1)=0.
      A(5,2)=SW(K4)
      A(5,3)=0.
      A(5,4)=C1
      A(5,5)=0.
```

```
      A(5,6)=0.
      A(5,7)=-(FLNL)*C1
      A(6,1)=0.
      A(6,2)=0.
      A(6,3)=-RW(K4)
      A(6,4)=-C1
      A(6,5)=0.
      A(6,6)=0.
      A(6,7)=0.
      A(7,1)=SR(K4)
      A(7,2)=0.
      A(7,3)= RW(K4)
      A(7,4) =-C1
      A(7,5)=0.
      A(7,6)=FLNL*C2*ST(K4)
      A(7,7)=0.
      C3 =PSP(K4)*FRQ2
      FSR=(TLR(J)-C3*THR(J))/RS(K4)
      FSI=(TLE(J)-C3*THE(J))/RS(K4)
      B(1,1)=RW(K4)*FSR
      B(1,2)=RW(K4)*FSI
      B(2,1)=-FSR
      B(2,2)=-FSI
      B(3,1)=0.
      B(3,2)=0.
      B(4,1)=0.
      B(4,2)=0.
      B(5,1)=0.
      B(5,2)=0.
      IF(M1-1) 440,440,441
  441 IF(L4-IT) 440,443,440
  440 EE1=0.
      EE2=0.
      EE3=0.
      EE4=0.
      GO TO 442
  443 EE1 =AXY1*FLNL
      EE2 =AXY2*FLNL
      EE3 =BXY1*FLNL
      EE4 =BXY2*FLNL
  442 B(6,1)=-RS(K4)*FLNL*THR(J)+EE1-SS(K4)*FSR
      B(6,2)=-RS(K4)*FLNL*THE(J)+EE2-SS(K4)*FSI
      B(7,1) =EE3
      B(7,2) =EE4
      CALL MATIN (A,7,B,2,CF9)
      TQR=B(5,1)
      EER=B(6,1)
      ANGR=B(7,1)
      TQE=B(5,2)
      EEI=B(6,2)
      ANGE=B(7,2)
C SAVE ALL VARIABLE SOLUTIONS, FIRST AND SECOND PASS
      TFPRR(M1,K4)=B(1,1)/FLNL
      TFPRE(M1,K4)=B(1,2)/FLNL
C TTPRR= TANGENTIAL TOOTH FORCE RING-PLANET
C TTRER= TANGENTIAL TOOTH FORCE RING-PLANET
      TTPCR(M1,K4)=C1*B(2,1)
      TTPCE(M1,K4)=C1*B(2,2)
C TTPCR= TOTAL TORQUE, PLANET-CARRIER, REAL
C TTPCE= TOTAL TORQUE, PLANET-CARRIER, IMAGINARY
      TPR(M1,K4)=B(3,1) /FLNL
```

```
      TPE(M1,K4)=B(3,2) /FLNL
C TPR= THETA-P-  ANGULAR DISPLACEMENT, PLANET-BODY - REAL
C TPE= THETA-P-  ANGULAR DISPLACEMENT, PLANET-BODY - IMAGINARY
      TBR(M1,K4)=B(4,1) /FLNL
      TBE(M1,K4)=B(4,2) /FLNL
C TBR= THETA-B - ANGULAR DISPLACEMENT, PLANET-CENTER, REAL
C TBE= THETA-B - ANGULAR DISPLACEMENT, PLANET-CENTER, IMAGINARY
      TTGRR(M1,K4)=EFR
      TTGRE(M1,K4)=EFI
C TTGRR= TOTAL TORQUE, GROUND-RING, REAL
C TTGRE= TOTAL TORQUE, GROUND-RING, IMAGINARY
      TFSPR(M1,K4)=FSR/FLNL
      TFSPE(M1,K4)=FSI/FLNL
C TTSPR= TOTAL TORQUE SUN-PLANET, REAL
C TTSPE= TOTAL TORQUE SUN-PLANET, IMAGINARY
CALCULATE TOTAL TORQUE SUN-PLANET - PLNST SUBROUTINE
      C3=RS(K4)*FSR
      C4=RS(K4)*FSI
CALCULATE TOTAL TORQUE PLANET-RING
      C5=C2*B(1,1)
      C6=C2*B(1,2)
C TEST DIAGNOSTIC
      IF(MDIAG) 600,608,608
C PRINT DIAGNOSTIC
C PRINT HEADING FOR DIAGNOSTICS
  600 IF(K4-1) 621,620,621
  620 WRITE(NW,703)
  621 WRITE(NW,700)
      WRITE(NW,701)L4,TBR(M1,K4),TBE(M1,K4),C3,C4,TTPCR(M1,K4),
     1 TTPCE(M1,K4)
      WRITE(NW,702)
      WRITE(NW,701)L4,TPR(M1,K4),TPE(M1,K4),C5,C6,TTGRR(M1,K4),
     1 TTGRE(M1,K4)
  608 K4=K4+1
      IF(K4-NPLG) 332,332,333
  332 L4=LEC(K4)
      RETURN
  333 L4=NS+2
      RETURN
  700 FORMAT(/4X,3HSTA,1X,24HANG. DISP.-PLANET CENTER,1X,
     1 22HTOT. TORQUE SUN-PLANET,2X,23HTOT TORQUE PLAN-CARRIER)
  701 FORMAT( 4X,3HNO.,5X,4HREAL,6X,9HIMAGINARY,5X,4HREAL,6X,9HIMAGINARY
     15X,4HREAL,6X,9HIMAGINARY /I7,1X,6E12.5)
  702 FORMAT(/ 4X,3HSTA,2X,22HANG. DISP.-PLANET BODY,2X,
     1 23HTOT. TORQUE PLANET-RING,2X,22HTOT. TORQUE GRND.-RING)
  703 FORMAT(/15X,              66HALL TORQUES GIVEN IN INCH-LB, AND ANGUL
     1AR DISPLACEMENTS IN RADIANS)
  705 FORMAT(12X,4HREAL,6X,9HIMAGINARY,5X,4HREAL,6X,9HIMAGINARY,5X,
     14HREAL,6X,9HIMAGINARY)
      END
```

Subroutine MATIN

```
C     MATRIX INVERSION WITH ACCOMPANYING SOLUTION OF LINEAR EQUATIONS   ANF40201
C                                                                       F4020002
      SUBROUTINE MATIN(A,N,B,M,DETER)
      DIMENSION IPIVO(7),A(7,7),B(7,2),INDEX(7,2),PIVOT(7)
      EQUIVALENCE (IROW,JROW), (ICOLU ,JCOLU ), (AMAX, T, SWAP)
C                                                                       F4020004
C                                                                       F4020008
C     INITIALIZATION                                                    F4020009
C                                                                       F4020010
   10 DETER =1.0                                                        F4020011
   15 DO 20 J=1,N                                                       F4020012
   20 IPIVO (J)=0                                                       F4020013
   30 DO 550 I=1,N                                                      F4020014
C                                                                       F4020015
C     SEARCH FOR PIVOT ELEMENT                                          F4020016
C                                                                       F4020017
   40 AMAX=0.0                                                          F4020018
   45 DO 105 J=1,N                                                      F4020019
   50 IF (IPIVO (J)-1) 60, 105, 60                                      F4020020
   60 DO 100 K=1,N                                                      F4020021
   70 IF (IPIVO (K)-1) 80, 100, 740                                     F4020022
   80 IF (ABS (AMAX)-ABS (A(J,K))) 85, 100, 100
   85 IROW=J                                                            F4020024
   90 ICOLU =K                                                          F4020025
   95 AMAX=A(J,K)                                                       F4020026
  100 CONTINUE                                                          F4020027
  105 CONTINUE                                                          F4020028
      IF(AMAX) 110,750,110
  110 IPIVO (ICOLU )=IPIVO (ICOLU )+1
C                                                                       F4020030
C     INTERCHANGE ROWS TO PUT PIVOT ELEMENT ON DIAGONAL                 F4020031
C                                                                       F4020032
  130 IF (IROW-ICOLU ) 140, 260, 140                                    F4020033
  140 DETER =-DETER                                                     F4020034
  150 DO 200 L=1,N                                                      F4020035
  160 SWAP=A(IROW,L)                                                    F4020036
  170 A(IROW,L)=A(ICOLU ,L)                                             F4020037
  200 A(ICOLU ,L)=SWAP                                                  F4020038
  205 IF(M) 260, 260, 210                                               F4020039
  210 DO 250 L=1, M                                                     F4020040
  220 SWAP=B(IROW,L)                                                    F4020041
  230 B(IROW,L)=B(ICOLU ,L)                                             F4020042
  250 B(ICOLU ,L)=SWAP                                                  F4020043
  260 INDEX(I,1)=IROW                                                   F4020044
  270 INDEX(I,2)=ICOLU                                                  F4020045
  310 PIVOT(I)=A(ICOLU ,ICOLU )                                         F4020046
  320 DETER =DETER *PIVOT(I)                                            F4020047
C                                                                       F4020048
C     DIVIDE PIVOT ROW BY PIVOT ELEMENT                                 F4020049
C                                                                       F4020050
  330 A(ICOLU ,ICOLU )=1.0                                              F4020051
```

```
  340 DO 350 L=1,N                                                      F4020052
  350 A(ICOLU ,L)=A(ICOLU ,L)/PIVOT(I)                                  F4020053
  355 IF(M) 380, 380, 360                                               F4020054
  360 DO 370 L=1,M                                                      F4020055
  370 B(ICOLU ,L)=B(ICOLU ,L)/PIVOT(I)                                  F4020056
C                                                                       F4020057
C     REDUCE NON-PIVOT ROWS                                             F4020058
C                                                                       F4020059
  380 DO 550 LI=1,N                                                     F4020060
  390 IF(LI-ICOLU ) 400, 550, 400                                       F4020061
  400 T=A(LI,ICOLU )                                                    F4020062
  420 A(LI,ICOLU )=0.0                                                  F4020063
      IF(T)430,550,430
  430 DO 450 L=1,N                                                      F4020064
  450 A(LI,L)=A(LI,L)-A(ICOLU ,L)*T                                     F4020065
  455 IF(M) 550, 550, 460                                               F4020066
  460 DO 500 L=1,M                                                      F4020067
  500 B(LI,L)=B(LI,L)-B(ICOLU ,L)*T                                     F4020068
  550 CONTINUE                                                          F4020069
C                                                                       F4020070
C     INTERCHANGE COLUMNS                                               F4020071
C                                                                       F4020072
  600 DO 710 I=1,N                                                      F4020073
  610 L=N+1-I                                                           F4020074
  620 IF (INDEX(L,1)-INDEX(L,2)) 630, 710, 630                          F4020075
  630 JROW=INDEX(L,1)                                                   F4020076
  640 JCOLU =INDEX(L,2)                                                 F4020077
  650 DO 705 K=1,N                                                      F4020078
  660 SWAP=A(K,JROW)                                                    F4020079
  670 A(K,JROW)=A(K,JCOLU )                                             F4020080
  700 A(K,JCOLU )=SWAP                                                  F4020081
  705 CONTINUE                                                          F4020082
  710 CONTINUE                                                          F4020083
  740 RETURN                                                            F4020084
  750 WRITE(1,760)
  760 FORMAT('MATRIX SINGULAR')
      STOP
      END
```

System Description of Sample Case

The torsional vibration system used in the sample case was taken from the UH-ID drive system. A schematic diagram of this system is given in Figure 76. Identification of the individual stations is given in the listing below. Data for these stations were scaled from a full-size assembly drawing or were taken from other information provided by the manufacturer.

Stations 1 - 4	Main system. These stations constitute the drive side of the spiral bevel pinion. The reflected inertia of the turbine and its gear drive has been included as a concentrated inertia at station 1. This simplification introduces no significant error for frequencies in the acoustic range. However, for lower frequencies, a more detailed system will be required.
Stations 5 - 8	First branch. These stations constitute the supported or the apex side of the spiral bevel pinion.
Station 9	Common station of first branch with main system; also, first member of simple gear set. This station is located at the bevel pinion center.
Stations 10 - 14	Second branch. These stations constitute the portion of the quill assembly below the main bevel gear.
Station 15	Common station of second branch with main system; also, second member of simple gear set. This station is located at the bevel gear center.
Stations 16 - 17	Main system. These stations constitute the portion of the quill assembly above the main bevel gear to the spline connecting the lower sun gear.
Station 18	Lower planetary stage. This station is located at the spline connection to the sun gear.
Station 19	Main system. This station starts at the spline end of the planet carrier.
Station 20	Upper planetary stage. This station is located at the spline connection to the sun gear.

Stations 21 - 24	Third branch. These stations constitute the lower portion of the mast assembly.
Station 25	Common station of third branch with main system. This station is located at the spline connection of the mast to the upper planet carrier.
Stations 26 - 39	Main system. These stations constitute the upper portion of the mast assembly. The rotor inertia has been applied at station 37.
Station 40	Terminal station of main system.

Input Listing of Sample Case

```
1 TEST EXAMPLE NO. 2      1-18-68
 40    0    3    1    1    1    2
     .1160000E08 .286
  1 .4827000E04 .1800000E01 .29      E01 .376     E01 .256     E01
  2 .47      E02 .167     E01 .315     E01 .315     E01 .2       E01
  3 .22      E03 .15      E01 .315     E01 .315     E01 .2       E01
  4 .0           .1005    E01 .36      E01 .360     E01 .2       E01
  5 .0           .44          .201     E01 .201     E01 .1       E01
  6 .86      E02 .65          .201     E01 .201     E01 .1       E01
  7 .0           .1       E01 .236     E01 .236     E01 .167     E01
  8 0.           .325         .360     E01 .36      E01 .2       E01
  9 .182     E02 .0           .0           .0           .0
 10 .0           .744         .47      E01 .47      E01 .395     E01
 11 .0           .693         .5154    E01 .5154    E01 .395     E01
 12 .4      E02 .45          .5154    E01 .5154    E01 .395     E01
 13 .0           .5396    E01 .434     E01 .434     E01 .395     E01
 14 .0           .155         .472     E01 .472     E01 .395     E01
 15 .274    E03 .2332    E01 .472     E01 .472     E01 .395     E01
 16 .134    E03 .1454    E01 .472     E01 .472     E01 .395     E01
 17 .0           .98          .429     E01 .429     E01 .395     E01
 18 0.0          .0           .0           .0           .0
 19 .0           .128     E01 .696     E01 .696     E01 .6       E01
 20 0.0          .0           .0           .0           .0
 21 .0           .1       E01 .35      E01 .35      E01 .312     E01
 22 .95     E02 .54          .35      E01 .35      E01 .312     E01
 23 .0           .1648    E02 .3375    E01 .3375    E01 .312     E01
 24 .0           .145     E01 .454     E01 .454     E01 .312     E01
 25 .386    E02 .115     E01 .454     E01 .454     E01 .312     E01
 26 .0           .156     E01 .422     E01 .422     E01 .312     E01
 27 .0           .5           .438     E01 .438     E01 .312     E01
 28 .76     E02 .5           .438     E01 .438     E01 .312     E01
 29 .0           .2           .476     E01 .476     E01 .312     E01
 30 .0           .149     E01 .404     E01 .404     E01 .312     E01
 31 .0           .1829    E02 .3555    E01 .3555    E01 .312     E01
 32 .0           .242     E01 .38      E01 .38      E01 .312     E01
 33 .0           .1374    E02 .3555    E01 .3555    E01 .312     E01
 34 .0           .251     E01 .38      E01 .38      E01 .312     E01
 35 .0           .1155    E02 .3555    E01 .3555    E01 .312     E01
 36 .0           .127     E01 .38      E01 .38      E01 .312     E01
 37 .1313   E08 .127     E01 .38      E01 .38      E01 .312     E01
 38 .0           .6275        .35      E01 .35      E01 .312     E01
 39 .0           .437         .35      E01 .35      E01 .312     E01
 40 .0           .1       E01 .0           .0           .0
  9 .2372   E01 .512     E01 .160156E-07 .0
 18 4.0          .336     E01 .182     E01
 18  .591   E01 .487     E02 .645     E01 .168     E02 .154     E02
 18  .85   E-07 .28     E-07 .62     E-06             .0
 20 8.0          .336     E01 .182     E01
 20  .459   E01 .7       E02 .645     E01 .244     E02 .17      E02
 20  .62   E-07 .22     E-07 .3      E-06
  5   9
 10  15
 21  25
  9  2800.          .4632813E-3 .0
```

Output Listing of Sample Case

TEST EXAMPLE NO. 2 1-18-68

TORSIONAL RESPONSE OF THE SYSTEM WITH GEARS,EPICYCLIC GEARS AND BRANCHES PN0336

STATIONS	BRG+EXT.CON.	BRANCHES	NO.OF FRQ	INP SETS	SR GEARS	PL GEARS
40	0	3	1	1	1	2

SHEAR MOD. LBS/IN**2	WT. DENSITY LBS/IN**3
0.11600E 08	0.28600E 00

ROTOR DATA

STA NO.	M.MOM.INERT. LBS-IN**2	LENGTH IN	STIFFN.DIA IN	MASS DIA IN	INNER DIA IN	CONC. COMPL. RAD/IN-LB
1	0.48270E 04	0.18000E 01	0.29000E 01	0.37600E 01	0.25600E 01	0.00000E 00
2	0.47000E 02	0.16700E 01	0.31500E 01	0.31500E 01	0.20000E 01	0.00000E 00
3	0.22000E 03	0.15000E 01	0.31500E 01	0.31500E 01	0.20000E 01	0.00000E 00
4	0.00000E 00	0.10050E 01	0.36000E 01	0.36000E 01	0.20000E 01	0.00000E 00
5	0.00000E 00	0.44000E 00	0.20100E 01	0.20100E 01	0.10000E 01	0.00000E 00
6	0.86000E 02	0.65000E 00	0.20100E 01	0.20100E 01	0.10000E 01	0.00000E 00
7	0.00000E 00	0.10000E 01	0.23600E 01	0.23600E 01	0.16700E 01	0.00000E 00
8	0.00000E 00	0.32500E 00	0.36000E 01	0.36000E 01	0.20000E 01	0.00000E 00
9	0.18200E 02	0.00000E 00	0.00000E 00	0.00000E 00	0.00000E 00	0.00000E 00
10	0.00000E 00	0.74400E 00	0.47000E 01	0.47000E 01	0.39500E 01	0.00000E 00
11	0.00000E 00	0.69300E 00	0.51540E 01	0.51540E 01	0.39500E 01	0.00000E 00
12	0.40000E 02	0.45000E 00	0.51540E 01	0.51540E 01	0.39500E 01	0.00000E 00
13	0.00000E 00	0.53960E 01	0.43400E 01	0.43400E 01	0.39500E 01	0.00000E 00
14	0.00000E 00	0.15500E 00	0.47200E 01	0.47200E 01	0.39500E 01	0.00000E 00
15	0.27400E 03	0.23320E 01	0.47200E 01	0.47200E 01	0.39500E 01	0.00000E 00
16	0.13400E 03	0.14540E 01	0.47200E 01	0.47200E 01	0.39500E 01	0.00000E 00
17	0.00000E 00	0.98000E 00	0.42900E 01	0.42900E 01	0.39500E 01	0.00000E 00
18	0.00000E 00	0.00000E 00	0.00000E 00	0.00000E 00	0.00000E 00	0.00000E 00
19	0.00000E 00	0.12800E 01	0.69600E 01	0.69600E 01	0.60000E 01	0.00000E 00
20	0.00000E 00	0.00000E 00	0.00000E 00	0.00000E 00	0.00000E 00	0.00000E 00
21	0.00000E 00	0.10000E 01	0.35000E 01	0.35000E 01	0.31200E 01	0.00000E 00
22	0.95000E 02	0.54000E 00	0.35000E 01	0.35000E 01	0.31200E 01	0.00000E 00
23	0.00000E 00	0.16480E 02	0.33750E 01	0.33750E 01	0.31200E 01	0.00000E 00
24	0.00000E 00	0.14500E 01	0.45400E 01	0.45400E 01	0.31200E 01	0.00000E 00
25	0.38600E 02	0.11500E 01	0.45400E 01	0.45400E 01	0.31200E 01	0.00000E 00
26	0.00000E 00	0.15600E 01	0.42200E 01	0.42200E 01	0.31200E 01	0.00000E 00
27	0.00000E 00	0.50000E 00	0.43800E 01	0.43800E 01	0.31200E 01	0.00000E 00
28	0.76000E 02	0.50000E 00	0.43800E 01	0.43800E 01	0.31200E 01	0.00000E 00
29	0.00000E 00	0.20000E 00	0.47600E 01	0.47600E 01	0.31200E 01	0.00000E 00
30	0.00000E 00	0.14900E 01	0.40400E 01	0.40400E 01	0.31200E 01	0.00000E 00
31	0.00000E 00	0.18290E 02	0.35550E 01	0.35550E 01	0.31200E 01	0.00000E 00
32	0.00000E 00	0.24200E 01	0.38000E 01	0.38000E 01	0.31200E 01	0.00000E 00
33	0.00000E 00	0.13740E 02	0.35550E 01	0.35550E 01	0.31200E 01	0.00000E 00
34	0.00000E 00	0.25100E 01	0.38000E 01	0.38000E 01	0.31200E 01	0.00000E 00
35	0.00000E 00	0.11550E 02	0.35550E 01	0.35550E 01	0.31200E 01	0.00000E 00
36	0.00000E 00	0.12700E 01	0.38000E 01	0.38000E 01	0.31200E 01	0.00000E 00
37	0.13130E 08	0.12700E 01	0.38000E 01	0.38000E 01	0.31200E 01	0.00000E 00
38	0.00000E 00	0.62750E 00	0.35000E 01	0.35000E 01	0.31200E 01	0.00000E 00
39	0.00000E 00	0.43700E 00	0.35000E 01	0.35000E 01	0.31200E 01	0.00000E 00
40	0.00000E 00	0.10000E 01	0.00000E 00	0.00000E 00	0.00000E 00	0.00000E 00

```
        SINGLE REDUCTION GEAR DATA

  STA   GEAR SET RADII (IN.)  COMBINED TANGENTIAL COMPLIANCES

        FIRST GEAR  SECOND GEAR   (IN/LB)
    9  0.23720E 01 0.51200E 01 0.16015E-07

            PLANETARY SET DATA

  STA    NO. OF        SUN        PLANET
  NO.   PLANETS    RADIUS(IN)  RADIUS(IN)
   18  0.40000E 01 0.33600E 01 0.18200E 01

  STA  WEIGHT(LB)     POLAR MASS MOMENTS OF INERTIA (LBS-IN**2)
  NO.    PLANET        SUN        PLANET       RING        CARRIER
   18  0.59100E 01 0.48780E 02 0.64500E 01 0.16800E 02 0.15400E 02

  STA      COMPLIANCE- LINEAR(IN./LB)                COM-ANG(RAD/LB)
  NO.  SUN-PLANET  PLANET-RING PLAN.-CAR.              RING-GROUND
   18   0.8500E-07  0.2800E-07  0.6200E-06              0.0000E 00

  STA    NO. OF        SUN        PLANET
  NO.   PLANETS    RADIUS(IN)  RADIUS(IN)
   20  0.80000E 01 0.33600E 01 0.18200E 01

  STA  WEIGHT(LB)     POLAR MASS MOMENTS OF INERTIA (LBS-IN**2)
  NO.    PLANET        SUN        PLANET       RING        CARRIER
   20  0.45900E 01 0.70000E 02 0.64500E 01 0.24400E 02 0.17000E 02

  STA      COMPLIANCE- LINEAR(IN./LB)                COM-ANG(RAD/LB)
  NO.  SUN-PLANET  PLANET-RING PLAN.-CAR.              RING-GROUND
   20   0.6200E-07  0.2200E-07  0.3000E-06              0.0000E 00

BRANCHES
 FIRST BRANCH  COMMON STATION
     5             9
    10            15
    21            25

          SINGLE REDUCTION GEAR- LINEAR EXCITATION (IN.)
  STA  FREQUENCY      REAL       IMAGINARY
    9  0.28000E 04 0.46328E-03 0.00000E 00
```

```
FREQUENCY =  0.280000E 04  CPS

   COMPUTED RESPONSE AT SIMPLE GEAR SET

STA  TANGENTIAL TOOTH FORCE (LBS)
        REAL       IMAGINARY
  9 -0.67609E 05 0.00000E 00

   COMPUTED RESPONSE AT PLANETARY GEAR SETS

      TANGENTIAL TOOTH FORCE AT EACH PLANET (LBS)
STA          SUN-PLANET                RING-PLANET
NO.      REAL       IMAGINARY      REAL       IMAGINARY
 13 -0.17161E 05 0.00000E 00-0.37611E 04 0.00000E 00
 20  0.11739E 05 0.00000E 00 0.82426E 04 0.00000E 00
// * ENDJOB
```

DESCRIPTION OF AUXILIARY COMPUTER PROGRAM

Input Variables, Format, and Instructions

Card 1 Title. Format (72H). This card precedes each set of input data.

a. Printing instructions, column 1.
For printer to skip a line, use 0.
For printer to go to the next sheet, use 1.

b. Title, columns 2 through 72.

Card 2 Control numbers. Format (15X, 2I5)

a. NF Total number of excitation cases.

Place the last digit of this number in column 20.

b. INT Identification as to whether this control card represents the last complete set of input data being submitted.
If more sets of input data follow, use 0.
If this is the last set, use 1.

Place this digit in column 25.

Card 3 Planetary geometry. Format (17X, 2E 12.4)
(Note: Card 7-A for the Main Program may be used.)

a. Blank Columns 1 through 5 are not read.

b. Blank Columns 6 through 17 are not read.

c. RS Pitch radius of the main sun gear, in.

Use columns 18 through 29.

d. RW Pitch radius of the planet gear, in.

Use columns 30 through 41.

Card 4 Planetary inertias. Format (5X, E 12.4, 12X, E 12.4)
(Note: Card 7-B for the Main Program may be used.)

a. Blank Columns 1 through 5 are not read.

b. PMS Weight of one planet gear, lb. This includes all components which rotate with the planet; everything between bearing surface and gear teeth. One-half the weight of any rolling elements in the bearing should be included.

Use columns 6 through 17.

c. Blank Columns 18 through 29 are not read.

d. PIP Moment of inertia of each planet gear, lb-in^2. This includes all components used in computing the weight, PMS.

Use columns 30 through 41.

Card 5 Planetary compliances. Format (5X, 2E12.4, 12X, E12.4)
(Note: Card 7-C for the Main Program may be used with the addition of item e.)

a. Blank Columns 1 through 5 are not read.

b. SS Combined linear compliance of each sun-planet gear mesh, tangential to its pitch circle; in.-lb. (See discussion under this item in card 7-C for the Main Program.)

Use columns 6 through 17.

c. SR Combined linear compliance of each planet-ring gear mesh, tangential to its pitch circle, in.-lb.

Use columns 18 through 29.

d. Blank Columns 30 through 41 are not read.

e. SQ Linear compliance of the local planet support in the planet carrier, tangential to the path of planet centers, in.-lb. This compliance is the combination of the compliance of the planet bearing and the compliance of any portion of the carrier which will deflect with a load on its individual planet. Excluded are the compliances of any part of the carrier which rigidly ties one planet support to another. Hence, if the carrier construction is such that there is a compliance between a hub and a rim-type member which supports all the planets collectively, this structural compliance may not be combined with the others.

Use columns 42 through 53.

Cards 6-1 to 6-NF Gear excitation data. Format (5X, 5E 12.4)
(Note: Cards 9 for the Main Program may be used.)

a. Blank Columns 1 through 5 are not read.

b. FRQ Frequency of the excitation, cps.

Use columns 6 through 17.

c. DSR The real or cosine component of the linear excitation in the sun-planet gear mesh tangential to the pitch circles, in.

Use columns 18 through 29.

d. DSE The imaginary or sine component of the linear excitation described above, in.

Use columns 30 through 41.

e. DRR The real or cosine component of the linear excitation in the planet-ring gear mesh tangential to the pitch circles, in.

Use columns 42 through 53.

f. DRE The imaginary or sine component of the linear excitation described just above, in.

Use columns 54 through 65.

Output Variables and Explanations

Input Data

Same as in input cards 1 to 6.

Calculated Data

Computed response forces for each planet - FSR, FSE, FRR, FRE, FCR, FCE

where: FSR and FSE - Real and imaginary components of tangential tooth force at the sun-planet mesh, lb.

FRR and FRE - Real and imaginary components of tangential tooth force at the planet-ring mesh, lb.

FCR and FCE - Real and imaginary components of tangential tooth force at the planet-carrier bearing, lb.

Computed response displacements for each planet - DPR, DPE, DBR, DBE

where: DPR and DPE - Real and imaginary components of angular displacement of planet about its own center relative to ground, rad.

DBR and DBE - Real and imaginary components of displacement of planet center, expressed as angular displacement about the planetary drive center, rad.

Program Listing of Source Deck

This program was written in FORTRAN II - Extended and may be compiled with FORTRAN IV. It was developed on the IBM 1800 computer. In the source deck listing which follows, the READ and WRITE statements are written with the variable NR to specify the reading unit and with the variable NW to specify the writing unit. To recompile the program for the IBM 7090, introduce the required unit numbers by making the necessary changes on the cards as noted in the listing.

In addition to the controlling portion of this planetary stage response program, named CHECK, there is one subroutine. This is MATIN which performs the matrix inversion that solves the simultaneous equations of the controlling program.

Running time on IBM 1800 was approximately

2.5 minutes for a first case with one excitation

.7 minute for each additional case with new planetary data

.2 minute for each additional excitation.

CHECK - Response Forces in Planetary Gear Stage.

```
      DIMENSION AA(5,5),A(5,5),B(5,2),BB(5,2)
C PN336A  REVISED 12-67
C REQUIRES SUBROUTINE MATIN -  A MATRIX (5,5)  ,- B MATRIX - (5,2)
C INITIALIZE READ UNIT AND PRINTER UNIT NOS. FOR IBM 1800
      NR=2
      NW=3
  203 READ(NR,101)
      READ(NR,102)NF,INT
C NF INDICATES TOTAL NO. OF FREQUENCIES
C INT =0, INDICATES THERE ARE MORE INPUT SETS
C INT= AN INTEGER OTHER THAN ZERO, INDICATES THERE ARE NO MORE INPUT SETS
      READ(NR,103)RS,RW
C RS= RADIUS OF SUN GEAR(INCHES)
C RW= RADIUS OF PLANET GEAR(INCHES)
      READ(NR,111)PMS,PIP
C PMS= WEIGHT OF ONE PLANET GEAR(LBS)
C PIP= POLAR MASS MOMENT OF INERTIA OF ONE PLANET GEAR(LBS-IN**2)
      READ(NR,112)SS,SR,SQ
C SR= LINEAR COMPLIANCE OF PLANET-RING(IN./LB)
C SS= LINEAR COMPLIANCE OF SUN-PLANET(IN./LB)
C SQ= LINEAR COMPLIANCE OF TOTAL CARRIER(IN./LB)
      WRITE(NW,101)
      WRITE(NW,109)NF,INT
      WRITE(NW,104)RS,RW
      WRITE(NW,113)PMS,PIP
      WRITE(NW,114)SS,SR,SQ
      RC=RS+RW
      RR=RC+RW
C RC= RADIUS OF CARRIER(IN.)
C RR= RADIUS OF RING(IN.)
      PMS=PMS/386.069
      PIP=PIP/386.069
      DO 206 I=1,5
      DO 206 K=1,5
  206 AA(I,K)=0.
      AA(1,1)=RW
      AA(1,2)=-RW
      AA(2,1)=1.
      AA(2,2)=1.
      AA(2,3)=-1.
      AA(3,3)=-SQ
      AA(3,5)=RC
      AA(4,1)=SS
      AA(4,4)=RW
      AA(4,5)=RC
      AA(5,2)=SR
      AA(5,4)=-RW
      AA(5,5)=RC
      DO 215 J=1,3
```

```
      BB(J,1)=0.
  215 BB(J,2)=0.
      MF=1
  222 READ(NR,115)FRQ,DSR,DSE,DRR,DRE
C FRQ= FREQUENCY FOR EXCITATION
C DSR= LINEAR EXCITATION  SUN GEAR,  REAL PART(IN.)
C DSE= LINEAR EXCITATION  SUN GEAR,  IMAGINARY PART.IN.)
C DRR= LINEAR EXCITATION RING GEAR,  REAL PART(IN.,
C DRE= LINEAR EXCITATION RING GEAR,  IMAGINARY PART(IN.)
      WRITE(NW,116)FRQ,DSR,DSE,DRR,DRE
C CORRECTION TO CHANGE TO LINEAR EXCITATION
      BB(4,1)=DSR
      BB(4,2)=DSE
      BB(5,1)=DRR
      BB(5,2) =DRE
      C1=FRQ*6.2831853
      FRE2=C1*C1
      DO 212 J=1,5
      DO 212 L=1,5
  212 A(J,L)=AA(J,L)
      A(1,4)=PIP*FRE2
      A(2,5)=PMS*RC*FRE2
      DO 213 J=1,5
      DO 213 L=1,2
  213 B(J,L)=BB(J,L)
      CALL MATIN(A,5,B,2,CF9)
      FSR=B(1,1)
      FRR=B(2,1)
      FCR=B(3,1)
      DPR=B(4,1)
      DBR=B(5,1)
      FSE=B(1,2)
      FRE=B(2,2)
      FCE=B(3,2)
      DPE=B(4,2)
      DBE=B(5,2)
      WRITE(NW,117)FSR,FSE,FRR,FRE,FCR,FCE
      WRITE(NW,118)DPR,DPE,DBR,DBE
      IF(NF-MF) 220,220,221
  221 MF=MF+1
      WRITE (NW,110)
      GO TO 222
  220 IF (INT) 201,203,201
  201 CALL EXIT
  101 FORMAT(/2H1
     1                    )
  102 FORMAT(15X,2I5)
  103 FORMAT(17X,2E12.4)
  104 FORMAT(/10X,18HPLANETARY SET DATA/
     125X,3HSUN,7X,6HPLANET/ 21X,10HRADIUS(IN),2X,10HRADIUS(IN)/
     210X,2E12.5)
  109 FORMAT(/10X,25HTOTAL NO. OF FREQUENCIES=,I10/
     1 10X,25HINDICATOR FOR INPUT SETS=,I10)
  110 FORMAT(/1H1)
  111 FORMAT(5X,E12.4,12X,E12.4)
  112 FORMAT(5X,2E12.4,12X,E12.4)
  113 FORMAT (/ 9X,10HWEIGHT(LB),2X,40HPOLAR MASS MOMENT OF INERTIA (LBS
     1-IN**2)/ 11X,6HPLANET,18X,6HPLANET/ 8X,E12.5,12X,E12.5)
  114 FORMAT(/13X,26HCOMPLIANCE- LINEAR(IN./LB)/
     19X,10HSUN-PLANET,2X,11HPLANET-RING,12X,13HLOCAL PL-CAR./
     28X,2E12.5,12X,E12.5)
```

```
115 FORMAT(5X,5E12.4)
116 FORMAT(/10X,9HFREQUENCY,2X,23HLINEAR EXCITATION (IN.)/
   122X, 8HSUN GEAR,4X,9HRING GEAR/ 8X,5E12.5)
117 FORMAT(/8X,7HOUTPUT-,5X,35HTOTAL TANGENTIAL TOOTH FORCES (LBS)//
    114X,12HSUN- PLANETS,12X,13HRING- PLANETS,9X,16HCARRIER- PLANETS/
    212X,4HREAL,6X,9HIMAGINARY,5X,4HREAL,6X,9HIMAGINARY,5X,4HREAL,
    36X,9HIMAGINARY/8X,6E12.5)
118 FORMAT (/13X,37HTOTAL ANGULAR DISPLACEMENTS (RADIANS)/
    I 14X,13HPLANETS- BODY,10X,15HPLANETS- CENTER/
    212X,4HREAL,6X,9HIMAGINARY,5X,4HREAL,6X,9HIMAGINARY/
    38X,4E12.5)
     END
```

Subroutine MATIN

```
C     MATRIX INVERSION WITH ACCOMPANYING SOLUTION OF LINEAR EQUATIONS   ANF40201
C                                                                       F4020002
      SUBROUTINE MATIN(A,N,B,M,DETER)
      DIMENSION IPIVO(5),A(5,5),B(5,2),INDEX(5,2),PIVOT(5)
      EQUIVALENCE (IROW,JROW), (ICOLU ,JCOLU ), (AMAX, T, SWAP)
C                                                                       F4020004
C                                                                       F4020008
C     INITIALIZATION                                                    F4020009
C                                                                       F4020010
   10 DETER =1.0                                                        F4020011
   15 DO 20 J=1,N                                                       F4020012
   20 IPIVO (J)=0                                                       F4020013
   30 DO 550 I=1,N                                                      F4020014
C                                                                       F4020015
C     SEARCH FOR PIVOT ELEMENT                                          F4020016
C                                                                       F4020017
   40 AMAX=0.0                                                          F4020018
   45 DO 105 J=1,N                                                      F4020019
   50 IF (IPIVO (J)-1) 60, 105, 60                                      F4020020
   60 DO 100 K=1,N                                                      F4020021
   70 IF (IPIVO (K)-1) 80, 100, 740                                     F4020022
   80 IF (ABS (AMAX)-ABS (A(J,K))) 85, 100, 100
   85 IROW=J                                                            F4020024
   90 ICOLU =K                                                          F4020025
   95 AMAX=A(J,K)                                                       F4020026
  100 CONTINUE                                                          F4020027
  105 CONTINUE                                                          F4020028
      IF(AMAX) 110,750,110
  110 IPIVO (ICOLU )=IPIVO (ICOLU )+1
C                                                                       F4020030
C     INTERCHANGE ROWS TO PUT PIVOT ELEMENT ON DIAGONAL                 F4020031
C                                                                       F4020032
  130 IF (IROW-ICOLU ) 140, 260, 140                                    F4020033
  140 DETER =-DETER                                                     F4020034
  150 DO 200 L=1,N                                                      F4020035
  160 SWAP=A(IROW,L)                                                    F4020036
  170 A(IROW,L)=A(ICOLU ,L)                                             F4020037
  200 A(ICOLU ,L)=SWAP                                                  F4020038
  205 IF(M) 260, 260, 210                                               F4020039
  210 DO 250 L=1, M                                                     F4020040
  220 SWAP=B(IROW,L)                                                    F4020041
  230 B(IROW,L)=B(ICOLU ,L)                                             F4020042
  250 B(ICOLU ,L)=SWAP                                                  F4020043
  260 INDEX(I,1)=IROW                                                   F4020044
  270 INDEX(I,2)=ICOLU                                                  F4020045
  310 PIVOT(I)=A(ICOLU ,ICOLU )                                         F4020046
  320 DETER =DETER *PIVOT(I)                                            F4020047
C                                                                       F4020048
C     DIVIDE PIVOT ROW BY PIVOT ELEMENT                                 F4020049
C                                                                       F4020050
  330 A(ICOLU ,ICOLU )=1.0                                              F4020051
```

```
  340 DO 350 L=1,N                                                      F4020052
  350 A(ICOLU ,L)=A(ICOLU ,L)/PIVOT(I)                                  F4020053
  355 IF(M) 380, 380, 360                                               F4020054
  360 DO 370 L=1,M                                                      F4020055
  370 B(ICOLU ,L)=B(ICOLU ,L)/PIVOT(I)                                  F4020056
C                                                                       F4020057
C     REDUCE NON-PIVOT ROWS                                             F4020058
C                                                                       F4020059
  380 DO 550 L1=1,N                                                     F4020060
  390 IF(L1-ICOLU ) 400, 550, 400                                       F4020061
  400 T=A(L1,ICOLU )                                                    F4020062
  420 A(L1,ICOLU )=0.0                                                  F4020063
      IF(T)430,550,430
  430 DO 450 L=1,N                                                      F4020064
  450 A(L1,L)=A(L1,L)-A(ICOLU ,L)*T                                     F4020065
  455 IF(M) 550, 550, 460                                               F4020066
  460 DO 500 L=1,M                                                      F4020067
  500 B(L1,L)=B(L1,L)-B(ICOLU ,L)*T                                     F4020068
  550 CONTINUE                                                          F4020069
C                                                                       F4020070
C     INTERCHANGE COLUMNS                                               F4020071
C                                                                       F4020072
  600 DO 710 I=1,N                                                      F4020073
  610 L=N+1-I                                                           F4020074
  620 IF (INDEX(L,1)-INDEX(L,2)) 630, 710, 630                          F4020075
  630 JROW=INDEX(L,1)                                                   F4020076
  640 JCOLU =INDEX(L,2)                                                 F4020077
  650 DO 705 K=1,N                                                      F4020078
  660 SWAP=A(K,JROW)                                                    F4020079
  670 A(K,JROW)=A(K,JCOLU )                                             F4020080
  700 A(K,JCOLU )=SWAP                                                  F4020081
  705 CONTINUE                                                          F4020082
  710 CONTINUE                                                          F4020083
  740 RETURN                                                            F4020084
  750 WRITE(1,760)
  760 FORMAT('MATRIX SINGULAR')
      STOP
      END
```

Input Listing of Sample Case

```
1 FORCES ON UPPER PLANET OPERATING ERRORS- SPIDER COMPLIANCE STUDY
                    3    1
                   3.36          1.82
      6.45                       4.59
      2.08    E-7 1.54    E-7              6.0     E-8
      644.0       -.000016      +.000049    -.000022     +.000004
     1288.0       +.000019      -.000018    +.000007     +.000004
     1932.0       -.000017      -.000001    +.000006     -.000004
```

Output Listing of Sample Case

```
FORCES ON UPPER PLANET OPERATING ERRORS- SPIDER COMPLIANCE STUDY

      TOTAL NO. OF FREQUENCIES=          3
      INDICATOR FOR INPUT SETS=          1

      PLANETARY SET DATA
                     SUN        PLANET
                RADIUS(IN)  RADIUS(IN)
                0.33600E 01 0.18200E 01

     WEIGHT(LB)  POLAR MASS MOMENT OF INERTIA (LBS-IN**2)
       PLANET                    PLANET
     0.64500E 01               0.45900E 01

         COMPLIANCE- LINEAR(IN./LB)
     SUN-PLANET  PLANET-RING              LOCAL PL-CAR.
     0.20800E-06 0.15400E-06               0.60000E-07

      FREQUENCY  LINEAR EXCITATION (IN.)
                  SUN GEAR    RING GEAR
     0.64400E 03-0.16000E-04 0.49000E-04-0.22000E-04 0.[illegible]E-05

    OUTPUT-      TOTAL TANGENTIAL TOOTH FORCES (LBS)

         SUN- PLANETS              RING- PLANETS          CARRIER- PLANETS
       REAL       IMAGINARY      REAL       IMAGINARY      REAL       IMAGINARY
    -0.62832E 02 0.86916E 02-0.62554E 02 0.88105E 02-0.12747E 03 0.17794E 03

         TOTAL ANGULAR DISPLACEMENTS (RADIANS)
          PLANETS- BODY            PLANETS- CENTER
       REAL       IMAGINARY      REAL       IMAGINARY
    0.25922E-05 0.11123E-04-0.14765E-05 0.20611E-05
```

```
FREQUENCY  LINEAR EXCITATION (IN.)
                SUN GEAR     RING GEAR
0.12880E 04 0.19000E-04-0.18000E-04 0.70000E-05 0.40000E-05

OUTPUT-     TOTAL TANGENTIAL TOOTH FORCES (LBS)

      SUN- PLANETS                RING- PLANETS            CARRIER- PLANETS
    REAL       IMAGINARY       REAL       IMAGINARY       REAL       IMAGINARY
0.41479E 02-0.21483E 02 0.42647E 02-0.23978E 02 0.90038E 02-0.48656E 02

     TOTAL ANGULAR DISPLACEMENTS (RADIANS)
      PLANETS- BODY              PLANETS- CENTER
    REAL       IMAGINARY       REAL       IMAGINARY
0.27307E-05-0.58307E-05 0.10429E-05-0.56358E-06
```

```
        FREQUENCY  LINEAR EXCITATION (IN.)
                    SUN GEAR     RING GEAR
      0.19320E 04-0.17000E-04-0.10000E-05 0.60000E-05-0.40000E-05

      OUTPUT-      TOTAL TANGENTIAL TOOTH FORCES (LBS)

           SUN- PLANETS              RING- PLANETS          CARRIER- PLANETS
         REAL       IMAGINARY      REAL       IMAGINARY     REAL       IMAGINARY
      -0.14284E 02-0.82036E 01-0.20412E 02-0.72544E 01-0.40710E 02-0.18137E 02

           TOTAL ANGULAR DISPLACEMENTS (RADIANS)
            PLANETS- BODY            PLANETS- CENTER
         REAL       IMAGINARY      REAL       IMAGINARY
      -0.63660E-05 0.98603E-06-0.47155E-06-0.21008E-06
// * ENDJOB
```

APPENDIX VI
PREDICTED NOISE LEVEL ANALYSIS

INTRODUCTION

The noise in the immediate environment of an enclosed gear system has its origin in the dynamic forces which are acting on the internal components. The actual mechanism by which these forces lead to the noise is very complex. It includes the transmission of the forces through the rotating elements, through the bearings, and into the casing which encloses the system. In the course of this transmission, the forces are subject to amplification or attenuation, according to the dynamic response of all the components forming the many simultaneous paths used. The casing itself responds to the forces applied at different points by vibrating in many modes, each different in amplitude and phase relationship. The means of support of the casing undoubtedly contributes to the variety of influences at work. Sound waves radiated by each vibrating portion of the casing reinforce and interfere with each other, according to their phase relationship and wave lengths, and the geometry of the casing. Noise levels in the immediate environment of the gearbox are directly influenced by all these variables. The shear complexity of the many mechanical and acoustical effects prohibits any detailed analysis which will relate noise levels around an actual gearbox to the vibration forces developed inside the box.

Any analysis useful for predicting noise levels will have to be, at least in part, based on empirical considerations. The analysis to be described is of this semi-empirical character. The empirical element results from one underlying assumption whose validity is substantiated only by the effectiveness of the analysis in predicting results later obtained by measurement. In one such case, an analysis using the same assumption has been shown to give confirmed results when applied to a marine gear application (Reference 5). The application of the analysis developed below to the helicopter gearbox in this study has also developed reasonable correlation with measured results (see Figure 40).

DESCRIPTION OF ANALYSIS AND CALCULATED RESULTS

Each sinusoidal excitation introduced into a power transmission system will develop a response force at the point of application. The force will also be sinusoidal and of the same frequency as the excitation. This excitation and force together represent mechanical energy being taken from the drive power and introduced into the system, also on a sinusoidal time basis (but double in frequency). When there is damping in the system, there is a net transfer of some energy to the points of damping where it is dissipated. The remainder of this energy is not dissipated but is simply returned to the drive, all within the time span of each of the sinusoidal cycles. The basis of the analysis that follows is the assumption that some small but predictable fraction of each pulse of this circulating or cycled mechanical energy is radiated from the housing of the gearbox in the form of acoustic energy. Furthermore, if the geometry of the radiating housing surfaces and the acoustic chamber enclosing it is known, the levels of sound pressure developed by this acoustic power can also be determined.

Let the excitation be expressed as

$$e = e_o \sin\omega t \tag{230}$$

where e_o = peak value of excitation

ω = angular frequency = $2\pi f$

t = time.

Then the response force will be

$$F = F_o \sin(\omega t + \theta) \tag{231}$$

where F_o = peak value of the response force, and θ = phase relationship of force relative to excitation.

The instantaneous work done or mechanical energy introduced by the excitation and force is

$$E_M = \int F de \tag{232}$$

Since the instantaneous excitation is a function of time,

$$de = \frac{\partial e}{\partial t} dt \tag{233}$$

From Equation (230),

$$de = \omega e_o \cos\omega t \, dt \tag{234}$$

When Equations (231) and (234) are substituted into Equation (232),

$$E_M = \omega e_o F_o \int \cos\omega t \cdot \sin(\omega t + \theta) dt \tag{235}$$

The integral is evaluated as follows:

$$\begin{aligned}
\int \cos\omega t \cdot \sin(\omega t + \theta) dt &= \int \cos\omega t [\sin\omega t \cdot \cos\theta + \cos\omega t \cdot \sin\theta] dt \\
&= \int [\sin\omega t \cos\omega t \cdot \cos\theta + \cos^2\omega t \cdot \sin\theta] dt \\
&= \int [\frac{\sin 2\omega t \cdot \cos\theta}{2} + \frac{(\cos 2\omega t + 1)\sin\theta}{2}] dt \\
&= \int [\frac{\sin(2\omega t + \theta) + \sin\theta}{2}] dt \\
&= -\frac{\cos(2\omega t + \theta)}{4\omega} + \frac{t \sin\theta}{2}
\end{aligned}$$

Equation (235) now becomes

$$E_M = -\left(\frac{e_o F_o}{4}\right) \cos(2\omega t + \theta) + \left(\frac{e_o F_o}{4}\right) 2\omega t \cdot \sin\theta \tag{236}$$

The second item on the right-hand side represents the energy transmitted to the dampers and dissipated there. When there is no damping in the system, the phase relationship θ will be 0° or 180°. In either case, this dissipated energy term is zero.

The first term represents the circulated or cycled mechanical energy, which, as noted above, proves to be sinusoidal with respect to time and with a frequency twice that of the excitation. The peak value of this energy is expressed by the coefficient of the cosine term, in which the significance of the minus sign is related to phase relationship.

$$E_{Mo} = \frac{e_o F_o}{4} \tag{237}$$

A fraction of this energy for each of its cycles is converted into acoustic energy.

$$E_A = \alpha E_{Mo}$$

$$E_A = \frac{\alpha e_o F_o}{4} \tag{238}$$

where E_A = acoustic energy released per cycle, and α = fraction of mechanical energy converted into acoustic energy.

To convert the acoustic energy term into acoustic power, the time duration of one energy cycle is introduced.

$$T_E = \frac{1}{f_E} = \frac{1}{2f} \tag{239}$$

where T_E = period of the energy cycle, f_E = frequency of the energy cycle, and f = frequency of the original excitation.

The acoustic power is taken as the rate of acoustic energy release as averaged over one energy cycle, and it may be written as

$$P_A = \frac{E_A}{T_E} = \frac{\alpha e_o F_o \cdot 2f}{4}$$

$$P_A = \frac{\alpha f e_o F_o}{2} \tag{240}$$

This power is the direct result of the excitation and response force at one point in the system. Where there is more than one excitation at the same

frequency, the acoustic power generated is taken as the sum of the individual contributors.

$$P_A = \frac{\alpha f}{2} \Sigma e_o F_o \tag{241}$$

This equation may be adapted to convenient units.

$$P_A = .565 \times 10^{-7} \alpha f \Sigma e_o F_o \tag{242}$$

where P_A = acoustic power, w

α = fraction of energy conversion

f = frequency of excitation, cps

e_o = peak of each sinusoidal excitation at the same frequency, μ in.

F_o = peak of the response force at each of the excitations, lb

To find the sound pressure level at the excitation frequency, the factor of housing geometry and the acoustic properties of the chamber enclosing the gearbox must be considered. Equation (242) will be adapted to a standard set of conditions, and a factor will be introduced to indicate the sound pressure attenuation or gain which results with departures from the standard. This standard uses the basic case of a spherical housing vibrating in the radial mode and located in a free field or in a chamber which does not reflect noise. For these conditions and in an atmosphere of air at 68°F and 29.5-in.Hg pressure, the relationship between sound pressure and sound power is (see Reference 3)

$$P_S^2 = \frac{P_A}{28.6\ r^2} \tag{243}$$

where P_S = sound pressure level under the standard conditions, μ bar

P_A = sound power, w

r = distance from the center of the noise-generating surface, ft

Under actual conditions, the sound pressure level will be

$$p^2 = \beta p_S^2 \tag{244}$$

where β = factor for the actual conditions of housing geometry and acoustic environment

When Equations (243) and (244) are combined,

$$p^2 = \frac{\beta P_A}{28.6\ r^2} \tag{245}$$

To express the sound pressure level in db, the sound pressure must first be related to the reference pressure P_o = .0002 μ bar.

Equation (245) becomes

$$\frac{p^2}{p_o^2} = \frac{\beta P_A}{28.6 r^2 (.0002)^2}$$

$$\frac{p^2}{p_o^2} = \frac{8.75 \times 10^{11}\ P_A}{r^2} \tag{246}$$

The sound pressure level in db is

$$L = 10 \log \frac{p^2}{p_o^2} \tag{247}$$

When Equations (242), (246), and (247) are combined,

$$L = 10 \log\left[\frac{4.94 \times 10^4\ \alpha\beta f \Sigma e_o F_o}{r^2}\right] \tag{248}$$

where L = sound pressure level, db

α = energy conversion factor

β = housing geometry and environment factor

f = frequency of excitation, cps

e_o = peak value of sinusoidal excitation, μ in.

F_o = response force at each excitation point, lb

r = radial distance to center of sound-radiating surface, ft

Very little information is available about the factors α and β for specific gearbox designs and environments. While it is possible that each might vary with frequency, at least two studies confirmed that their product remains fairly constant, at least over the frequency ranges studied. The marine gearing study mentioned previously covered the range of from 50 to 2000 cps. The helicopter transmission study contained in this report investigated the

range of from 500 to 10,000 cps. In the former study, the gearbox had a housing of flat, steel plates with welded ribs and was operated in a marine environment. The value used for the combined factor, $\alpha\beta$, was $.7 \times 10^{-3}$ adjusted to the definition used in the above analysis. In the present study, the predicted noise levels for the comparison with measured results were calculated using this same factor, but they were further adjusted for the different housing material. This adjustment was based on the difference in material density. The same kinetic energy in bodies of differing mass would give different amplitudes of motion, as the following analysis shows.

For equal kinetic energy,

$$(KE_1)_1 = (KE)_2 \tag{249}$$

$$\frac{M_1 V_1^2}{2} = \frac{M_2 V_2^2}{2} \tag{250}$$

The velocity-squared ratio becomes

$$\frac{V_2^2}{V_1^2} = \frac{M_1}{M_2} \tag{251}$$

When similar geometry and constant scaling factors are assumed, the mass is proportional to material density,

$$\frac{M_1}{M_2} = \frac{\gamma_1}{\gamma_2} \tag{252}$$

Since sound pressure produced by a vibrating surface is directly proportional to the surface velocity,

$$\frac{P_2^2}{P_1^2} = \frac{V_2^2}{V_1^2} \tag{253}$$

From Equations (242) and (246) combined,

$$\frac{P_2^2}{P_1^2} = \frac{(\alpha\beta)_2}{(\alpha\beta)_1} \tag{254}$$

When Equations (251) through (254) are combined,

$$\frac{(\alpha\beta)_2}{(\alpha\beta)_1} = \frac{\gamma_1}{\gamma_2} \tag{255}$$

or $$(\alpha\beta)_2 = \frac{\gamma_1}{\gamma_2}(\alpha\beta)_1 \tag{256}$$

The previously-mentioned combined factor for steel is

$$(\alpha\beta)_{stl} = .7 \times 10^{-3}$$

The steel-to-magnesium density ratio is

$$\frac{\gamma_{stl}}{\gamma_{mag}} = \frac{.284}{.065} = 4.37$$

Therefore, the factor selected for the largely magnesium housing of the UH-1D transmission housing was

$$(\alpha\beta)_{mag} = .7 \times 10^{-3} \times 4.37 = 3.08 \times 10^{-3} \tag{257}$$

The use of the foregoing analysis, specifically Equation (248) and the factor stated in Equation (257), is illustrated by the set of noise calculations summarized in Table XXXV. The data for these calculations came from the calculated results for the UH-1D, under cruise flight conditions. The gear excitation values are those shown in Table VII. All, except for the bevel gear, were directly calculated with the computer program described in Appendix IV. The force values are those shown in Table VIII. These were calculated with the computer programs described in Appendix V.

After calculating the sound pressure level for each of several excitation frequencies, it is often desirable to display the results as they would be analyzed in third-octave bands by typical instrumentation. Two difficulties arise. First, the band-pass filter for each third octave will pass some part, but not all, of the signal from adjacent bands. With the aid of the filter characteristic, it is possible to find this reduction in db level for the particular frequency and, from this, to find the db level contributing to the third-octave band reading. Second, when more than one noise component is admitted into the particular band, either as full-level contributors whose frequency actually lies within the band or as reduced-level contributors from adjacent bands, the analyzer performs the combination in a special manner. Although the instrument simply records the sum of the individual power levels, when these are evaluated in units of db, the combination is not one of simple addition. Figures 77 and 78 have been provided to assist in coping with the two difficulties. The former is a typical third-octave filter characteristic in a form which permits ready evaluation of filter attenuation in terms of db. The second figure assists in finding the db of the combination of two sound levels when each is given in db. If more than two are to be combined, the result of one combination can be combined with the next sound level in the same manner.

TABLE XXXV. COMPUTATION OF SOUND PRESSURE LEVELS OF GEAR NOISE COMPONENTS - CRUISE FLIGHT CONDITION

Noise Component Source	Freq.* (Hz) f	Excit.* (μ in) e_o	Force* (lb) F_o	No. of Meshes n	Sum of Excit.x Force $\Sigma e_o F_o$	Calculation with log values**					Noise Level (db) L
						$\log f$	$\log \Sigma e_o F_o$	$\log \frac{4.94 \times 10^4}{r^2}$	$\log \alpha \beta$	Sum of Logs	
UP-1 Sun		174	234	8	326×10^3						
Ring		156	234	8	292						
Total	644				618×10^3	2.81	5.79	4.69	-2.52	10.77	107.7
UP-2 Sun		88	83	8	58.4×10^3						
Ring		54	87	8	37.6						
Total	1288				96.0×10^3	3.11	4.98	4.69	-2.52	10.26	102.6
UP-3 Sun		57	20	8	9.1×10^3						
Ring		48	25	8	9.6						
Total	1932				18.7×10^3	3.29	4.27	4.69	-2.52	9.74	97.4
LP-1 Sun		132	73	4	38.6×10^3						
Ring		141	73	4	41.2						
Total	1982				79.8×10^3	3.30	4.90	4.69	-2.52	10.37	103.7
B -1 Bevel	3190	120	910	1	109×10^3	3.50	5.04	4.69	-2.52	10.71	107.1
LP-2 Sun		70	870	4	244×10^3						
Ring		52	707	4	147						
Total	3964				391×10^3	3.60	5.57	4.69	-2.52	11.34	113.4
LP-3 Sun		46	217	4	39.4×10^3						
Ring		48	340	4	65.3						
Total	5946				104.7×10^3	3.78	5.02	4.69	-2.52	10.97	109.7

*Freq. from Table I
Excit. from Table VII
Force from Table VIII

**From Equation (248) rewritten as the sum of the log values with $r = 1$ ft and $\alpha = 3.08 \times 10^3$

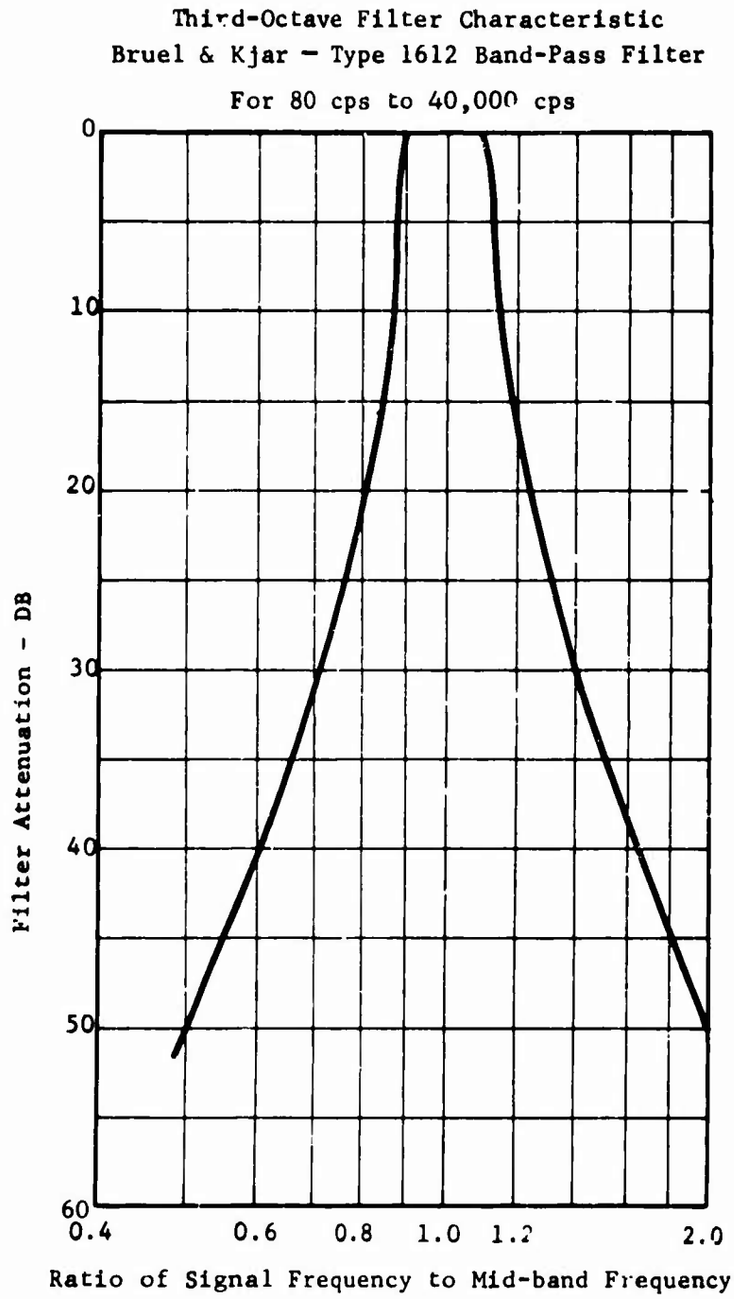

Figure 77. Third-Octave Filter Characteristic.

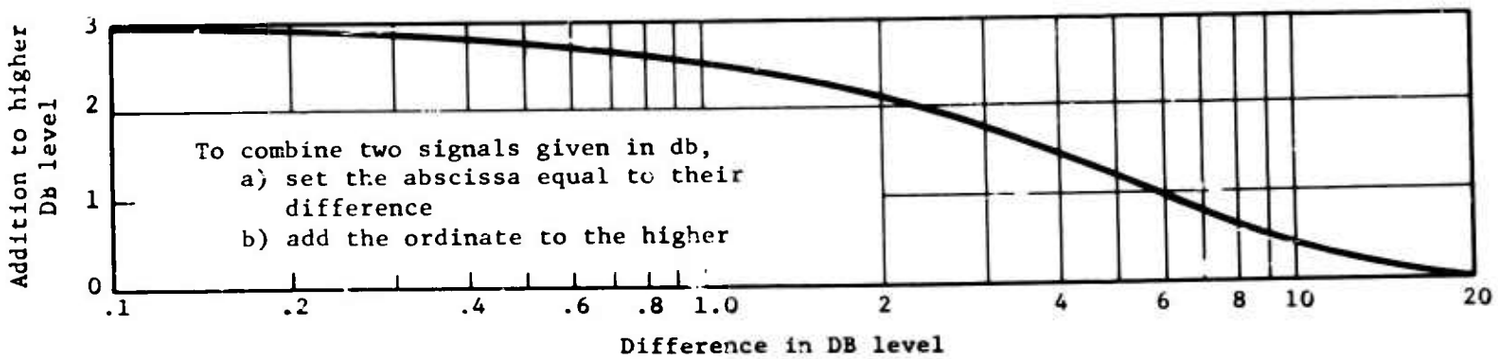

Figure 78. Curve for Calculating DB Level of Combination of DB Levels of Two Signals.

The conversion of the set of individual noise components into a third-octave band display is illustrated by the calculations summarized in Table XXXVI. In this table, under each of the third-octave band midpoints, the successive calculation steps are shown. First, the ratio of noise component excitation frequency to band midpoint frequency is found for each of the frequencies that are close to the band midpoint frequency. With this ratio the proper filter attenuation factor is taken from Figure 77. This factor is subtracted from the corresponding individual noise level value to give the attenuated component noise level passed by the filter. For each band, all of these attenuated levels are combined to give the resultant noise level at the particular third octave band.

TABLE XXXVI. COMBINATION OF GEAR NOISE COMPONENTS SIMULATING THIRD-OCTAVE ANALYSIS - CRUISE FLIGHT CONDITION

Noise Component Source	Freq. (Hz)	Noise* Level (db)	Third Octave Band Midpoints - Hz											
			640	800	1000	1250	1600	2000	2500	3200	4000	5000	6400	8000
			Frequency Ratios											
UP-1	644		1.61	.81	.64									
UP-2	1288				1.29	1.03	.80							
UP-3	1932						1.21	.97	.77					
LP-1	1982						1.24	.99	.79					
B -1	3190								1.27	1.00	.80			
LP-2	3964									1.24	.99	.79		
LP-3	5946											1.19	.93	.74
			Filter Attenuation in db (from Frequency Ratios and Figure 77)											
UP-1	644	107.7	0	20	37									
UP-2	1288	102.6			24	0	21							
UP-3	1932	97.4					17	0	25					
LP-1	1982	103.7					20	0	22					
B -1	3190	107.1							22	0	21			
LP-2	3964	113.4								19	0	22		
LP-3	5946	109.7										15	0	27
			Noise Level Passed in Each Band in db											
UP-1	644	107.7	107.7	87.7	70.7									
UP-2	1288	102.6			78.6	102.6	81.5							
UP-3	1932	97.4					80.4	97.4	72.4					
LP-1	1982	103.7					83.7	103.7	81.7					
B -1	3190	107.1							85.1	107.1	96.1			
LP-2	3964	113.4								94.4	113.4	91.4		
LP-3	5946	109.7										94.7	109.7	82.7
Combined Noise Levels**			107.5	88.0	80.0	102.5	87.0	104.5	87.0	107.5	113.5	96.5	109.5	82.5

*Noise Level from Table XXXV

**Combined Noise Level found by use of Figure 78 and rounded to nearest .5 db.

BLANK PAGE

Unclassified
Security Classification

DOCUMENT CONTROL DATA - R & D

(Security classification of title, body of abstract and indexing annotation must be entered when the overall report is classified)

1. ORIGINATING ACTIVITY (Corporate author)
Mechanical Technology Incorporated
Latham, New York

2a. REPORT SECURITY CLASSIFICATION
Unclassified

2b. GROUP

3. REPORT TITLE
ANALYSIS OF NOISE GENERATED BY UH-1 HELICOPTER TRANSMISSION

4. DESCRIPTIVE NOTES (Type of report and inclusive dates)
Final Report (June 21, 1966 to September 21, 1967)

5. AUTHOR(S) (First name, middle initial, last name)
Irving Laskin
Frederic K. Orcutt
Eugene E. Shipley

6. REPORT DATE
June 1968

7a. TOTAL NO. OF PAGES
316

7b. NO. OF REFS
11

8a. CONTRACT OR GRANT NO.
DA-44-177-AMC-416(T)

b. PROJECT NO.
Task 1G121401D14414

c.

d.

9a. ORIGINATOR'S REPORT NUMBER(S)
USAAVLABS Technical Report 68-41

9b. OTHER REPORT NO(S) (Any other numbers that may be assigned this report)
MTI-67TR83

10. DISTRIBUTION STATEMENT
This document has been approved for public release and sale; its distribution is unlimited.

11. SUPPLEMENTARY NOTES

12. SPONSORING MILITARY ACTIVITY
Department of the Army
U. S. Army Aviation Materiel Laboratories
Fort Eustis, Virginia 23604

13. ABSTRACT

A method of computing helicopter gearbox noise from design and operating data is presented. Measurements on UH-1D helicopters are used to provide a basis for this computation method. Its validation is shown by a comparison between calculated and measured noise spectrums. The method is used to quantitatively evaluate several kinds of noise-reducing design changes.

The most objectionable noise is shown to originate in the meshing action of the gear teeth. The variable tooth deflection under the heavy tooth loading together with some contribution from the manufactured tooth profile errors act to excite vibrations in the gearbox drive components. Each gear mesh produces up to three noise components whose frequencies correspond to the gear tooth meshing rates and their second and third harmonics. The gear-induced vibration is transmitted to the gearbox casing which serves to "broadcast" the gear noise. Calculations of excitation, vibration forces, and noise radiation is accomplished with the aid of several computer programs.

Calculations on the UH-1D gearbox reveal that a variety of design modifications will be required to reduce all high-level noise components, and that some modifications must be carefully optimized to avoid increasing one component while reducing another.

DD FORM 1 NOV 65 1473 REPLACES DD FORM 1472, 1 JAN 64, WHICH IS OBSOLETE FOR ARMY USE.

Unclassified
Security Classification

Unclassified
Security Classification

14. KEY WORDS	LINK A ROLE	LINK A WT	LINK B ROLE	LINK B WT	LINK C ROLE	LINK C WT
Helicopters						
Noise Measurements						
Gearbox Noise Calculation						
Gearbox						
Noise						
Vibration						
Design for Noise Reduction						
Gear						
Measurement						
Spur Gear Teeth						
Deflection						
Load Transfer						
Planetary Gearing						
Vibration						
Noise						
Calculation						

Unclassified
Security Classification

5744-68